

**STUDY OF ACOUSTICAL AND THERMODYNAMIC
PROPERTIES OF GRAPHENE OXIDE (GO) AND
REDUCED GRAPHENE OXIDE (rGO) IN WATER AND
SOME ORGANIC SOLVENTS**

A Thesis

Submitted in partial fulfillment of the requirements for the
award of the degree of

DOCTOR OF PHILOSOPHY

in

Physics

By

ALOK JAIN

(Reg. No. 41400132)

Supervised By

**Dr. Kailash Chandra Juglan
Professor, Department of Physics**



LOVELY
PROFESSIONAL
UNIVERSITY

Transforming Education Transforming India

**LOVELY PROFESSIONAL UNIVERSITY
PUNJAB
2020**

CANDIDATE'S DECLARATION

I, Alok Jain, hereby declare that the thesis entitled “STUDY OF ACOUSTICAL AND THERMODYNAMIC PROPERTIES OF GRAPHENE OXIDE (GO) AND REDUCED GRAPHENE OXIDE (rGO) IN WATER AND SOME ORGANIC SOLVENTS,” submitted to Lovely Faculty of Physical Sciences, Lovely Professional University, Phagwara, in partial fulfillment of the requirement for the award of the degree of Doctor of Philosophy in Physics is the original work carried out by me under the supervision of Prof. Kailash Chandra Juglan. No part of the thesis has been formed the basis for the award of any degree or diploma at any other university or institute.

Alok Jain

Reg. No. 41400132

CERTIFICATE

I certify that the thesis entitled ‘STUDY OF ACOUSTICAL AND THERMODYNAMIC PROPERTIES OF GRAPHENE OXIDE (GO) AND REDUCED GRAPHENE OXIDE (rGO) IN WATER AND SOME ORGANIC SOLVENTS,’ submitted to the Lovely School of Sciences, Lovely Professional University, Punjab, for the award of the degree of DOCTOR OF PHILOSOPHY in PHYSICS is the result of research work carried out by Mr. Alok Jain under my guidance and supervision.

Signature of Supervisor

Prof. Kailash Chandra Juglan

Head of Physics Department

Lovely Professional University

Jalandhar -Delhi, Grand Trunk Road

Phagwara-144411, Punjab, India

ABSTRACT

Carbon has always been a fascinating material among the scientific community. A lot of research on carbon has been done in the last century. Diamond and graphite were the two allotropes that are available for centuries. In the previous decade of a 20th-century new allotrope of the carbon comes into existence named nanotubes. The nanotubes have incredible properties that are used in many fields like technology, science, and medicine. In the previous decade, another incredible material of carbon was found. This material also has some excellent properties, which have dominated the scientific community's attention. The material is a few layers of the graphite that is detached from its structure. These few layers of the graphite are named “*graphene*.” Graphene has some remarkable properties like the highest electron mobility, excellent thermal properties, superior conductivity, and many more. All these fascinating properties make the graphene a good contender for research and applications.

The research of the nanofluids/nanosuspension also picks up the pace with the advancement in nanotechnology. Nanofluids are the nanoparticles dispersed in some base fluids. Nanofluids/nanosuspension shows remarkable properties over the fluids with micro and macroparticles. This study revolves around the excellent features of the GO and rGO to be used as nanosuspension. GO, and rGO is not very dispersive in many of the organic solvents, but it shows some excellent dispersive and stable properties with individual solutions such as water, N, N Dimethylformamide (DMF), Ethylene Glycol (EG), Tetrahydrofuran (THF), and, N-Methyl-2-pyrrolidone (NMP). These five solvents were selected for the dispersion of the GO and rGO in the selected solvents.

This thesis entitles “*Study of acoustical and thermodynamic properties of graphene oxide (GO) and reduced graphene oxide (rGO) in water and some organic solvents*” deals with the production of graphene oxide and reduced graphene oxide and their characterization. Many characterization techniques like FESEM, EDS, FTIR, XRD, and RAMAN were used to characterize the prepared GO and rGO. The result of the characterization has been discussed in the details in the thesis. This prepared powder is

dispersed in the organic solvents selected for the study. The use of the ultrasonication helps to disperse this prepared powder in the solvent such that they become stable and dispersive. The prepared nanosuspension was characterized by different characterization techniques like UV-Vis, DLS, and HRTEM. The results of all the tests are discussed in the thesis with all the required details. The Study of thermoacoustic properties of graphene oxide and reduced graphene oxide with some organic solvent at different temperatures has been done in this thesis. The thermodynamic properties of the liquid mixture become the topic of interest nowadays. These properties are beneficial in the pharmaceutical, petrochemical, and chemical industries. This study helps to understand the molecular and particle-particle interactions present in the mixture. The awareness of different thermoacoustic properties is beneficial as solute stability in the different solvent; also, the blending consequences of the suspension mixture are tough to understand. The thermoacoustic properties of the different concentrations of the prepared solution are calculated by interferometer, densitometer, and viscometer.

Different series of the samples were prepared with concentrations 0 mg/ml, 0.2 mg/ml, 0.4 mg/ml, 0.6 mg/ml, 0.8 mg/ml, and 1.0 mg/ml of GO and rGO in water, DMF, NMP, THF and EG. All these samples under study were gone through the intensive ultrasonication for stability and studied at four different temperatures (298, 303, 308, and 313 K).

In this thesis, we divided the study into five sections. In all the sections, ultrasonic velocity, density, and viscosity were measured with the help of instruments. We have used these measured values to measure the derived parameters like adiabatic compressibility, acoustical impedance, attenuation, bulk modulus, relaxation time, and intermolecular free length have been calculated for all the prepared samples. In this study, the impact of the calculated and derived values on intermolecular and particle-particle interaction is discussed.

ACKNOWLEDGMENT

With great pleasure, I express my sincere and profound gratitude to my supervisor Prof. Kailash Chander Juglan, for his erudite and invaluable guidance throughout my research work. It is by virtue of his patience, motivation, exuberance, and immense knowledge that led to the completion of my Ph.d. Work. His guidance helped me throughout my research work and inditing of the thesis. I could not have imagined a better guide for my Ph.D.

I would extend my thanks to Mr. Navdeep Singh Dhaliwal, Head, Department of Examination, for his kind support and suggestions throughout my research work. I would also like to thank Prof. Ramesh Thakur, HOS, School of Physical Sciences, for his inspiration and regular support for my research work.

I want to convey a special thanks to my dearest friend Dr. Neeraj Batra, who has consistently encouraged and supported me in my research work. I would also thank Mr. Sonu, Mr. Ankur Gupta, Mr. Mohit Sharma, and Mr. Arvind Sharma, for their generous behavior and moral support. Also, I feel fortunate to have Mr. Gurmel Singh, Dr. Amit Dutt, Ms. Shreya, Dr. Nitin Tandon, and my old classmate and friend Mr. Vishal Sharma, as my good friends who always motivated me throughout my work.

Finally, I would like to thank my family for their consistent inspiration, encouragement, and moral support throughout my life. It is because of the blessings of my father and mother, which enabled me to complete this research work. I can never forget the love and affection I got from them. No amount of words could express my appreciation to them.

Last but not least, I appreciate the patience, support, and understanding of my wife, Mrs. Neeru Shamra; without her help, the work would never have been completed. I would also express affection for my duo Saksham Jain and Naman Jain, who is always a source of happiness for me.

Alok Jain

CONTENTS

Title	Page No.
Declaration.....	i
Certificate.....	ii
Abstract	iii
Acknowledgment	v
Contents.....	vi
List of Tables	x
List of Figures.....	xi
List of symbols and abbreviations used.....	xviii
1 Introduction	
1.1 Origin of carbon nanomaterial.....	1
1.2 Different carbon allotropes.....	3
1.3 Fluids and Suspensions.....	8
1.4 Techniques to prepare nanosuspension.....	10
1.5 Choice of Base Fluid.....	14
1.6 Acoustical parameters.....	18
1.7 References.....	21
2 Review of Literature	
2.1 A brief view of relevant literature.....	25
2.2 References.....	48
3 Objectives and methodology	
3.1 Objectives.....	53
3.2 Research Methodology.....	53
3.3 Calculation of other parameters.	68
3.4 Structures of the chemical used in the experiment.....	69

3.5	Description of the chemical used in the study.....	71
3.6	References.....	72
4	Result and Discussion	
4.1	Characterization of GO.....	74
4.2	Characterization of rGO.....	78
4.3	Characterization of GO Nanosuspension.....	83
4.4	Characterization of rGO Nanosuspension.....	87
4.5	Reference.....	90
	Section 1 (Part A)	
4.6	Introduction.....	92
4.7	Material and Method.....	93
4.8	Characterization of GO and Water-GO nanosuspension.....	94
4.9	Data Table.....	95
4.10	Result and Discussion.....	101
4.11	Reference.....	113
	Section 1 (Part B)	
4.12	Introduction.....	117
4.13	Material and method.....	118
4.14	Characterization of RGO and Water-rGO nanosuspension.....	119
4.15	Data Table.....	121
4.16	Result and Discussion.....	127
4.17	References.....	139
	Section 2	
4.18	Introduction.....	143
4.19	Experimental.....	144
4.20	Data table.....	146
4.21	Result and Discussion.....	158
4.22	References.....	169

Section 3 (Part A)	
4.23	Introduction..... 172
4.24	Material and Method..... 173
4.25	Characterization of GO and NMP-GO nanosuspension..... 175
4.26	Data Table..... 176
4.27	Result and Discussion..... 182
4.28	References..... 192
Section 3 (Part B)	
4.29	Introduction..... 196
4.30	Materials and Methods..... 197
4.31	Characterization of NMP-RGO Nanosuspension..... 199
4.32	Data Table..... 201
4.33	Result and Discussion..... 205
4.34	References..... 212
Section 4	
4.35	Introduction..... 214
4.36	Material and Method..... 215
4.37	Characterization of THF-GO and THF-rGO Nanosuspension..... 217
4.38	Data Table..... 219
4.39	Result and Discussion..... 227
4.40	References..... 233
Section 5	
4.41	Introduction..... 235
4.42	Material and Method..... 236
4.43	Characterization of EG-GO and EG-rGO Nanosuspension..... 237
4.44	Data Table..... 240
4.45	Result and Discussion..... 248
4.46	References..... 254

5	Summary and Conclusion	
5.1	Summary.....	256
5.2	Conclusion.....	260
5.3	Future Prospective.....	261
6	List of publications and conferences attended	
6.1	List of Publications.....	262
6.2	Paper Communicated.....	262
6.3	Research Paper presented in conferences.....	262

LIST OF TABLES

Table 1.1	General properties of 5 basic fluids
Table 3.1	Sample details
Table 3.2	Chemical used in the study with structure
Table 4.1	UV Cutoff wavelength for the liquids under study.
Table 4.2	Water-GO Nanosuspension 1
Table 4.3	Water-GO Nanosuspension 2
Table 4.4	Water-RGO Nanosuspension 1
Table 4.5	Water-RGO Nanosuspension 2
Table 4.6.	DMF-GO Nanosuspension 1
Table 4.7	DMF-GO Nanosuspension 2
Table 4.8	DMF-rGO Nanosuspension 1
Table 4.9	DMF-rGO Nanosuspension 2
Table 4.10	NMP-GO Nanosuspension 1
Table 4.11	NMP-GO Nanosuspension 2
Table 4.12	NMP-rGO Nanosuspension 1
Table 4.13	NMP-rGO Nanosuspension 2
Table 4.14	THF-GO Nanosuspension 1
Table 4.15	THF-GO Nanosuspension 2
Table 4.16	THF-rGO Nanosuspension 1
Table 4.17	THF-rGO Nanosuspension 2
Table 4.18	EG-GO Nanosuspension 1
Table 4.19	EG-GO Nanosuspension 2
Table 4.20	EG-rGO Nanosuspension 1
Table 4.21	EG-rGO Nanosuspension 2

LIST OF FIGURES

- Figure 1.1 Graphite structure and diamond structure
- Figure 1.2 C60 structure of fullerene
- Figure 1.3 Carbon SWCNT, MWCNT, and CNF
- Figure 1.4 Graphene Sheet, Graphene Oxide sheet and Reduced Graphene Oxide Sheet
- Figure 1.5 Nanofluid, colloidal suspension and nanosuspension
- Figure 1.6 Water molecule
- Figure 1.7 DMF molecule
- Figure 1.8 EG molecule
- Figure 1.9 THF molecule
- Figure 1.10 NMP molecule
- Figure 3.1 Nova Nano SEM 450
- Figure 3.2 Nova Nano SEM 450 with EDS attachment
- Figure 3.3 HRTEM JOEL JEM-2100
- Figure 3.4 FTIR Perkin Elmer Spectrum 2
- Figure 3.5 XRD Panalytical X'Pert Pro
- Figure 3.6 Raman Spectrometer Airix STR-500
- Figure 3.7 UV-Vis Spectrometer Shimadzu UV-1800
- Figure 3.8 DLS Malvern Zetasizer Nano ZS90
- Figure 3.9 Ultrasonic Interferometer Mittal M-81
- Figure 3.10 Pyknometer Density bottle with a thermometer
- Figure 3.11 Rotational Viscometer Labman LMDV 200
- Figure 4.1 (a) shows the FESEM Micrograph for prepared GO samples at 50000 magnification and 2 μm scale (b) shows the FESEM Micrograph for prepared GO sample at 200000 X Magnification at 500 nm scale.
- Figure 4.2 shows the EDX with elemental analysis for the prepared GO sample

- Figure 4.3 shows the FTIR spectra for the prepared GO sample
- Figure 4.4 shows the XRD spectra for the prepared GO sample
- Figure 4.5 shows the RAMAN spectra for the prepared GO sample
- Figure 4.6 (a) shows the FESEM Micrograph for prepared rGO samples at 1 μm magnification. (b) shows the FESEM Micrograph for prepared rGO sample at 500 nm Magnification.
- Figure 4.7 shows the EDS with elemental analysis for the prepared rGO sample
- Figure 4.8 shows the FTIR spectra for the prepared rGO sample
- Figure 4.9 shows the XRD spectra for the prepared rGO sample
- Figure 4.10 shows the RAMAN spectra for the prepared rGO sample
- Figure 4.11 shows the UV-Vis spectra of GO nanosuspensions.
- Figure 4.12 (a) shows the HRTEM Micrograph for prepared GO samples at 100 nm magnification. (b) shows the HRTEM Micrograph for prepared GO sample at 50 nm Magnification.
- Figure 4.13 Shows the particle size distribution of the GO in different solvent
- Figure 4.14 shows the UV-Vis spectra of GO nanosuspensions.
- Figure 4.15 (a) shows the HRTEM Micrograph for prepared rGO samples at 100 nm magnification. (b) shows the HRTEM Micrograph for prepared rGO sample at 50 nm Magnification.
- Figure 4.16 Shows the particle size distribution of the rGO in different solvent
- Figure 4.17 FESEM Micrograph for GO
- Figure 4.18 EDS for GO
- Figure 4.19 FTIR for GO
- Figure 4.20 XRD for GO
- Figure 4.21 Raman Spectra for GO
- Figure 4.22 UV-Vis for Water-GO nanosuspension

Figure 4.23	DLS for Water-GO nanosuspension
Figure 4.24	The velocity of sound in Water-GO nanosuspension
Figure 4.25	The density of Water-GO nanosuspension
Figure 4.26	The viscosity of Water-GO nanosuspension
Figure 4.27	Adiabatic Compressibility of Water-GO nanosuspension
Figure 4.28	Acoustical Impedance of Water-GO nanosuspension
Figure 4.29	Attenuation of sound in Water-GO nanosuspension
Figure 4.30	The bulk modulus of Water-GO nanosuspension
Figure 4.31	The relaxation time of Water-GO nanosuspension
Figure 4.32	Intermolecular Free Length of Water-GO nanosuspension
Figure 4.33	FESEM of rGO
Figure 4.34	EDS of rGO
Figure 4.35	FTIR of rGO
Figure 4.36	XRD of rGO
Figure 4.37	RAMAN Spectra of rGO
Figure 4.38	UV-VIS spectra of rGO
Figure 4.39	DLS of Water-rGO Nanosuspension
Figure 4.40	The ultrasonic velocity of Water-rGO Nanosuspension
Figure 4.41	The density of Water-rGO Nanosuspension
Figure 4.42	The viscosity of Water-rGO Nanosuspension
Figure 4.43	Adiabatic Compressibility of Water-rGO Nanosuspension
Figure 4.44	Acoustical Impedance of Water-rGO Nanosuspension
Figure 4.45	Attenuation of a sound wave in Water-rGO Nanosuspension
Figure 4.46	The bulk modulus of Water-rGO Nanosuspension
Figure 4.47	The relaxation time of Water-rGO Nanosuspension
Figure 4.48	Intermolecular Free Length of Water-rGO Nanosuspension
Figure 4.49	(a) FESEM micrograph of GO (b) FESEM micrograph of rGO
Figure 4.50	(a) EDS Spectra of GO (b) EDS Spectra of rGO
Figure 4.51	(a) FTIR Spectra of GO (b) FTIR Spectra of rGO

- Figure 4.52 (a) XRD Spectra of GO (b) XRD Spectra of rGO
- Figure 4.53 (a) RAMAN Spectra of GO (b) RAMAN Spectra of rGO
- Figure 4.54 (a) TEM Spectra of GO (b) TEM Spectra of rGO
- Figure 4.55 (a) UV-VIS Spectra of DMF-GO (b) UV-VIS Spectra of DMF-rGO
- Figure 4.56 (a) DLS Study of DMF-GO (b) DLS Study of DMF-rGO
- Figure 4.57 (a) Ultrasonic Velocity Study of DMF-GO (b) Ultrasonic Velocity Study of DMF-rGO
- Figure 4.58 (a) The density of DMF-GO (b) Density of DMF-rGO
- Figure 4.59 (a) The viscosity of DMF-GO (b) Viscosity of DMF-rGO
- Figure 4.60 (a) Adiabatic Compressibility of of DMF-GO (b) Adiabatic compressibility of DMF-rGO
- Figure 4.61 (a) Acoustical Impedance of DMF-GO (b) Acoustical Impedance of DMF-rGO
- Figure 4.62 (a) Attenuation of sound wave in DMF-GO (b) Attenuation of a sound wave in DMF-rGO
- Figure 4.63 (a) Bulk Modulus of DMF-GO (b) Bulk Modulus of a sound wave in DMF-rGO
- Figure 4.64 (a) Relaxation Time of DMF-GO (b) Relaxation Time of DMF-rGO
- Figure 4.65 (a) Intermolecular Free Length of DMF-GO (b) Intermolecular Free Length of DMF-rGO
- Figure 4.66 FESEM of GO
- Figure 4.67 EDS of GO
- Figure 4.68 FTIR of GO
- Figure 4.69 XRD of GO
- Figure 4.70 Raman of GO
- Figure 4.71 DLS of GO
- Figure 4.72 Ultrasonic Velocity of NMP-GO Nanosuspension

- Figure 4.73 The density of NMP-GO Nanosuspension
- Figure 4.74 The viscosity of NMP-GO Nanosuspension
- Figure 4.75 Adiabatic Compressibility of NMP-GO Nanosuspension
- Figure 4.76 Acoustical Impedance of NMP-GO Nanosuspension
- Figure 4.77 Attenuation of Ultrasound in NMP-GO Nanosuspension
- Figure 4.78 The bulk modulus of NMP-GO Nanosuspension
- Figure 4.79 Relaxation Time of NMP-GO Nanosuspension
- Figure 4.80 Intermolecular Free Length of NMP-GO Nanosuspension
- Figure 4.81 HRTEM image of rGO
- Figure 4.82 DLS particle size of the NMP-rGO Nanosuspension
- Figure 4.83 Ultrasonic study of NMP-rGO Nanosuspension
- Figure 4.84 The density of NMP-rGO Nanosuspension
- Figure 4.85 The viscosity of NMP-rGO Nanosuspension
- Figure 4.86 Adiabatic Compressibility of NMP-rGO Nanosuspension
- Figure 4.87 Acoustical Impedance of NMP-rGO Nanosuspension
- Figure 4.88 Attenuation of ultrasound waves in NMP-rGO
Nanosuspension
- Figure 4.89 Bulk Modulus of NMP-rGO Nanosuspension
- Figure 4.90 Relaxation Time of NMP-rGO Nanosuspension
- Figure 4.91 Intermolecular free length of NMP-rGO Nanosuspension
- Figure 4.92 (a) HRTEM image of GO (b) HRTEM image of rGO
- Figure 4.93 (a) DLS image of THF-GO Nanosuspension (b) DLS image of
THF-rGO Nanosuspension
- Figure 4.94 (a) Ultrasonic Velocity of THF-GO Nanosuspension (b)
Ultrasonic Velocity of THF-rGO Nanosuspension
- Figure 4.95 (a) The density of THF-GO Nanosuspension (b) Density of
THF-rGO Nanosuspension
- Figure 4.96 (a) The viscosity of THF-GO Nanosuspension (b) Viscosity of
THF-rGO Nanosuspension

- Figure 4.97 (a) Adiabatic Compressibility of THF-GO Nanosuspension
(b) Adiabatic Compressibility of THF-rGO Nanosuspension
- Figure 4.98 (a) Acoustical Impedance of THF-GO Nanosuspension (b)
Acoustical Impedance of THF-rGO Nanosuspension
- Figure 4.99 (a) Attenuation of Ultrasonic Waves in THF-GO
Nanosuspension (b) Attenuation of Ultrasonic Waves in THF-
rGO Nanosuspension
- Figure 4.100 (a) Bulk Modulus of THF-GO Nanosuspension (b) Bulk
Modulus of THF-rGO Nanosuspension
- Figure 4.101 (a) Relaxation Time of THF-GO Nanosuspension (b)
Relaxation Time of THF-rGO Nanosuspension
- Figure 4.102 (a) Intermolecular free Length of THF-GO Nanosuspension
(b) Intermolecular free Length of THF-rGO Nanosuspension
- Figure 4.103 (a) HRTEM image of GO (b) HRTEM image of rGO
- Figure 4.104 (a) DLS image of EG-GO Nanosuspension (b) DLS image of
EG-rGO Nanosuspension
- Figure 4.105 (a) Ultrasonic Velocity of EG-GO Nanosuspension (b)
Ultrasonic Velocity of EG-rGO Nanosuspension
- Figure 4.106 (a) The density of EG-GO Nanosuspension (b) Density of EG-
rGO Nanosuspension
- Figure 4.107 (a) The viscosity of EG-GO Nanosuspension (b) Viscosity of
EG-rGO Nanosuspension
- Figure 4.108 (a) Adiabatic Compressibility of EG-GO Nanosuspension (b)
Adiabatic Compressibility of EG-rGO Nanosuspension
- Figure 4.109 (a) Acoustical Impedance of EG-GO Nanosuspension (b)
Acoustical Impedance of EG-rGO Nanosuspension
- Figure 4.110 (a) Attenuation of Ultrasonic Waves in EG-GO
Nanosuspension (b) Attenuation of Ultrasonic Waves in EG-
rGO Nanosuspension

Figure 4.111 (a) Bulk Modulus of EG-GO Nanosuspension (b) Bulk Modulus of EG-rGO Nanosuspension

Figure 4.112 (a) Relaxation Time of EG-GO Nanosuspension (b) Relaxation Time of EG-rGO Nanosuspension

Figure 4.113 (a) Intermolecular free Length of EG-GO Nanosuspension (b) Intermolecular free Length of EG-rGO Nanosuspension

List of the symbol and abbreviations used

u	Speed of sound
T	Temperature
ρ	Density
η	Viscosity
β	Adiabatic compressibility
f	Frequency
Z	Acoustic impedance
K	Bulk Modulus
τ	Relaxation time
L_f	Intermolecular free length
α	Attenuation of the ultrasonic wave in a sample.
GO	Graphene Oxide
rGO	Reduced graphene oxide
EG	Ethylene Glycol
NMP	N-Methyl-2-pyrrolidone
THF	Tetrahydrofuran
DMF	N, N Dimethylformamide
FESEM	Field emission scanning electron microscope
EDS	Energy dispersive spectroscopy
HRTEM	High resolution transmission electron microscope
FTIR	Fourier transform infrared microscopy
XRD	X-Ray diffraction
RAMAN	Raman Spectroscopy
Water-GO	Water Graphene Oxide nanosuspension
Water-rGO	Water reduced Graphene Oxide nanosuspension

DMF-GO	N, N Dimethylformamide graphene oxide nanosuspension
DMF-rGO	N, N Dimethylformamide reduced graphene oxide nanosuspension
NMP-GO	N-Methyl-2-Pyrrolidone graphene oxide nanosuspension
NMP-rGO	N-Methyl-2-Pyrrolidone reduced graphene oxide nanosuspension
THF-GO	Tetrahydrofuran graphene oxide nanosuspension
THF-rGO	Tetrahydrofuran reduced graphene oxide nanosuspension
EG-GO	Ethylene Glycol graphene oxide nanosuspension
EG-rGO	Ethylene Glycol reduced graphene oxide nanosuspension

CHAPTER 1: INTRODUCTION:

Carbon is a building block of our life [1]; it is one of the most abundant elements that exist in-universe, earth crust, and most probably in the human body. Carbon exists in different states like a diamond, graphite, and a wide number of structures with other elements ranging from tiny molecular chains to huge molecular chains [1]. The existence of different hybridization states of carbon can create more allotropes than any other known element presents on earth. However, the best known since old times are diamond and graphite [2]. The use of the diamond in the ancient times were mostly as a precious gem, but graphite was used to make tools in ancient history as we are building tools nowadays also the weak dispersion forces between the adjacent sheets plays a vital role in the lubrication properties of the graphite. We know the sp^3 hybridization of the carbon atoms in the diamond structure leads to the most durable natural formation available because of this structure, a diamond is transparent with excellent insulation properties [2]. On the other hand, graphite follows sp^2 hybridization, which gives the characteristics like soft material and unique electrically conductive properties. As for the structural differences, diamond consists of sp^3 hybridized carbon atoms, while graphite is based on sp^2 hybridized carbon atoms stacked in layers. But this is all just the beginning since carbon, and its allotropes found their application almost everywhere. And in our case, we will be looking through the typical orifice on a small portion of its use in acoustic and intermolecular interaction study.

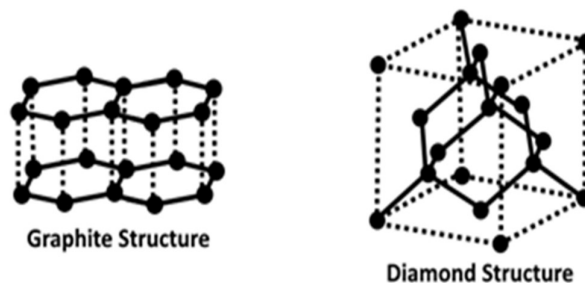


Figure 1. Graphite structure and diamond structure

1.1 Origin of carbon nanomaterial: Development in the field of material science and

chemistry leads to further investigation of different allotropes and forms of carbon atoms [2]. Improvement in the various physical and chemical properties leads to more and more applications related to the carbon element. There are many famous names in the arsenal of the carbon-like nanoribbons (NR), nanotubes (NT), single-wall nanotubes (SWCNTs), multiwall nanotubes (MWCNTs), graphene oxide (GO) and reduced graphene oxide (rGO) and graphene (G). Nanomaterials like nanoribbons, graphene, or single-walled carbon nanotubes (SWCNTs) show ballistic electron transport, which offers the possibility for construction of high-speed sensors [3-5]. In particular, SWCNTs are a great example of another advantage, and that is the combination of morphology, biocompatibility, and electronic properties, which allows direct wiring with active sites of redox enzymes and thus leads to direct electron transfer, better sensitivity, and lower detection limits. However, it is worth mentioning that carbon materials have one significant disadvantage, and that is their heterogeneity in nature.

Carbon nano allotropes could be generally sorted into two main groups by the powerful covalent bond in the structure which they have created. The first group is the build-up of mostly sp^2 hybridized carbon atoms. They are highly packed in hexagonal (honeycomb) crystal lattice, but they could also contain (and usually do) some amount of sp^3 hybridized atoms at the edges and due to disruptions, which are present in the crystal lattice on the basal plane. Typical representatives of this group are graphene and graphene-like structures such as nanoribbons or quantum dots, CNTs, fullerenes, and fullerene-like structures such as onion-like nanospheres (multi-shell fullerenes). The second group is the build-up of mostly sp^3 hybridized carbon atoms, and thus they cannot be considered as graphene derivatives. Typically, with only one chief representative – nanodiamond. In this work, a more favourable classification of carbon nanostructures is used. It is based on the dimension in space. In this way, carbon nano allotropes could have resorted into three main groups; 0D structures such as fullerenes and fullerene-like allotropes, quantum dots and nanodiamonds, 1D structures represented by nano horns, nanofibers, and CNTs, and finally, 2D structures with the most significant representative, i.e., graphene and other graphene-like structures such as graphene nanoribbons [6].

1.2 Different carbon allotropes:

1.2.1 Fullerenes: Fullerenes are new carbon allotropes in which carbon atoms are arranged in cage-like structure, as shown in figure 2. The most common and abundant form of the fullerene is Buckminsterfullerene, where 60 carbon atoms are arranged to form a sphere-like structure. Commonly it is also known as C₆₀. The shape of a molecule of the Buckminster is icosahedron in which carbon atoms are resembling a soccer ball consist of 12 pentagons and 20 hexagons. C₆₀ fullerene is the most stable structure having no two pentagons side by side [7].

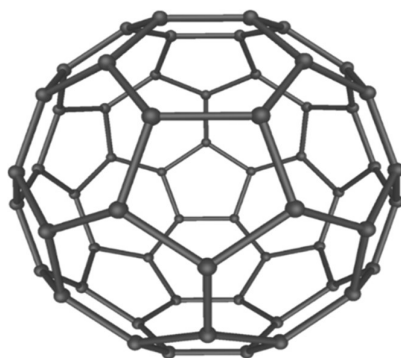


Figure 2: C₆₀ structure of fullerene

The C₆₀ molecule is highly symmetrical, and there are around 120 symmetrical operations like rotation and reflection can be applied to this molecule. All these symmetrical operations map the molecule on to the molecule itself. Two different kinds of bond lengths exist inside the fullerene molecule. One is the bond length of the C-C in the pentagon, and the other is the C-C bond length in the case of the hexagon. The bond length in the case of the pentagon is 1.45 Å, and in the case of hexagon, it is 1.40 Å. Each carbon atom forms bond with sp² hybridization with the other three carbon atom. All orbitals are arranged 120° to each other and centered along XY-Plane. The size of the C₆₀ molecule is approximately 7 Å. [1]

Fullerites is the crystalline state of weakly bound C₆₀ molecules condensed to form solid. This condensed solid-state of C₆₀ is weakly bonded and insulating. The colour of this solid is yellow and turns pink when dissolved in toluene. The polymerization of

the Buckyball can be initialized with exposure of the intense UV light; with this, Buckyball starts forming bonds with the adjacent balls. At lower temperatures, Buckyball spins freely in their crystalline position below $-183\text{ }^{\circ}\text{C}$ the movement of the buckyballs gets restricted and stuck. If we heat the C60 closer to $1500\text{ }^{\circ}\text{C}$ than molecules turn into graphite in the absence of the air. [8-10]

Fullerenes have many applications in the field of biology, pharmaceutical, medical, superconductor, HIV Protease Inhibitors, etc. There are two big problems associated with applications of the fullerene. The first problem associated with the fullerene is that it approximately 100 to 1000 times expensive (as per purity) as compare to gold, which restricts the application in many fields where cost plays a big role. This high cost involved in the preparation of the fullerene is the use of high temperature during the manufacturing process. Another problem associated with the fullerene application is insolubility and instability of the C60 powder in the water. This problem is solved by manufacturing the fullerene derivatives, which are soluble to water. Another possible application of the fullerene is in medicine, where cost sometimes is not a big issue. [11],[12]

C60 is the novel form of fullerene; other than this, fullerene is having carbon atoms between range from 30 to 980. All these fullerenes follow the different structures. As more and more hexagons and pentagons are added to the soccer ball structure of fullerenes, the molecule begins to loosen its shape and get flattened. Some fullerenes are shaped like a rugby ball, pentagonal shape, and asteroids. As the molecule loses its roundness, symmetrical properties also get disturbed. Fullerene is the low-density powder, which is soluble in organic compounds like carbon disulfide, toluene, etc.[10]

1.2.2 Carbon dots and carbon nanodiamonds: Carbon nanodots are the type of nanomaterial with excellent optical properties and having a particle size of less than 10 nm. The major application of the carbon dots is in the field of photoluminescence, where the full spectrum of the sunlight is used in the photoluminescence properties of the carbon dots. The light-induced electrical properties extend the application of carbon dots in many fields of science. [13],[14]

Carbon nanodiamonds follow the truncated octahedral structure having a size of about 1 – 10 nm. Carbon nanodiamonds possess many astonishing properties like chemical inertness, hard, optically transparent, and high thermal conductivity. These extraordinary properties of the nanodiamonds lead to many applications. The common synthetic nanodiamond does not have any functional group attached to its structure, so for the various applications, further treatment will be required to attach functional groups to the surface of the nanodiamonds. One of the applications of the surface-functionalized nanodiamond is in the purification of intact protein from the urine sample. [15], [16]

1.2.3 Carbon nanotubes (CNT) and carbon nanofiber (CNF): Carbon nanotube is the king of inventions in the last decade. Due to its amazing properties, CNT has excellent applications in many research fields, including nanotechnology, electronics, optics, medicines, architecture, automobile, and manufacturing industries. Since the size to tensile strength is very high for the CNT, which makes them best in the market to use where material needs to be reliable, but weight needs to be light. Like sports rackets, bikes, combat jackets, concrete, etc. In the field of electromagnetism, CNT can be used very well in areas like conductive films, optical ignition, electric bulb filament, superconductive properties, and electromagnetic antenna applications. [17-19]

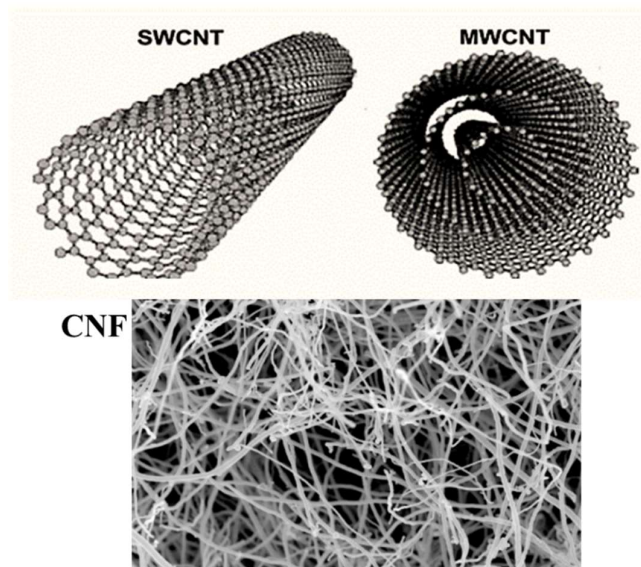


Figure 3: Carbon SWCNT, MWCNT and CNF

There are many chemical applications of the CNT, which can be briefed as water filters, air pollution filters, hydrogen storage applications, containers for biotech, etc. in the field of mechanical applications like oscillators, membranes, actuators, IR detectors, and thermal radiation for satellites. All the above-discussed form of the CNT is due to its high mechanical, electrical, thermal, and optical properties.[20-22]

Carbon nanofibers (CNF) has been discovered in the late 19th century. They belong to a dimensional structure group of the carbon allotropes with sp^2 hybridization. CNF is considered a big brother of CNT with the same properties as excellent strength to weight ratio with good thermal and electrical properties. The length of the CNF varies from 50 – 200 nm. As compare to CNT inner space of the CNF is not empty, which makes them dense as compared to CNT. As CNT, there are many applications for CNF. CNF has excellent use in lithium-ion batteries supercapacitor. The addition of the CNF in thermoplastic leads to increase strength as well as the tensile strength of the thermoplastic. CNF can also be easily modified and integrated into the living tissues in the field of biomedical. But toxicity always remains the issue, and still work is going on. Due to high electrical conductivity, thermal conductivity and tensile strength is choice material to improve applications.[23-25]

1.2.4 Graphene Oxide (GO), Reduced Graphene Oxide (rGO), and Graphene (G): Graphene is a material of the 21st century, and intensive research is going on to study the different applications a property of this wonder material. Graphene is a 2D sheet of graphite separated by the chemical or mechanical route. In this material, carbon atoms are arranged in a chicken wore pattern. This material has many new properties like very high electrical and thermal conductivity, good mechanical strength and unmatched optical properties, etc. Nowadays, many research groups are working on this fascinating material to know more and more about this material. Graphene cannot be produced directly; instead, it can be manufactured by reducing the graphite sheets chemically to separate the graphene layers. Oxidation of the graphite sheet is one method that adds oxygen in between the sheets of the graphite; this oxygen act as a functional group and a group of graphite sheets with oxygen functional group is known as graphene oxide (GO). This added oxygen group in between the sheets can be

removed chemically, and the graphite sheets after the removal of the oxygen functional group are called reduced graphene oxide (rGO). Series of chemical reductions reduce the GO to rGO.[26-28]

There are many methods available to produce GO as well as rGO. Many methods are very cost-effective and simple, also. Properties of rGO are almost like graphene; the difference is that the rGO contains more defects as compared to pristine G sheets. Sometimes some functional group also gets attached to the oxygen, which changes the properties of the rGO, or it can also be considered as functionalized rGO. The production of the G sheet is a costly and time-consuming process, but the conversion of carbon to GO and rGO can be done on the industrial scale. rGO is still an attractive candidate over pure G because of the cost of production. rGO can be used for the same applications where pure G sheets can be used like composites, ink, conductive nanofluids, and electronics. The process used to produce the rGO and GO extremely important as it will have a huge impact on the quality of the final rGO. The process defines how much closer to the graphene sheets we reached in terms of properties.[26], [29-31]

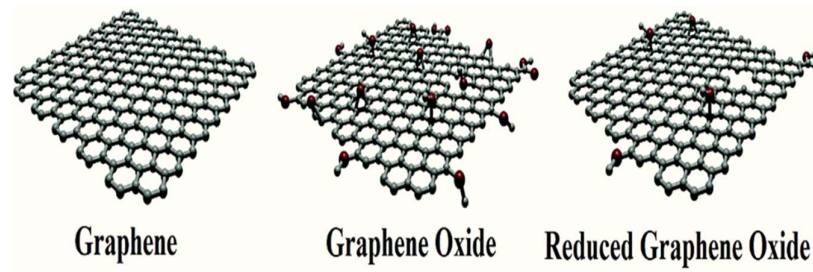


Figure 4: Graphene Sheet, Graphene Oxide sheet and Reduced Graphene Oxide Sheet

Many processes exist to produce the rGO. Some method uses a chemical approach, some uses thermal, and some use a mechanical approach to convert carbon to rGO. Some of the ways produce very high-quality rGO, which is very close to the G sheets in properties. Some functional rGO can be created for some typical applications like antennas etc. G sheets are known for the fantastic features like high electron mobility at room temperature that is $15,000 \text{ cm}^2\text{V}^{-1}\text{s}^{-1}$, which is quite high as compared to other

materials available. It has been suggested that the electron transport properties of G sheets are based on Dirac's equation, which is based on the relativity. The electron transport properties also depend on the temperature; it was proved that electron mobility $28000 \text{ cm}^2\text{V}^{-1}\text{s}$ is achievable with G sheets. In the study, it was also found that on SiO_2 substrate electron mobility became independent of the temperature range of 10 K to 100 K. because extremely high electron mobility properties graphene can be used as high-speed transistors where extremely high switching is needed. G sheets also possess high stiffness and good thermal conductivity. It is also the thinnest 2-Dimensional material that exists on earth.[32-34]

1.3 Fluids and Suspensions:

We know the matter exists in three different states called solid, liquid, and gas. Solids have a definite shape and a particular volume; on the other hand, liquids have fixed volume, but the form is not fixed. It takes the shape of the container in which it is placed. In the case of gasses, neither we have a definite form, nor we have a particular volume. Atoms in the solids are separated by a certain distance and attached with a spring-like bond. These atoms vibrate, which leads to the lattice vibration of the solids. These bonds can be stretched and compressed based on the external force applied. Due to the existence of these bonds' solids can sustain externally applied stress. There is always a fixed distance between the atoms in solids. If the compression is used, atoms will be forced to come closer to each other, but when the decompressive force is applied, atoms will be pulled away from each other. The permanent deformation of the solids occurs after the application of a high tensile or compression force. On the other hand, atoms in the liquid do not get compressed, but they begin to flow on the application of external stress. If we close the liquid in the container and apply some external pressure, then the atoms of the liquid also come closer to each other under the application of stress. So, some fluids can even tolerate compression up to particular strength. We know atoms in the gases separated by more considerable distances as compared to solids and liquids. Because of the more significant range of atoms, the forces between the atoms are minimal as compare to solids and liquids. Most of the gasses can be compressed easily, but liquids cannot compress easily. Both gasses and

liquid can be combined in a single category, which is called fluids.

When we add the solid powder (a disperse phase) particles in the liquid phase (continuous phase) without talking about particle size, then this mixture is called dispersion. If the size of the particles added is ranged up to 1 micron, then the suspension is known as a colloidal or colloidal suspension. If the size of the particles is greater than the 1 micron, than the suspension is known as coarse dispersion or coarse suspension. If the size of the particles added to the continuous phase is from 100 – 500 nm, then the suspension is known as nanosuspension, and if the particle size is less than 100 nm, than the term nanosuspension is replaced by nanofluids. The size of the particles affects the properties of the suspension to a large extent.[35-37]

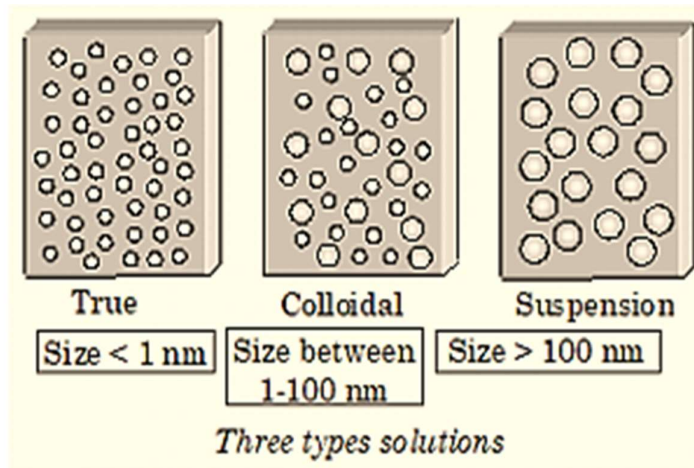


Figure 5: Nanofluid, colloidal suspension and nanosuspension

1.3.1 Nanofluids: Nanofluids are the class of colloidal suspensions containing particles or liquid droplets in the size range of 1 – 100 nm. There are a different kind of the nanoparticles can be used in the nanofluids like oxides, CWNT, MWNTs, carbides, ceramics, metals, etc. All these particles are used to enhance the properties of the base fluid. It is well known that nanoparticles have a high surface as compared to their counterpart, which helps to improve the thermal, chemical, electrical, and mechanical properties. There are many organic and inorganic liquids are available, which can be

used as the base fluids. Some of the commonly used base fluids are water, ethylene glycol, natural oils, etc. Nanofluids have many applications like coolant, heat exchanger in electronic cooling systems.[38-40]

1.3.2 Nanosuspension: On the other hand, Nanosuspensions are also the liquid suspension of nanoparticles, having a dimension between 100 nm to 500 nm. The number of solid particles can be used for the manufacturing of nanosuspension like oxides, carbides, CNTs, etc. Nanosuspension is used rigorously in the field of medicine, with many benefits over the normal colloidal and coarse dispersion. It enhances the desolation rate and absorption rate of the drug. It also helps in surface modification of the drug for the site-specific drug delivery. It increases the thermal and electrical conductivity of the nanosuspension. The medical field gives enormous opportunities in the area of nanosuspension drug delivery.[41-43]

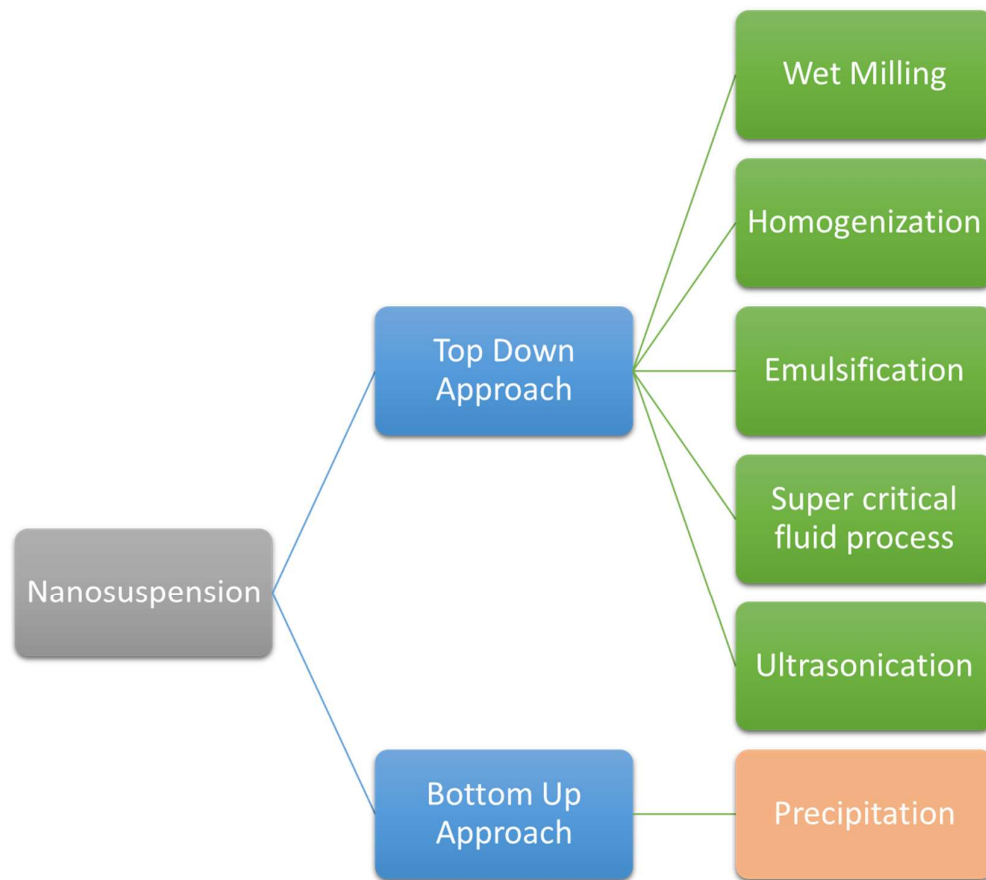
The fundamental difference in the nanofluid and nanosuspension is the size of the particles with which they are dealing; otherwise, both are advanced versions of the suspension. The primary research associated in this field is related to medicine and drug manufacturing and the use of nanosuspension in the field of heat transfer fluid. There are some new research areas like conductive ink, stable nanosuspension without modifiers, and surfactants that also attracts many researchers. In Lithium-Ion battery manufacturing, nanofluid can play a vital role.

1.4 Techniques to prepare nanosuspension:

Generally, the nanoparticles are produced in the liquid media via the disintegration process; the product formed in this manner is usually known as nanosuspension. There are different types of techniques available to produce nanoparticles. These techniques are broadly divided into two approaches. A first approach is a top-down approach in which particle in the micron is reduced to nano by the disintegration process.

Processes like wet milling, homogenization, emulsification, supercritical fluid process, and ultrasonication are top-down approaches. The second approach is the Bottom-up approach in which we build up nanoparticles by precipitation of the dissolved molecules in the liquid. So, the size of the particles increases in the bottom-up approach

from molecules to nano. Precipitation is the process used in the bottom-up approach. The disadvantage of the milling technique is contamination and incomplete recovery of products from the milling media due to wear and tear of ceramic balls during milling. The precipitation approach can be used where the amount of nanosuspension is needed less in volume. Techniques like ultrasonication can be used effectively in the case of the industrial production of the nanosuspension with controlled results without surfactants and stabilizers. Another method, micro fluidization technology, also produces stable and well dispersible nanosuspensions.[44]



1.4.1 Top-Down Approach:

1.4.1.1 Milling Techniques: Milling is the process of grinding micro size particles to nano-size particles. During the milling process, metals or ceramic balls are used for the

operation of milling. These moving balls produce localized pressure on the powder to break them into a fine powder. The mill consists of three main parts chambers, shaft, and grinding balls. These grinding balls can either be of metals or of ceramic depending upon the type of the powder we are using for the reduction. The mixture of the water and powder is added to the chamber and closed tightly under the controlled temperature and pressure conditions. When the chamber starts rotating, the mixture inside, along with the balls, also starts to turn. With this rotation ball inside the chamber increases in height and falls back to the bottom of the chamber to crush the powder beneath. This impact of the balls on the wet powder at the bottom and unto the walls of the chamber helps to break the powder into a smooth paste. Generally, the mill media is made up of zirconia or ceramic with high abrasion resistance. The high energy impact of the balls in milling media helps to reduce the size of the powder into nano dimensions. The change in temperature, pressure, ball size, ball material, mill rotation speed, and amount of powder change the overall product we are going to get after milling. The advantage of this milling process is easy to use instruments and the ability to produce both dilute and concentrated nanosuspension. It yields highly disperse nanosized particles. The major disadvantage associated with this technique is the residue of milling media can contaminate the overall product.[45]

1.4.1.2 Homogenization: homogenization process based on the principle of cavitation. This technique is used in the poorly soluble water-based suspensions. In this method, micro size powder is passed through the nanosized high-pressure homogenizer, due to the presence of high pressure and nano-sized aperture a cavity produces, which creates pressure on the powdered particles. This external pressure generated on the particles reduces the size of the particles to nano dimensions. The primary concern with this method is to take a small portion of the powder sample at a time; otherwise, the problem of nozzle clogging can occur. To reduce the particles into nano dimensions take a lot of effort and many cycles. Disso tube is the technology that can be used to formulate very dilute or highly concentrated nanosuspension at the industry level. Disso cell works on the principle of the homogenization. The significant advantage associated with this technique is very little contamination. Powder soluble, either inorganic or inorganic liquids, can be used for the preparation of nanosuspensions. The major

drawback of this process is the raw material used in the process is processed microparticles and repeated the process to produce nanoparticles.[46]

1.4.1.3 Emulsification: this technique work on the principle of emulsification using a high-speed stirrer. This technical solution of the given powder is prepared and followed by the emulsification in another solution, which is non-soluble for the offered powder. Evaporation of the first solvent leads to the precipitation of the powder. The speed of the stirrer can control the growth of the particles and aggregation. The advantages of these techniques are high drug, solubilization, long shelf life, ease of manufacture. The disadvantages of this technique are the use of a high amount of surfactants and stabilizers. [47]

1.4.1.4 Super Critical fluid process: Critical temperature of the substance is the temperature at and above which vapours of the material cannot be liquified, no matter how much pressure is applied, and critical pressure is the pressure required to liquefy a gas at its critical temperature. A supercritical fluid is a particular type of fluid whose temperature and pressure are more significant than its critical temperature and pressure, where the liquid and gas phase cannot be districted. This process helps to create nanoparticles with the size range from 5 – 2000 nm. Poorly soluble powder with supercritical CO₂ at critical pressure is required for this process. The advantage of this process is the production of highly soluble powder. The disadvantage of this process is that only those powder can be used which are soluble in the supercritical fluid. The use of high pressure and high temperature also restrict this technology to be used in the industry.[48]

1.4.1.5 Ultrasonication: The process of the sonication involves the agitation of nanoparticles with the help of high-frequency sound energy. High-frequency sound waves produce high impact energy on the fluid particles. This energy helps to apply pressure on the particles, which further breaks it down. The application of the sound more than 20000 Hz is known as ultrasonic sound. Many types of ultrasonicator are available nowadays, like probe-type sonicator or bath type sonicator. The stability of the nanosuspension can also be increased with the addition of stabilizers and surfactants. The dispersion of the powder increases with the viscosity of the fluid.

Suppose the base fluid is of less viscosity, than it will be difficult to achieve proper dispersion. In case if the dispersion of the powder is good, then it helps to increase the viscosity of the fluid. No study has defined the minimum and maximum time of sonification to achieve proper dispersion with good stability. Some researchers have suggested the prolonged use of the ultrasonication technique helps to increase the dispersion. Many studies are available where the comparison between particle size and ultrasonication time is given as a variable to understand the stability of the prepared suspension. The advantage of this process is the ease of use, and the disadvantage is less control over the reduction of particle size. [49],[50]

1.4.2 Bottom-Up Approach:

1.4.2.1 Precipitation: Precipitation technique is applied to prepare microparticles of the powder which poorly soluble in the given fluid. Then in the presence of surfactants, the powder is firstly dissolved in the solvent, then it is added with miscible antisolvent. The rapid mixing of the solvent and antisolvent leads to the supersaturation of the powder, which creates very fine particles of the powder. This method of precipitation is purely dependent upon two phases. The first phase is the nuclei formation of the powder, and the second phase is the growth of this powder nuclei. To prepare a nanosuspension, there should be a high nucleation rate but a slow growth rate, which will help to generate more nucleus. These light nuclei will help developing nanoparticle in the solvent. Both nucleation and growth depend highly on the temperature and pressure conditions. Advantage of this process simplicity of the process and low-cost equipment involved. The disadvantage of this process is powder needs to be soluble in at least one of the liquids, and antisolvent needs to be miscible with solvent. The growth and crystallization process needs to be taken care of under controlled temperature and pressure.[51]

1.5 Choice of Base Fluid:

For the current study large number of the fluids are available for the preparation of nanosuspension of graphene oxide and reduced graphene oxide, but with the help of a literature survey, five pure solvents have been chosen to prepare the well-dispersed

suspension. Let us discuss the pure fluids.[52],[53]

1.5.1 Water: Water is the most abundant liquid present on earth. Water got some fantastic properties, which make it one of the most valuable liquid presents on earth. The chemical recipe of the water is H_2O . Each molecule of the water has two hydrogen molecules covalently connected with single oxygen. It is a universal solvent and able to dissolve more substances as compared to many other liquids.

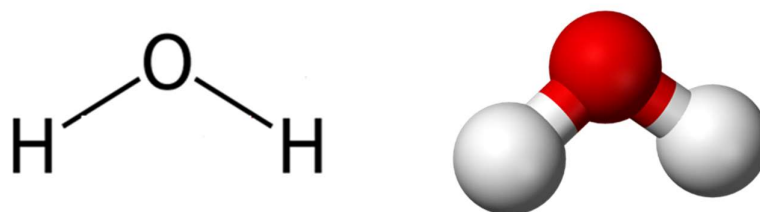


Figure 6: Water molecule

1.5.2 N, N Dimethylformamide (DMF): DMF is an organic compound which is commonly abbreviated as DMF. DMF is a colourless liquid that is immiscible with water. Generally, DMF is odourless, but sometime DMF with impurities has some foul smell. It is a polar solvent with a high simmering point. The first use of the DMF is a solvent with a low vaporization rate used in the manufacture of pesticide adhesive, synthetic leather, surface coating, etc. DMF mostly penetrate through all the plastics and make them swell. It is advantageous in suspending and separating carbon nanotubes.

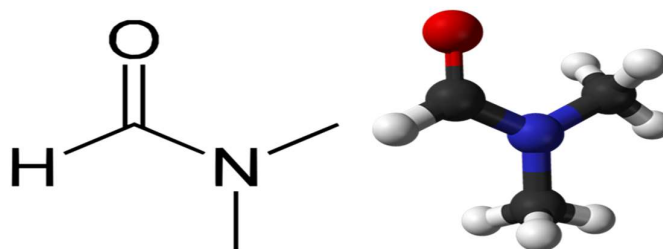


Figure 7: DMF molecule

1.5.3 Ethylene Glycol (EG): EG is an organic compound with chemical formula $C_2H_6O_2$. EG is an odourless, colourless, and sweet viscous liquid. Ethylene oxide reacts with water to produce ethylene glycol. It can also be produced from carbon monoxide. The primary use of the EG is antifreeze formulation and application in the production of polyesters. EG can be used as the fluid in the thermal heat pumps where the heat can either be taken into the system or taken out of the system. The mixture of the ethylene glycol and water further gives benefits like use as a coolant, antifreeze solution and helps to prevent corrosion. It can be used as a dehydrating agent and vaccines. EG is mildly toxic. It is very dangerous for children because it is sweet and can attract kids.

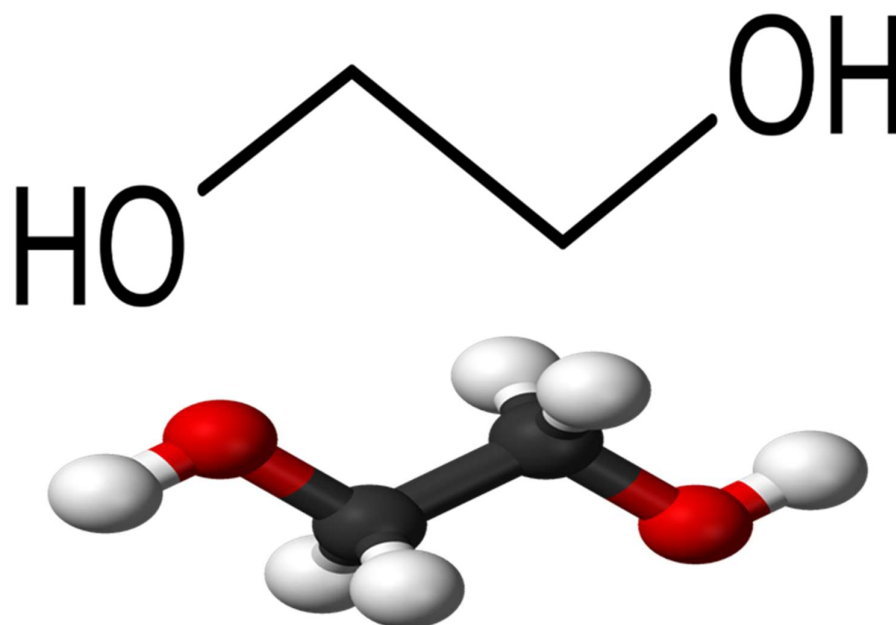


Figure 8: EG molecule

1.5.4 Tetrahydrofuran (THF): THF is an organic compound that is a cyclic ether. It is a colourless low viscosity liquid which is water-miscible. THF is a polar solvent, and that is why it is an excellent solvent. This polymer is primarily used to produce fibers like spandex. THF is an industrial solvent that is used to dissolve PVC and varnishes. Recently THF is also used in 3D printing when using PLA plastics. THF is a non-toxic liquid that can easily penetrate through the skin and cause dehydration. It is highly flammable.

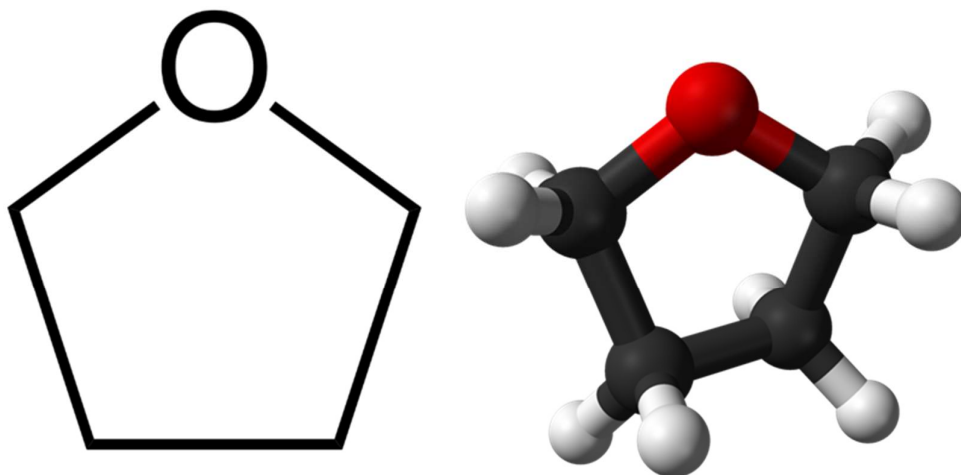


Figure 9: THF molecule

1.5.5 N-Methyl-2-pyrrolidone (NMP): NMP is an organic compound consist of 5-member cyclic amide. It is a colourless and odourless liquid. It is miscible with water and most of the available organic compounds.

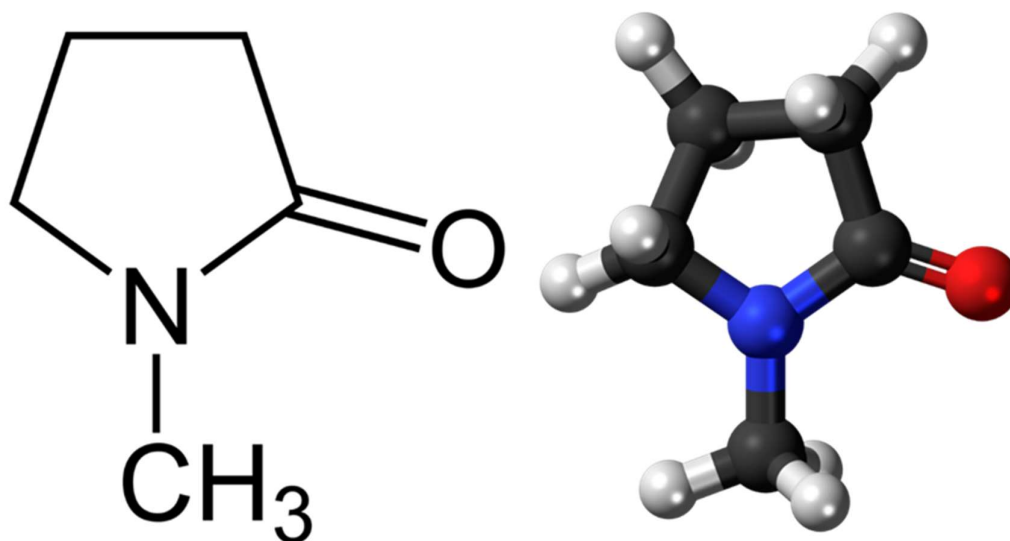


Figure 10: NMP molecule

It is a dipolar aprotic solvent which is used in the petrochemical and plastic industries

as a solvent. Approximately 25000 – 30000 tons of NMP are produced annually. It is widely used as a paint stripper and treatment of textile resins. It is used as the formation of oral as well as transdermal drugs. NMP is infuriating to the nose, face, eyes, and throat. It penetrates through the skin very quickly. After getting absorbed into the skin, it dissolves the natural oils, which cause dry, rough, and cracked skin.

Table 1.1 General properties of 5 basic fluids.					
Property	Water	DMF	EG	THF	NMP
Chemical Formula	H ₂ O	C ₃ H ₇ NO	C ₂ H ₆ O ₂	C ₄ H ₈ O	C ₅ H ₉ NO
Chemical Name	Water	N, N-Dimethylformamide	Ethane-1,2-diol	Oxolane	N-Methyl-2-Pyrrolidone
Molecular weight (g mol ⁻¹)	18	73.095	62.068	72.107	99.133
Density (kg L ⁻¹)	0.998	0.948	1.1132	0.8876	1.03
Boiling Point (K)	373	425	470	339	477
Viscosity (mPas)	1.002	0.920	1.60	0.46	1.89

1.6 Acoustical parameters:

An ultrasonic interferometer at a frequency of 2 MHz will be used to measure ultrasonic velocity. Density will be measured with the help of a specific gravity bottle, and viscosity will be measured using Oswald's viscometer. From these three experimental values, parameters like adiabatic compressibility, intermolecular free length, acoustic impedance, ultrasonic attenuation, and relaxation time have been calculated using standard formulae. [54]

1.6.1 Density measurement: The density of pure liquids, as well as its mixtures, can be measured using the relative measurement method. The density of the fluid can be

measured by employing a 25ml specific gravity flask at different concentrations. The measured density was measured with a formula,

$$\rho_2 = \frac{w_2}{w_1} \rho_1$$

Where, w_1 = weight of distilled water, w_2 = weight of the experimental liquid, ρ_1 = Density of water, ρ_2 = Density of experimental liquid

1.6.2 Viscosity measurement: The viscosity of the mixture has measured using an Ostwald's viscometer. Viscosity can be determined using the relation:

$$\eta_2 = \eta_1 \frac{t_2 \rho_2}{t_1 \rho_1}$$

Where, η_1 = viscosity of water, η_2 = viscosity of experimental liquid, t_1 = time of flow of water, t_2 = flow of experimental liquid, ρ_1 = Density of water, ρ_2 = density of experimental liquid.

1.6.3 Ultrasonic velocity: The principle of the ultrasonic device is based on the standing waves produced by the ultrasound between two reflecting plates. This instrument can measure the wavelength of the ultrasonic wave, which helps to determine the ultrasonic velocity of the samples. The formula for the wavelength calculation can be given as:

$$\lambda = 2d/n$$

Now from the understanding of wavelength (λ), the velocity (U) can be attained by the relation:

$$U = \lambda f = 2df$$

Where U=velocity of the ultrasonic wave, f= frequency of particle vibration, λ =wavelength of wave

1.6.4. Acoustics impedance: It is the resistance which is offered to the propagation of the ultrasonic wave in a material, and can be described as the product of density (ρ) and

acoustic velocity (U)

$$Z = \rho U$$

This impedance is crucial for acoustic transmission and reflection at the border of two materials having different acoustics impedances.

1.6.5 Adiabatic compressibility: It is the fractional reduction of volume per unit rise of pressure when no heat flows in or out. These alterations are related to the compressibility of the medium but thermodynamic relations:

$$\beta = \frac{1}{v} \frac{dv}{dp}$$

This can also be computed from the speed of sound as well as density of medium using equations of Newton's as

$$\beta = (U^2 \rho)^{-1}$$

Where, ρ = Density of medium, U = Ultrasonic velocity in the medium,

1.6.6. Relaxation time: It is the amount of the time taken by medium particles to modify their original mean positions inside the medium following displacement by ultrasonic waves. Its value is characterizing by the medium. Relaxation time for binary mixture can be calculated from the relation.

$$\tau = \frac{4\beta\eta}{3}$$

It can also be written as:

$$\tau = \frac{4\eta}{3\rho U^2}$$

Where τ =Relaxation time, β =Adiabatic compressibility, η =Viscosity of mixture

1.6.7. Intermolecular free length: The distances between the surfaces of neighbouring molecules that is given by the relation:

$$L_f = K_T (\beta)^{1/2}$$

Where, β = Adiabatic compressibility of the mixture, K_T = Temperature of dependent Jacobson's constant, $K_T = (93.875 + 0.375 K) 10^{-8}$ where T = temperature in Kelvin.

1.6.8. Ultrasonic attenuation: Rate of decrease of energy when an ultrasonic wave is transmitting in a medium labelled as attenuation and depends upon the properties of the medium. The sound attenuation increases with an increase in the frequency and usually related to the square of sound frequency. So ultrasonic attenuation can be expressed as:

$$\frac{\alpha}{f^2} = \frac{8\pi^2 \eta}{3\rho U^3}$$

Where, f = frequency of the wave

1.7 References.

- [1] S.K. Tiwari, V. Kumar, A. Huczko, R. Oraon, A. De Adhikari, and G.C. Nayak, Crit. Rev. Solid State Mater. Sci. **41**, 257 (2016).
- [2] A. Hirsch, Nat. Mater. **9**, 868 (2010).
- [3] C. Peng, S. Zhang, D. Jewell, and G.Z. Chen, Prog. Nat. Sci. **18**, 777 (2008).
- [4] R. Kiruba, M. Gopalakrishnan, T. Mahalingam, and A.K.S. Jeevaraj, **2**, 50 (2013).
- [5] J. Sandler, M.S.P. Shaffer, T. Prasse, W. Bauhofer, K. Schulte, and A.H. Windle, **40**, 5967 (1999).
- [6] G. Xiong, C. Meng, R.G. Reifenberger, P.P. Irazoqui, and T.S. Fisher, Electroanalysis **26**, 30 (2014).
- [7] A.K. Geim and K.S. Novoselov, Nat. Mater. **183** (2007).
- [8] A. Sáenz, L.I. López, A. Castañeda, and L. Farías, Fullerenes Chem. Nat. Sources Technol. Appl. **189** (2014).
- [9] R.E. Smalley, Sci. Am. **265**, 54 (1991).

- [10] A.P.A. Reasenber, L.M. Jones, and J.R. Finnerty, **265**, 1251 (1994).
- [11] P. Anilkumar, F. Lu, L. Cao, P. G. Luo, J.-H. Liu, S. Sahu, K. N. Tackett II, Y. Wang, and Y.-P. Sun, *Curr. Med. Chem.* **18**, 2045 (2012).
- [12] U. Sagman, *Perspect. Fuller. Nanotechnol.* 145 (2002).
- [13] F. Zu, F. Yan, Z. Bai, J. Xu, Y. Wang, Y. Huang, and X. Zhou, *Microchim. Acta* **184**, 1899 (2017).
- [14] J. Wang and J. Qiu, *J. Mater. Sci.* **51**, 4728 (2016).
- [15] S. Telles, S.K. Reddy, and H.R. Nagendra, *J. Chem. Inf. Model.* **53**, 1689 (2019).
- [16] Y. Xing and L. Dai, *Nanomedicine* **4**, 207 (2009).
- [17] M.S. Dresselhaus, G. Dresselhaus, and R. Saito, *Carbon N. Y.* **33**, 883 (1995).
- [18] M. Moniruzzaman and K.I. Winey, *Macromolecules* **39**, 5194 (2006).
- [19] A.C. Dillon, K.M. Jones, T.A. Bekkedahl, C.H. Kiang, D.S. Bethune, and M.J. Heben, *Nature* **386**, 377 (1997).
- [20] M. Ohfuchi, and Y. Miyamoto, *Carbon N. Y.* **114**, 418 (2017).
- [21] P.W. Barone, S. Baik, D.A. Heller, and M.S. Strano, *Nat. Mater.* **4**, 86 (2005).
- [22] Q. Zheng and Q. Jiang, *Phys. Rev. Lett.* **88**, 3 (2002).
- [23] K.P. De Jong and J.W. Geus, *Catal. Rev.* **42**, 481 (2000).
- [24] Y. Yu, L. Gu, C. Wang, A. Dhanabalan, P.A. Van Aken, and J. Maier, *Angew. Chemie - Int. Ed.* **48**, 6485 (2009).
- [25] W. Fang, S. Yang, X.-L. Wang, T.-Q. Yuan, and R.-C. Sun, *Green Chem.* **19**, 1794 (2017).
- [26] I. Roy, G. Sarkar, S. Mondal, D. Rana, A. Bhattacharyya, N.R. Saha, A.

- Adhikari, D. Khastgir, S. Chattopadhyay, and D. Chattopadhyay, *RSC Adv.* **6**, 10557 (2016).
- [27] S. Zhou, H. Zhang, Q. Zhao, X. Wang, J. Li, and F. Wang, *Carbon N. Y.* **52**, 440 (2013).
- [28] L. Feng and Z. Liu, *Nanomedicine* **6**, 317 (2011).
- [29] H. Zhang, X. Tian, C. Wang, H. Luo, J. Hu, Y. Shen, and A. Xie, *Appl. Surf. Sci.* **314**, 228 (2014).
- [30] H. Wang, H. Tian, S. Wang, W. Zheng, and Y. Liu, *Mater. Lett.* **78**, 170 (2012).
- [31] U. Male, J.K.R. Modigunta, and D.S. Huh, *Polym. (United Kingdom)* **110**, 242 (2017).
- [32] K.I. Bolotin, K.J. Sikes, Z. Jiang, M. Klima, G. Fudenberg, J. Hone, P. Kim, and H.L. Stormer, *1* (2008).
- [33] K.S. Novoselov, Z. Jiang, Y. Zhang, S. V. Morozov, H.L. Stormer, U. Zeitler, J.C. Maan, G.S. Boebinger, P. Kim, and A.K. Geim, *Science (80-.)*. **315**, 1379 (2007).
- [34] Y. Wu, Y.M. Lin, A.A. Bol, K.A. Jenkins, F. Xia, D.B. Farmer, Y. Zhu, and P. Avouris, *Nature* **472**, 74 (2011).
- [35] J. Hemalatha, T. Prabhakaran, and R. Pratibha Nalini, *Microfluid. Nanofluidics* **10**, 263 (2011).
- [36] M.L.S. Srinivasan, *J. Therm. Anal. Calorim.* (2017).
- [37] M. Leena and S. Srinivasan, *J. Mol. Liq.* **206**, 103 (2015).
- [38] S.K. Verma, D.K. Singh, D.K. Pandey, and R.R. Yadav, **36**, 535 (2013).
- [39] D. Wen and Y. Ding, *J. Thermophys. Heat Transf.* **18**, 481 (2004).
- [40] M.S. Liu, M.C.C. Lin, and C.C. Wang, *Nanoscale Res. Lett.* **6**, 1 (2011).

- [41] A. Jain, P. Kaur, and K.C. Juglan, *J. Phys. Conf. Ser.* **1531**, 0 (2020).
- [42] J.G. Thattil, K.K. Kumar, and B.D. Kumar, *J. Bio Innov.* **7**, 660 (2018).
- [43] H. Journals and R. Article (2016).
- [44] P. Zuo, X. Lu, Z. Sun, Y. Guo, and H. He, *Microchim. Acta* **183**, 519 (2016).
- [45] E. Merisko-Liversidge and G.G. Liversidge, *Adv. Drug Deliv. Rev.* **63**, 427 (2011).
- [46] Y. Zhou, Q. Fang, B. Niu, B. Wu, Y. Zhao, G. Quan, X. Pan, and C. Wu, *Colloids Surfaces B Biointerfaces* **172**, 372 (2018).
- [47] Y. Li, X. Zhao, Y. Zu, and Y. Zhang, *Int. J. Pharm.* **490**, 324 (2015).
- [48] R. Campardelli and E. Reverchon, *J. Food Eng.* **149**, 131 (2015).
- [49] D. Xia, P. Quan, H. Piao, H. Piao, S. Sun, Y. Yin, and F. Cui, *Eur. J. Pharm. Sci.* **40**, 325 (2010).
- [50] X. Mei and J. Ouyang, *Carbon N. Y.* **49**, 5389 (2011).
- [51] X. Zhang, Q. Xia, and N. Gu, *Drug Dev. Ind. Pharm.* **32**, 857 (2006).
- [52] S. Park, J. An, I. Jung, R.D. Piner, S.J. An, X. Li, A. Velamakanni, and R.S. Ruoff, *Nano Lett.* **9**, 1593 (2009).
- [53] J.I. Paredes, A. Marti, J.M.D. Tasco, and A. Marti, *Langmuir* **24**, 10560 (2008).
- [54] K. Kaur, K.C. Juglan, and H. Kumar, *AIP Conf. Proc.* **1860**, (2017).
- [55] P. Kaur, N. Chakraborty, S. Singh, K.C. Juglan, and H. Kumar, *J. Phys. Conf. Ser.* **1531**, (2020).
- [56] B. Kaur and K.C. Juglan, *J. Polym. Eng.* **33**, 851 (2013).

CHAPTER 2: REVIEW OF LITERATURE

Hummer and Offeman (1957): presented a study in which they claimed one method to exfoliate the graphene layers. They claimed to transfer graphite to graphite oxide with the help of chemical oxidation. The process involved the addition of potassium chlorate in the mixture of carbon under controlled temperature and pressure conditions. The significant achievement of the Hummer and Offeman is to accomplish the final graphite oxide without the addition of water in concentrated sulphuric acid, sodium nitrate, and potassium permanganate. The whole process got completed in less than 2 hours and under the temperature of 45 °C. As per the author, the well-oxygenated samples have a carbon to oxygen proportion lay in among 2 to 3.[1]

H. P. Boehm et. al. (1994): has reported the nomenclature for the graphite compounds. It included compounds that retain the layers of graphitic structures. In this nomenclature, those compounds are not included, which undergoes sp^3 hybridization and makes covalent bonds to carbon heteroatoms. The rules are described for the structure notations. The suffix “ene” was used for the polycyclic aromatic compounds. The newest addition in this list is a single layer group of carbon sheets following sp^2 hybridization. This compound is known as “Graphene”. [2]

Dongsheng Wen et. al. (2004): has reported the preparation of the carbon nanotube and water nanosuspension with sodium dodecylbenzene sulfonate as the stabilizer. Researchers have discussed the effect of temperature and particle loading on the thermal conductivity of prepared samples. The thermal conductivity of the prepared nanofluid surges with increasing the particle concentration this upsurge is non-linear even at deficient levels of attention. The thermal conductivity to surges with a rise in temperature, and this dependence is also nonlinear. It has been reported that at the temperature, less than 30 °C thermal conductivity shows the linear relationship, but after 30 °C this dependence is nonlinear. For the nanofluid prepared with SDBS, the temperature should not be more than 60 °C; it makes the nanofluid unstable. The enhanced thermal conductivity is due to the networking of the CNT in the nanofluid.[3]

Charles M. Hensen (2004) had reported the solubility parameters of the different

solvents. Researchers have studied many numbers of liquids for the solubility parameter studies. They use the technique of geometrical means of interaction between two pure liquids. The hundreds of HSP is given in the handbook of the Hansen Solubility Parameter. The solubility parameter is used in many applications to dissolve one liquid into another. The settings for mixed solvents are found by volume additivity of respective parameters. The distances between the materials (Ra) can be given by equation

$$Ra^2 = 4(\delta_{D1} - \delta_{D2})^2 + (\delta_{P1} - \delta_{P2})^2 + (\delta_{H1} - \delta_{H2})^2$$

Another useful parameter given in this study is, Red number

$$RED = \frac{Ra}{Ro}$$

Where Ro is called the radius of the Hansen solubility parameter, the excellent solvent will have $RED < 1$ and progressively weaker will have increasing values.[4]

A. K Geim and K. S. Novoselov (2007): has reported the astonishing properties of the graphene. Graphene is getting popular day by day. This two-dimensional material shows some exceptional features. Due to its excellent properties, several new potential applications have been discussed in this paper. Graphene can have numerous numbers of applications, some of which are like use in composites and conductive plastics. Another potential use of the graphene can be in capacitive batteries. The large surface area of the graphene can be used as the surface to store many charges for super capacitance. Graphene powder shows some excellent emitting properties which can be used in the upcoming sensors. Graphene can be used to make gas sensors, which will be better than the sensors made up of carbon nanotubes.

Narasimha H Ayachit et. al. (2007): has reported the ultrasonic parameters for some nematic liquid, namely 4, 4' – azoxy anisole and 4,4'-dibutoxy azoxy benzene in diluted solutions. It has been reported that structural changes arising because of transition can be explained better by the ultrasonic studies. The study informs about the phase transition, pre-transitional effect. The values of velocity, Rao's number,

compressibility, is instrumental in understanding the structural behaviour. If the quantity of the sample is less than molecular characterization, information can be used to find the intermolecular interaction between particle and particle and between particle and fluid.[5]

J I Paredes et.al. (2008) had stated the distribution of GO in different organic solvents. The dispersion of the graphene oxide can be stabilize using surfactants or stabilizers, but in some of the application use of stabilizers and surfactants is not possible. Hence, they identified the several solvents in which prepared graphite oxide can be into individual GO sheets, forming dispersion with long term stability. Go was prepared by Hummer's method, and it was under vacuum and then peeled of the filter papers in the form of films. Go dispersion was tested in three following organics solvents acetone, methanol, ethanol, 1-proposal, ethylene glycol, dimethyl sulfoxide (DMSO) N, N Dimethylformamide (DMF), N-methyl-2-pyrrolidone (NMP), pyridine, tetrahydrofuran (THF), dichloromethane, O-xylene, and n-hexane. Insolvent water content was leu than 0.1%. Because water is a universal solvent for the preparation of graphite oxide dispersion in water. The distribution of the solution was characterized by UV-vis absorption spectroscopy and AFM. The results of UV-Vis show good dispersion in the case of water, ethylene glycol, DMF, NMP, and THF. Distribution of the water is used mostly to disperse GO for the chemical reactions; with this study, water can be replaced by another organic solvent for better colloidal dispersion.

K I Bolotin et. al. (2008): has reported the low-temperature graphene shows the near ballistic transport properties over micron dimensions, and the declared value for the mobility is $170\ 000\ \text{cm}^2/\text{V}\cdot\text{s}$. It was proved the higher temperatures, the resistivity of the pure graphene increases with a rise in temperature. The deduced upper bound of the deformation potential in high density is comparable to the values from graphite, but this deformation varies very much for the electrons and holes concentrations, large carrier density, $n > 0.5 \times 10^{11}\ \text{cm}^{-2}$,. At temperature 240 K, the mobility is $120000\ \text{cm}^2/\text{V}\cdot\text{s}$, which is higher than in any known semiconductor.

Changgu Lee et. al. (2008): has reported the elastic properties and intrinsic breaking strength of the monolayer graphene membrane prepared. The declared value of the

elastic strain and elastic stiffness is 340 Nm^{-1} and 690 Nm^{-1} . The breaking strength is reported as 42 Nm^{-1} for defect-free sheets. These values make the graphene the most robust material measured at an atomic level.[6]

P Simon et. al. (2008): has reported the review article for the advance supercapacitor material available. In this study, it is said that nanoporous carbon can be tuned at the angstrom level for the use of electrolyte. Carbon nanotubes can be used as flexible and printable devices. It has been reported that some nano nitride and nano metal oxide can posse's high energy density for the super capacitance. It has been reported that the nanoarchitecture of electrodes leads to further improvement in power delivery. Supercapacitors in the future will come closer to the batteries in maintaining the high energy density for a longer time; it has been observed that capacitive energy has low energy loss than those of batteries. The increasing the life and energy efficiency of the supercapacitor can serve as the energy solution for the future.[7]

Yuyan Shao et. al. (2009): had reported the specific electronic structure of graphene. Graphene shows remarkable properties which can be used as electrochemical sensors for bioanalysis. Graphene shows superior properties as compared to carbon nanotubes. A novel chemical method for the synthesis of the graphene has been proposed. Out of all available techniques to produce the graphene, the electrochemical route to deliver graphene is promising for industry-scale production. Doping of the surface of the graphene further enhances the properties. The use of graphene as a catalyst and biosensor can be done only after increasing the functional group on the surface. In has been discussed that graphene can be an excellent material for an electrode for the use of electroanalysis and electrocatalysis.[8]

Weiwei Cai et. al. (2009) has reported the use of thermal chemical vapor deposition for large are FLG and graphite films with layer varying from few to hundred on the surface of the metal. After the growth, films are transferred to other substrates, and the metal ion is dissolved in iron chloride etching. The optical and electrical properties of these prepared sheets were studied. Experimentally it was calculated that sheet resistance is meager that is $200 \Omega/\text{m}$ for FLG, and approximately 85 % of the light is transmitted through the prepared samples. It was found that the amount of transmittance

depends very less on the incident angle.[9]

Sungjin Park et. al. (2009) had reported the production of a homogenous colloidal suspension of chemically modified graphene sheets. GO has prepared with the Hummers method. Since the graphene oxide is hydrophilic, it gets agglomerated as soon as it is dispersed in water. It was found the problem of the agglomeration occurs if the liquid does not have the right amount of the cohesive energy. In this research, GO is dispersed in DMF with different particle loading. To avoid agglomeration of the dispersed powder, ultrasonication is being used. Similarly, many dispersions of GO sheets in other organic solvents than water is prepared; other solutions used are ethanol, dimethyl sulfoxide, acetonitrile, acetone, tetrahydrofuran, diethyl ether, toluene, and 1,2 – dichlorobenzene with the same procedure. It was also reported that GO was not appropriately dissolved in the solvents where Hansen Solubility Parameter is less than ten or greater than 30. The optimum range of the excellent dispersion as per the Hansen solubility parameter is from 10 to 30. This study will be perfect for a variety of applications and a wide range of colloidal suspension for fundamental research.[10]

R S Vajjha et. al. (2009): has reported the density values for the 60:40 mixture of EG/W, which is very close to the literature values. The calculation of the density values for Al_2O_3 and Sb_2O_5 : SnO_2 nanofluids shows the agreement with Pak and Cho equations. The density of the nanofluid increases with the increase in the particle loading; this increase is because of the addition of high-density particles in the fluid. There is a maximum of 8 % deviation from the Pak and Cho equation for ZnO nanofluid. With the increase in the particle loading, the variance increases from 8%. One equation with a correction factor was derived from this study.[11]

Yanwu Zhu et.al (2010) reported the properties of graphene and graphene oxide like morphology and structure, electronic properties, mechanical properties, optical properties, Raman Spectroscopy of graphene, and thermal properties of graphene. In the application, part graphene can be used as a field-effect transistor, many types of sensors, transparent conductive films, clean energy devices, graphene polymers nanocomposites. Further, the different techniques of synthesis of graphene and graphene oxide were included in the same umbrella.[12]

Kai Yang et.al (2010) reported the use of nanographene sheets in polyethylene glycol with a particle size of 27nm. The researcher said the effect of coating and size affect the behaviour of the suspension. As per the study, the suspension can be used to treat tumors. Graphene particles are excellent conductors of heat, and this property can be used to treat cancer with the heat at specific areas. The researcher also reported the combination of the chemotherapy drug with the prepared suspension to fight cancer in the near future.[13]

J. Hemlatha et. al. (2010): has reported the preparation of the nanosized Al_2O_3 in ethylene glycol of various concentrations. The acoustical parameters of these fluids have been calculated at a different range of temperatures. The comparison of micro and nanofluid has been provided in this paper for the reference. They reported the particle liquid communication in microfluid decline with a rise in the particle concentration, but for the nanofluid, the particle fluid interaction surges up to a critical concentration than start decreasing. Since the inner particle distance is longer at low concentration, but higher concentration interparticle length decreases because of the number of particles in the system increases, which helps in increasing the particle-particle interaction. SEM micrographs also show the agglomeration of the particles at elevated concentrations. The nanofluid shows the different behavior as compare to the nanofluids because in nanofluid particle possesses a higher surface area as compared to its counterpart. Such studies help to understand the reasons behind the anomalous behavior of nanofluids as compare to normal fluids.[14]

G. Paul et. al (2010): has reported the review on the thermal conductivity of the available nanofluid. It has been reported that the transient hot-wire method one of the most natural ways which can be used for the calculation of thermal conductivity. This method helps to produce accurate and repeatable results. Here nanofluid prepared based on the water, ethylene glycol with ZrO_2 , and TiO_2 with a two-step physical preparation method. It has been reported that the thermal conductivity of the prepared nanofluid is more than that of the base fluid. Thermal conductivity also increases with an increase in particle loading. The results demonstrate a remarkable rise in thermal conductivity with the surge in volume percentage. These nanofluids can be used for engineering

applications.[15]

F. Torrasi et. al. (2011) have reported the formulation of ink with graphene for inkjet printing. The flakes prepared with the standard, modified hummers method. After the production of the wafers, sonification of the dispersion of flakes and GO was done for 9 hours. This technique of exfoliation is called liquid-phase exfoliation. The resulting ink was characterized by Optical absorption spectroscopy, TEM, XRD, and RAMAN spectroscopy. The graphene can also be dispersed in the water using bare salt as a surfactant. Prepared ink was used to print a thin-film transistor. The printed transistor has the electron mobility up to $95 \text{ cm}^2\text{V}^{-1}\text{s}^{-1}$ and an ON/OFF ratio 4×10^5 . [16]

Soujit Sen Gupta et. al. (2011): has reported the preparation of nanofluid containing graphene nanosheets. The graphene was prepared with a three-step reduction method (a) pre-reduction, (b) sulfonation, and (c) post-reduction. Characterization of the prepared graphene was done with TEM and DLS. Nanofluid was characterized by UV-Vis and DLS plot. The thermal conductivity of the prepared nanofluid was experimentally calculated using the transient hot-wire method. It has been observed that the thermal conductivity of the nanofluid is quite high, even at low particle concentrations. The thermal conductivity increases with the rise in the temperature as well as particle loading. This is strange as in the case of CNT and GO nanofluid, there was no temperature dependence found. The possible mechanism of this behavior could be the Brownian motion and percolation hybrid. Brownian motion surges with the rise in temperature, and agglomeration explain the increase in thermal conductivity. [17]

Kumar Sastry et. Al. (2012) had done the studies on the molecular interaction of the tertiary mixture of ethyl hydroxyl benzoate by ultrasonic measurement. The ultrasonic velocity was calculated using a single crystal adjustable path interferometer working at 2 MHz at 303 K. densities and viscosity were computed using a specific gravity bottle and Oswald viscometer, respectively. The parameter like acoustic impedance, adiabatic compressibility, intermolecular free length, relaxation time, molar volume, internal pressure, and free volume is considered using standard relations. The measured value of sound velocity and density were decreasing while viscosity finds the increasing trend for reducing the concentration of X_2 . Due to the presence of solute-solvent interaction

through molecular association, ultrasonic velocity varies in the mixture. The increase in shear velocity with an increase in the concentration confirms the existence of solute-solvent communication. Both adiabatic compressibility, intermolecular free length, and relaxation time had shown an increasing trend. Molar volume and free volume had shown a decreasing trend, which was suggesting a specific interaction between the component of the mixture and particular communication between the components of the mix. The decreasing trend of the free volume was due to the close association between solute and solvent molecules. The decreasing trend of the relaxation time confirms the formation of hydrogen bonding between hydroxyl group (--OH) of 2PN and CH group of hydroxyl benzoate restrict the free internal association of the molecules. The decreasing trend of Gibb's free energy and Helmholtz free energy indicates the presence of collaboration between the molecules of the mixtures. The dipole-dipole interaction through hydrogen bonding between ethyl hydroxyl benzoate and alkanol enhance the decrease incompressibility and free length. The increased value of free volume and a decrease in internal pressure confirms the increasing magnitude of interaction.[18]

Veronica Strong et. al. (2012) had reported the production of graphene-based material with a step green method. This produced material is low-cost, simplistic, and multipurpose to create the patterning of graphene films in stable states. The infrared laser with low power was used in the experiment for the reduction of graphene oxide. The use of laser not only gives better reduction it also helps to produce an unusual pattern of printable devices. The intensity of the laser also helps in controlling the various properties of produced films. A flexible all-organic gas sensor was fabricated and tested. The produced LSG also shows exceptional electrochemical activities that surpass the features of carbon-based electrodes. This technique can further be used to prepare batteries, sensors, and electrocatalyst.[19]

Songfeng Pei et. al. (2012): had reviewed the different methods to oxidized carbon to GO and rGO. They discuss an interactive route to increase mass-scale production in industries. As per discussion, the full reduction of the GO to G is still tricky. At the same time, the partial reduction of the GO can be made with the number of methods

available. The structure and chemistry of the GO and rGO are mentioned in the paper, which helps to increase the scientific understanding of the final product. Different functional groups like hydroxyl group and epoxy group removal have been discussed in the chemical method. It has also been clarified that the functional groups which get attached to the defect sites are challenging to remove. A low defect rGO was prepared with the combination of chemical reduction and thermal annealing by removing most of the functional groups. Future research needs to be around the reduction mechanism and controlled oxidation of the GO. It can help to facilitate the application of graphene as semiconductors used in the transistors.[20]

M Nabeel Rashin et. al. (2012): has reported the preparation of stable nanofluid of CuO in coconut oil without any surfactants. Characterization of the prepared nanofluid was done with the help of XRD and SEM. The acoustical parameters of the prepared nanofluid have been calculated experimentally. It has been observed that molecular interactions are taking place between particles and oil. Particles interact well with base oil at a lower concentration, but as the level increases more than 1.5 wt.%, the particle-particle interaction dominates as compare to particle-fluid communication. At higher temperatures, the Brownian motion of the base oil increases, which decreases the effect of particle and particle interaction, which helps nanofluid to have good particle fluid interaction at a higher level of particle loading also.[21]

X Han et. al (2013) had studied the printable surfactant-free graphene ink directly from graphite. As per the author, the manufacturing of graphene had been reported by many researchers, but scalable graphene with a non-toxic solvent was needed. Here it has been reported that surfactant-free graphene ink with a solvent exchange method to switch from NMP to Water/Ethanol cross solvent. For the printed graphene film, both sheet resistance and light transmission has been calculated. The purpose of coating to glass and plastic has been demonstrated in the study. The prepared ink is without any surfactants and can be used for future applications like flexible electronics, biological sensors, and supercapacitors.[22]

Ji Chen et. al. (2013) had reported the improved Hummers method without the use of sodium nitrate to convert carbon powder to graphene oxide. This method helps to

eliminate the toxic gases from the experiment and helps to remove the waste liquid easily. Removal of the gasses and waste liquid will ultimately decrease the production cost of the graphene oxide. The properties of the produced GO are like properties of the GO produced with the conventional method. Also, the overall yield is not affected. This method helps to generate graphene at the industry level without harming our environment.[23]

Mishra Sujata and Paikaraj Rita (2013): has reported the acoustical and thermodynamical parameter study of two polar liquids Dehpa and N-Butyl bromide, at different temperatures. The variation of calculated parameters with particle loading shows the dominance of dipole-dipole interaction with weak dispersive forces present in the system. The large surface area of the two liquids shows the supremacy of dispersive forces. The strength of the dipole-dipole is maximum at equimolar concentration, and it decreases with the increase in the particle loading. The excess values become more and more cynical with the rise of temperature; this shows the increase in the intermolecular interaction. [24]

Dash Ashok Kumar and Paikaray Rita (2013) has reported the intermolecular interaction studies of dimethylacetamide in diethyl ether and acetone. DMAC is a dipolar solvent with excellent thermal and chemical stability. The thermoacoustic parameter like adiabatic compressibility, acoustic impedance, molar volume, etc. was calculated for the ternary mixture. It has been reported that there is intermolecular interaction exists between components of the ternary mixtures. The negative values suggest the strong interaction between the molecules of the ternary mixture. The negative value also indicates the existence of the dispersive forces. The molecular interaction also gets disturbed with the increase in the frequency of a fixed amount of particle loading.[25]

Balwinder Saini et, al. (2013) had studied the molecular interaction in β - Alanine-water-methanol solutions. In a study Balwinder et. Al reported the solute-solute and solute-solvent communication for β -alanine-water- methanol solution. β -alanine was used with a purity of 99.9%. Triply distilled degassed water was used for the preparation of the solution. All solutions were made on a mass basis using an analytical

mettle balance having an accuracy of ± 0.1 mg. The density of solutions was measured using a capillary pyrometer. The viscosity of the solutions was measured using a suspended level viscometer. The ultrasonic velocity of the solutions was measured with the help of multi-frequency ultrasonic interferometers at 4 MHz. Density increases with an increase in concentrations of β -alanine in aqueous solutions along with different levels of aqueous methanol. An increase in density with an increase in concentrations may attribute to the rise in hydrophilic interactions. The study reveals that the ultrasonic velocity for the solutions increases while compressibility decreases. The upsurge in the speed might be due to the cohesion carried by ionic hydration. The apparent molar volume was calculated using the standard equation. The values of apparent molar volume were fitted into Marconi's equation by the least square method. The amount of apparent molar volume shows an increasing behavior and become more positive as the concentration of the solute increase. The limiting values of the apparent molar volume indicate robust solute-solvent interaction. The negative values of apparent molar compressibility in different concentrations of aqueous methanol solutions may be attributed to the lack of structural compressibility of the solvent molecule. The positive values of (slope) for β -alanine in various concentrations of methanol in the water suggest that solute-solvent interactions are relatively more reliable. [26]

Jilei Liu et. al. (2013): has reported the green and cost-effective approach to produce high-quality graphene. The carbon was taken from the pencil cores. This carbon had been used to prepare high-quality graphene oxide with electrochemical reaction. An electrochemical cell with two electrodes was set up to start the exfoliation process. The static potential of 1 V was applied initially, and then it was ramped up to 7 V. The polarity of the electrodes was changed after 7 to 8 minutes. Prepared GO flakes were further used for characterization with TEM, SEM, AFM, RAMAN, and XRD. These results are auspicious for the scale-up production of the graphene oxide. This method is eco-friendly, green, and cost-effective. [27]

Maher F El-Kady et. al. (2014): has reported the progress of the supercapacitor for hybrid and electric vehicles. There is a very high mounting demand in developing the hybrid supercapacitor to overwhelm the energy density boundaries. The researcher has

been reported the high-performance supercapacitor based on graphene and MnO₂. The reported ultrahigh value of volumetric capacitance is 1100 F/cm³. It is near to the theoretical value of 1380 F/g. It has been described that the energy density varies between 22 to 43 Wh/l liable upon the configuration of the device. This reported value of the super capacitance is more significant than all commercially available supercapacitors. A simple system for the production of a supercapacitor array for high voltage usage. These arrays can be integrated with solar cells for efficient and green energy. [28]

M. Nabeel et. al. (2014): has reported the synthesis of various concentrations of Cobalt Ferrite nanofluid. The prepared nanofluid was stable and having no phase separation. In this study, the author published the ultrasonic and magnetic parameter study of the prepared nanofluid under various concentrations, temperature, and magnetic fields. It has been reported that interparticle interaction between nanoparticle is very minute in the absence of a magnetic field; as the magnetic field applied, the interparticle interaction increase and forms the chain-like structure. It is confirmed that the change in the temperature and ultrasonic parameters leads to the domination of cohesion forces over thermal expansion. The effect of the magnetic field changes the overall structure of the nanofluid with a variation. It agitates the liquid nanofluid and particle tries to accumulate with each other. It is also confirmed that an increase in the magnetic field at high value of temperature increases the magnetic effect within the samples of nanofluids even at low concentrations. [29]

G.R. Bedare et al (2014) had done the experimental studies on Binary mixture of Methyl methacrylate in 1, 4-Dioxane of 303K temperature. As per the study, liquid combinations contain polar and non-polar components are of immense reputation in productions such as petrochemical and pharmaceutical, and Methyl methacrylate polymers and copolymers are used in waterborne, solvent and coatings. Exteriors latex paint based on emulsions containing methyl methacrylate is used widely solvent, and emulsion polymers containing methyl methacrylate are also used in adhesive, leather coating, paper coating, inks, floor polishing, textile finishing. In far this study, ultrasonic interferometers working at 2MHz frequency are used. A double-walled

measuring cell attached with electronically digitally operated water has been used. Ostwald's viscometer was used for the viscosity measurement of pure liquids and liquid mixtures. Various acoustical parameters such as adiabatically compressibility intermolecular free length, Acoustical impedance, internal pressure, and relaxation time have been calculated with the help of the standard expressions. [30]

A.O. Deshmukh et. al. (2014) had studied the molecular interaction in 3-(Chloroaryl)-5-Aryl-1 substituted pyrazines in dioxane densities were measured with the help of capillary pycnometer ultrasonic velocities were calculated using a crystal interferometer at a frequency of 1MHz. All acoustic parameters were computed for all different percentages of 2, 4-dioxane intermolecular free length surges with a rise in the proportion of organic solvent in dioxane water mixture at different temperatures with a decrease in free length velocity increases. Intermolecular free distance upsurges linearly with the increased concentration of substituted pyrazines. Which, directs that here is essential interaction amid the ion and solvent molecular signifying an indorsing structure behavior of the added solute. The values of relatives association increase for all concentrations decrease with an increase in the percentage of solution at different temperatures. [31]

M. Abdelkader (2015): has reported the production of crumpled graphene with a low-cost manufacturing process. Graphene oxide was manufactured using the electrochemical process in which synthesized graphene oxide is taken as an anode and stainless-steel rod acts as a cathode. The eutectic composition of KCl and LiCl is used as the electrolyte. The argon gas was flushed into the sealed vessel. A constant voltage is provided during the whole experiment. The sample was washed thoroughly after removing from the reactor; further washing is done to remove any metal ion in the prepared sheets of graphene. The prepared product is characterized using XPS, FTIR, SEM, RAMAN, etc. with this method; the oxygen content was reduced from 30% to less than 5%. The electrical conductivity of the prepared graphene film is about 2300S/m². It reported that the surface area of the produced film is 565 m²/g, which is quite high. The specific capacitance measure comes out to be 255 F/g. [32]

Guoxing Zhu et. al. (2015): IN this method author demonstrated the simple method to

coat the CN form with rGO. This produced composite can be cut in different shapes and sizes. The amount of rGO in the final product can be tuned with the help of the amount of GO in the starting. This method can be used at the industry level. The product was tested for the application of a supercapacitor. The produced product is lightweight conductive and presents excellent electrochemical charge storage capabilities. The product was characterized with the help of SEM, TEM, AFM, XPS, FTIR, and CV profile. The specific capacitance of 162 F/g has been described in this paper, which is quite high. The Graphene microstructures influence the high value of the capacitance performance. [33]

Kirandeep Kaur et. al. (2015): has reported the intermolecular interaction study of chloroform with methanol. The results show the intermolecular interaction in the binary mixture. It can be seen in the results that a decrease in the ultrasonic velocity with a surge in particle loading can be related to the reduction of the intermolecular free length of the binary liquid. Both density and ultrasonic velocity increase with the increase in concentration. All other parameters like compressibility, free length, attenuation, and relaxation time decrease with a rise in the concentration. The reduction in the calculated setting suggests the weak interaction exists between molecules of the binary mixture. The linear increase with the concentration indicates the absence of any complex formation in the binary mixture. [34]

P J Thakre and J.B. Thakre (2015) has studies the intermolecular interaction of alcohol acetic acid, and TEA (tri-ethyl amine) chemicals used in the study were procured from merch Mumbai with purity 99.5%. Samples were formulated by mingling the components of liquids in volume proportion ultrasonic velocity in the liquid combinations were calculated using an ultrasonic interferometer working at 3 MHz frequency and three different temperatures 303K, 308K, and 313K. The density of the system was measured on electronic balance with a calibrated density bottle. Ostwald's viscometer was used for the viscosity calculations of unadulterated liquids and liquid mixtures. The experimentally measured values of ultrasonic velocity, density, and viscosity were used to evaluate various thermodynamic parameters like compressibility, intermolecular free length, and available volume. The variation of the

free period was no linear; it shows the concave nature. The value of free length decreases with concentration, becomes minimum, and again increases with a mole fraction of TEA. It concludes there is a significant interaction in liquid mixtures ultrasonic velocity decrease with the upsurge of intermolecular free length because of its inverse relationship. This indicates that molecules are closer to each other in the system. It was understood in the order that accessible volume changes with the composition of the system. As the concentration of the TEA increases, available volume decreases at concentration 0.14, it becomes minimum and again increases. The accessible volume also shows concave behavior. The observed value of free volume was owed to the close connotation between solute and solvent. Non-linear variation of all the parameters measured for the ternary liquid mixture indicates the existence of interaction amid the different molecules of the compound of the mix. For the observed molecular interaction, hydrogen bond development and accountable for the communication in the fluid mixture. [35]

S. Elengovan (2015) had studied the intermolecular interaction in a binary combination of N-Methyl Formate with 1 Butanol at 308 K. various thermal and acoustical parameters have been calculated for the binary mixture at a temperature of 308K. The excess values have been calculated experimentally. The results suggest that there is a specific kind of hydrogen bonding that exists between the carboxyl group of methyl formate and the hydroxyl group of butanol. [36]

Tumberphale et al. (2015) had studied the molecular interaction in the binary mixture of ethanol in ethylene diamine at 3 MHz frequency. Ethanol is used in fuel additives, medical wipes, and effective against most bacteria, fungi, and viruses. EDA is mainly used as an intermediate in the production of bleach activator fungicides, chelating agents, plastic lubricants, textile resin, polyamides, and fuel additives. In this study, Ethylene, Diamine, and Ethanol were of AR grade, with 99.9% purity procured from S.D Fine chemicals and Spectro Chem. Pvt Ltd Mumbai. The density and viscosity of pure liquid and liquid mixtures were determined using the pycnometer and Oswald's viscometer, respectively. The ultrasonic velocity of the mixture had been measured using an ultrasonic fixed frequency interferometer.

The experimental values of density, viscosity, and ultrasonic velocity were used to calculate various acoustical parameters such as adiabatic compressibility, free length, acoustical impedance, relative association, relaxation time, effective molecular weight, molar volume by standard relation. The increase in ultrasonic velocity with a mole fraction of EDA indicates that there is intermolecular interaction exists within mixtures. The maximum change in the slope means complex formation. The decrease in adiabatic compressibility with an increase in the concentration of EDA indicated the dipolar-induced dipolar interaction leading to a contraction in the volume, which further leads to a decrease in adiabatic compressibility as well as intermolecular free length. The increasing trend of acoustical impedance supports the possibility of the intermolecular interaction between solute and solvent molecules. The decreasing trend in relaxation time indicates the significance of molecular interaction. The negative values of the excess free length confirm the intermolecular interaction in the system. The negative values of adiabatic compressibility further verified the strong molecular interaction between unlike molecules. Positive values also approved this of excess velocity over the entire range. The discussion of the various parameter in this study concludes the strong interaction between ethanol and the EDA system. The non-linear behaviour of acoustic parameters suggests the formation of a complex in the mixture.[37]

Vijayta Gupta et. al. (2015) had reported the fluid-particle interaction of CuO Nanofluid using an ultrasonic technique. Studied had shown the preparatory method to obtain CuO Nanofluid. Nano Fluid of various Nanoparticle concentration in ethylene glycol was formulated by scattering a quantified amount of CuO Nanoparticle in Nanofluid. The velocity value of ultrasonic wave broadcast through nanofluid samples was calculated utilizing a multi-frequency ultrasonic interferometer. A specific gravity bottle measured the density of the fluid, and Oswald's viscometer measured viscosity. Various parameters like adiabatic compressibility, intermolecular free length, relaxation time, absorption coefficient, acoustical impedance, Gibb's free energy, free volume, Rao's number, and Wada constant were measured for prepared Nanofluid using experimentally calculated values. The peak of the ultrasonic velocity is at 0.6 wt.% of CuO. This peak and increase show the stable particle and fluid interaction present in the suspension. The increase in the Brownian motion decrease in the velocity

of the sample. The speed first declines with the rise in the particle loading, but with the increased interaction between the particle and fluid communication, this velocity starts to decrease. The same happens with the value of adiabatic compressibility and intermolecular free length; their values also decrease up to 0.6 wt.% but increases after this. The tremendous amount of acoustical impedance indicates the numerous interactions between particle and fluid exist in this system. [38]

I M Mahbubul et. al. (2015): in this study, the effect of the ultrasonication process on the colloidal suspension was studied. The dispersion of aluminium oxide 0.5 % was prepared with water has been sonicated for 1 to 5 hours with different amplitude. It was noted with the help of SEM micrographs that the prepared powder was agglomerated before suspended into the water. After the addition of the powder into water, it was pragmatic that 1 hour of ultrasonication is not enough for the proper dispersion of nanoparticles in water. It was observed that 5 hours of the dispersion gives outstanding results in terms of dispersion of powder in water. It was detected that the accumulation of the particles decreases by the upsurge in the sonication time; also, the value of zeta potential suggests that the dispersion becomes more stable after the 5 hours of ultrasonication. Maximum zeta potential worth 58.4 mV achieved after 3 hours of continuous sonication. With the help of ultrasonication, better particle dispersion, lower cluster dimensions, and the superior value of the zeta potential can be achieved with 50% sonicator power. The optimum duration of ultrasonication was found to be between 3 to 5 hours. [39]

Mohan Leela et. al. (2015): has reported the dispensation and blend of the stable TiO₂-EG nanofluid of different concentrations. Ultrasonic and thermal properties parameters have been calculated at room temperature. The ultrasonic investigation leads to the molecular level understanding of the solute and solvent interaction. It is confirmed in this study that molecular interaction is pronounced in the case of ethylene glycol. It is proved in this paper that there is an interaction between solute and solvent. It was shown that there is stronger molecular interaction exist between the component of the nanofluids. [40]

Haifeng Jaing et. al. (2015): has reported the processing and synthesis of CNT based

nanofluids. The stability of the CNT-water nanofluid was measured with various sedimentation time. The data has been collected experimentally with changing concentrations and changing temperatures. As per the study, the thermal conductivity increases with the increase in the concentration of CNT concentration, but this increase is not linear. The thermal conductivity does not change much with the change of the temperature of the nanofluid. A model for the calculation of the thermal conductivity has been proposed in the study, and this model gives the higher and lower limit to the thermal conductivity calculation. The chain-like agglomeration of carbon nanotubes is better to increase the thermal conduction, which enhances the thermal conductivity of the nanofluid to achieve higher cooling rates for coolants.[41]

Emad Sadeghinezhad et. al. (2016): has reported the review of the development in the graphene oxide nanofluids. It helps to understand the different parameters of the nanofluid, which affect the overall thermal performance of nanofluid. Long term stability of the graphene nanofluid is a critical issue in the aspect of the nanofluid application. It has been reported that how the thermal conductivity of the nanofluid is based on the concentration, size of particles, base fluid, temperature, the acidity of the solution, and additives. Usually, the thermal conductivity increases with the rise in the particle loading. An increase in the thermal conductivity does not depend upon the applied temperature. Agglomeration of the particles has an important role that influences the thermal conductivity of nanofluid. It has been reported that the addition of a small number of particles also changes the optical properties drastically. Graphene nanofluid requires further investigation. [42]

Shanxing Wang et. al. (2016): Has stated the deposition of the TiO₂ nanoparticles on the plane of reduced graphene oxide by the solvothermal reaction. Nanofluid of prepared TiO₂ and Graphene Oxide has been prepared with water with different concentrations. Ultrasonication has been used extensively to develop the nanofluid without the addition of the external surfactants. The zeta potential has been measured to be between -46.49 to -36.44 mV once the particle concentration is 0.024 and 0.051 wt.%, respectively. The result might be due to the presence of TiO₂ particles on the surface of the graphene oxide. It has been reported that the thermal conductivity of the

prepared nanofluid is better than the Graphene-based nanofluids. As per the author, this nanofluid can be a promising material because of its exceptional properties. [43]

Milad Rabbani Esfahani et. al. (2016): has reported the processing and synthesis of the graphene oxide films. After manufacturing with the modified hummers method further, characterization was done using XRD, SEM, and UV-Vis spectroscopy. The nanofluid of Graphene Oxide films is prepared with Distilled water as base fluid with different concentrations. The different sizes of the graphene oxide film have been added to the base fluid to make nanofluids. The zeta potential is amplified for -31 to -51 mV by increasing the concentration of the graphene oxide films from 0.011 % to 0.5 wt. %. The viscosity of the prepared sample also increases with an increase in particle loading. At the same time, the viscosity of all prepared samples decreases with an increase in the temperature. Thermal conductivity is also measured for prepared nanofluids. Increasing the concentration of the GO films increases the agglomeration and reduces the Brownian motion, results in a significant increase in thermal conductivity. [44]

Khushboo et.al (2016) had reported the acoustical and thermodynamic parameters of ZnO and nematic liquid mixture. The study was done on the Anton Paar densimeter. Ultrasonic velocity was calculated experimentally 3 MHz transducers. It has been observed that the sound speed decreases with a rise in the particle loading linearly. On the other hand, sound velocity increases with the increase in the temperature of the system. The density of the mixture shows the continuous decrease with the surge in the temperature, and on the other hand, the intermolecular distance increases with the increase in the mean free path; it has been observed by evaluating different parameters that there is a weak interaction between the fluid and the particles.[45]

Indranil Roy et. al. (2016): has reported the synthesis and processing of the graphene oxide from the carbon electrode of the waste cell batteries. Chemical reduction of the carbon is made to synthesize GO, and further reduction is made to obtain rGO. Characterization of the prepared GO and RGO has been completed with XRD, RAMAN, SEM, etc. zeta potential results show the negative values, which prove the excellent stability of the dispersion. TEM images help to identify rippled and crumbled structures of RGO. The amount of current passes through RGO sheets is higher than

GO. The conductivity is approximately 479 mS/cm, which is high as compare to GO 0.0086 mS/cm. the voltage-current characterization of GO is non-linear, but for rGO, this behaviour is linear. [46]

H Zhang et. al. (2017): had reported the synthesis of the rGO with the help of a modified Hummers method. Prepared CRGO is dispersed in water with different concentrations. Prepared nanofluid was tested for stability, thermal conductivity, and rheological studies. The -50.9-mV value of the zeta potential suggests the excellent dispersion stability of the nanofluid at PH value 12. Prepared nanofluid also shows excellent thermal conductivity for the sample with a concentration of 1 mg/ml at 60 °C. The rheological behaviour of the prepared nanofluids exhibits the Newtonian behaviour at higher values of stress. Characterization of the ready samples was done with the help of XRD, XPS, TEM, and zeta potential, etc. [47]

C Selvam et. al. (2017): has reported the preparation of nanofluid with graphene platelet in the base fluid of water and water and ethylene glycol. Prepared nanofluid is studied for thermal properties experimentally. For the testing of the stability of the nanofluid UV-Vis and zeta potential were performed, the results of these two tests confirm the stability of the prepared nanofluid. The thermal conductivity of the nanofluid increases significantly as we increase the particle loading. The highest thermal conductivity was found to be 18% at 0.45 wt.% of GnP/Water-EG were compared with the Maxwell-Garnett theory. It has been reported that there is interfacial thermal resistance that exists between water and ethylene glycol, and further research can proceed on the removal of this interfacial thermal resistance and enhancement of the thermal conductivity.[48]

Kirandeep Kaur et. al. (2017): has reported the thermoacoustic molecular interaction in the combination of glycerol and ethylene glycol. It has been stated that there is a linear increase or decrease of all the acoustical parameters. These parameters propose the existence of molecular interaction in the binary mixture. There is a constant value seen for Wada's number, Rao's number, and Vander Waal constant, which shows the non-attendance of any multifaceted development in the mixture. The reduction in the internal pressure, Gibb's energy, and enthalpy suggest the stronger molecule-molecule

interaction present in the liquid under study.[49]

Ashkan Afshari et. al. (2018): has reported the experimental verification of hybrid nanofluid manufacturing and rheological studies. Nanofluids consist of MWNT and aluminium oxide in a combination of water plus ethylene glycol. The volume fraction of the nanoparticles increases by weight percentage. The viscosity of the nanofluid declines with the surge in the temperature of the prepared nanofluid. Dynamic viscosity decreases in the rise of the element loading. Nanofluid also shows Newtonian behaviour at specific values of the mole fraction 0.0625, 0.125, 0.25, and 0.5 %. Nanofluid also shows non-Newtonian behaviour for the mole fraction of 0.75% and 1%. It was proved experimentally that viscosity increases in general with an increase in particle loading. A scientific equation was provided to foresee the viscosity of the nanofluid with reasonable accuracy. [50]

Kirandeep Kaur et. al. (2018): has reported the temperature-dependent study of PEG-400 and PEG-4000 in sorbitol solution. The partial molar properties have been determined experimentally at different temperature and 0.1 MPa pressure. There is a presence of solute and solvent collaboration in the ternary classification. The negative values at lesser temperatures suggest the healthy interaction between PEG and water molecules. This interaction further upsurges with a rise in the sorbitol concentration in the water. The positive worth of the partial molar volume and partial molar isentropic compression in the ternary system. [51]

A Nanda et. al. (2018): has reported the preparation of silver nanoparticles with a one-step chemical method. UV-Vis analysis of the prepared nanoparticles confirmed the size of nanoparticles is 15nm. These nanoparticles are used to make homogenous nanofluid of silver nanoparticles of various concentration with the help of a stirrer. The ultrasonic studies were done at room temperature to study the values like adiabatic compressibility, intermolecular free length, and acoustic impedance. This intermolecular investigation gives the inside of prepared nanofluid. They observed that flake liquid communication declines with the rise in the particle loading in the microfluid samples. Still, in the case of nanofluids, this particle fluid interaction surges with the surge in the particle loading up to critical concentration 2 ml above which

particle and particle interaction increases. Particle fluid interaction favours the increase in velocity.[52]

Nabparna Chakraborty et. al. (2018): has stated the calculation of acoustical parameters of ethylene glycol, diethylene glycol, triethylene glycol, in D Panthenol. With the help of molar and partial molar measurements, it has been proved that there is molecule-molecule interaction that is dominating. When the molar mass of the glycols increases, then the interaction between molecules also increases.[53]

Ashima Thakur et. al. (2019): has reported the collaboration of glycols in a methanol solution of methylparaben with the help of ultrasonic velocity. The apparent molar volume and apparent molar isentropic compressibility have been calculated with the help of an experimental study. It has been reported that there is a strong collaboration that exists amid solute and solvent in the prepared mixture. The partial molar volume increases with the increasing temperature shows the strong intermolecular interaction for all the working temperatures. Compressibility surges with the rise in the heat for entire ternary systems. [54]

Renna R Meena et. al. (2019): had reported the dispersion of CuO nanostrips in two types of transformer oil with different concentration. CuO was synthesized using the wet chemical method and disperse in the two-transformer oil one is made in 1997, and the other is made in 2017. Characterization of the prepared sample was done using XRD, EDAX, TEM, SEM, and UV-Vis. UV-Vis spectroscopy, along with zeta potential, shows the prepared colloidal suspension shows excellent stable colloidal properties. The ultrasonic velocity, density, and viscosity are measure at a different temperature level using nanofluid instruments. Similar behaviour of both of the oil has been observed and reported in the paper. [55]

Ebtisam Saeed et. al. (2019): has reported the synthesis of two different products from the graphene nanoplatelets to improve nanoparticle stability in the nanofluid. Characterization helps to prove the complete oxidation of the graphene oxide surface. This removal of the oxygen from the surface of the graphene oxide helps to stabilize the nanofluids. Thermal conductivity of the nanofluid increases to the base fluid ahead

to values of 50.80% for xGnP/PG, 7.20% for xGOnP/PG, and 13.30% for r-xGOnp/PG, which exposes that afterward oxidation of graphene oxide nanofluids show a decrease in the thermal conductivity. After the reduction of the graphene oxide, the thermal conductivity of the prepared nanofluids again increases. It has been reported; thermal conductivity is almost independent of the temperature. Prepared nanofluid shows the non-Newtonian behaviour; as the concentration increase, the apparent Newtonian plateau begins to visible in the rheological behaviour. It has been suggested that the functionalization of the graphene sheets can further enhance the overall properties of the nanofluids. [56]

Adeel Arashad et. al. (2019): In this study, the focus is on the stability of the nanofluid, which restricts the application of the nanofluid in heat transfer. This study also includes the fundamental synthesis, preparation, characterization, and stability of the nanofluids. The research consists of the influence of parameters like concentration, particle size, purity, temperature, surface properties, and shear rate on the thermal conductivity of the concocted samples. The graphene nano-fluids can be used on applications like electronic heat transfer, heat pipes, heat exchanger, and solar collectors. It has been seen that the thermal conductivity of the nanofluid increases with the increase in the concentration of particles and temperature. It has also been reported that the heat transfer rate in prepared nanofluid is higher than nanofluid prepared with metal oxides. [57]

Ashima Thakur et. al. (2019): has reported the sound velocity, density of ethylene glycol, and propylene glycol in the solution of methanol, propyl 4-hydroxybenzoate calculated with the help of experiment. The data has been derived experimentally. For all the mixtures, apparent molar volume increases with the increase in the temperature. It shows the intermolecular interaction for PG in methanol is stronger as compare to EG in methanol solution of propylparaben. The compressibility also increases with the increase in the temperature. The positive value of the apparent molar expansibility shows the solute-solvent interaction in the mixture. The less than zero values of the isentropic compressibility give control to the penetration effect over the solvent intrinsic compressibility. [58]

Prashant B Kharat et. al. (2019): has reported the ultrasonic parameter calculation for the nickel ferrite nanofluid with water. Nanoparticles for the nickel ferrite were synthesized used chemical route and characterized with the help of XRD, SEM, etc. Colloidal stability of the nanofluid is reported as 11 days without phase separation. Superparamagnetic characteristics were observed in the prepared nanoparticles. The purity of the sample was confirmed using composition spectra. The thermoacoustic investigation is an inexpensive choice in contrast to other techniques like DLS, PSA, and thermal conductivity, etc. It helps to illustrate the particle-particle and fluid-particle interaction of the prepared nanofluids.[59]

2.2 REFERENCES

- [1] W.S. Hummers and R.E. Offeman, J. Am. Chem. Soc. **80**, 1339 (1958).
- [2] H. Boehm, R. Setton, and E. Stumpp, Int. UNION Pure Appl. Chem. **66**, 1893 (1994).
- [3] D. Wen and Y. Ding, J. Thermophys. Heat Transf. **18**, 481 (2004).
- [4] C.M. Hansen, Prog. Org. Coatings **51**, 77 (2004).
- [5] N.H. Ayachit, S.T. Vasan, F.M. Sannaningannavar, and D.K. Deshpande, J. Mol. Liq. **133**, 134 (2007).
- [6] C. Lee, X. Wei, J.W. Kysar, and J. Hone, Science (80-.). **321**, 385 (2008).
- [7] P. Simon and Y. Gogotsi, Nat. Mater. **7**, 845 (2008).
- [8] Y. Shao, J. Wang, H. Wu, J. Liu, I.A. Aksay, and Y. Lin, Electroanalysis **22**, 1027 (2010).
- [9] W. Cai, Y. Zhu, X. Li, R.D. Piner, and R.S. Ruoff, Appl. Phys. Lett. **95**, 3 (2009).
- [10] S. Park, J. An, I. Jung, R.D. Piner, S.J. An, X. Li, A. Velamakanni, and R.S. Ruoff, Nano Lett. **9**, 1593 (2009).
- [11] R.S. Vajjha, D.K. Das, and B.M. Mahagaonkar, Pet. Sci. Technol. **27**, 612

(2009).

[12] Y. et. al. Zhu, *Adv. Mater.* **22**, 3906 (2010).

[13] K. Yang, S. Zhang, G. Zhang, X. Sun, S.T. Lee, and Z. Liu, *Nano Lett.* **10**, 3318 (2010).

[14] J. Hemalatha, T. Prabhakaran, and R. Pratibha Nalini, *Microfluid. Nanofluidics* **10**, 263 (2011).

[15] G. Paul, M. Chopkar, I. Manna, and P.K. Das, *Renew. Sustain. Energy Rev.* **14**, 1913 (2010).

[16] F. Torrisi, T. Hasan, W. Wu, Z. Sun, A. Lombardo, T. Kulmala, G.W. Hsieh, S.J. Jung, F. Bonaccorso, P.J. Paul, D.P. Chu, and A.C. Ferrari, *ACS Nano* **6**, 2992 (2012).

[17] S. Sen Gupta, V.M. Siva, S. Krishnan, T.S. Sreeprasad, P.K. Singh, S. Sen Gupta, V.M. Siva, S. Krishnan, and T.S. Sreeprasad, **084302**, (2011).

[18] A. June, **3**, 500 (n.d.).

[19] V. Strong, S. Dubin, M.F. El-Kady, A. Lech, Y. Wang, B.H. Weiller, and R.B. Kaner, *ACS Nano* **6**, 1395 (2012).

[20] S. Pei and H.M. Cheng, *Carbon N. Y.* **50**, 3210 (2012).

[21] M.N. Rashin and J. Hemalatha, *Int. J. Math. Comput. Phys. Electr. Comput. Eng.* **6**, 386 (2012).

[22] X. Han, Y. Chen, H. Zhu, C. Preston, J. Wan, Z. Fang, and L. Hu, *Nanotechnology* **24**, (2013).

[23] J. Chen, B. Yao, C. Li, and G. Shi, *Carbon N. Y.* **64**, 225 (2013).

[24] M. Sujata and P. Rita, *Res. J. Chem. Sci.* **3**, 24 (2013).

[25] A.K. Dash and R. Paikaray, *Res. J. Phys. Sci.* **4**, 130 (2013).

- [26] B. Saini, B. Rani, and R.K. Bamezai, *Russ. J. Phys. Chem. A* **88**, 47 (2014).
- [27] J. Liu, H. Yang, S.G. Zhen, C.K. Poh, A. Chaurasia, J. Luo, X. Wu, E.K.L. Yeow, N.G. Sahoo, J. Lin, and Z. Shen, *RSC Adv.* **3**, 11745 (2013).
- [28] M.F. El-Kady, M. Ihns, M. Li, J.Y. Hwang, M.F. Mousavi, L. Chaney, A.T. Lech, and R.B. Kaner, *Proc. Natl. Acad. Sci.* **112**, 4233 (2015).
- [29] M.N. Rashin and J. Hemalatha, *Ultrasonics* **54**, 834 (2014).
- [30] G.R. Bedare, **1**, 1 (2014).
- [31] A.O. Deshmukh and P.B. Raghuwanshi, *Int. J. ChemTech Res.* **8**, 375 (2015).
- [32] A.M. Abdelkader, *J. Mater. Chem. A* **3**, 8519 (2015).
- [33] G. Zhu, C. Xi, Y. Liu, J. Zhu, and X. Shen, *J. Mater. Chem. A* **3**, 7591 (2015).
- [34] K. Kaur, K.C. Juglan, and H. Kumar, *J. Chem. Eng. Data* **62**, 3769 (2017).
- [35] P.J. Thakare and J.B. Thakare, *IJSR* 205 (2015).
- [36] S. Elangovan, *Int. J. ChemTech Res.* **8**, 223 (2015).
- [37] U.B. Tumberphale, R.S. Kawale, N.P. Pawar, and V.G. Kalamse, *Int. J. Phys. Math. Sci.* **5**, 25 (2015).
- [38] V. Gupta, U. Magotra, A.K. Sharma, and M. Sharma, *J. Chem. Pharm. Res.* **7**, 313 (2015).
- [39] I.M. Mahbubul, R. Saidur, M.A. Amalina, E.B. Elcioglu, and T. Okutucu-Ozyurt, *Ultrason. Sonochem.* **26**, 361 (2015).
- [40] M. Leena, S. Srinivasan, and M. Prabhakaran, *Nanotechnol. Rev.* **4**, 449 (2015).
- [41] H. Jiang, Q. Zhang, and L. Shi, *J. Taiwan Inst. Chem. Eng.* **55**, 76 (2015).
- [42] E. Sadeghinezhad, M. Mehrali, R. Saidur, M. Mehrali, S. Tahan Latibari, A.R.

- Akhiani, and H.S.C. Metselaar, *Energy Convers. Manag.* **111**, 466 (2016).
- [43] S. Wang, Y. Li, H. Zhang, Y. Lin, Z. Li, W. Wang, Q. Wu, Y. Qian, H. Hong, and C. Zhi, *J. Mater. Sci.* (2016).
- [44] M.R. Esfahani, E.M. Languri, and M.R. Nunna, *Int. Commun. Heat Mass Transf.* (2016).
- [45] Khushboo, A. Devi, P. Malik, and H. Kumar, *J. Mol. Liq.* **214**, 145 (2016).
- [46] I. Roy, G. Sarkar, S. Mondal, D. Rana, A. Bhattacharyya, N.R. Saha, A. Adhikari, D. Khastgir, S. Chattopadhyay, and D. Chattopadhyay, *RSC Adv.* **6**, 10557 (2016).
- [47] H. Zhang, S. Wang, Y. Lin, M. Feng, and Q. Wu, (2017).
- [48] C. Selvam, D. Mohan Lal, and S. Harish, *J. Therm. Anal. Calorim.* **129**, 947 (2017).
- [49] K. Kaur, K.C. Juglan, and H. Kumar, *AIP Conf. Proc.* **1860**, (2017).
- [50] A. Afshari, M. Akbari, D. Toghraie, and M.E. Yazdi, *J. Therm. Anal. Calorim.* **132**, 1001 (2018).
- [51] K. Kaur, K.C. Juglan, and H. Kumar, *J. Mol. Liq.* **268**, 700 (2018).
- [52] A. Nanda, A. Tiadi, S.K. Mallik, R. Giri, and G. Nath, *IOP Conf. Ser. Mater. Sci. Eng.* **360**, (2018).
- [53] N. Chakraborty, H. Kumar, K. Kaur, and K.C. Juglan, *J. Chem. Thermodyn.* **126**, 137 (2018).
- [54] A. Thakur, K.C. Juglan, H. Kumar, and K. Kaur, *J. Mol. Liq.* **288**, 111014 (2019).
- [55] Reena R. Meena¹, Sunil H. Chaki, Ankurkumar J. Khimani, and M. P. Deshpande, *Mater. Res. Express* **1** (2019).

- [56] E. Saeed, M.M. Piñeiro, C. Hermida-Merino, and M.J. Pastoriza-Gallego, *Nanomaterials* **9**, (2019).
- [57] A. Arshad, M. Jabbal, Y. Yan, and D. Reay, *J. Mol. Liq.* **279**, 444 (2019).
- [58] A. Thakur, K.C. Juglan, H. Kumar, and K. Kaur, *Phys. Chem. Liq.* **00**, 1 (2019).
- [59] P.B. Kharat, S.D. More, S.B. Somvanshi, and K.M. Jadhav, *J. Mater. Sci. Mater. Electron.* **30**, 6564 (2019).

CHAPTER 3: OBJECTIVES AND METHODOLOGY

3.1 Objectives

The aim of studying acoustical properties of Graphene Oxide and Reduced Graphene Oxide suspensions with organic liquids was started by framing the following objectives:

- 1) Preparation and characterization of Graphene Oxide (GO) and Reduced Graphene Oxide (RGO).
- 2) To find ultrasonic velocity, density, and viscosity of Graphene Oxide (GO) and Reduced Graphene Oxide (RGO) with water and some organic solvents at different temperatures.
- 3) To derive various acoustical and thermodynamic parameters.
- 4) To examine various molecular interactions on the basis of acoustical and thermodynamic parameters.

3.2 Research Methodology:

3.2.1 Preparation of Graphene Oxide (GO): A beaker of 1000ml capacity have been taken and kept on a magnetic stirrer. In a big tub, an ice bath has been made around the beaker. This ice bath will help to keep the temperature of the reaction mixture below 10 °C. A digital thermometer is placed inside the beaker to note the heat of the reaction. In this beaker, we add 345 ml of sulphuric acid was added with continuous stirring. When the temperature of the mixture gets below 10 °C, 15 gm of the carbon powder, along with 7.5 gm of sodium nitrate added to the mix for at least 25 minutes. After 25 minutes of continuous string in an ice bath will bring the temperature of the mixture close to zero. As soon as the temperature approaches zero, we will start adding 45 gm of potassium permanganate gradually to the mix. While the reaction is exothermic, the temperature of the mixture begins to rise; at this point, controlling the amount of potassium permanganate in the mix will help to maintain the temperature of the system below 90 °C. This mixture is kept on a magnetic stirrer for about 2 hours. Now the ice bath has been removed, and the beaker was shifted to a water bath with a temperature of 40 °C. This increase in temperature will trigger the oxidation process. After 30

minutes in the water bath, the mixture was again shifted to magnetic stirrer until the colour of the mixture transforms from black to yellowish-brown. After the change of the colour, the combination was yet placed on the magnetic stirrer with an ice bath setup. With the continuous magnetic stirring and 500 ml of distilled water was added to the mixture gradually with the temperature of the mix below 90 °C. after about 8 hours, 30% mixture of hydrogen peroxide in water was progressively added to the reaction mixture very gradually. The addition of the hydrogen peroxide will remove any excess potassium ions from the reaction mixture and stops the oxidation process. Add more water for washing and diluting the brew. After overnight, the decantation of the water can be done by removing the top layer of water from the mixture. This layer will remove the excess water from the reaction mixture. Washing of the prepared samples was done thoroughly to maintain the quality of the product. Two washing with dilute hydrochloric acid will remove excess metal ion from the reaction mixture. After completion of the filtration, the process mixture was kept in the sonicator for ultrasonication treatment. This treatment will help to break the graphene oxide. The reaction mixture was dried in a vacuum and at 40 °C. The dried mixture was ground to get GO powder.[1-4]

3.2.2 Preparation of Reduced Graphene Oxide (rGO): Here, we are going to process GO prepared in the last step. Powder of GO (2mg/ml) was dispersed in 500 ml distilled water. Sonication of the prepared mixture was done using ultrasonication. The pH of the colloidal suspension was checked, and if required, few drops of ammonia added to the suspension to maintain the pH in the range of 9 to 10. Hydrazine monohydrate (1 µl/3ml) was added to the suspension very gradually. Now the colloidal suspension was kept on magnetic stirring for 4 hours with maintaining the temperature up to 90 °C. Later, the mixture will start to precipitate in black colour. This black colour precipitation is rGO. After complete precipitation, the mixture was washed and filtered. The mixture was dried in a vacuum at 40 °C.[5-7]

3.2.3 Characterization of GO and RGO: Following characterization techniques were used to characterize the GO and rGO.

3.2.3.1 Field Emission Scanning Electron Microscope (FESEM): Nova Nano

FESEM 450 used for SEM Micrography. This model provides micrographs with a high definition of clarity and actual nanoscale information of the sample under study. The Resolution provided in this model is 1.6 nm at 1 kV. The magnification provided by this SEM is 500000X.

SEM is an electron optical system, which uses an electron gun to produce a beam of electrons with the help of tungsten filament. The electron microscope generally uses magnetic lenses, whose optical strength can be changed by controlling the amount of current passing through the coil. The condenser lens is placed close to the object; this lens helps to control the diameter of the electron beam.



Figure 3.1 Nova Nano SEM 450

The use of the objective lens after the condenser lens is for focusing the final beam on to the object. This gives better control of the focus. The sample stage of the SEM can perform horizontal as well as vertical movement in a very smooth manner. The vertical movement helps to get the depth of the sample under study. There is a secondary electron detector in the SEM. There is a very high vacuum generated inside the SEM chamber 10^{-3} to 10^{-4} Pa. resolution of the SEM can reach up to 1nm to 20 nm. Magnification of the SEM can be from range 10 to 3000000 X. [8],[9]

3.2.3.2 Energy-dispersive spectroscopy (EDX): This system is integrated as the external device in Nova Nano FESEM 450. this system integrates to capture a

backscatter electron from the specimen. This liquid-cooled system read the energy of the X-rays and converts them into useful information. The detector is mounted on the FESEM, as shown in figure 3.2. In old technology, silicon-lithium crystal was used to detect these electrons along with the nitrogen cooling system. Now with the advancement in science and technology, the silicon detector has replaced the old sensors. This new detector can even work without a cooling system.

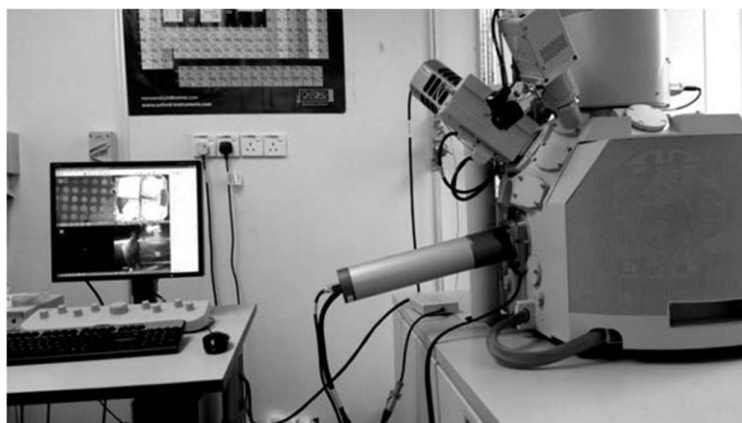


Figure 3.2 Nova Nano SEM 450 with EDS attachment

The principle of the EDX depends upon the ionization. In the detector, incoming X-rays get absorbed by the crystal, and this produces a free electron in the crystal. The number of electrons produced by an individual X-ray will generate a specific amount of current that is detected by the system. Each characteristic X-ray generated by different elements makes an unusual amount of the current in the system. The X-ray generated ultimately helps to identify the intensity of the elements present in the sample under study.[10]

3.2.3.3 High-resolution transmission electron microscopy (HRTEM): In this study, we used HR-TEM; Joel JEM-2100 Plus electron microscope with a working voltage of 80 to 200 kV, magnification of 15,000,00 lakh, Resolution of 0.194 nm (point), attached with Charge Couple Device (CCD).

Transmitted electrons interact with atoms within the sample via elastic and inelastic scattering. Electrons that undergo inelastic scattering have a change in energy after they are transmitted through the sample, whereas elastically scattered electrons maintain

their initial transmitted power and, therefore, can be more useful for the final data interpretation. The electrons that undergo elastic scattering leave the sample and move through the lenses of the microscope to form the high-resolution image.



Figure 3.3 HRTEM JOEL JEM-2100

Inelastically scattered electrons are generally not used in this technique, but they can produce data from the sample using a method called EELS, electron energy loss spectroscopy. HR-TEM relies on a principle called ‘phase contrast’ for image formation, which can often come with some problems when used at such a small scale. When the image is formed through the objective lens of the microscope, there is some significant oscillation present due to the little scaling used, which can often reduce the quality of the Resolution of the image. A function called the phase contrast transfer function (TF) describes how these limitations affect image formation. The TF is universal for all lenses and for all specimens used so it can be easily measured in all scenarios and used to predict the Resolution produced in specific procedures. There are many different applications for HR-TEM currently used, and there are even more options after potential development. It is often used for the study of crystals, but also materials such as metals, semiconductors, and nanoparticles. Particular focus is usually aimed around defects in these materials at the atomic level. [11]

3.2.3.4 Fourier-transform infrared spectroscopy (FTIR): In this study, we used Perkin-Elmer Spectrum 2 with ATR & Pellet accessories. Spectrum 2 has standard, high performance, room temperature LiTaO₃ detector with a total range of 350 to 8300 cm⁻¹ at the best Resolution of 0.5. The instrument is connected to a PC with spectrum software.



Figure 3.4 FTIR Perkin Elmer Spectrum 2

The basic principle of the FTIR is the amount of light absorbed by the sample between the applied range of the frequency. In FTIR beam of many wavelengths shines on the given sample. The beam used in this is carrying all the wavelengths. These many wavelengths of the beams act as the source of light for the Michelson interferometer. In this interferometer, one mirror is fixed, and another mirror is moving with the help of a motor; as the mirror moves, each wavelength of the light forms the interference pattern. Each different wavelength produces a different interference pattern at the contrasting settings of the mirrors. Now when the sample is placed between mirrors and source of light, a specific part of the wavelength is absorbed by the elements present in the sample. This absorbed spectrum is omitted from the interference pattern of the wavelength. This interference pattern is studied with the help of Fourier transformation. Computer programming helps to generate useful information in the form of graphs from this interference pattern. The primary role of the Fourier transformation is to convert a distance on the mirrors into the gap between the waves.[12]

3.2.3.5 X-ray diffraction (XRD): To study the crystal structure and to predict the presence of a particular element in the compound, we use XRD. In this study, Panalytical X'pert Pro was used to take XRD intensity graphs. This instrument is excellent for studying powdered samples. This module uses the Cu K α as the source to produce X-Rays of 1.54 Å. This instrument is proficient for high-resolution measurements. The sample holder is made up of aluminum. XRD works at the voltage of 40 kV and 40 mA.



Figure 3.5 XRD Panalytical X'Pert Pro

The principle of the XRD is based on the constructive interface of the monochromatic X-ray produced by cathode ray with the crystal structure. The X-rays produced by the Cu K α source pass through the collimator and falls on the sample. We know the constructive interference pattern will be formed when the incoming X-Rays after reflection travel the same pathlength for constructive interference or odd pathlength for the destructive interference. This can be understood with the help of Bragg's Law ($n\lambda=2d \sin \theta$). This law depends on the d, which is space between the lattices and θ , which is a diffraction angle. Each element has a unique crystal structure and lattice spacing. This combination gives a different pattern for the different available elements. The XRD pattern of the components can be analogs to the fingerprint pattern. Each

different element has a different XRD pattern. This is a compelling technique to find and verify the presence of certain different elements in the given samples.[13]

3.2.3.6 RAMAN Spectroscopy: For the prepared samples, the RAMAN spectroscope model Airix STR-500 is used for the Raman Characterization. This spectroscope offers a resolution of 0.3 cm^{-1} and can measure up to 50 cm^{-1} . This system provides a focal length of 500 mm with $f/6.5$. This system offers a fully automated imaging system. The laser available in the system is 325 nm, 532 nm, and 785 nm.

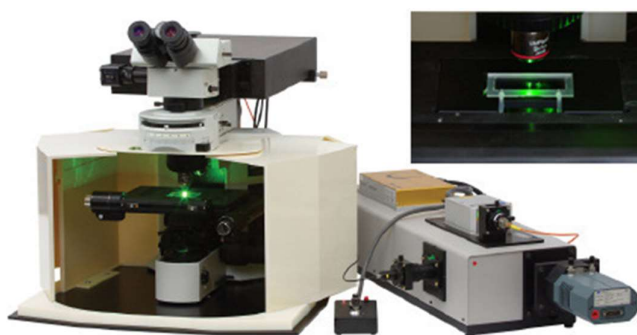


Figure 3.6 Raman Spectrometer Airix STR-500

Raman spectroscopy depends upon the change in the polarizability of molecular bonds. When the photon of light falls on the electron cloud of the molecular bonds, the electron cloud interacts with incoming photons. This interaction changes the polarizability of the molecular bond and gives rise to Raman active modes. There are many examples of the molecular relationship like carbon-carbon exist in nature where the polarizability of the molecular bond changes with the interaction of incoming photons. The changes in the polarizability are minimal and cannot be observed in FTIR. Raman is a weak effect, so the components of the Raman spectra should be well matched and synchronized. The incident photon interacts with the molecule and then scatter. This incident and disperse molecules have a difference in the energy due to changes in the rotational and vibrational energy of the molecule. This change provides information on the energy level present in the molecules.[14]

3.2.4 Preparation of nanosuspension samples: Top-down approach has been used to prepare nanosuspension. Prepared samples were mixed well and sonicated for at least 5 hours to get continuous dispersion without any phase separation. The following set of

samples, as described in the below table, have been prepared for the further collection of studies. Each sample consists of 20 ml of liquid and some specific amount of GO/RGO, as mentioned in the table. These samples have been measured with precision.

Table 3.1: Sample details

Water		DMF		NMP		THF		EG	
Section 1		Section 2		Section 3		Section 4		Section 5	
20 ml Water + 4 mg GO	20 ml Water + 4 mg RGO	20 ml DMF + 4 mg GO	20 ml DMF + 4 mg GO	20 ml NMP + 4 mg GO	20 ml NMP + 4 mg RGO	20 ml THF + 4 mg RGO	20 ml THF + 4 mg RGO	20 ml EG + 4 mg GO	20 ml EG + 4 mg RGO
20 ml Water + 8 mg GO	20 ml Water + 8 mg RGO	20 ml DMF + 8 mg GO	20 ml DMF + 8 mg GO	20 ml NMP + 8 mg GO	20 ml NMP + 8 mg RGO	20 ml THF + 8 mg RGO	20 ml THF + 8 mg RGO	20 ml EG + 8 mg GO	20 ml EG + 8 mg RGO
20 ml Water + 12 mg GO	20 ml Water + 12 mg RGO	20 ml DMF + 12 mg GO	20 ml DMF + 12 mg GO	20 ml NMP + 12 mg GO	20 ml NMP + 12 mg RGO	20 ml THF + 12 mg RGO	20 ml THF + 12 mg RGO	20 ml EG + 12 mg GO	20 ml EG + 12 mg RGO
20 ml Water + 16 mg GO	20 ml Water + 16 mg RGO	20 ml DMF + 16 mg GO	20 ml DMF + 16 mg GO	20 ml NMP + 16 mg GO	20 ml NMP + 16 mg RGO	20 ml THF + 16 mg RGO	20 ml THF + 16 mg RGO	20 ml EG + 16 mg GO	20 ml EG + 16 mg RGO
20 ml Water + 20 mg GO	20 ml Water + 20 mg RGO	20 ml DMF + 20 mg GO	20 ml DMF + 20 mg GO	20 ml NMP + 20 mg GO	20 ml NMP + 20 mg RGO	20 ml THF + 20 mg RGO	20 ml THF + 20 mg RGO	20 ml EG + 20 mg GO	20 ml EG + 20 mg RGO

3.2.5 Characterization of nanosuspension: Following characterization techniques that were used to confirm the occurrence of GO and rGO in the nanosuspension and size of the particles in the nanosuspension.

3.2.5.1 Ultraviolet-visible spectroscopy (UV-Vis): In this study, the presence of solvent in the liquid suspension, UV-Vis spectroscopy can be used. In this study, Shimadzu UV-1800 UV-Vis spectrophotometer was used to study UV-Vis spectroscopy. This spectrometer offers the wavelength range from 190 to 1100 nm with a spectral bandwidth of 1 nm. The light source used in this spectrometer is deuterium and tungsten halogen lamps.



Figure 3.7 UV-Vis Spectrometer Shimadzu UV-1800

The principle of the UV-Vis spectroscopy is the absorption of UV and visible light by the chemical compounds. The absorption of energy by the mixture creates interaction between the electron cloud and incoming photons. This interaction produces distinct spectra for the compound under study. As soon as the photon falls on the sample under investigation, an electron from the ground energy level gets excited and moves to an excited energy level. The difference between the energy level is exactly equals to the energy of the incident photon. The deexcitation of the electrons from an excited state to the ground again produces the photon whose power is equivalent to the incoming photon. The emission of the photon produces spectra, which are known as UV-Vis spectra for the sample under study. In molecules, there are two types of electron clouds

are present one is known as bonding, and the other is known as antibonding. An electron can move from one highest occupied molecular orbit to a lower occupied molecular orbit. If the gap between these orbitals is less than the wavelength absorbed will be high and vice versa. UV-Vis also used as the liquid chromatography in which the principle of working is Beer-Lambert law. According to this law, the absorption of the light by the solution is directly proportional to the concentration of the absorbing sample and pathlength traveled by the light.

$$A = \epsilon l c$$

Where ϵ is the molar attenuation coefficient, l is the pathlength of the light passing through the solution, and c is the concentration of the attenuating species. The absorption of ultraviolet light by a chemical compound will produce a distinct spectrum which aids in the identification of the mixture.[15]

3.2.5.2 Dynamic light scattering (DLS): In this study, the size of the particles in the suspension, dynamic light scattering can be used. In this study to study the DLS Malvern ZetaSizer Nano-ZS90 system has been used. This set up uses the He-Ne laser with a wavelength of 633nm is used. This instrument can measure particle size form the range of 0.3 nm to 5 μm . A minimum of 20 μl of the sample is required for the study of the particle size, and 150 μl is necessary for the zeta potential study. The temperature of the system can vary from 0 to 90 $^{\circ}\text{C}$.



Figure 3.8 DLS Malvern Zetasizer Nano ZS90

Dynamic Light Scattering (DLS) is based on the random motion of the particles. As per the theory, particles on the solute are always in motion and collides with the molecules of the solvent. In this process, energy is a transfer from solute molecules to solute particles as we know small particles move fast as compare to the larger particles. If we know all other parameters which can affect the movement of the particles in the solvent, then the size of the particles in a liquid can be determined with the help of the Stokes-Einstein equation.

$$D = \frac{k_B T}{6 \pi \eta R}$$

Where D is the diffusion coefficient or speed of the particle. k_B is the Boltzmann Constant. η is the viscosity of the solvent, and R being the hydrodynamic radius.

In the DLS setup sample is taken in a small cuvette. Incident laser falls on the sample and gets scattered. Scattered rays are detected at some angle to calculate the diffusion coefficient. This diffusion coefficient further helps to calculate the hydrodynamic radius with the help of the Stokes-Einstein equation.[16]

3.2.6 Measurement of Ultrasonic Velocity: To calculate the ultrasonic velocity of the sample, we used Mittal interferometer M -81 with a fixed frequency of 2 MHz. This instrument consists of a multifrequency generator, a measuring cell with 10 ml capacity, an ultrasonic wave generator, and a reflector which can move freely inside the measuring cell, water bath to maintain the temperature of the liquid under study. The least count of the micrometer used is 0.01 mm.

In this method, the sound waves are produced by a piezoelectric crystal. The wavelength of the sound wave is measured with the variable path interferometer at a fixed frequency of the sound wave. The velocity of the sound wave can be calculated from this wavelength. The measuring cell of the ultrasonic interferometer is made up of the doubled walled brass cell with the chromium coating. This doubled wall cell allows the circulation of the water around the sample to keep the temperature under control. The piezoelectric crystal of fixed frequency produces ultrasonic waves. There are movable metallic plates parallel to the quartz plates, which reflect the sound wave

in the medium. These reflected waves interfere with the incoming waves. When the distance between the two waves is exactly equated to half of the wavelength of a sound wave standing waves are produced in the liquid. This length of the measuring cylinder is noted with accuracy, and at this point, the current in the system is maximum.[17]



Figure 3.9 Ultrasonic Interferometer Mittal M-81

Now, if the distance of the two parallel reflectors increased or decreased, the variation is exactly equated to half of the wavelength, and the current is maximum at this point. We know

$$U = \lambda \times f$$

Where U is the velocity of the sound in the given medium, λ is the wavelength, and f is the known frequency of the sound wave. Samples of 10 ml have been used for the studies, and the temperature has been varied form range 298 K to 313 K.

3.2.7 Measurement of Density: Density calculation has been done with the help of a 10 ml pycnometer with a built-in thermometer. Capacity within 10% insignificant volume imprinted on the flask, side tube lid has a minor opening for air outflow, a thermometer is used to record the reading from 298 K to 313 K, standard taper 10/18 thermometer joint, standard taper 5/12 cap, Bodies numbered for easy identification, 50mL size is for specific gravity of pigments according to ASTM.

A sample of 15 ml has been taken for ultra-sonification. Ultrasonication for 2 hours

helps to redistribute samples. A water bath has been prepared to maintain the desired temperature. Fifteen readings for each sample has been taken to remove any experimental error. A total of 825 reading has been made with this setup.[18]



Figure 3.10 Pycnometer Density bottle with termometer

3.2.8 Measurement of Viscosity: To measure the viscosity of the prepared samples, Labman LMDV 200 Rotational Digital Direct Reading Viscometer is used in this study. This instrument can be used to calculate the velocity of Newtonian as well as non-Newtonian fluids.



Figure 3.11 Rotational Viscometer
Labman LMDV 200

This model has a measuring range of 40 to 40000000 mPa.s with six standard spindles. The speed range is from 0.5 to 200, with 54 variations. This instrument has temperature monitoring and measurement accuracy of 1% and a repeatability accuracy of 0.5% and 220 V 50 Hz power supply.

The rotational viscometer works on the principle of torque produced in the spindle when it moves inside the liquid under study. More is the viscosity of the sample; less will be the speed of the spindle and vice-versa. If the speed of the rotating rod is known, then the viscosity of the fluid can be measured by the assistance of mathematical calculations. A sample of 15 ml has been taken for ultra-sonification. Ultrasonication for 2 hours helps to redistribute samples. [9]

3.3 Calculation of other parameters: Some parameters can be calculated with the help of velocity, density, and viscosity.

3.3.1 Acoustics impedance: It is the resistance which is offered to the propagation of the ultrasonic wave in a material, and can be described as the product of density (ρ) and acoustic velocity (U)

$$Z = \rho U$$

This impedance is crucial for acoustic transmission and reflection at the border of two materials having different acoustics impedances.

3.3.2 Adiabatic compressibility: It is the fractional reduction of volume per unit rise of pressure when no heat flows in or out. These alterations are related to the compressibility of the medium but thermodynamic relations:

$$\beta = \frac{1}{v} \frac{dv}{dp}$$

This can also be computed from the speed of sound as well as density of medium using equations of Newton's as

$$\beta = (U^2 \rho)^{-1}$$

Where, ρ = Density of medium, U = Ultrasonic velocity in the medium,

3.3.3 Relaxation time: It is the amount of the time taken by medium particles to modify their original mean positions inside the medium following displacement by ultrasonic waves. Its value is characterizing by the medium. Relaxation time for binary mixture can be calculated from the relation.

$$\tau = \frac{4\beta\eta}{3}$$

It can also be written as:

$$\tau = \frac{4\eta}{3\rho U^2}$$

Where τ =Relaxation time, β =Adiabatic compressibility, η =Viscosity of mixture

3.3.4 Intermolecular free length: The distances between the surfaces of neighbouring molecules that is given by the relation:

$$L_f = K_T (\beta)^{1/2}$$

Where, β = Adiabatic compressibility of the mixture, K_T = Temperature of dependent Jacobson's constant, $K_T = (93.875 + 0.375 K) 10^{-8}$ where T = temperature in Kelvin.

3.3.5 Ultrasonic attenuation: Rate of decrease of energy when an ultrasonic wave is transmitting in a medium labelled as attenuation and depends upon the properties of the medium. The sound attenuation increases with an increase in the frequency and usually related to the square of sound frequency. So ultrasonic attenuation can be expressed as:

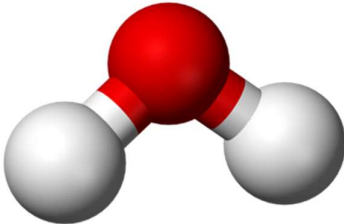
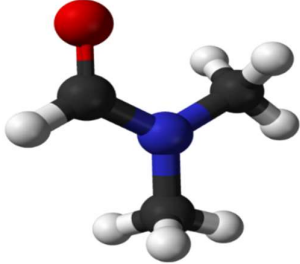
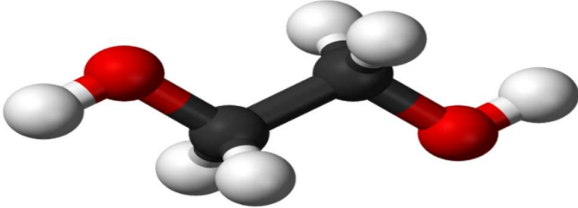
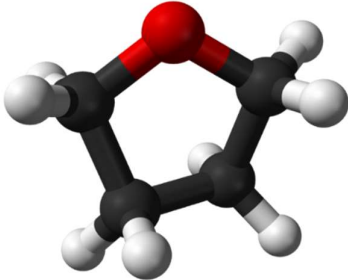
$$\frac{\alpha}{f^2} = \frac{8\pi^2\eta}{3\rho U^3}$$

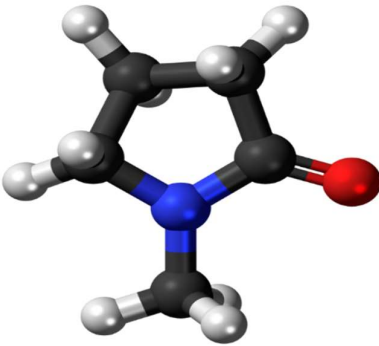
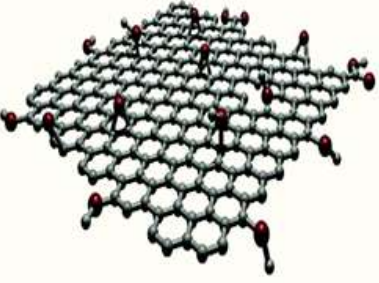
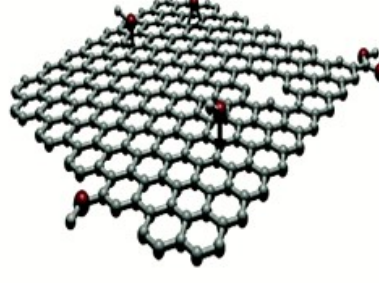
Where f = frequency of the wave.

3.4 Structures of the chemical used in the experiment: Following structures have

been used in the study.

Table 3.2 Chemical used in the study with structure

Name of the Chemical	Structure
Water	
N, N Dimethylformamide (DMF)	
Ethylene Glycol (EG):	
Tetrahydrofuran (THF)	

<p>N-Methyl-2-pyrrolidone (NMP)</p>	
<p>Graphene Oxide</p>	
<p>Reduced Graphene Oxide</p>	

3.5 Description of the chemical used in the study:

Sr. No	Chemical	Supplier	Purification Method	Purity Grade
1	Graphite Powder	Loba Chemical	None	AR
2	Sodium Nitrate	Loba Chemical	None	AR
3	Potassium permanganate	CDH	None	AR
4	Hydrochloric Acid	CDH	None	AR
5	Ammonia	CDH	None	AR
6	Sulphuric Acid	Avantar	None	AR
7	Hydrogen peroxide	Fisher Scientific	None	AR

8	Hydrazine monohydrate	Sigma Aldrich	None	AR
9	N-Methyl-2-pyrrolidone	CDH	None	AR
10	Tetrahydrofuran	CDH	None	AR
11	Ethylene Glycol	Sigma Aldrich	None	AR
12	N, N Dimethylformamide	Loba Chemical	None	AR
13	Water	Double Distilled	Double Distilled	Double Distilled

3.6 References.

- [1] W.S. Hummers and R.E. Offeman, *J. Am. Chem. Soc.* **80**, 1339 (1958).
- [2] J. Chen, B. Yao, C. Li, and G. Shi, *Carbon N. Y.* **64**, 225, (2013).
- [3] R. Muzyka, M. Kwoka, Ł. Smędowski, N. Díez, and G. Gryglewicz, Xinxing Tan Cailiao/New Carbon Mater. **32**, 15 (2017).
- [4] D. C.C. Marcano, D. V. V Kosynkin, J.M. Berlin, A. Sinitskii, Z.Z. Sun, A. Slesarev, L.B. Alemany, W. Lu, and J.M. Tour, *ACS Nano* **4**, 4806 (2010).
- [5] T. Remyamol, H. John, and P. Gopinath, *Carbon N. Y.* **59**, 308, (2013).
- [6] W. Feng, Y. Wang, J. Chen, L. Wang, L. Guo, J. Ouyang, D. Jia, and Y. Zhou, *Carbon N. Y.* **108**, 52 (2016).
- [7] C. Zhao, M. Shen, Z. Li, R. Sun, A. Xia, and X. Liu, *J. Alloys Compd.* **689**, 1037 (2016).
- [8] M. Zhong, Y. Song, Y. Li, C. Ma, X. Zhai, J. Shi, Q. Guo, and L. Liu, *J. Power Sources* **217**, 6 (2012).
- [9] M. Joshi, A. Bhattacharyya, and S.W. Ali, *Indian J. Fibre Text. Res.* **33**, 304 (2008).
- [10] J.L. Lv, S.R. Zhai, C. Gao, N. Zhou, Q. Da-An, and B. Zhai, *Chem. Eng. J.* **289**,

261 (2016).

[11] J. Lin, Z. Peng, Y. Liu, F. Ruiz-Zepeda, R. Ye, E.L.G. Samuel, M.J. Yacaman, B.I. Yakobson, and J.M. Tour, *Nat. Commun.* **5**, 1 (2015).

[12] Y. Wang, X. Wu, and W. Zhang, *Mater. Lett.* **165**, 71 (2016).

[13] M. Zong, Y. Huang, N. Zhang, and H. Wu, *J. Alloys Compd.* **644**, 491, (2015).

[14] A.C. Ferrari, *Solid State Commun.* **143**, 47, (2007).

[15] Z. Luo, L. Zhu, Y. Huang, and H. Tang, *Synth. Met.* **175**, 88, (2013).

[16] I. Roy, G. Sarkar, S. Mondal, D. Rana, A. Bhattacharyya, N.R. Saha, A. Adhikari, D. Khastgir, S. Chattopadhyay, and D. Chattopadhyay, *RSC Adv.* **6**, 10557, (2016).

[17] I. Saxena, R. Pathak, V. Kumar, and R. Devi, *Int. J. Appl. Res.* **1**, 562 (2015).

[18] M. Nabeel Rashin and J. Hemalatha, *J. Mol. Liq.* **197**, 257, (2014).

CHAPTER 4: RESULT AND DISCUSSION

In the section methodology, we discussed the preparation of the GO and rGO. In this section, we will discuss the characterization of prepared GO and rGO. As examined in the earlier chapters, we have prepared a total of 55 samples for the acoustical and thermo-dynamical study of liquid nanosuspensions. The characterization of the prepared nanosuspension and research discussed in this chapter.

4.1 Characterization of GO:

As discussed, earlier GO prepared with the Hummers method. In this chapter, we will discuss the characterization of GO with FESEM, EDX, FTIR, XRD, and RAMAN. This characterization will lead us to the conclusion that the prepared sample is GO chemically, and oxidation of the carbon powder has been successful with the Hummers method.

4.1.1 FESEM: we have used Nova Nano Sem 450 for the characterization of the solid GO powder. In figure 4.1, there are two micrographs 4.1(a) at the 50000 X magnification and 2 μm scale. The micrograph in figure 4.1 (b) is at 200000 X magnification and 500 nm scale. In figure 4.1(a), the edges of the prepared GO sheets are visible. These sheets are stack on each other. The size of the layers is higher than 2 μm as it can compare with the scale. The crumbled sheets are overlapped with each other to form GO. [1-3]

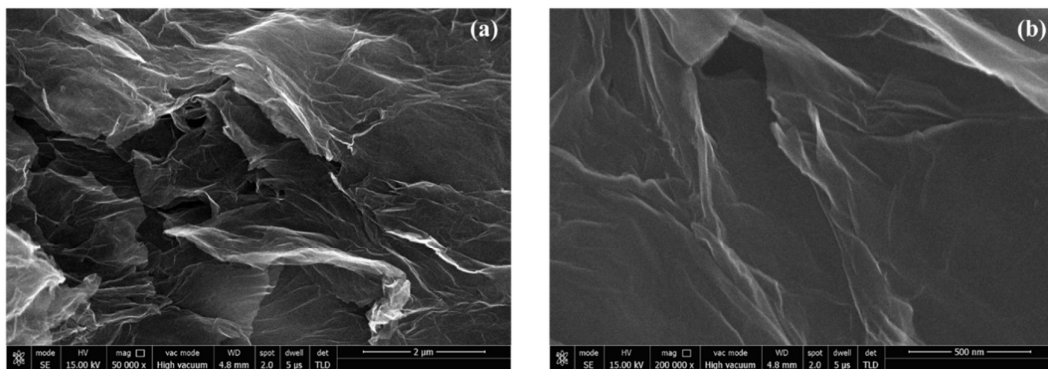


Figure 4.1 (a) shows the FESEM Micrograph for prepared GO samples at 50000 magnification and 2 μm scale Figure 4.1 (b) shows the FESEM Micrograph for prepared GO sample at 200000 X Magnification at 500 nm scale.

In figure 4.1 (b) is the magnified image of 4.1(a) in which two graphene sheets are visible who are separated by some gap. The separation of edges leads to the conclusion that the prepared sample has some sheet kind of structure, which is evident in the SEM micrographs. It can also mention that the GO sheets prepared are having a size of more than 2 μm in the powder form. Sheets are clustered on each other but good in size.

4.1.2 EDX: EDX spectra obtained from the backscattered electron in SEM, a specialized attachment called EDX, is used to study the energy corresponding to the backscatter electron. This energy helps to determine the element with which electron has interacted. This study contributes to determine the chemical composition of the prepared sample and shows the impurity elements if present in the product. Figure 4.2 shows the EDX of the ready GO sample. [4],[5]

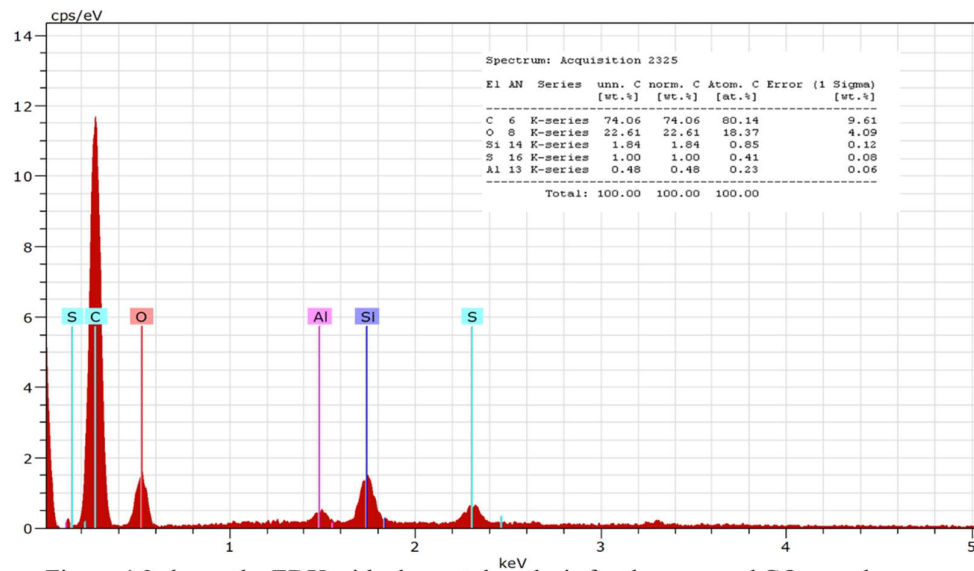


Figure 4.2 shows the EDX with elemental analysis for the prepared GO sample

In this graph it mentions the type of elements present in the prepared GO sample and their composition. There is approximately 74.06 % of the carbon content present in the GO sample, 22.61 % of the oxygen content, which is quite good and shows the proper oxidation of the specimen during a chemical reaction. There is a bit of impurity also present in the sample that is of silicon 1.64 %, sulphur 1 %, and aluminium 0.48 %. The total Carbon and oxygen content are 96.67 %, which is quite useful for laboratory preparation, and there is a contamination of approximately 3.33 % in the sample.

4.1.3 FTIR: shows the FTIR spectra of the prepared GO sample with the help of the Perkin-Elmer Spectrum 2 instrument. FTIR is a preliminary study done to make sure the product form after the chemical reaction is transformed into what we wanted. FTIR helps to understand the absorption of light by the different molecular bonds present in the sample under study.

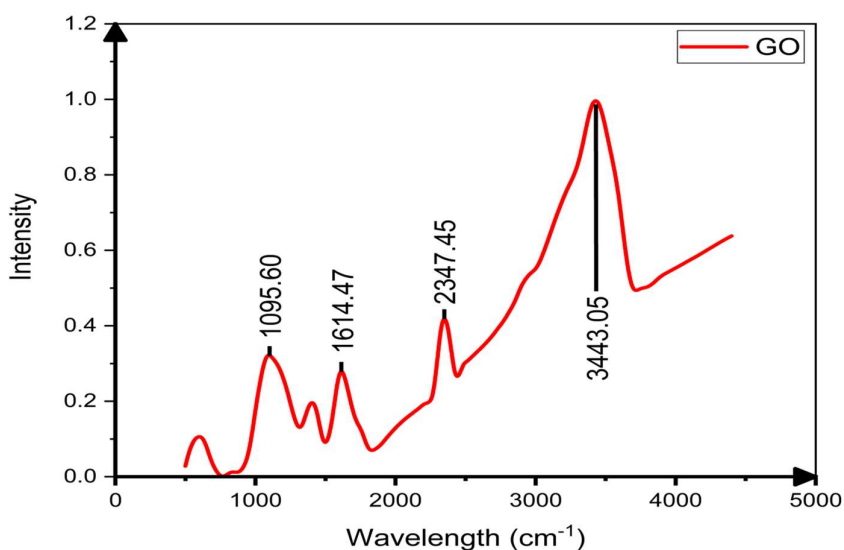


Figure 4.3 shows the FTIR spectra for the prepared GO sample

In this sample under study, the peak present at 1109.16 cm^{-1} corresponds to the stretching vibration of Carbon and oxygen bond. The peak at 1618.33 cm^{-1} corresponds to the elemental Carbon and carbon vibration. Carbon-carbon vibration is also known as the Skelton vibration of the graphene network. Peaks at 2345 cm^{-1} again correspond to the carbon-oxygen bond present in carbon dioxide, and peak at 3435 cm^{-1} corresponds to the hydroxyl group present in the water molecule. The dominance of the water molecule in the sample might be there was due to the moisture present in the prepared GO sample. This study helps to dry the sample under vacuum further. The presence of carbon and carbon bond absorption in the FTIR study confirms the presence of the graphene network in the prepared sample. [6-8]

4.1.4 XRD: The XRD spectrum study was done with the help of the Panalytical

X'Pert Pro instrument. XRD study is based on the Bragg's Law, which helps to understand the interference pattern we obtain in the XRD study.

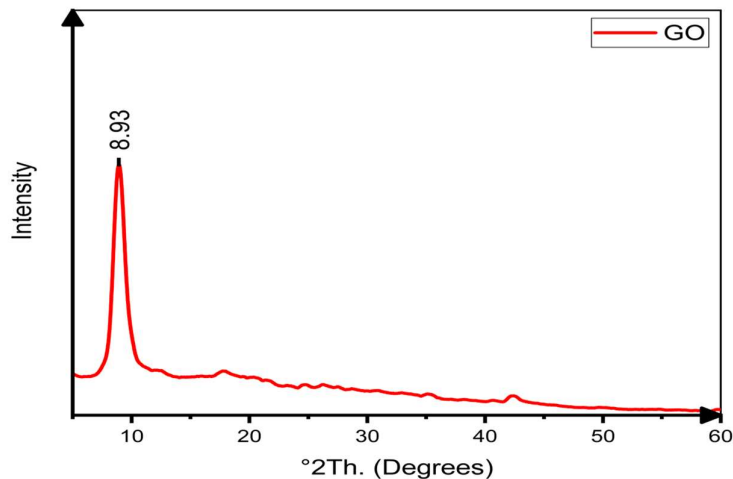


Figure 4.4 shows the XRD spectra for the prepared GO sample

The peak at an angle $8^{\circ}.93'$ is a low angle peak. As per Bragg's law, the bond length of the two atoms of the different planes is inversely proportional to the incident angle. There will be more separation between the atoms of the adjacent plane; less will be the angle. In our study, the angle comes out to be quite low, and this corresponds to the fact that the distance between adjacent planes is vast. In our case, the gap between the two planes is significant because the oxygen atom takes empty places between the layer of carbon atoms. This occupation by the oxygen atom increases the d spacing between the planes, which again confirms the proper oxidation of the prepared GO sample. As per the literature, the plane corresponds to this peak is 001^{1,2}. The calculated value of d for this peak comes out to be 98.76 nm. [9-11]

4.1.5 Raman Spectra: Raman studies of our sample were completed using Airix STR 500. This instrument helps to measure the rotational and vibrational level of the sample under examination, which cannot be measured with the FTIR instrument.

Figure 4.5 corresponds to the Raman Spectroscopy graph of GO. Raman spectra consist of two peaks; the first peak is at 1352.37 cm^{-1} , which is known as the defect peak of the graphene network. The D-bands in both spectra is strong, confirming the lattice

distortions of graphene basal planes.

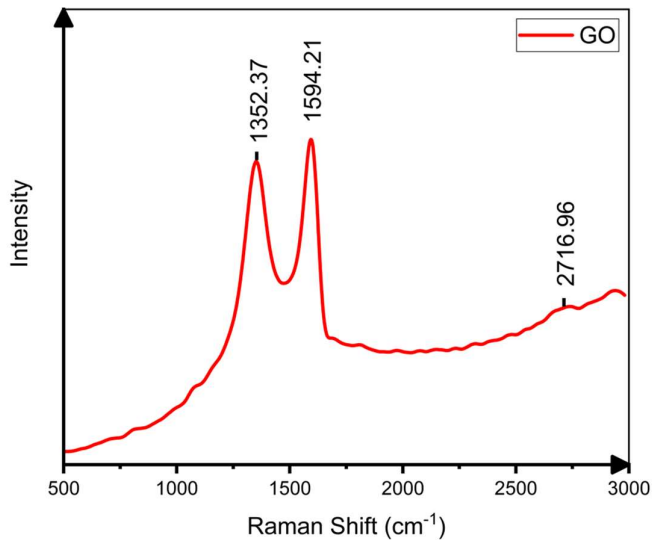


Figure 4.5 shows the RAMAN spectra for the prepared GO sample

The second peak corresponds to the 1594.21 cm^{-1} , which is known as the graphene structure peak. As seen in figure 4.5, the intensity value of the graphene network peak is more significant as compared to the graphene defect peak. The I_D/I_g ratio is 0.93, which corresponds to the excellent oxidation of graphite. I_D/I_g corresponds to the superb structure retainment by the graphene network in the prepared GO sample. [12-14]

4.2 Characterization of rGO:

As discussed, earlier rGO prepared with the help of reduction with hydrazine monohydrate. In this chapter, we will discuss the characterization of rGO with FESEM, EDX, FTIR, XRD, and RAMAN. This characterization will lead us to the conclusion that the prepared sample is rGO chemically, and oxidation of the carbon powder has been successful after reduction with hydrazine hydrate.

4.2.1 FESEM: we have used Nova Nano Sem 450 for the characterization of the solid rGO powder. In figure 4.6, there are two micrographs 4.6(a) at the 100000 X magnification and $1 \mu\text{m}$ scale. The micrograph in figure 4.1 (b) is at 200000 X

magnification and 500 nm scale. In figure 4.6(a), the edges of the prepared rGO sheets are visible. These sheets are stack on each other. The size of the layers is higher than 1 μm as it can compare with the scale. The crumbled sheets are overlapped with each other to form the rGO network.

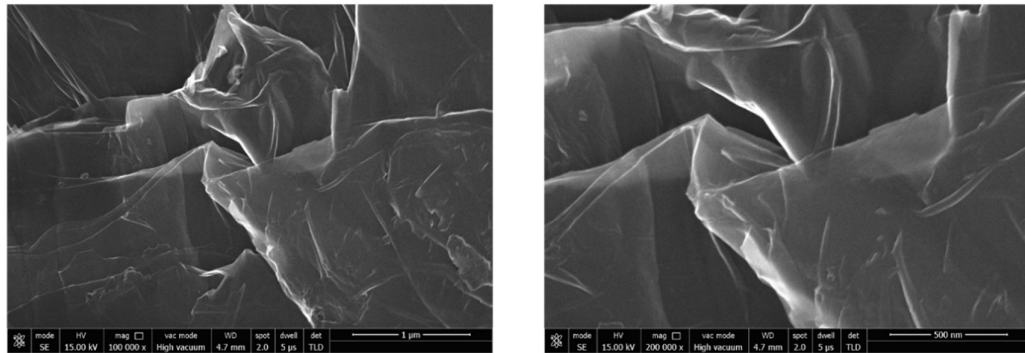


Figure 4.6 (a) shows the FESEM Micrograph for prepared rGO samples at 1 μm magnification. Figure 4.6 (b) shows the FESEM Micrograph for prepared rGO sample at 500 nm Magnification.

In figure 4.6 (b) is the magnified image of 4.6 (a) in which two graphene sheets are visible who are separated by some gap. The separation of edges leads to the conclusion that the prepared sample has some sheet kind of structure, which is evident in the SEM micrographs. It can also mention that the rGO sheets prepared are having a size of more than 1 μm in the powder form. Sheets are clustered on each other but good in size. [1-3]

4.2.2 EDX: EDX spectra obtained from the backscattered electron in SEM, a specialized attachment called EDX, is used to study the energy corresponding to the backscatter electron. This energy helps to determine the element with which electron has interacted. This study contributes to determine the chemical composition of the prepared sample and shows the impurity elements if present in the product. Figure 4.7 shows the EDX of the ready rGO sample.

In this graph, it mentions the type of elements present in the prepared rGO sample and their composition. There is approximately 86.83 % of the carbon content present in the GO sample, 8.56 % of the oxygen content, which is quite good and shows the proper oxidation of the specimen during a chemical reaction. There is a bit of impurity also present in the sample that is of Boron 4.91 %. The total Carbon and oxygen content are

95.39 %, which is quite useful for laboratory preparation, and there is a contamination of approximately 4.91 % in the sample. [4],[5]

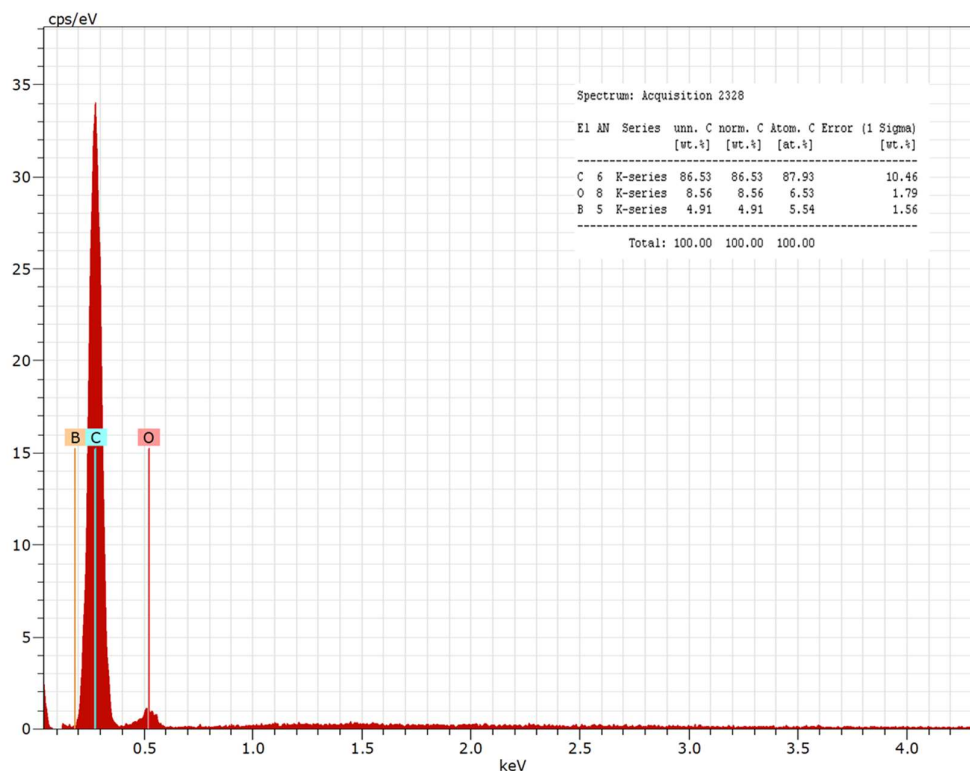


Figure 4.7 shows the EDS with elemental analysis for the prepared rGO sample

4.2.3 FTIR: shows the FTIR spectra of the prepared rGO sample with the help of the Perkin-Elmer Spectrum 2 instrument. FTIR is a preliminary study done to make sure the product form after the chemical reaction is transformed into what we wanted. FTIR helps to understand the absorption of light by the different molecular bonds present in the sample under study.

In this sample under study, the peak present at 923.93 cm^{-1} corresponds to the stretching vibration of Carbon and oxygen bond. The peak at 1234.48 cm^{-1} corresponds to the Carbon and oxygen bond present in epoxy stretching. The peak at 1539.24 cm^{-1} corresponds to the elemental Carbon and carbon vibration. Carbon-carbon vibration is also known as the Skelton vibration of the graphene network. Peaks at 2341 cm^{-1} again

correspond to the carbon-oxygen bond present in carbon dioxide. [6-8]

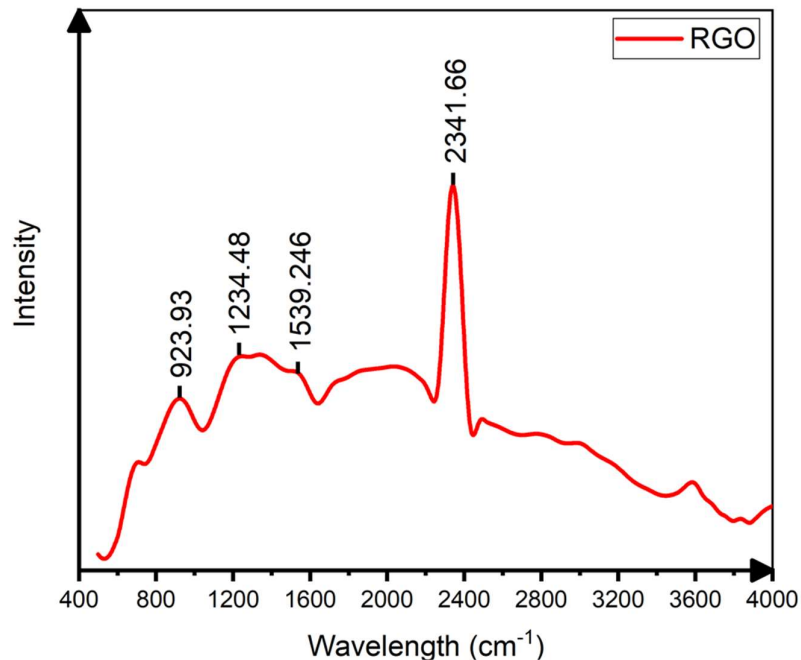


Figure 4.8 shows the FTIR spectra for the prepared rGO sample

4.2.4 XRD: The XRD spectrum study was done with the help of the Panalytical X'Pert Pro instrument. XRD study is based on the Braggs Law, which helps to understand the interference pattern we obtain in the XRD study.

The peak at an angle $26^{\circ}.47'$ is a low angle peak. As per Bragg's law, the bond length of the two atoms of the different planes is inversely proportional to the incident angle. There will be more separation between the atoms of the adjacent plane; less will be the angle. In our study, the angle comes out to be $26^{\circ}.47'$, and this corresponds to the fact that the distance between adjacent planes is less. In our case, the gap between the two planes is significantly less because the oxygen atom is removed from places between the layer of carbon atoms. This removal of the oxygen atom decreases the d spacing between the planes, which again confirms the proper reduction of the prepared rGO sample. As per the literature, the plane corresponds to this peak is 111. The calculated

value of d for this peak comes out to be 33.63 nm. [9-11]

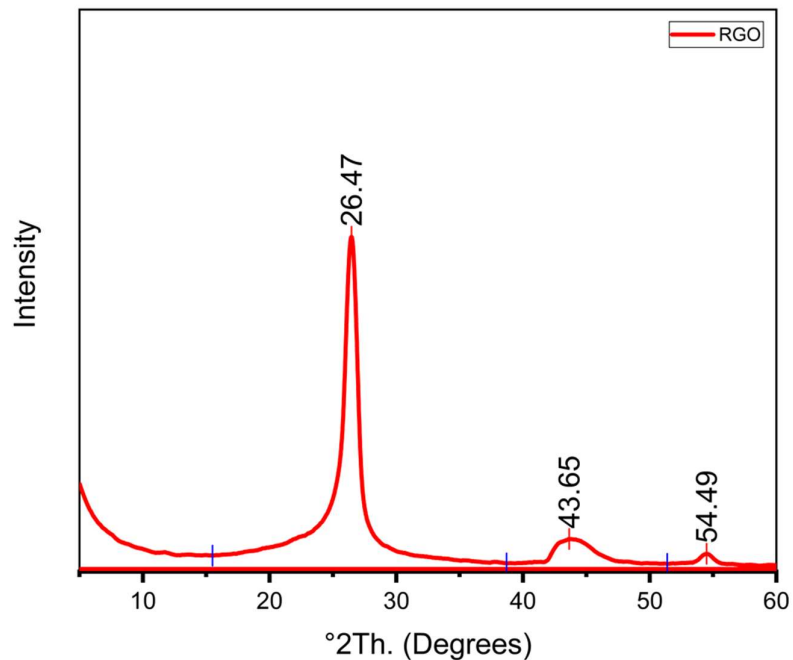


Figure 4.9 shows the XRD spectra for the prepared rGO sample

4.2.5 Raman Spectra: Raman studies of prepared samples were completed using Airix STR 500. This instrument helps to measure the rotational and vibrational level of the sample under examination, which cannot be measured with the FTIR instrument.

Figure 4.10 corresponds to the Raman Spectroscopy graph of rGO. Raman spectra consist of three peaks; the first peak is at 1336.38 cm^{-1} , which is known as the defect peak of the graphene network. The D-bands in both spectra is strong, confirming the lattice distortions of graphene basal planes. The second peak corresponds to the 1565.96 cm^{-1} , which is known as the graphene structure peak. The third peak at 2682.66 cm^{-1} is called a 2D maximum, which is a result of a double resonance-enhanced two phonon process involving two TO phonons around the K point. As seen in figure 4.5, the intensity value of the graphene network peak is more significant as compared to the graphene defect peak. The 2D peak also corresponds to the defect peak. The I_D/I_G ratio

is 0.41, which corresponds to the excellent reduction of rGO with hydrazine monohydrate. I_D/I_g corresponds to the superb structure retainment by the graphene network in the prepared GO sample. [12-14]

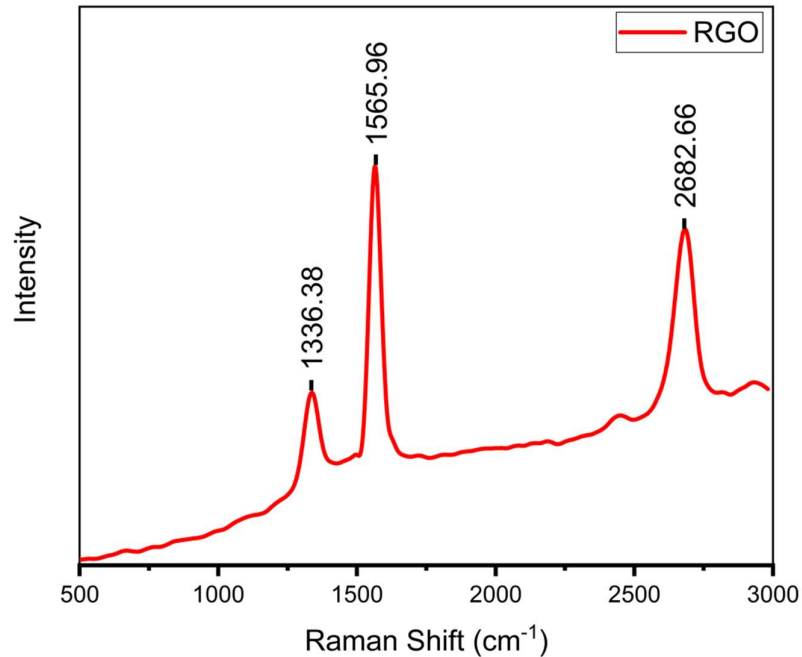


Figure 4.10 shows the RAMAN spectra for the prepared rGO sample

4.3 Characterization of GO Nanosuspension

Nanosuspension of the GO has been prepared with the help of ultrasonication, as discussed in methodology. The ultrasonication helps to decrease the particle size of the GO particles in the solvent, and extensive ultrasonication helps to increase the stability of the solution.

4.3.1 UV-VIS: The prepared nanosuspension studied for the presence of the GO particles in the nanosuspension. Shimadzu UV 1800 instrument was used for the UV-Vis studies. The principle of the UV-Vis is based on the absorption of the incoming light in the range of 190-1100 nm.

Figure 4.11 shows the UV-Vis spectra of GO suspension with water, NMP, DMF, THF, and EG. As per literature, when we study the pure liquid, each liquid has its characteristic spectra. Each liquid has a different cut-off wavelength for which UV-Vis spectra are not detected because of liquid own frequency range falls in that region. In table 4.1, the cut-off frequency of the liquid is provided. [15],[16]

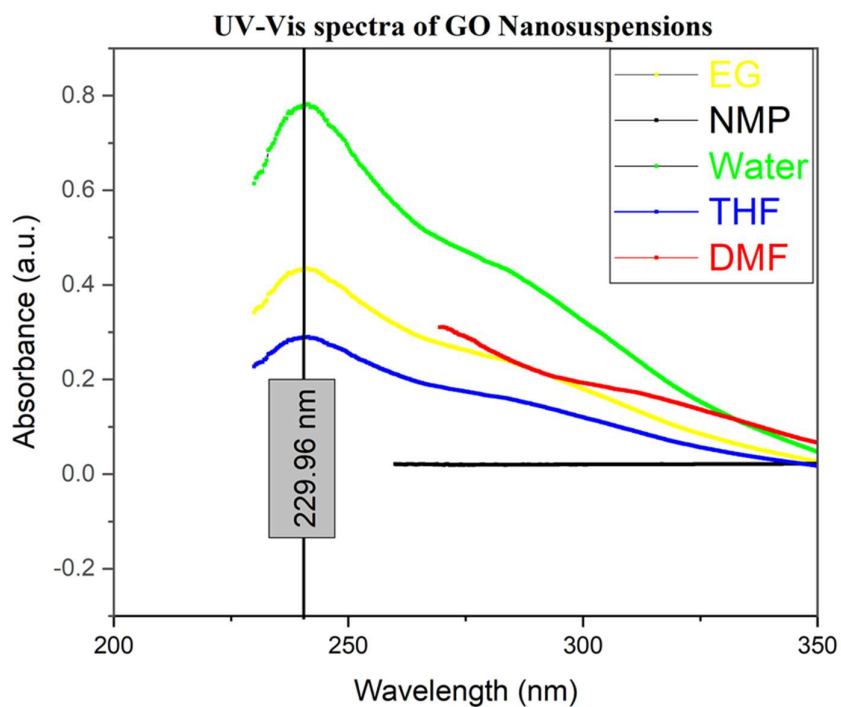


Figure 4.11 shows the UV-Vis spectra of GO nanosuspensions.

Table 4.1 UV Cutoff wavelength for the liquids under study.	
Liquid	UV cut-off wavelength
Water	190 nm
DMF	268 nm
THF	220 nm
NMP	280 nm
EG	180 nm

Before starting the study of each pure sample has been studied for the reference. In this study, we took 4 ml of the sample in the quartz cuvette diluted to the minimum. This sample was placed in the UV-Vis instrument for the spectra study. Similarly, we studied the spectra of all the prepared nanosuspension. The UV cut-off wavelength of the water is 190 nm. As per literature, the peak of GO presence is in the range of 225 to 240 nm. In figure 4.11, we found a peak at 229.9 nm. Samples of water, THF, and EG show the presence of GO. In the case of NMP, the UV cut-off wavelength is 280 nm. That is why there is not any hint of the existence of GO can be given by this liquid. In the case of DMF, the UV cut-off wavelength is 268 nm, but a slope of the graph is increasing just gives a hint of the presence of GO. Here we approve the presence of the GO in the liquids understudy with the help of UV-Vis spectroscopy.

4.3.2 HRTEM: In this research, we study liquid samples for High-resolution tunneling microscope micrographs. Here we used a drop of the liquid nanosuspension sample to examine the GO particle in the nanosuspension. TEM study completed with the help of the JOEL JEM-2100 plus electron microscope with a working voltage of 80 to 200 kV, magnification of 15,000,00 lakh, Resolution of 0.194 nm (point), attached with Charge Couple Device (CCD).

The morphology of GO, consisting of thin stacked flakes of shapes and having well defined multifaceted composition at the edge, can be seen in figure 4.12 (a) and 4.12 (b). GO sheets shows the different thickness and sheet-like morphology.

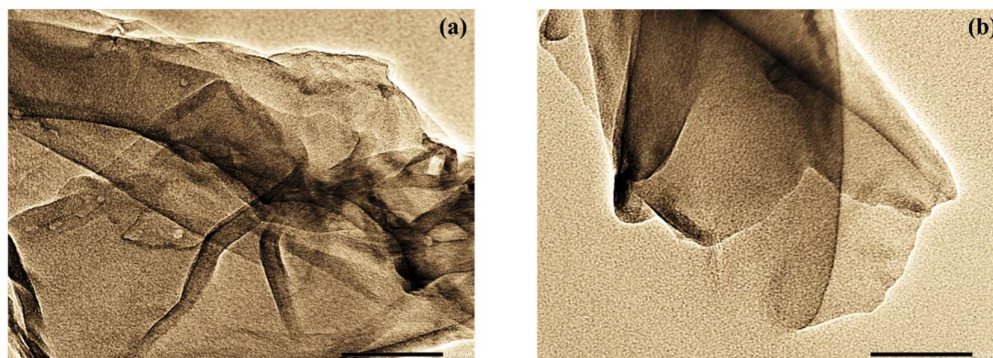


Figure 4.12 (a) shows the HRTEM Micrograph for prepared GO samples at 100 nm magnification. Figure 4.12 (b) shows the HRTEM Micrograph for prepared GO sample at 50 nm Magnification.

The dark colour in the figures shows the compact stacking of the graphene oxide sheets or the presence of the oxygen atoms between the layers; on the other hand, light colours show the thin stacking of films of few-layer GO. The disordered and unwrinkled structure was owing to no removal of oxygen atoms and a high degree of exfoliation during the oxidation process. Moreover, irregular shapes and unorganized particle sizes were caused by cracking of the structure.

4.3.3 DLS: The measurement standard of Dynamic Light Scattering (DLS) depends on the Zigzag movement of particles. Here in this study, there is some sample, which is an exhibit. DLS allows measurement of colloids, such as Solid particles, polymers dispersed in solvent Emulsions. We used quartz cuvettes to measure the samples. While pouring the sample into the cuvette, make sure there are no air bubbles in the sample. The z-values of the hydrodynamic diameter is plotted in figure 4.13.

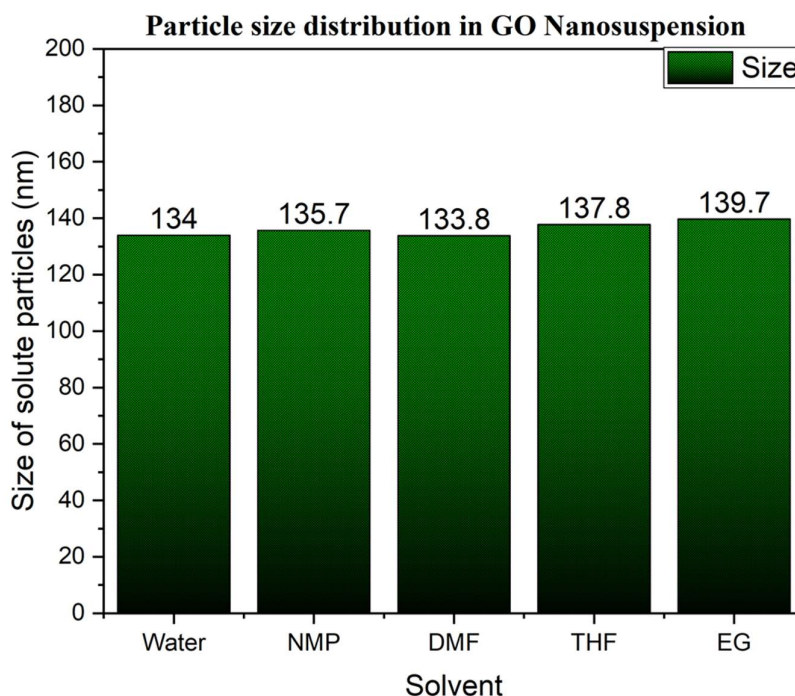


Figure 4.13 Shows the particle size distribution of the GO in different solvent

We calculated the hydrodynamic diameter for all samples prepared. The average size

of the particles comes out to be from 134 to 140 nm in the case of GO suspension. The prepared sample has a range of sizes between 100 to 500 nm. So, we can say our sample is a nanosuspension, as described in the literature. [5], [17-18]

4.4 Characterization of rGO Nanosuspension

Nanosuspension of the rGO has been prepared with the help of ultrasonication, as discussed in methodology. The ultrasonication helps to decrease the particle size of the rGO particles in the solvent, and extensive ultrasonication helps to increase the stability of the solution.

4.4.1 UV-VIS: The prepared nanosuspension studied for the presence of the rGO particles in the nanosuspension. Shimadzu UV 1800 instrument was used for the UV-Vis studies. The principle of the UV-Vis is based on the absorption of the incoming light in the range of 190-1100 nm. Figure 4.14 shows the UV-Vis spectra of GO suspension with water, NMP, DMF, THF, and EG. As per literature, when we study the pure liquid, each liquid has its characteristic spectra. Each fluid has a different cut-off wavelength for which UV-Vis spectra are not detected because of liquid own frequency range falls in that region. In table 4.14, the cut-off frequency of the liquid is provided.

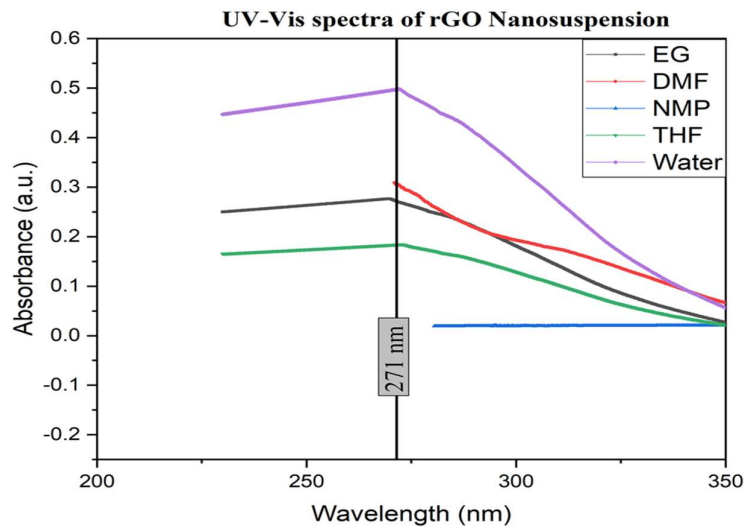


Figure 4.14 shows the UV-Vis spectra of GO nanosuspensions.

Before starting the study of each pure sample has been studied for the reference. In this study, we take 4 ml of the sample in the quartz cuvette diluted to the minimum. We place this sample in the UV-Vis instrument for the spectra study. Similarly, we have studied the spectra of all the prepared nanosuspension. The UV cut-off wavelength of the water is 190 nm. As per literature, the peak of rGO presence is in the range of 260 to 275 nm. In figure 4.14, their peak is a peak at 271 nm. Samples of water, THF, DMF, and EG show the presence of GO. In the case of NMP, the UV cut-off wavelength is 280 nm. That is why there is not any hint of the existence of GO can be given by this liquid. In the case of DMF, the UV cut-off wavelength is 268 nm, but a slope of the graph is increasing to the top just gives a hint of the presence of rGO. The presence of the rGO in the liquids was approved with the help of UV-Vis studies. [15], [16]

4.4.2 HRTEM: We studied the liquid samples with a High-resolution tunneling microscope for micrographs. A drop of the fluid nanosuspension sample was used to study the rGO particle in the nanosuspension. TEM study completed with the help of the JOEL JEM-2100 plus electron microscope with a working voltage of 80 to 200 kV, magnification of 15,000,00 lakh, Resolution of 0.194 nm (point), attached with Charge Couple Device (CCD).

The morphology of rGO, consisting of thin stacked flakes of shapes and having well defined multifaceted composition at the edge, can be seen in figure 4.15 (a) and 4.15 (b). rGO sheets show the different thicknesses and sheet-like morphology. The dark colour in the figures shows the compact stacking of the reduced graphene oxide sheets or the presence of the oxygen atoms between the layers; on the other hand, light colours show the thin stacking of films of few-layer rGO. The disordered and unwrinkled structure was owing to no removal of oxygen atoms and a high degree of exfoliation during the reduction process. Moreover, irregular shapes and unorganized particle sizes were caused by cracking of the structure.

4.4.3 DLS: The measurement standard of Dynamic Light Scattering (DLS) centered on the Zigzag movement of particles. This measurement inhibits the variety of samples that are evaluated with this technique. DLS allows analysis of colloids, such as Solid particles, polymers dispersed in a solvent Emulsions. Quartz cuvettes were used to

measure the samples. While pouring the sample into the cuvette, make sure there are no air bubbles in the sample. The z-values of the hydrodynamic diameter are plotted in figure 4.16.

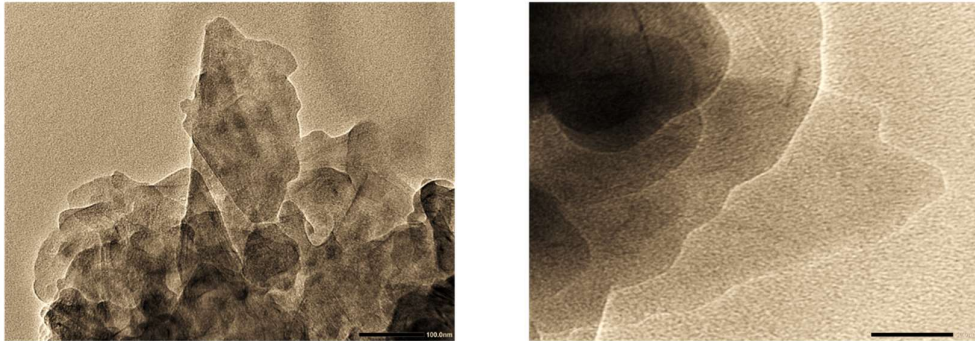


Figure 4.15 (a) shows the HRTEM Micrograph for prepared rGO samples at 100 nm magnification. Figure 4.15 (b) shows the HRTEM Micrograph for prepared rGO sample at 50 nm Magnification.

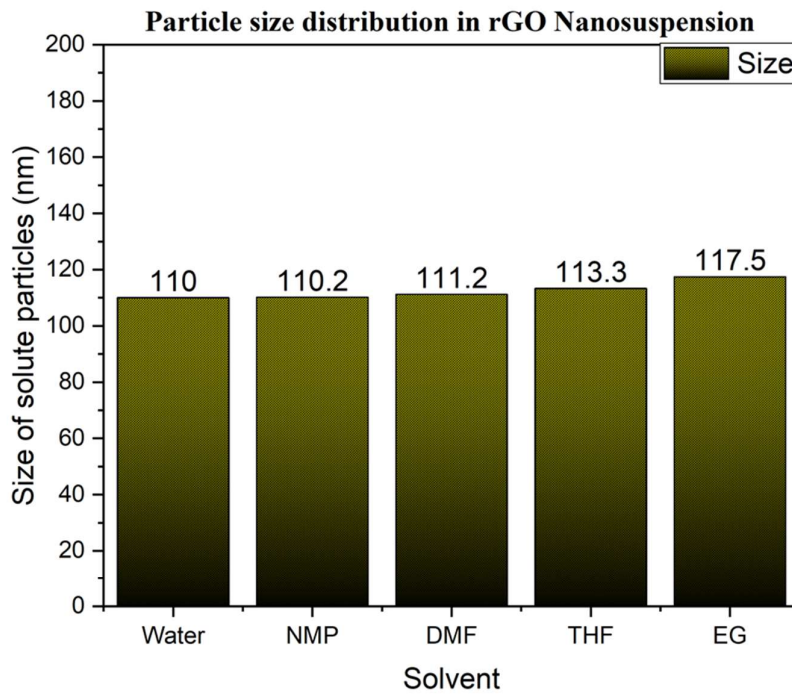


Figure 4.16 Shows the particle size distribution of the rGO in different solvent

We calculated the hydrodynamic diameter for all the prepared samples. The average size of the particles comes out to be from 110 to 120 nm in the case of rGO suspension. The ready sample has a range of sizes between 100 to 500 nm. So, we can say our sample is a nanosuspension, as described in the literature. [5], [17], [18].

4.5 Reference.

- [1] X. Han et al., *Nanotechnology*, **24**, 20 (2013).
- [2] S. Sheshmani and M. A. Fashapoyeh, *ACTA Chem*, **60**, 813 (2013).
- [3] S. Pei and H. M. Cheng, **50**, 3210 (2012).
- [4] L. Wang, Y. Huang, and H. J. Huang, *Mater. Lett.*, **124**, 89 (2014).
- [5] I. Roy, *RSC Adv.*, **6**, 10557 (2016).
- [6] Y. Wang, X. Wu, W. Zhang, J. Li, C. Luo, and Q. Wang, *Synth. Met.*, **229**, 82 (2017)
- [7] G. Zhu, C. Xi, Y. Liu, J. Zhu, and X. Shen, *J. Mater. Chem. A*, **3**, 7591 (2015)..
- [8] Z. Luo, L. Zhu, Y. Huang, and H. Tang, *Synth. Met.*, **175**, 88 (2013).
- [9] Marcano et al., *ACS Nano*, **4**, 4806 (2010).
- [10] J. Liu et al., *RSC Adv.*, **3**, 11745 (2013).
- [11] M. Zong, Y. Huang, and N. Zhang, *Appl. Surf. Sci.*, **345**, 272 (2015).
- [12] P. Su, H. L. Guo, L. Tian, and S. K. Ning, *Carbon N. Y.*, **50**, 5351 (2012).
- [13] W. Feng et al, *Carbon N. Y.*, **108**, 52 (2016).
- [14] S. Stankovich et al., *Carbon N. Y.*, **45**, 1558 (2007).
- [15] J. I. Paredes, A. Marti, J. M. D. Tasco, and A. Marti, *Langmuir*, **24**, 10560 (2008).
- [16] D. Li, M. B. Müller, S. Gilje, R. B. Kaner, and G. G. Wallace, *Nat. Nanotechnol.*,

3, 101 (2008).

[17] J. Ma, J. Liu, W. Zhu, and W. Qin, *Colloids Surfaces A Physicochem. Eng. Asp.*, **538**, 79 (2018).

[18] H. Bao et al., *Small*, **7**, 1569 (2011).

Section 1 (Part A)

Study of Water-GO Nanosuspension

4.6 Introduction

Nanosuspension is a colloidal dispersion of nanoparticles that can be controlled by various techniques. The particle size range for solid particles in nanosuspensions is typically smaller than one micron with a median particle size ranging between 100 and 500 nm. [30]. Dispersion of nanoparticle in a base fluid can offer a tremendous change in its properties, and because of the extraordinary properties shown by various nanoparticles of metals, metals oxides, ceramic, and Carbon, it becomes the attraction for many researchers. One fascinating feature of nanofluids is that they have anomalously high thermal conductivity [15], [33], [36], which makes nanosuspension durable material for the next generation of coolants for improving the design and performance of thermal management systems. [44]. The Brownian motion of nanoparticles in a base liquid is proposed to be one of the significant physical mechanisms of the thermal conduction of nanofluids. Therefore, it is vital to investigate the movements of nanoparticles in nanosuspension. Ultrasonication is an accepted technique for the study of such Brownian motion and dispersing aggregated nanoparticles for the preparation of aqueous nanosuspensions [48]. Most of the studies have focused on the effect of sonication time on the stability of nanosuspensions, and all of them used continuous ultrasonic waves to sonication [26]. The ultrasonic properties of solid-liquid suspensions in the micrometer size of the particles can cause changes in ultrasonic velocity and ultrasonic attenuation that can affect the thermal conductivity of nanofluids. More specifically, there is an increasing interest mostly in the acoustic properties for acoustic telemetry suspensions via drilling fluids, as well as the rising market for ultrasonic components. Several scientists have researched ultrasonic propagation behavior by suspending solid particles, especially in the nanometre scale of a fluid, intending to find a process that allows vital information to be derived from the behavior of ultrasonic materials, such as particle size, density, and mechanical properties of the constituents. Due to their relatively large surface-to-volume ratio, nanoparticles arrested in base liquid substantially expose some new

features that are not always present in either of the pure components. Hence it is essential to investigate the influence of nanoparticles on the properties of the base liquid to anticipate the final properties of the complex fluids effectively.

Graphene is one of the most significant finds of the last decade in terms of many physical and chemical properties. Since its evolution in 2004 range of features has been reported like: high electron mobility, high thermal conductivity, impermeable to gasses, most durable material ever published, etc. Despite all of these excellent properties still, there are several challenges associated with this material, like industrial-scale productivity, the stability of GO in different available solvents [6], [10], [18], [37].

In the present work, we have conducted a study of ultrasonic waves in colloidal dispersion of GO nanoparticles with different concentrations in water to take advantage of the GO properties in the form of nanosuspension. Structural, morphological, and fluid-particle interaction studies have been completed and compared. Various acoustical parameters like ultrasonic velocity, density, viscosity were calculated at a temperature range of 298 to 313 K and explained.

4.7 Material and Method

4.7.1 Reagent and chemicals

Graphite powder, sodium nitrate procured from Sigma Aldrich, KMnO_4 , HCL, H_2SO_4 , and Ammonia has been taken from CDH. H_2O_2 has been purchased from fisher scientific. All chemicals used in this research were of AR grade and used without additional purification. Throughout the experiment, double distilled water was used.

4.7.2 Methods

Graphene Oxide was prepared using Hummers Method. In short, 3g of graphite powder and 6g of NaNO_3 was added in the glass flask containing 120 ml of H_2SO_4 kept on an ice bath maintaining 0 °C. After continuous stirring of 45 minutes, 12 gm of KMnO_4 was added in the suspension, very slowly maintaining the temperature below 90 °C. The mixture is maintained close to 0 °C and kept on continuous stirring for 2 hours. After this mixture is placed in the water bath maintained at 40 °C to increase the

oxidation reaction. The color of the mixture begins to change from black to brown. Eventually, 30% of the H_2O_2 is applied to the solution to halt the reaction. The solution is treated with distilled water and sprayed with HCl to remove excess metal ions. The paste is adequately cleaned, purified, and air-dried with 2 liters of distilled water. Synthesized GO is spread by continuous ultrasonicate in distilled water. Suspension of various concentrations was prepared without adding any further chemical treatment. [1], [12], [26], [28].

4.8 Characterization of GO and Water-GO nanosuspension

Nova Nano FESEM 450 with attached EDAX was used for the micro-level imaging of prepared samples. Shimadzu 8400S spectrometer was used for the Fourier transform spectroscopy in range from 400 to 4000 cm^{-1} . Panalytical X'Pert Pro with wavelength 1.54 \AA used for the XRD spectra. Confocal Raman Spectrometer Airix STR 500 was used to study the Raman spectrometric studies. Shimadzu UV-1800 spectrometer was used to review the UV-Vis studies of the prepared nanosuspension samples. The average particle size in nanosuspension was verified with the help of Malvern Zetasizer Nano ZS90. The ultrasonic velocity of the prepared samples calculated with the help of Mittal Interferometer M – 81 with a fixed frequency of 2 MHz. Density was calculated with the help of a pycnometer. The labman model of LMDV-200 was used to calculate the viscosity of all prepared samples.

4.9 Data Table

Table 4.2. Water-GO Nanosuspension 1

Concentration (mg/ml)	Temperature(T) (K)	Average Velocity(U)	Density(ρ)	Viscosity(η)	Adiabatic Compressibility(β)
		(m/s) $U = \lambda \times f$	(Kg/m ³)	(Pa-s)	(1/Pa) $\beta = 1/ (U^2 \times \rho)$
0	299	1498.461	997	0.00089	4.47E-10
0.2	299	1501.538	1005	0.015014	4.41E-10
0.4	299	1504.615	1004.3	0.015044	4.40E-10
0.6	299	1506.550	1003.3	0.015822	4.39E-10
0.8	299	1507.692	1002.4	0.01602	4.39E-10
1	299	1510.460	1000.8	0.016612	4.38E-10
0	304	1507.692	995.4	0.000797	4.42E-10

0.2	304	1510.846	1003.2	0.014089	4.37E-10
0.4	304	1512.923	1002.1	0.01425	4.36E-10
0.6	304	1514.850	1001.2	0.0151	4.35E-10
0.8	304	1515.846	1000.3	0.015075	4.35E-10
1	304	1518.692	999.4	0.015978	4.34E-10
0	309	1516.150	993.8	0.000719	4.38E-10
0.2	309	1519.080	1002.1	0.0136	4.32E-10
0.4	309	1521.170	1001	0.01382	4.32E-10
0.6	309	1524.050	1000.1	0.014575	4.30E-10
0.8	309	1526.140	998.7	0.014675	4.30E-10
1	309	1529.320	998.1	0.015528	4.28E-10
0	314	1525.310	992.2	0.000653	4.33E-10

0.2	314	1528.540	1000.8	0.013263	4.28E-10
0.4	314	1530.230	999.5	0.01346	4.27E-10
0.6	314	1532.230	998.1	0.014289	4.27E-10
0.8	314	1534.860	996.9	0.01426	4.26E-10
1	314	1537.150	995.5	0.01462	4.25E-10

Table 4.3 Water-GO Nanosuspension 2

Concentration (mg/ml)	Temperature(T) (K)	Acoustical impedance(Z) (Pa. s/m³) Z = ρ × U	Attenuation (α/f²) (m⁻¹) α/f² = 8π²η /3ρU³	Bulk Modulus(K) (Pa) K = ρ U²	Relaxation Time(τ) (s) τ = 4βη/3	Intermolecular Free Length (L_f) (L_f = K_T × β^{1/2})
0	299	1493966.154	6.97567E-15	2238650821	5.30E-13	4.59E-10
0.2	299	1509046.154	1.16024E-13	2265890840	8.83E-12	4.54E-10
0.4	299	1511085.231	1.15625E-13	2273602086	8.82E-12	4.52E-10
0.6	299	1511521.615	1.21257E-13	2277182889	9.26E-12	4.51E-10
0.8	299	1511310.769	1.22606E-13	2278591621	9.37E-12	4.51E-10
1	299	1511668.368	1.26641E-13	2283314603	9.70E-12	4.50E-10
0	304	1500756.923	6.14258E-15	2262679669	4.70E-13	4.59E-10
0.2	304	1515680.862	1.07068E-13	2289960600	8.20E-12	4.53E-10

0.4	304	1516100.215	1.07965E-13	2293743003	8.28E-12	4.52E-10
0.6	304	1516667.82	1.14071E-13	2297524247	8.76E-12	4.52E-10
0.8	304	1516300.908	1.1376E-13	2298478899	8.74E-12	4.51E-10
1	304	1517781.092	1.20006E-13	2305042470	9.24E-12	4.50E-10
0	309	1506749.87	5.45797E-15	2284458815	4.20E-13	4.58E-10
0.2	309	1522270.068	1.01792E-13	2312450015	7.84E-12	4.53E-10
0.4	309	1522691.17	1.03126E-13	2316272127	7.96E-12	4.52E-10
0.6	309	1524202.405	1.08242E-13	2322960675	8.37E-12	4.51E-10
0.8	309	1524156.018	1.0869E-13	2326075465	8.41E-12	4.50E-10
1	309	1526414.292	1.1436E-13	2334375905	8.87E-12	4.49E-10
0	314	1513412.582	4.87604E-15	2308423345	3.77E-13	4.57E-10
0.2	314	1529762.832	9.75646E-14	2338303679	7.56E-12	4.51E-10

0.4	314	1529464.885	9.88144E-14	2340433051	7.67E-12	4.51E-10
0.6	314	1529318.763	1.04637E-13	2343268088	8.13E-12	4.50E-10
0.8	314	1530101.934	1.04013E-13	2348492254	8.10E-12	4.49E-10
1	314	1530232.825	1.06313E-13	2352197387	8.29E-12	4.49E-10

4.10 Result and Discussion

4.10.1 Morphological and elemental analysis

Figure 4.17 corresponds to the FESEM image of the GO sample at 200000 X magnification. The picture shows how layers of Carbon are stacked together in GO. The EDS graph of GO shows the present content of Carbon and oxygen present in the prepared samples, which come out to be 74.33% and 24.46%, respectively, in figure 4.18. A large amount of oxygen content present in the prepared sample shows the excellent oxidation of Carbon. It proves the conversion of graphite powder into GO. [35], [46].

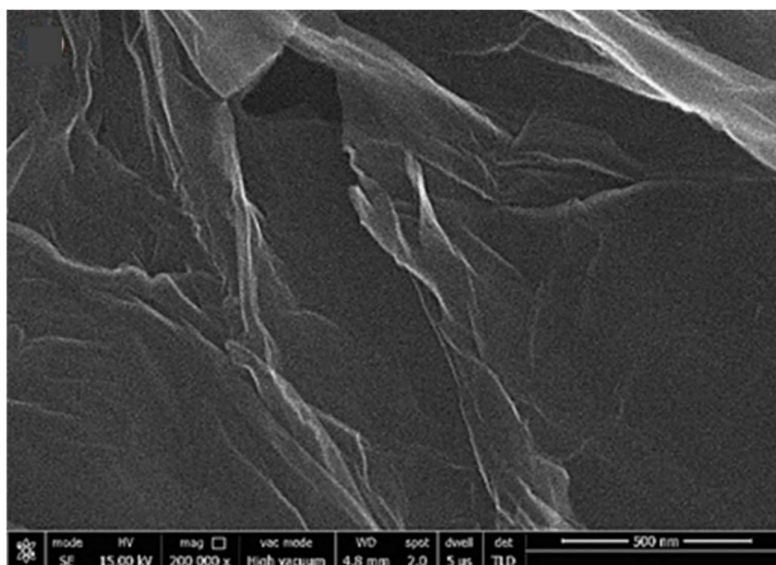


Figure 4.17 FESEM Micrograph for GO

Figure 4.19 corresponds to the FTIR spectrum of GO. Peaks at 1116.82 cm^{-1} correspond to alkoxy C—O stretching vibration and C—O epoxy stretching vibrations. 1618.33 cm^{-1} correspond to C=C Skelton vibrations of the Graphene network; 2345.51 cm^{-1} shows the presence of CO_2 [24], [47], [49]. XRD spectra of GO is shown in figure 4.20. The sharp peak at 8.93 contributed toward the (001) crystal plane of GO. The lower value of angle corresponds to the increase in the interplanar distance of the layers of Graphene because of oxygen atoms trapped inside these layers [21-23]

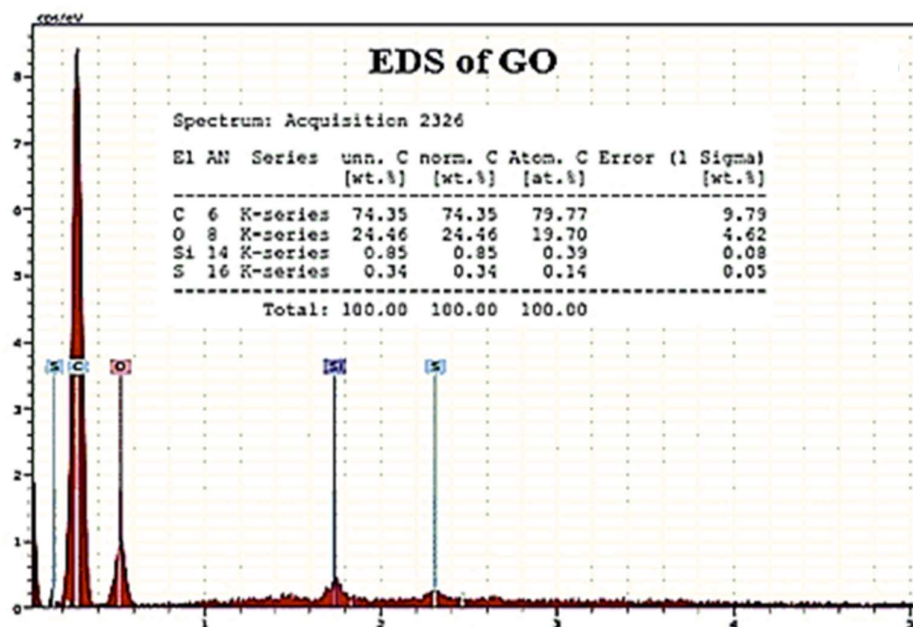


Figure 4.18 EDS for GO

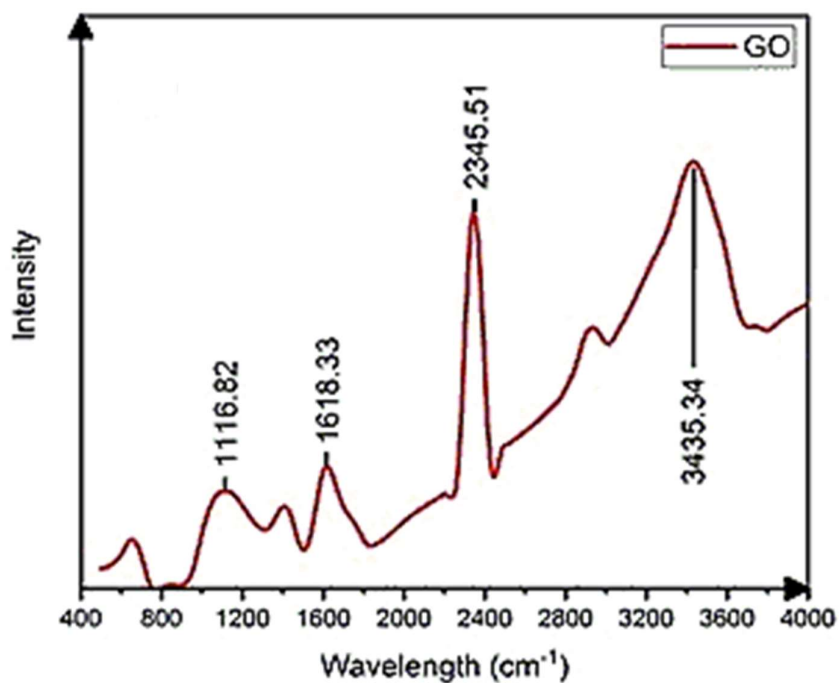


Figure 4.19 FTIR for GO

The peak at 1352.37 cm⁻¹ in figure 4.21 corresponds to defects in the graphene network,

and the second peak at 1594.21 cm^{-1} corresponds to the Graphene Network peak, respectively. The intensity ratio of structure defect and Graphene network ratio is $I_D/I_G = 0.84$ which

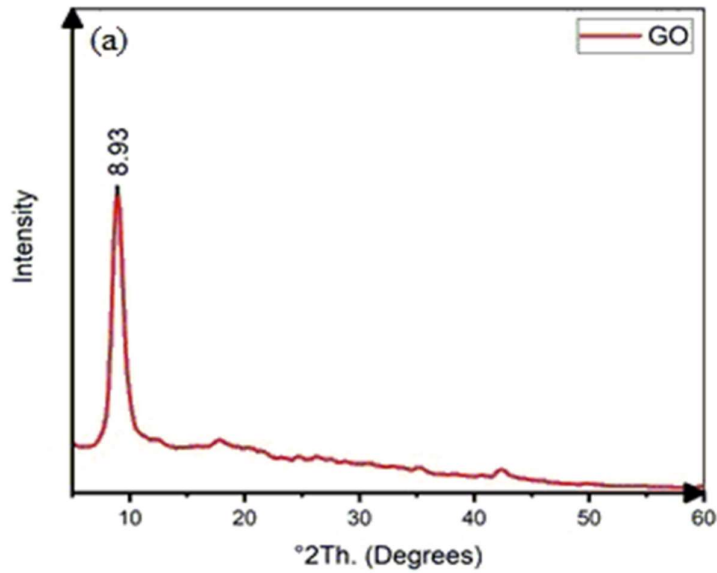


Figure 4.20 XRD for GO

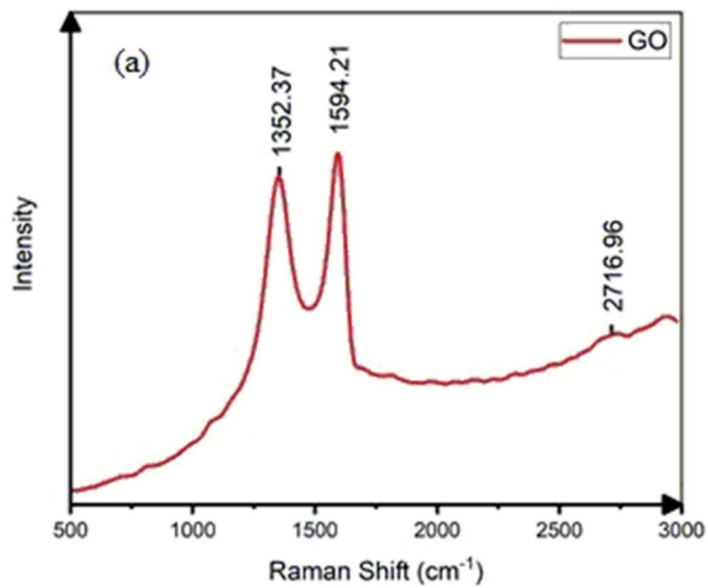


Figure 4.21 Raman Spectra for GO

corresponds to the excellent structure retainment of the graphene network. [8], [39], [40]

4.10.2 Colloidal Stability analysis

The nanosuspension of water-GO was prepared with the help of extensive ultrasonication. The UV-Vis spectra are shown in figure 4.22. The peaks at the position of 239 nm confirm the presence of GO in the nanosuspension [12], [20]. The average diameter of GO in water is obtained using a dynamic light scattering (DLS) shown in figure 4.21. It is seen that the average size of the GO is in the array of 130 to 155 nm for all five prepared samples [4], [25], [35]. With the help of average particle size calculation by DLS, we can categorize the prepared sample as nanosuspension.

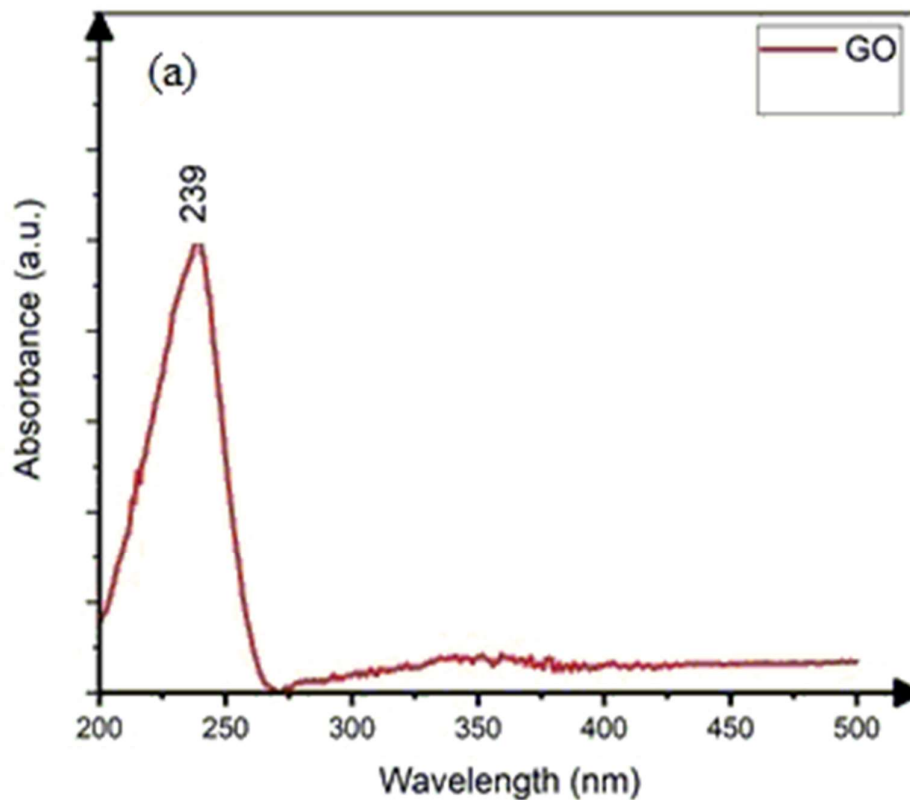


Figure 4.22 UV-Vis for Water-GO nanosuspension

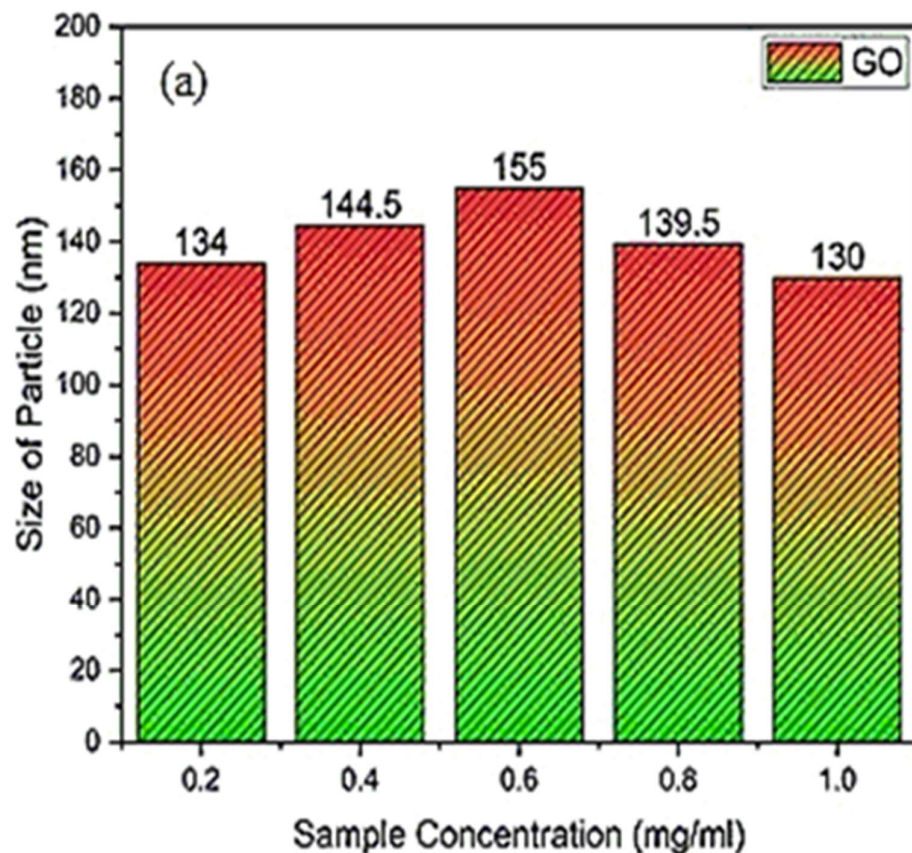


Figure 4.23 DLS for Water-GO nanosuspension

4.10.3 Thermoacoustic analysis

The following parameters have been measured in the study.

4.10.3.1 Ultrasonic Velocity

Ultrasonic velocity is one of the most important parameters for understanding the intraparticle and intermolecular interaction of nanosuspension specimens. The ultrasonic speed of double distilled water and its solution was measured at four different temperatures (298, 303, 308, and 313 K) and 1atm pressure. The reading of velocity, density, and viscosity was repeated several times for accuracy. All measurements for pure water are matched with literature to prevent error. The dissimilarity of ultrasonic

velocity with the concentration of nanosuspension and temperature contributes to the understanding of the liquid. Figure 4.24 indicates the difference of ultrasonic velocity with the concentration of GO in the fluid.

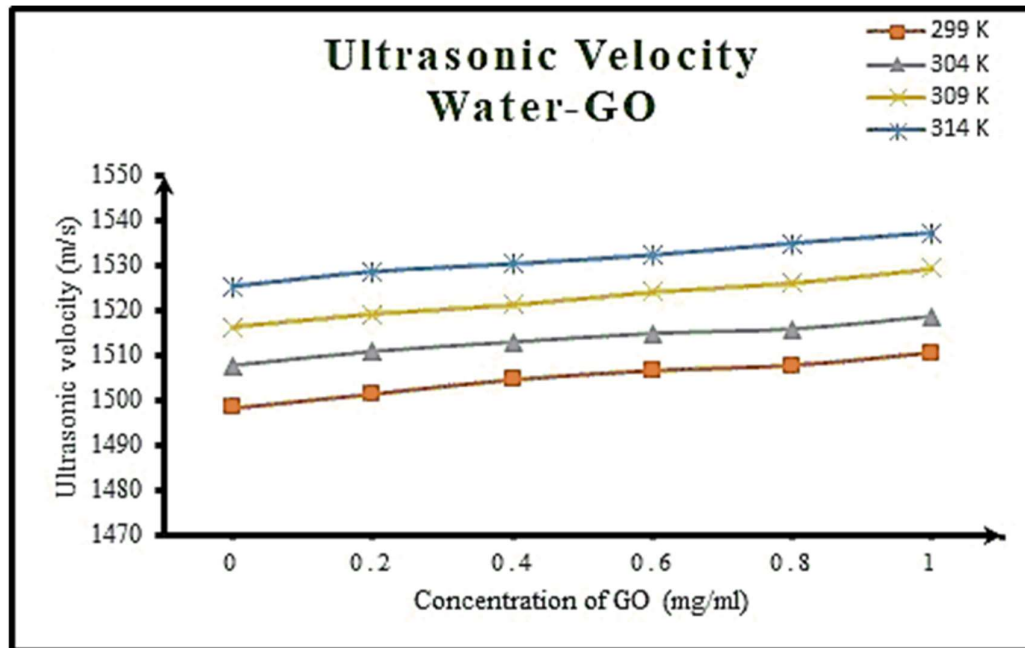


Figure 4.24 Velocity of sound in Water-GO nanosuspension

Ultrasonic velocity grows in water-GO nanosuspension with the upsurge in the concentration of the particles. The increment in the ultrasonic speed has been accredited to the dominance of intramolecular interaction over intermolecular interaction. With the growth in the concentration of the particles, there is a likelihood of an increase in the Brownian motion of nanosuspension and an increase in the surface layer, which further helps to increase the ultrasonic velocity. Growth in the temperature of the nanosuspension also increases in the Brownian motion of the fluid molecules, which further increases the speed of the fluid. [5], [19], [31], [42]

4.10.3.2 Density

As shown in Figure 4.25, as soon as the GO particle has been added to the pure water, density increases from 997 kg/m^3 to 1005 kg/m^3 for water-GO nanosuspension at 0.2 mg/ml . After this continuous decrease in the density of the prepared nanosuspension with

a rise in the concentration of the particles can be seen. The decline in density is due to an increase in intramolecular interaction rather than intermolecular interaction. Density drops with the rise in the temperature of nanosuspensions [34], [45]

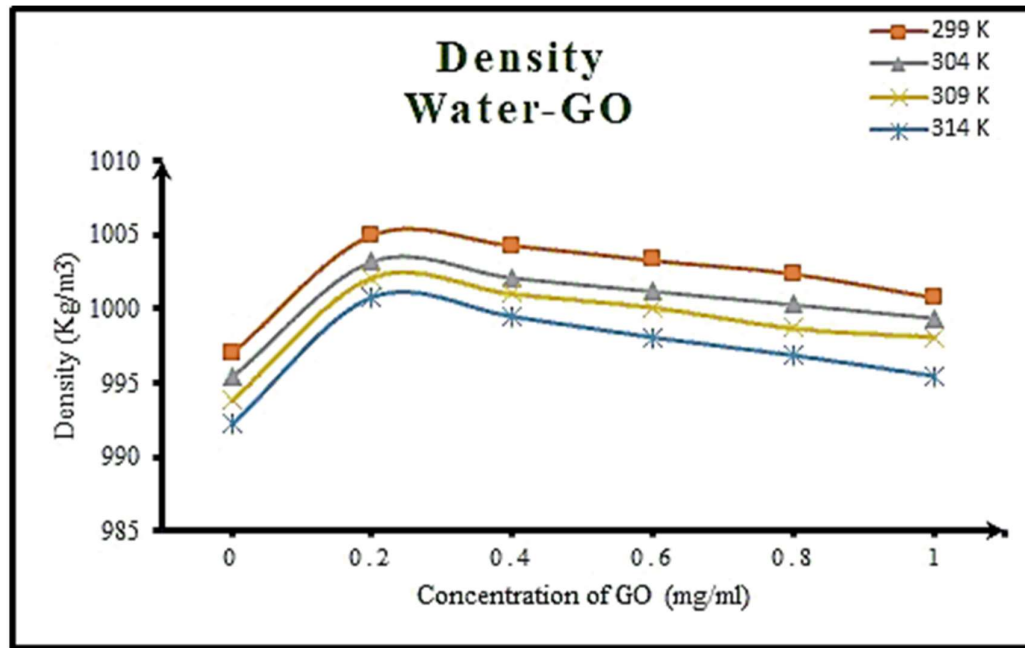


Figure 4.25 Density of Water-GO nanosuspension

4.10.3.3 Viscosity

The viscosity of the water-GO nanosuspension declines with a rise in temperature due to the increase in the Brownian motion of the water molecules, as shown in figure 4.26. The increase in the temperature flow of nanosuspension also becomes easy. Viscosity also increases slightly with an increase of particle loading in nanosuspension, which is due to a restriction in the flow produced by GO nanoparticles. These particles get tangled with each other to restrict the flow of liquids [2], [31], [33].

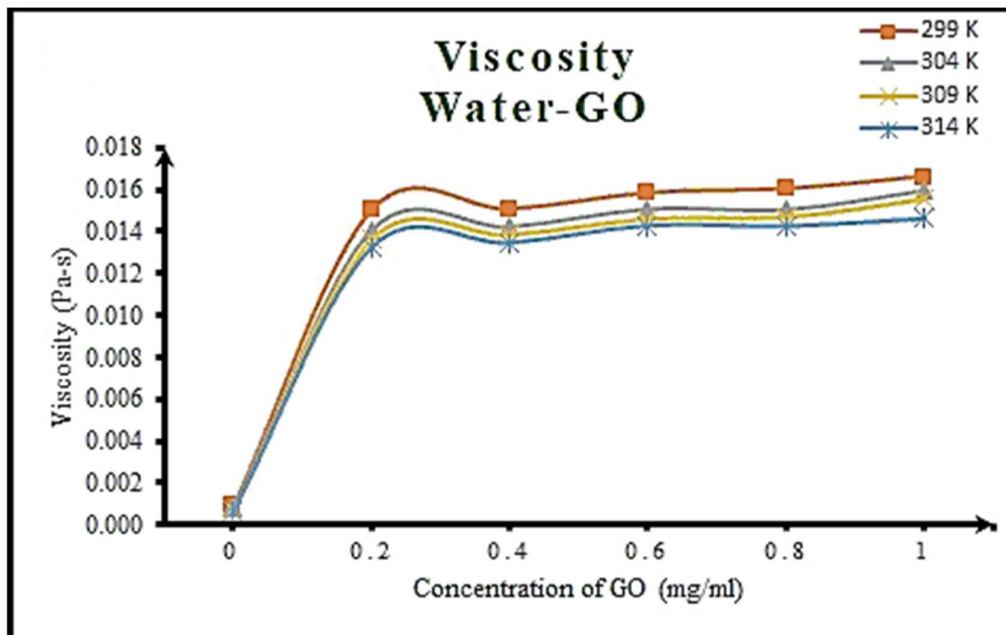


Figure 4.26 Viscosity of Water-GO nanosuspension

4.10.3.4 Adiabatic Compressibility

Figure 4.26 shows a decrease in adiabatic compressibility with a rise in the concentration of the particles.

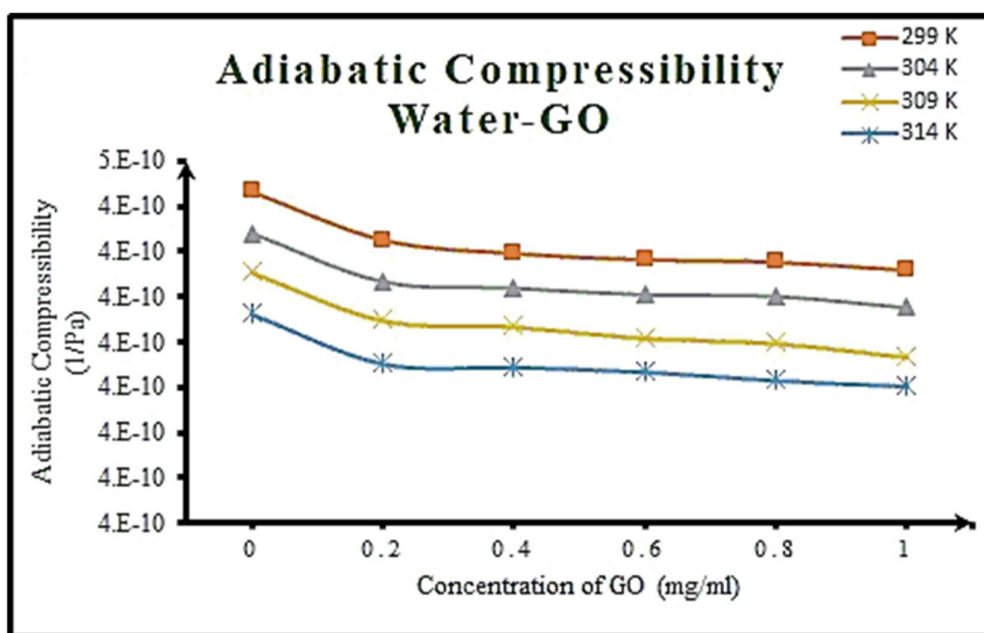


Figure 4.27 Adiabatic Compressibility of Water-GO nanosuspension

Decreased adiabatic compressibility with increased concentration of the particles promotes fluid-particle interaction. Besides, adiabatic compressibility also decreases with an increase in system temperature [11], [14], [17], [42]

4.10.3.5 Acoustic Impedance

Figure 4.28 shows an increase in the value of acoustic impedance in nanosuspension with an increase in the number of particles. Increased amounts of acoustic impedance suggest that there is a significant collaboration between nanoparticles and liquid, which can affect the structural arrangement.

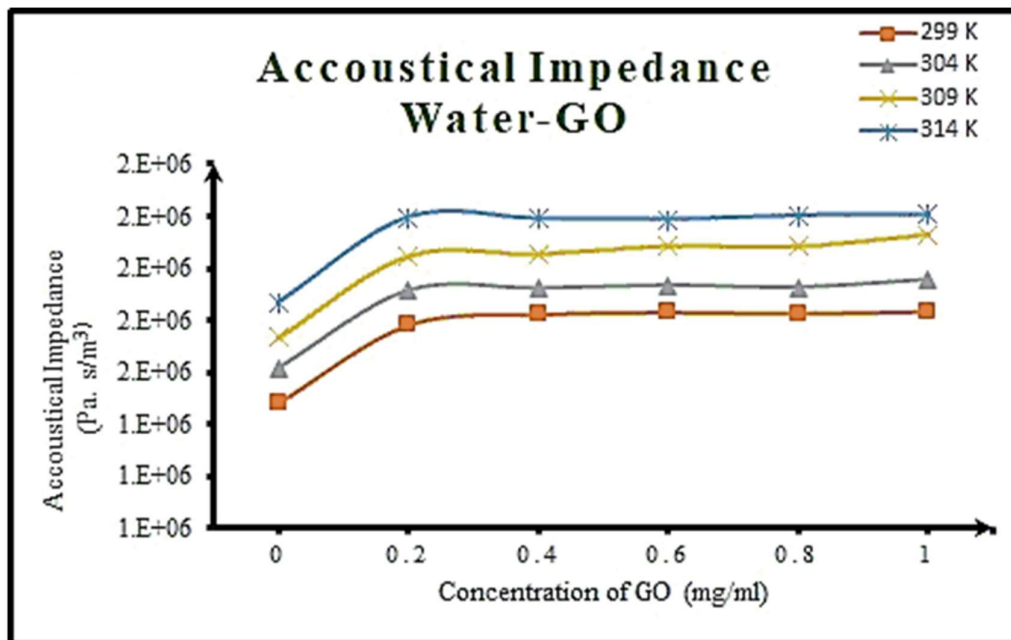


Figure 4.28 Acoustical Impedance of Water-GO nanosuspension

On the other side, the acoustic impedance for nanosuspensions increases with an uprise in temperature that can be due to the rise in the Brownian motion of base fluid molecules. Increasing particle-fluid interactions at lower concentrations widens the intermolecular gap, which provides resistance to the propagation of ultrasonic waves. [9], [16], [27], [38], [43]

4.10.3.6 Ultrasonic attenuation

Figure 4.29 demonstrates the attenuation of ultrasound waves when going through prepared nanosuspensions. Ultrasonic attenuation increases dramatically with the addition of nanoparticles to the base fluid because the network of these particles can block most of the ultrasonic waves from reaching the other end. Therefore, with the rise in the density of the samples, the attenuation decreases only marginally. Moreover, the reliance on attenuation on temperature can be seen in all other nanosuspension preparations.

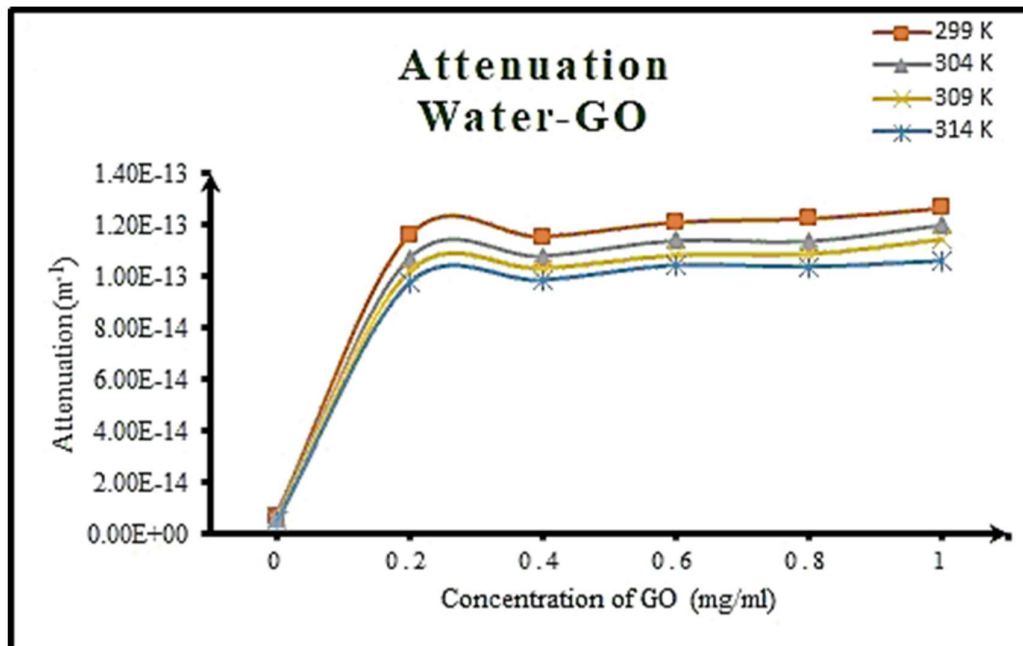


Figure 4.29 Attenuation of sound in Water-GO nanosuspension

As the temperature rises, the magnitude of the attenuation declines because of the rate of Brownian motion increases in the base liquid [13], [41]

4.10.3.7 Bulk Modulus

It can be described as the resistance of the liquid or fluid to the stress applied. In Figure 14, the bulk modulus tends to increase for the water-GO nanosuspension with the growth in the count of the particles in nanosuspension. Bulk modulus also increases with increased temperature.

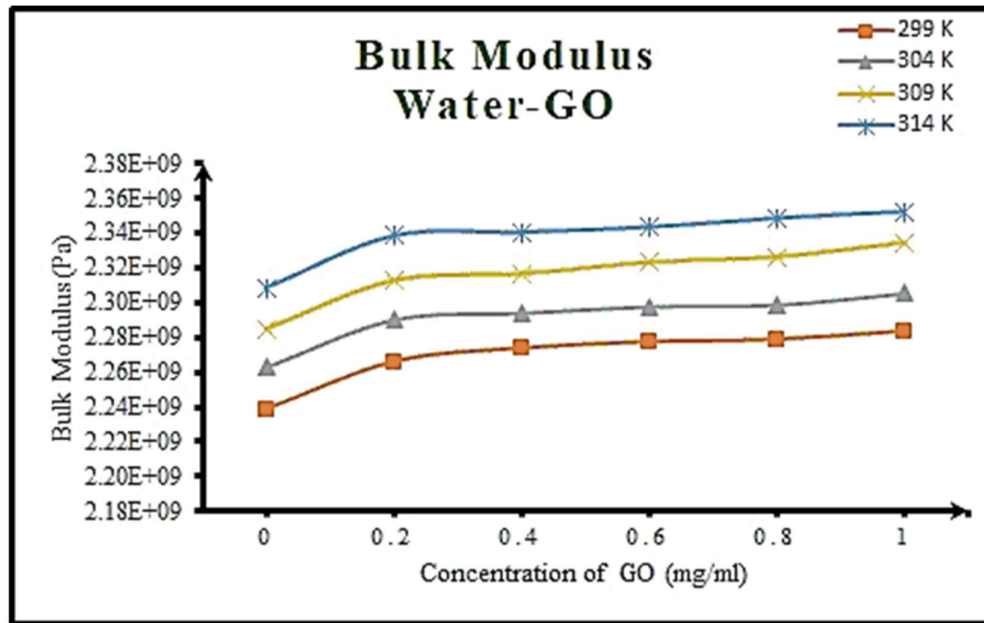


Figure 4.30 Bulk modulus of Water-GO nanosuspension

An increase in bulk modulus or reduction in compressibility attributes to the fact that robust collaboration forces act between molecules of the base fluid after the dispersion of GO nanoparticles in water [3], [7].

4.10.3.8 Relaxation Time

Figure 4.31 indicates the relaxation time of the water-GO nanosuspension. Relaxation time is the duration of molecular re-arrangement during the propagation of ultrasonic waves from the fluid. It can be seen clearly in Figure 4.31 that relaxation time rises from 5.3×10^{-13} s to 8.83×10^{-12} s purely because of the introduction of GO nanoparticles to pure water. Besides, a slight increase in relaxation time is seen in nanosuspensions. Relaxation time declines with an increase in temperature as the Brownian motion of water molecules rise with an increase in temperature [7], [29].

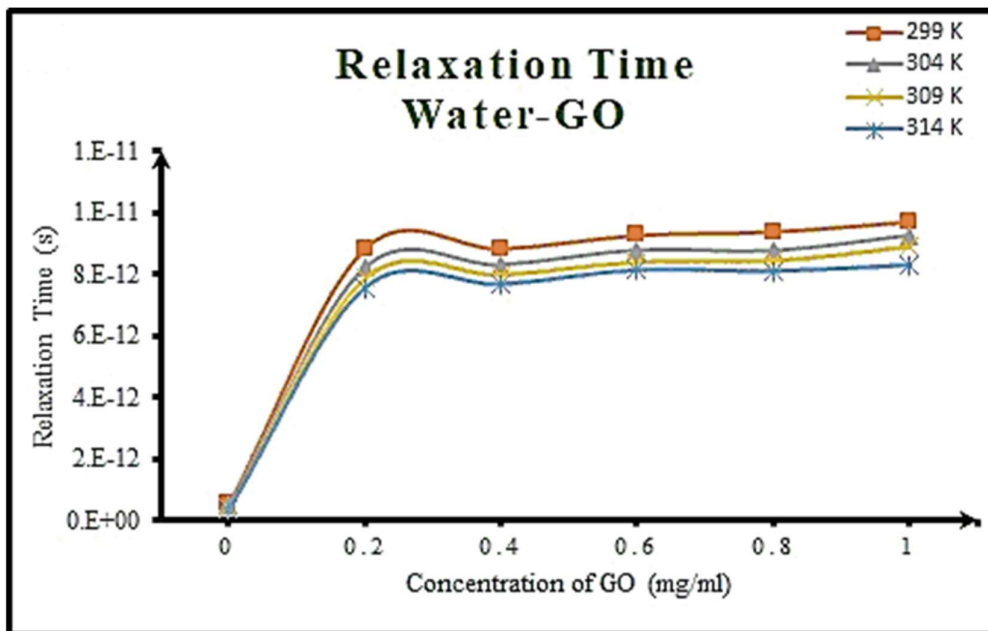


Figure 4.31 Relaxation time of Water-GO nanosuspension

4.10.3.9 Intermolecular free length

It can be clearly understood from Figure 4.32 that the intermolecular free length is a function of temperature.

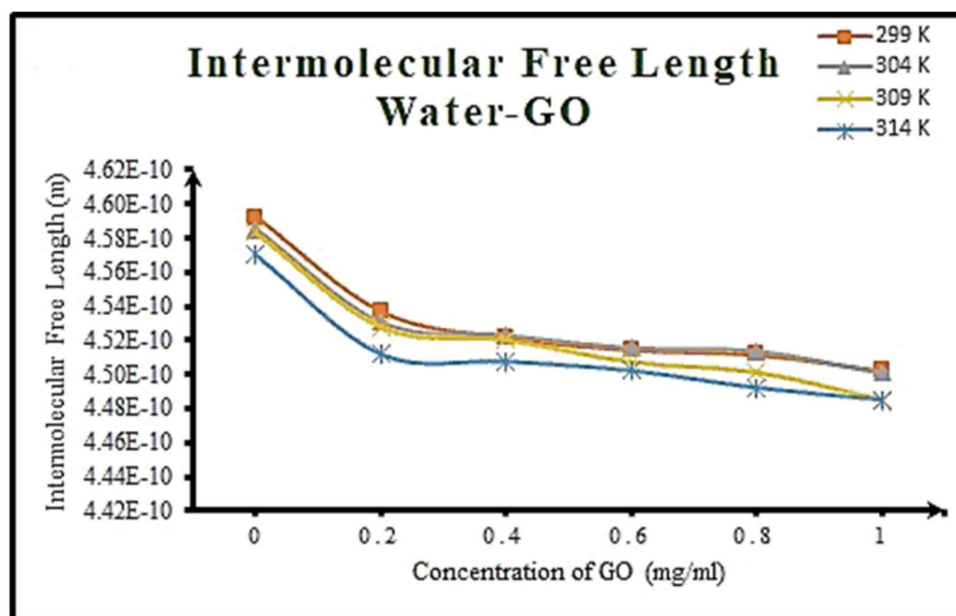


Figure 4.32 Intermolecular Free Length of Water-GO nanosuspension

As the temperature rises, the free intermolecular free length reduces as the relaxation period increases. Therefore, the intermolecular free length falls with an increase in the density of nanoparticles in the base liquid. This activity is the result of liquid and particle interactions in nanosuspension [9], [16].

4.11 References

- [1] Abulizi, A. et al. The Journal of Physical Chemistry C, **4(3)**, 6426, (2013).
- [2] Ashima, Juglan, K. C. and Kumar, H., Journal of Chemical Thermodynamics. Elsevier Ltd, **140**, 105916 (2020).
- [3] Ayachit, N. H. et al., Journal of Molecular Liquids, **133**, 134, (2007)
- [4] Bao, H. et al., Small, **7**, 1569, (2011)
- [5] Chakraborty, N. et al., Journal of Chemical and Engineering Data., **203**, 76, (2020)
- [6] El-Kady, M. F. et al., Science, **335**, 1326, (2012)
- [7] Elangovan, S. and Mullainathan, S., Indian Journal of Physics, **87**, 659. (2013).
- [8] Feng, W. et al., Carbon. Elsevier Ltd, **108**, 52, (2016).
- [9] Gupta, V., Sharma, A. K. and Sharma, M., Journal of Chemical and Pharmaceutical Research, **6(1)**, 714, (2014).
- [10]. Haque, A. K. M. M. et al., **12**, 3202, (2015).
- [11] Hemalatha, J., Prabhakaran, T. and Pratibha Nalini, R., Microfluidics and Nanofluidics, **10**, 263, (2011)
- [12] Hummers, W. S. and Offeman, R. E., Journal of the American Chemical Society, **80**, 1339, (1958)
- [13] Kaur, K. and Juglan, K. C. C., Der Pharma Chemica, **7(2)**, 160, (2015).
- [14] Kaur, K., Juglan, K. C. and Kumar, H., Journal of Molecular Liquids. Elsevier

B.V, **268**, 700, (2018).

[15] Kharat, P. B. et al., Journal of Materials Science: Materials in Electronics. Springer US, **30(7)**, 6564, (2019)

[16] Khushboo et al., Journal of Molecular Liquids, **214**, 145, (2016).

[17] Kumar, H. et al., Journal of Molecular Liquids. Elsevier B.V., **221**, 526, (2016).

[18] Lee, C. et al., Science, **321(5887)**, 385, (2008).

[19] Leena, M., Srinivasan, S., and Prabhakaran, M., Nanotechnology Reviews, **4(5)**, 449, (2015)

[20] Li, D. et al., Nature Nanotechnology, **3(2)**, 101, (2008).

[21] Liu, J. et al., RSC Advances, **3(29)**, 11745, (2013).

[22] Liu, P., Huang, Y. and Zhang, X., **95**, 107, (2014)

[23] Liu, P., Yao, Z., and Zhou, J., Ceramics International. Elsevier, **41(10)**, pp. 13409, (2015).

[24] Luo, Z. et al., Synthetic Metals. Elsevier B.V., **175**, 88, (2013)

[25] Ma, J. et al., Colloids and Surfaces A: Physicochemical and Engineering Aspects. Elsevier B.V., **538**, 79, (2018)

[26] Mahbulul, I. M. et al., Ultrasonics Sonochemistry. Elsevier B.V., **26**, 361, (2015)

[27] Manon, P. et al., AIP Conference Proceedings, **1860**, 1, (2017)

[28] Naficy, S. et al., Materials Horizons, **1(3)**, 326, (2014)

[29]. Naik, A. B., Indian Journal of Pure and Applied Physics, **53(1)**, 27, (2015)

[30] Pardeike, J. et al., International Journal of Pharmaceutics. Elsevier B.V., **420(1)**, 93, (2011).

- [31] Parveen, S. et al., *Applied Acoustics*, **70(3)**, pp. 507, (2009)
- [32] Hummers, Offeman, **208**, 1937, (1957).
- [33] Rabbani, M., Mohseni, E., and Rao, M., *International Communications in Heat and Mass Transfer*. Elsevier Ltd, **76**, 308, (2016)
- [34] Ranjini, K., Mahalingam, T. and Jeevaraj, A. K. S., **204**, 256, (2012)
- [35] Roy, I. et al., *RSC Adv.*, **6(13)**, 10557, (2016)
- [36] Sadeghinezhad, E. et al., *Energy Conversion and Management*. Elsevier Ltd, **111**, 466, (2016)
- [37] Sheshmani, S. and Fashapoyeh, M. A., **25**, 813, (2013).
- [38] Sonika and Thakur, R. C., *Research Journal of Pharmaceutical, Biological, and Chemical Sciences*, **6**, 664, (2015)
- [39] Stankovich, S. et al., *Carbon*, **45(7)**, 1558, (2007)
- [40] Su, P. et al., *Carbon*. Elsevier Ltd, **50**, 5351, (2012)
- [41] Tajik, B. et al., *Powder Technology*, **217**, 171, (2012)
- [42] Thakur, A. et al., *Physics and Chemistry of Liquids*. Taylor & Francis, **9**, 1, (2019)
- [43] Thakur, R. C. et al., *Journal of Materials and Environmental Science*, **6(5)**, 1330, (2015)
- [44] Torrisi, F. et al., *ACS Nano*, **6(4)**, 2992, (2012)
- [45] Vajjha, R. S., Das, D. K. and Mahagaonkar, B. M., *Petroleum Science and Technology*, **27**, 612, (2009)
- [46] Wang, L., Huang, Y. and Huang, H. J., *Materials Letters*. Elsevier, **124**, 89, (2014)
- [47] Wang, Y. et al., *Synthetic Metals*. Elsevier, **229**, pp. 82, (2017)

- [48] Zhang, H. et al., *Applied Thermal Engineering*, **119**, 132, (2017)
- [49] Zhu, G. et al., *Journal of Materials Chemistry A*, **3(14)**, 7591, (2015)
- [50] Thakur, R. C. et al., *Asian Journal of Chemistry*, 28(10), 2331, (2016).

Section 1 (Part B)

Study of Water-rGO Nanosuspension

4.12 Introduction

Nanosuspensions are the colloidal dispersion of nanosized particles ranging from 100 – 500 nm in the base fluid [4]. The nanoparticles used in the nanosuspension are typically made from metals, oxides, carbides, or nanotubes of Carbon. As we know, heat transfer takes place on the surface of the particle, so for the better heat transfer application, nanosized particles can play a very vital role because of the extremely high surface area available in these particles. Nanosized particles have a high thermal conductivity that can be used in various fields like electronics, where the dissipation of heat from the electronic components is always a challenge [5–7]. Another potential area can be the use of these particles in ink for electronic device printing for the production of flexible and more conductive electronic devices [8]. The choice of the base fluid in these nanosuspensions can further increase the properties, e.g., the use of water as a base fluid can help to improve the process of heat exchange as water is one of the best coolant available. But, the main objective and goal in nanosuspension research are to develop nanosuspension with stability for industrial applications [4], [9]. Ultrasonication is an accepted technique for dispersing aggregated nanoparticles for the preparation of aqueous nano-suspensions [10]. It has been found in the literature that the increase in the stability of nanosuspension with the rise in the sonication time. Stabilization of the nanosuspension also depends on the choice of the nanoparticle and the choice of sonication time. So, the first challenge is to prepare stable nanosuspension, which can be used for industrial applications.

Graphene is one of the most significant finds in the last decade in terms of many physical and chemical properties. Since its evolution, the number of features like high electron mobility, high electron density, high thermal conductivity, the most durable material, etc. [11–13]. Despite all these excellent properties, there are some difficulties associated with this material like industrial-scale productivity and preparation of the good stable suspension. A different peer group has reported many methods for the

production of graphene (G), graphene oxide (GO) and reduced graphene oxide (RGO), and the stable suspension [14].

In this paper, we prepared RGO nanosuspension with different concentrations in water. Structural, morphological, and fluid interaction studies have been completed and compared. Intermolecular interaction between Water-rGO nanosuspension was observed at different concentrations and temperatures in the range of 298 to 313 K. The adiabatic compressibility, acoustic impedance, mean free pathway were evaluated and examined by ultrasonic approach. Nonetheless, the attenuation coefficient of the ultrasonic wave propagating through all specimens is calculated.

4.13 Material and method:

4.13.1 Materials

Graphite powder, sodium nitrate obtained from Loba Chemical, KMnO_4 , HCl , and Ammonia was taken from CDH, and H_2SO_4 was obtained from Avantar. H_2O_2 was gathered from a fisher scientific, Hydrazine monohydrate was purchased from Sigma Aldrich with an AR grade. All the chemicals used in work are AR grade. Double distilled water was used throughout the experiment.

4.13.2 Methods

The original Hummers Method is used to prepare to GO. In 1000 ml beaker, 345 ml of H_2SO_4 has been taken and put to the continuous magnetic stirrer [15]. An ice bath has been made around the beaker to maintain the temperature of the bath below ten °C. 15 gm of Graphite Powder, and 7.5 gm of NaNO_3 has been added to continuously stirring H_2SO_4 with the heat of the bath is close to zero Celsius. After 30 minutes of continuous stirring, 45 gm of KMnO_4 has been added to the mixture very slowly, such as to maintain the reaction temperature below 90 °C. The mixture is left for continuous stirring for 2 hours after that beaker has been placed in a water bath at the temperature of 40 °C for 1 hour to increase the rate of oxidation. The color of the mixture changes from black to greenish-brown. After 1 hour, the mixture is placed on the magnetic stirrer and ice bath. With continuous stirring, the mixture is diluted with 500 ml of

distilled water very slowly, maintaining the reaction temperature below 90 °C. After leaving the mixture overnight, distilled water 100 ml with 30% H₂O₂ added to the mix to remove any excess KMnO₄ and to stop the oxidation reaction. The further mixture was diluted with distilled water and left for the decantation process overnight. Then we remove the top layer of water, and the remaining solution is filtered. Continuous addition of distilled water has been added during the filtration process helps to remove excess KMnO₄ and metal ions. Approximately 5 liters of distilled water was used during the filtration process. Following the completion of the filtration, the processed mixture was again mixed with 500 ml of distilled water and added to 8-hour ultrasonication, which helps to reduce GO.

The mixture was left to dry in the vacuum and to grinded for GO powder. A colloidal suspension of GO powder in double-distilled water (2 mg/ml) is prepared by ultrasonication of GO in 500 mL of liquid for 1 hour. A few drops of Ammonia have been added to the solution to adjust the PH of the solution in a range of 9 to 10. Hydrazine monohydrate (1 µl for 3 mg of GO) was then added to the suspension. Continuous magnetic string and temperature maintenance up to 95 °C for 3 hours yielded black precipitate of RGO powder [16]. After cooling to room temperature, the powder was filtered through the filter, and the vacuum was dried. Synthesized RGO nanoparticles are dispersed in double distilled water by ultrasound for 24 h to obtain a homogenous suspension of different concentrations without any phase separation and sedimentation. As with many peer groups, it is indisputable that ultrasound improves reliability and dispersion of the suspension [10]. Nanosuspensions with different concentrations (0.2mg / ml, 0.4mg / ml, 0.6mg / ml, 0.8mg / ml and 1.0mg / ml) are prepared without the introduction of any surfactants [17].

4.14 Characterization of RGO and Water-rGO nanosuspension

Both FE-SEM Imaging and elemental analysis has been done with the help of Nova Nano FE-SEM 450, which provides an ultra-high-resolution description and nanoscale information of the sample. The FE-SEM is attached with an EDAX detector for the measurement of the elemental and chemical composition of materials. The surface morphology of RGO particles is analyzed with FE-SEM operating at 15 KV. FE-SEM

is the first test to see the surface morphology of the RGO samples. EDS helps to understand the chemical composition of the RGO samples, which gives an insight into the chemical composition of the sample under study. FTIR spectra were recorded using Shimadzu 8400S spectrometer in the range of wavenumber 400 to 4000 cm^{-1} using a He-Ne laser. It is a Pre-Primary test to detect the skeleton vibrations of C=C, which presents in Graphene. XRD of the RGO sample was performed using a Panalytical X'Pert Pro instrument, which uses Cu-K α radiation of wavelength 1.54 Å. The increment in the scan speed is taken as 0.02 s, and reading is taken for 2θ ranging from 0° to 60°. It is one of the most critical tests to see the proper removal of oxygen from GO samples. Raman Spectra of powder RGO sample is taken with the help of Airix STR 500 confocal Raman Spectrometer, which uses a solid-state laser beam of 532 nm at 30mW. It is the first test to know the structure retainment by the RGO samples after the chemical reduction of RGO from GO. UV spectra of the prepared nanosuspension taken with the help of Shimadzu UV-1800 spectrometer. 20 μl of prepared EG-RGO suspension is diluted with 4 ml of pure EG in the quartz cuvette for the UV spectrometry. The range of wavelengths for the study is between 200 nm to 600 nm. All five samples are prepared and measured in the same conditions. This test is used to verify the presence of RGO in the suspension. The average diameter of RGO in water is obtained using a dynamic light scattering (DLS) instrument by Malvern Zetasizer Nano ZS90. This test is used to find the count and size of the particles present in the suspension. Thermoacoustic properties of the sample were measured with the help of Mittal Interferometer M – 81 with a fixed frequency of 2 MHz for ultrasonic velocity, pycnometer for density measurement, and LABMAN model of LMDV-200 for viscosity measurement with attached constant temperature digital water bath.

4.15 Data Table

Table 4.4 Water-RGO Nanosuspension 1					
Concentration (mg/ml)	Temperature(T) (K)	Average Velocity(U) (m/s) $U = \lambda \times f$	Density(ρ) (Kg/m³)	Viscosity(η) (Pa-s)	Adiabatic Compressibility(β) (1/Pa) $\beta = 1/ (U^2 \times \rho)$
0	299	1498.461538	997	0.00089	4.47E-10
0.2	299	1501.62	1003.5	0.015742	4.42E-10
0.4	299	1503.69	1002.3	0.01587	4.41E-10
0.6	299	1506.69	1000.9	0.016212	4.40E-10
0.8	299	1508.77	1000.2	0.0163778	4.39E-10
1	299	1510.77	998.5	0.01631	4.39E-10
0	304	1507.692308	995.4	0.000797	4.42E-10

0.2	304	1509.85	1002.3	0.015044	4.38E-10
0.4	304	1512	1001.1	0.015122	4.37E-10
0.6	304	1515.15	999.8	0.015271	4.36E-10
0.8	304	1518.08	998.8	0.015482	4.34E-10
1	304	1520	997.5	0.01545	4.34E-10
0	309	1516.1500	993.8	0.000719	4.38E-10
0.2	309	1518.23	1000.9	0.014411	4.33E-10
0.4	309	1521.23	1000	0.014711	4.32E-10
0.6	309	1524.23	999.01	0.014914	4.31E-10
0.8	309	1526.15	998.1	0.015075	4.30E-10
1	309	1528.08	997	0.01493	4.30E-10
0	314	1525.3100	992.2	0.000653	4.33E-10

0.2	314	1528.46	1000.1	0.013828	4.28E-10
0.4	314	1531.31	998.8	0.01443	4.27E-10
0.6	314	1535.46	998.2	0.014362	4.25E-10
0.8	314	1537.38	997.3	0.014775	4.24E-10
1	314	1538.38	996.5	0.014529	4.24E-10

Table 4.5 Water-RGO Nanosuspension 2

Concentration (mg/ml)	Temperature(T) (K)	Acoustical impedance(Z) (Pa. s/m³) Z = ρ × U	Attenuation (α/f²) (m⁻¹) α/f² = 8π²η /3ρU³	Bulk Modulus(K) (Pa) K = ρ U²	Relaxation Time(τ) (s) τ = 4βη/3	Intermolecular Free Length (L_f) (L_f = K_T × β^{1/2})
0	299	1493966.154	6.97567E-15	2238650821	5.30E-13	4.59E-10
0.2	299	1506871.038	1.21813E-13	2262740734	9.28E-12	4.54E-10
0.4	299	1507150.8	1.22442E-13	2266291064	9.34E-12	4.54E-10
0.6	299	1508046.021	1.24509E-13	2272157859	9.51E-12	4.52E-10
0.8	299	1509070.985	1.25351E-13	2276839869	9.59E-12	4.52E-10
1	299	1508503.077	1.24549E-13	2279000033	9.54E-12	4.51E-10
0	304	1500756.923	6.14258E-15	2262679669	4.70E-13	4.59E-10

0.2	304	1513318.8	1.14656E-13	2284878570	8.78E-12	4.54E-10
0.4	304	1513663.2	1.14896E-13	2288658758	8.81E-12	4.53E-10
0.6	304	1514849.569	1.15455E-13	2295228264	8.87E-12	4.52E-10
0.8	304	1516255.231	1.16492E-13	2301792075	8.97E-12	4.51E-10
1	304	1516200	1.15961E-13	2304624000	8.94E-12	4.50E-10
0	309	1506749.87	5.45797E-15	2284458815	4.20E-13	4.58E-10
0.2	309	1519597.177	1.08173E-13	2307099191	8.33E-12	4.54E-10
0.4	309	1521230.769	1.09871E-13	2314143053	8.48E-12	4.52E-10
0.6	309	1522721.012	1.10841E-13	2320977049	8.57E-12	4.51E-10
0.8	309	1523254.154	1.11716E-13	2324720186	8.65E-12	4.50E-10
1	309	1523492.692	1.10346E-13	2328014026	8.55E-12	4.50E-10
0	314	1513412.582	4.87604E-15	2308423345	3.77E-13	4.57E-10

0.2	314	1528614.385	1.01808E-13	2336428294	7.89E-12	4.52E-10
0.4	314	1529470.123	1.05786E-13	2342089365	8.21E-12	4.50E-10
0.6	314	1532696.172	1.04498E-13	2353393664	8.14E-12	4.48E-10
0.8	314	1533233.677	1.07197E-13	2357169867	8.36E-12	4.48E-10
1	314	1533000.269	1.05291E-13	2358344030	8.21E-12	4.47E-10

4.16 Result and Discussion

4.16.1 Morphological and elemental analysis

Figure 4.33 corresponds to the FESEM image of the RGO sample at 50000 X magnification. In these images, lamellar morphology with few-layered structures is visible. Wrinkles and separated layers at the scale of 2 μ m confirm the formation of RGO and conversion of GO into RGO, respectively. The EDS graph of RGO is shown in figure 4.34. It is visible from the chart that carbon content is 86.35%, and oxygen content is 8.56%. The reduced amount of oxygen content shows the complete removal of oxygen content while reducing the sample from GO to RGO. It proves the conversion of GO into RGO [2], [18].

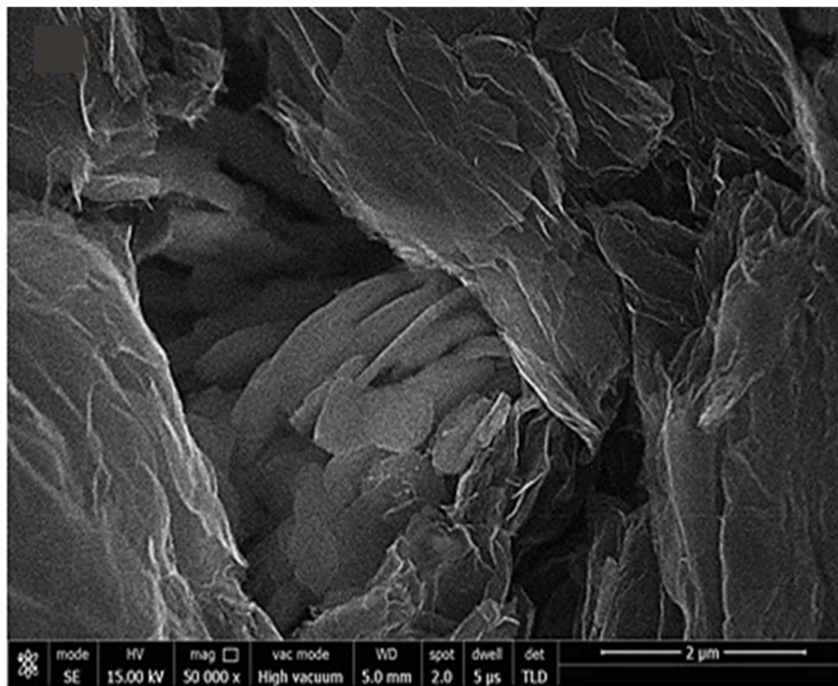


Figure 4.33 FESEM of rGO

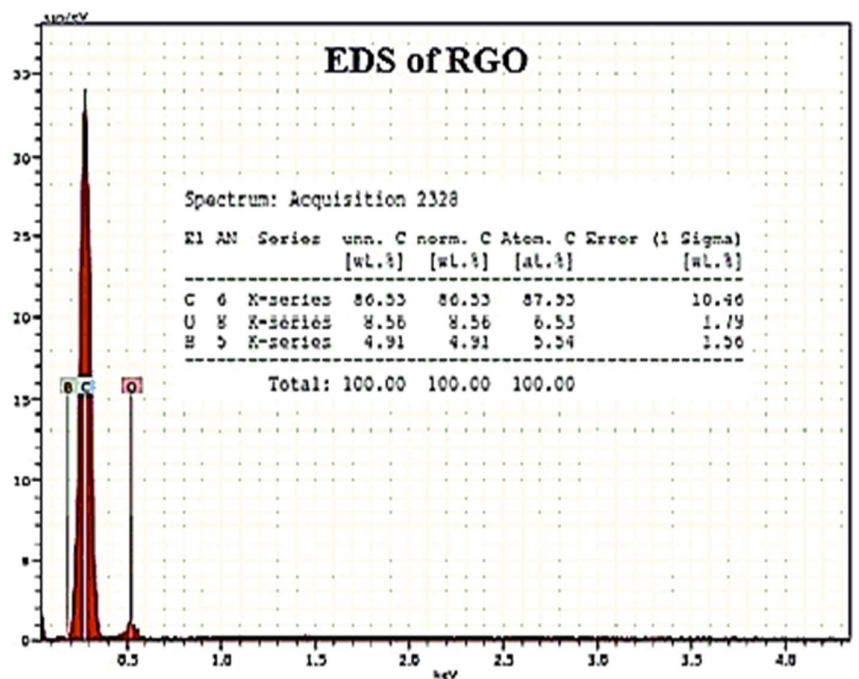


Figure 4.34 EDS of rGO

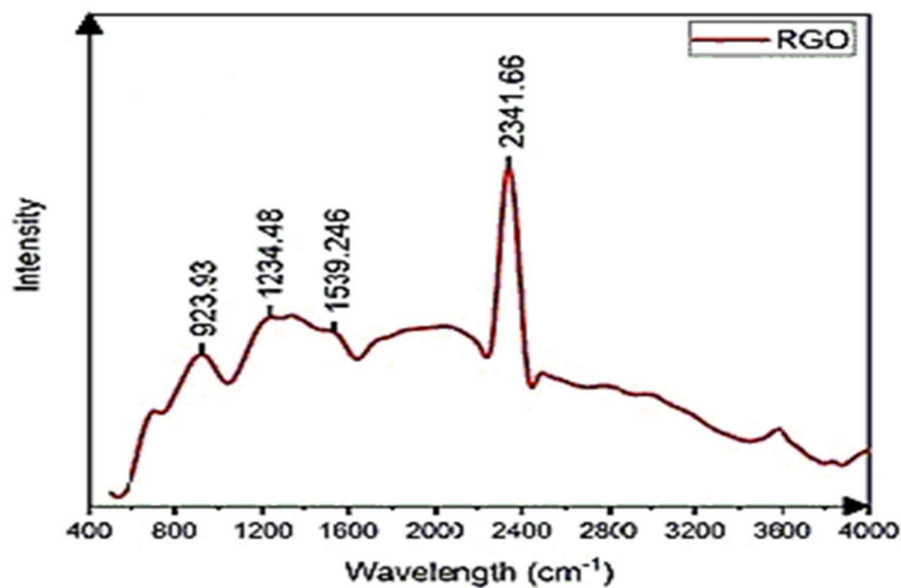


Figure 4.35 FTIR of rGO

Figure 4.35 corresponds to the FTIR spectrum of RGO. Peaks at 923.93 cm⁻¹, 1234.48 cm⁻¹ correspond to alkoxy C—O stretching vibration and C—O epoxy stretching

vibrations. 1539.24 cm^{-1} correspond to C=C Skelton vibrations of Graphene network, 2341.66 cm^{-1} correspond to CO_2 respectively [19–21].

XRD spectra of RGO is shown in figure 4.36. The sharp peak at $26^\circ.43'$ in figure 4.36 contributed to the graphene-like structure (002) and the complete removal of oxygen content from RGO. The peak of RGO at angle $26^\circ.43'$ confirms the removal of trapped oxygen from layers of Graphene by hydrazine monohydrate and a decrease in the interplanar distance between layers [22–24]. Figure 4.37 corresponds to the Raman spectroscopy graph of the RGO samples.

In figure 4.37, the peak at 1336.38 cm^{-1} correspond to defect in the Graphene network, 1565.96 cm^{-1} correspond to the Graphene Network peak, and 2682.66 cm^{-1} correspond to the 2D defect peak in the graphene network. The intensity ratio of structure defect and Graphene network ratio is $I_D/I_G = 0.41$, which corresponds to good structure retainment of the graphene network [25–27].

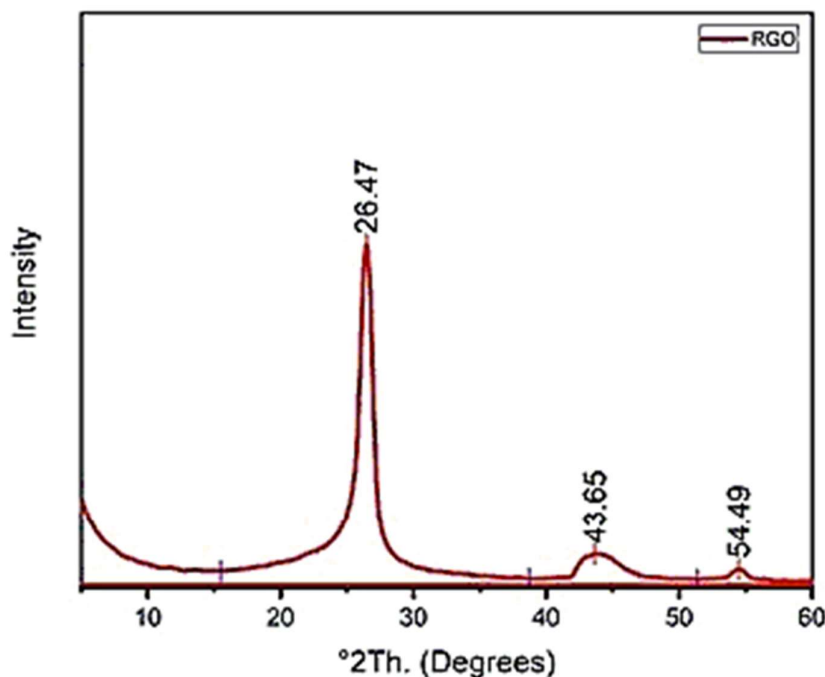


Figure 4.36 XRD of rGO

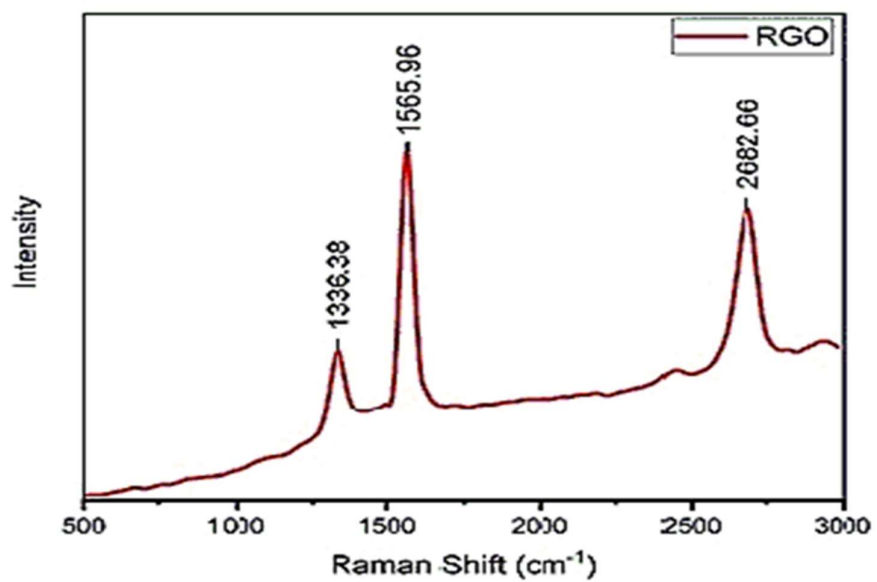


Figure 4.37 RAMAN Spectra of rGO

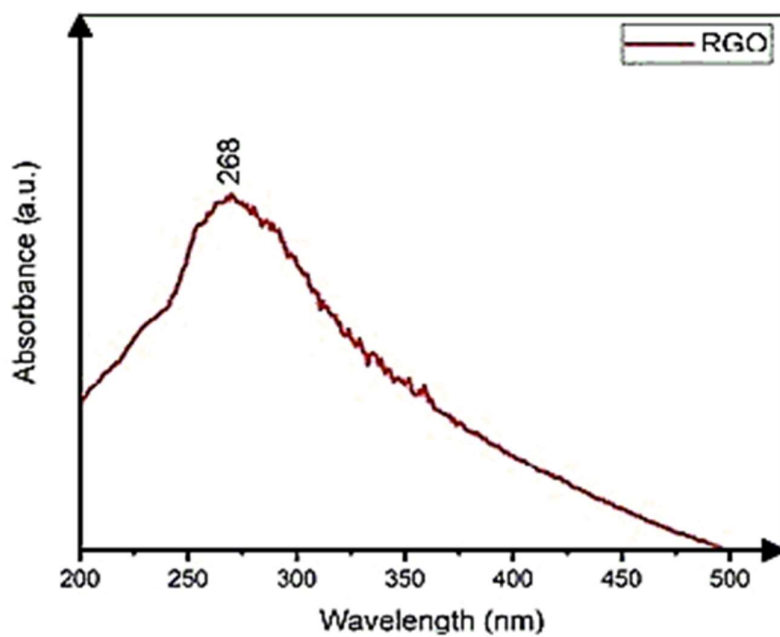


Figure 4.38 UV-VIS Spectra of rGO

4.16.2 Colloidal Stability analysis

The nanosuspension of RGO with water was prepared with the help of extensive ultrasonication. The UV-Vis spectra are shown in figure 4.38 confirms the presence of RGO in the nanosuspension. The peaks at the position 268 nm represent the presence of RGO in the nanosuspension [15], [28].

The average diameter of RGO in water is obtained using a dynamic light scattering (DLS) shown in figure 4.39. It is seen that the average size of the RGO is in the range of 109 nm to 119 nm for all five prepared samples [2], [29,30]. With the help of particle size calculation by DLS, we can call the prepared suspension as nanosuspension.

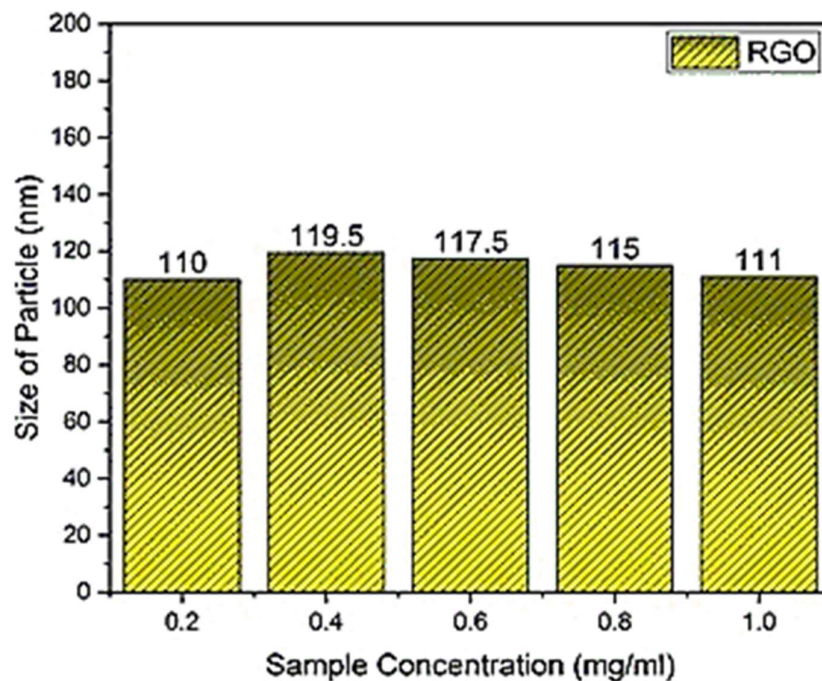


Figure 4.39 DLS of Water-rGO Nanosuspension

4.16.3 Thermoacoustic analysis

4.16.3.1 Ultrasonic Velocity

Ultrasonic velocity is the most crucial parameter to understand the intraparticle and

intermolecular interaction in the nanosuspension samples. The ultrasonic speed of double distilled water and their solution were measured at four different temperatures (298, 303, 308, and 313K) and 1atm pressure. The velocity, density, and viscosity reading were repeated several times for accuracy. All the measurements for pure water were matched with literature to avoid any error. The dissimilarity of ultrasonic velocity with the concentration of the nanosuspension and temperature helps to find the insight of the fluid. Figure 4.40 displays the divergence of ultrasonic velocity with the concentration of RGO in water.

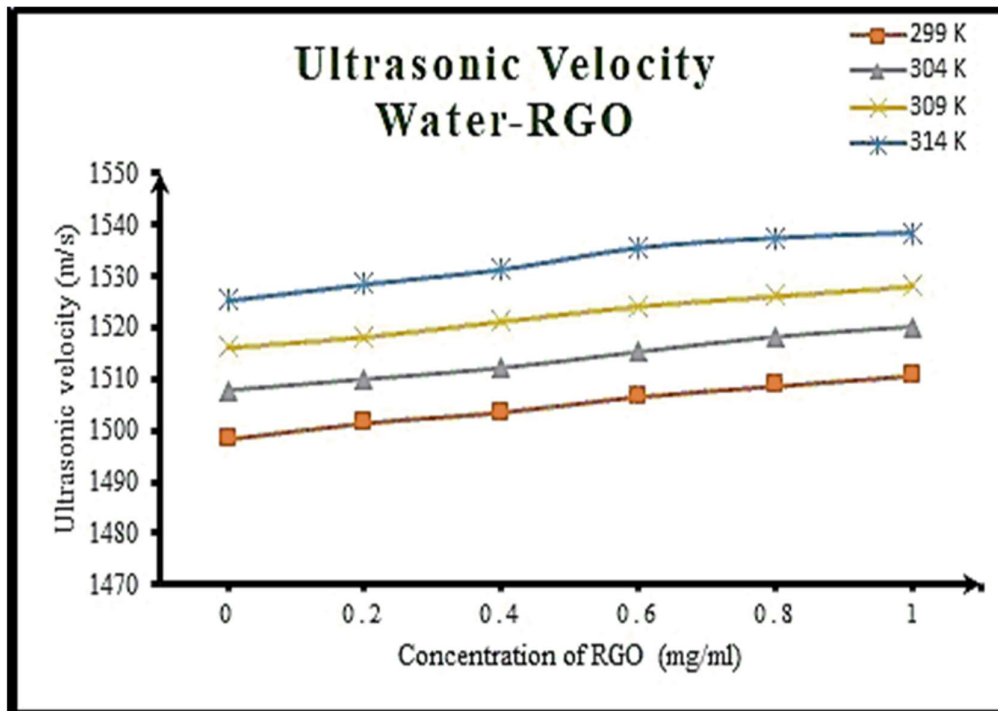


Figure 4.40 Ultrasonic velocity of Water-rGO Nanosuspension

Ultrasonic velocity increases in water-RGO nanosuspension with the rise in the concentration of the particles. The upsurge in the ultrasonic velocity has been accredited to water-RGO interaction, and it further guarantees the dominance of intramolecular interaction over intermolecular interaction. With the rise in the concentration of the particles, there is a possibility of an increase in the Brownian motion of nanosuspension molecule and an increase in the surface layer, which further helps to increase the

ultrasonic velocity. An increase in the temperature of the nanosuspension also increases in the Brownian motion of the fluid molecules, which further increases the speed of the fluid [31,32].

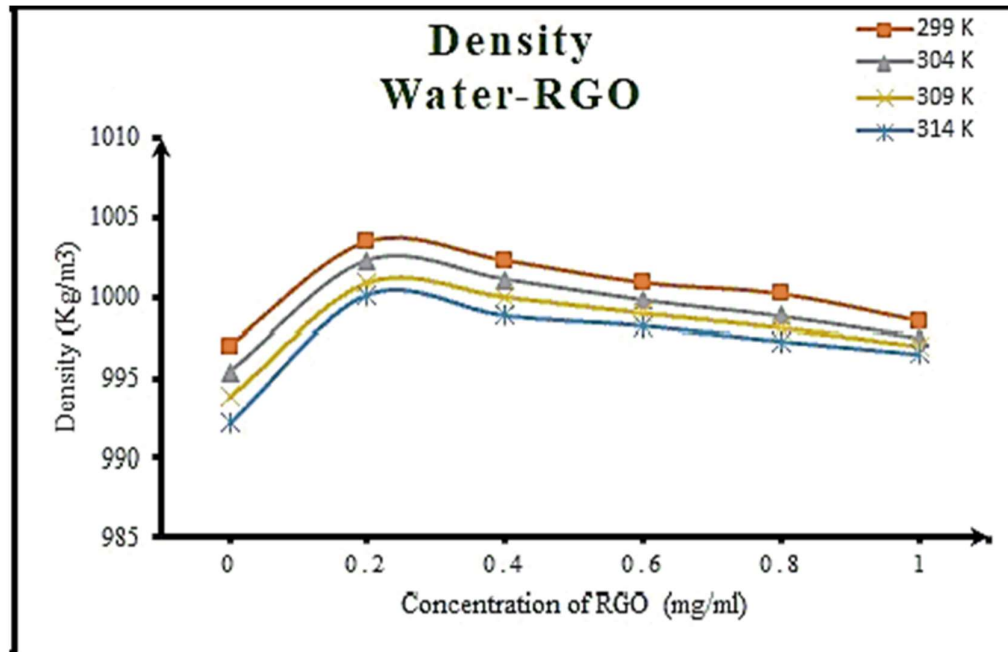


Figure 4.41 Density of Water-rGO Nanosuspension

4.16.3.2 Density

As seen in figure 4.41, as soon as the RGO particle added to the pure water, density increases from 997 to 1003.5 kg/m³ in the case of RGO nanosuspension for 0.2mg/ml. After this, a continuous decrease can be seen in the density of the prepared nanosuspension with an increase of particle concentration. The increase in density is due to the rise in intramolecular interaction than intermolecular interaction. Water-RGO shows the same decreasing trend. Density declines with the increase in the temperature of both nanosuspensions [33,34].

4.16.3.3 Viscosity

Figure 4.42 shows the viscosity of Water-RGO nanosuspension declines with the rise in the temperature because of the increase in the Brownian motion of the molecules of water. With the rise in the temperature flow of nanosuspension also gets easy. Viscosity

also increases slightly with the addition of particle loading in the nanosuspension, which may be due to restriction in the flow produced by the RGO nanoparticles. These particles get tangled with each other to restrict the flow of liquids [5], [32].

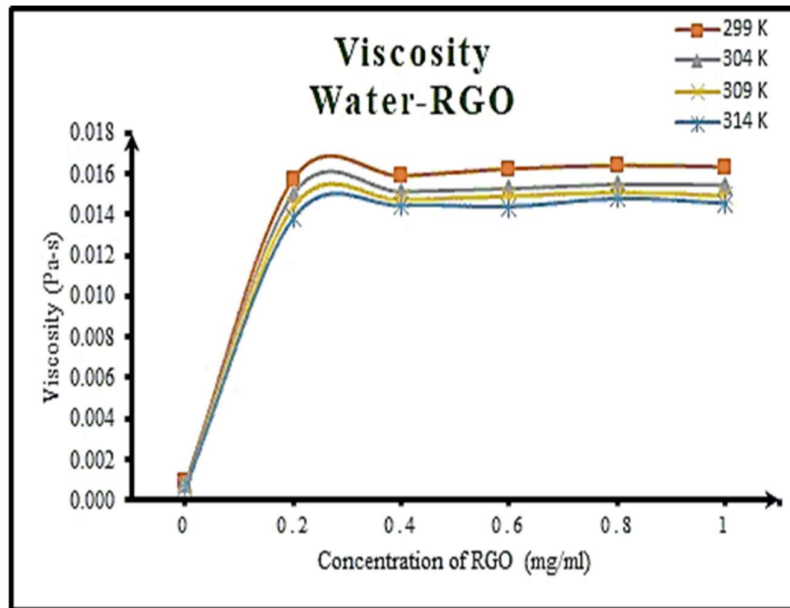


Figure 4.42 Viscosity of Water-rGO Nanosuspension

4.16.3.4 Adiabatic Compressibility

Figure 4.43 displays the decrease of adiabatic compressibility with the rise in the concentration of the particles. The reduction in the adiabatic compressibility with an increase in the concentration of the particles supports fluid-particle interaction. Further, adiabatic compressibility also decreases with an increase in the temperature of the system in [35, 36].

4.16.3.5 Acoustic Impedance

In figure 4.44, there is an increase in the value of acoustical impedance in the nanosuspensions with the rise in the concentration of the particles. The higher values of the acoustical impedance suggest that there is substantial interaction between the nanoparticles and base liquid molecules, which may affect the structural arrangement. On the other hand, the acoustical impedance of both nanosuspensions declines with the rise in the temperature that may be due to an increase in the Brownian motion of the

base liquid molecules. The increasing particle-fluid interactions at lower concentrations increase the intermolecular distance, which creates resistance in the propagation of ultrasonic waves [37, 38].

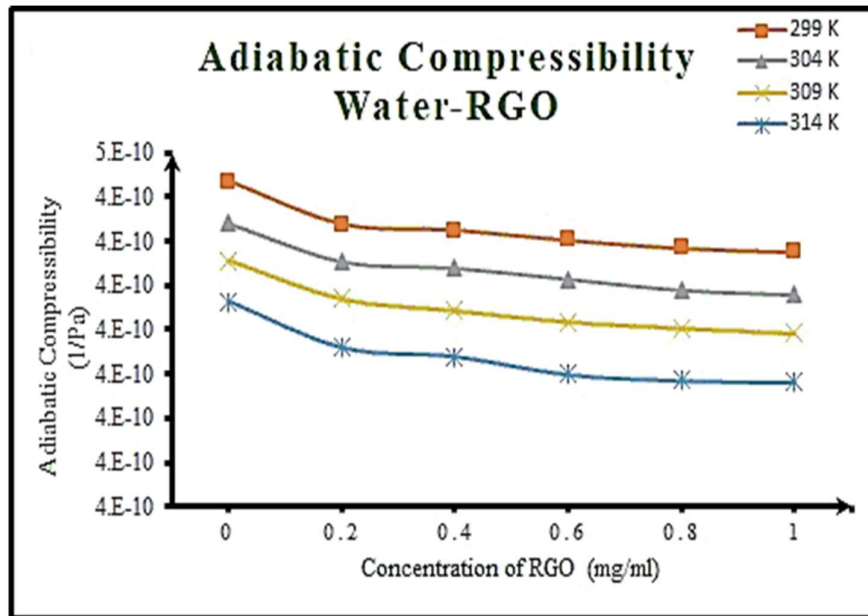


Figure 4.43 Adiabatic Compressibility of Water-rGO Nanosuspension

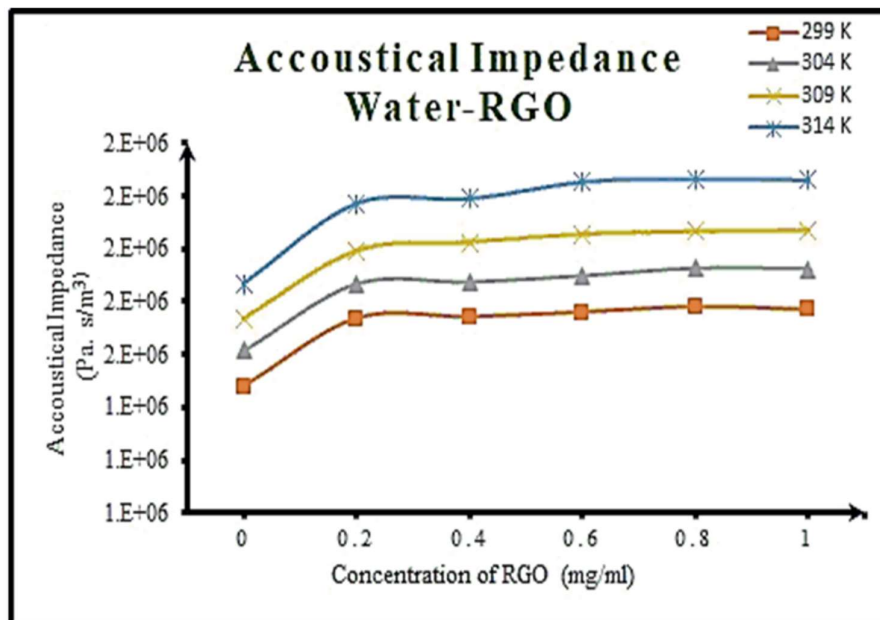


Figure 4.44 Acoustical Impedance of Water-rGO Nanosuspension

4.16.3.6 Ultrasonic attenuation

Figure 4.45 represents the attenuation of the ultrasonic waves while passing through prepared nanosuspensions. Ultrasonic attenuation increases dramatically with the addition of the nanoparticle to the base fluid because the network of these particles may block most of the ultrasonic waves from reaching to the other end. Further, the attenuation increases very slightly with the increase of concentration of the particles. Also, the dependency of attenuation on temperature can be seen in both prepared nanosuspension. It can be seen that as the temperature rises, the value of the attenuation declines because with heat, the Brownian motion, the base fluid increases [39, 40].

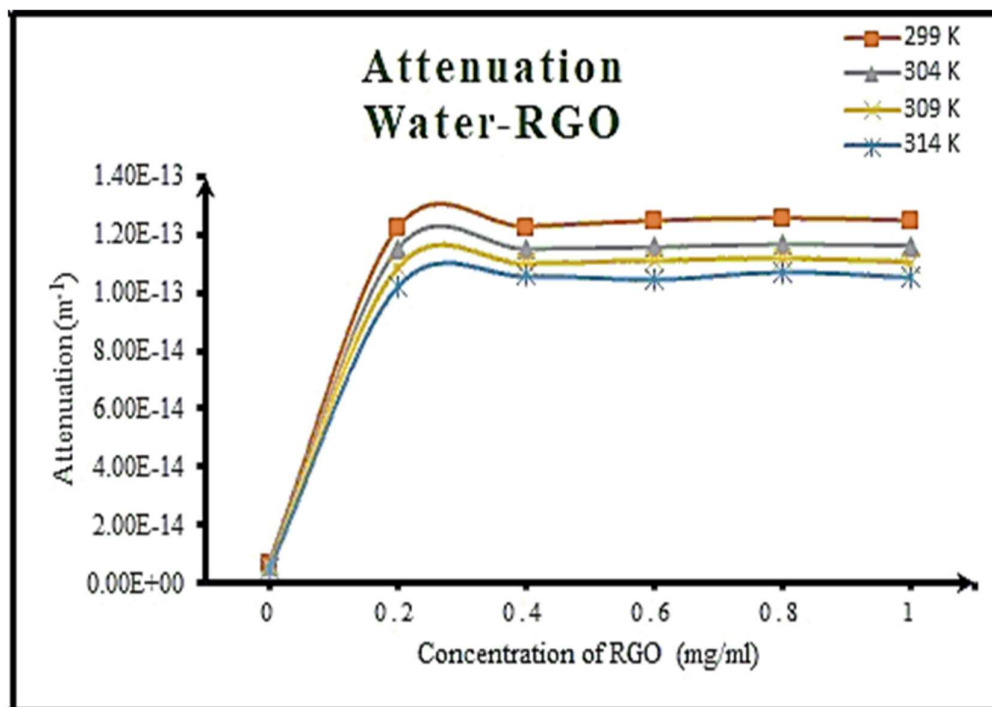


Figure 4.45 Attenuation of sound wave in Water-rGO Nanosuspension

4.16.3.7 Bulk Modulus:

Bulk modulus Can be defined as the resistance of the liquid or fluid to the applied stress. In figure 4.46, bulk modulus increases for the Water-RGO nanosuspension with the increase in the concentration of the particles. Bulk modulus also increases with the rise

in temperature. A surge in bulk modulus or a decrease in incompressibility is attributed to the fact that powerful, cohesive interaction forces work among molecules/atoms after the dispersion of RGO nanoparticles in liquid [41, 42].

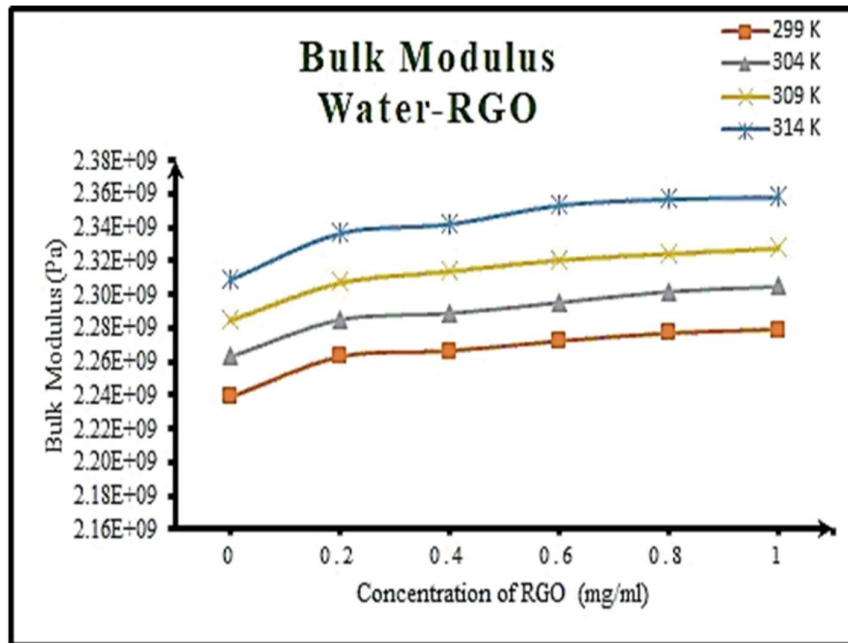


Figure 4.46 Bulk modulus of Water-rGO Nanosuspension

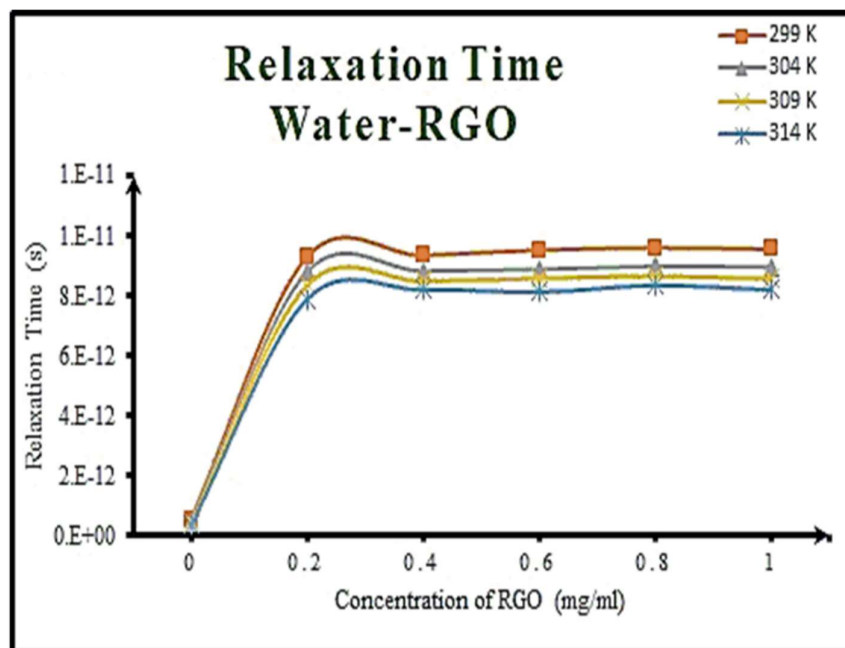


Figure 4.47 Relaxation time of Water-rGO Nanosuspension

4.16.3.8 Relaxation Time

Figure 4.47 represents the relaxation time of the water-rGO nanosuspension. Relaxation time is the molecular rearrangement time during the process of transmission of ultrasonic waves. It can be seen clearly in figure 15(a) and 15(b) that relaxation time increase from 5.3×10^{-13} s to 9.28×10^{-12} s because of the addition of RGO nanoparticles in the pure water. Further, a slight increase in the relaxation time is seen in both nanosuspension. Relaxation time decreases with the increase in the temperature as the Brownian motion of the water molecules increases with the rise in the heat of [42 43].

4.16.3.9 Intermolecular free length

In figure 4.48, it can be understood clearly that intermolecular free length is a function of temperature. As the temperature rises, the intermolecular free length declines as the relaxation time increases. Further, the intermolecular free length decreases with the increase in the concentration of the nanoparticles in the base fluid. This behavior is the response of fluid and particle interaction in the prepared nanosuspension [37, 38].

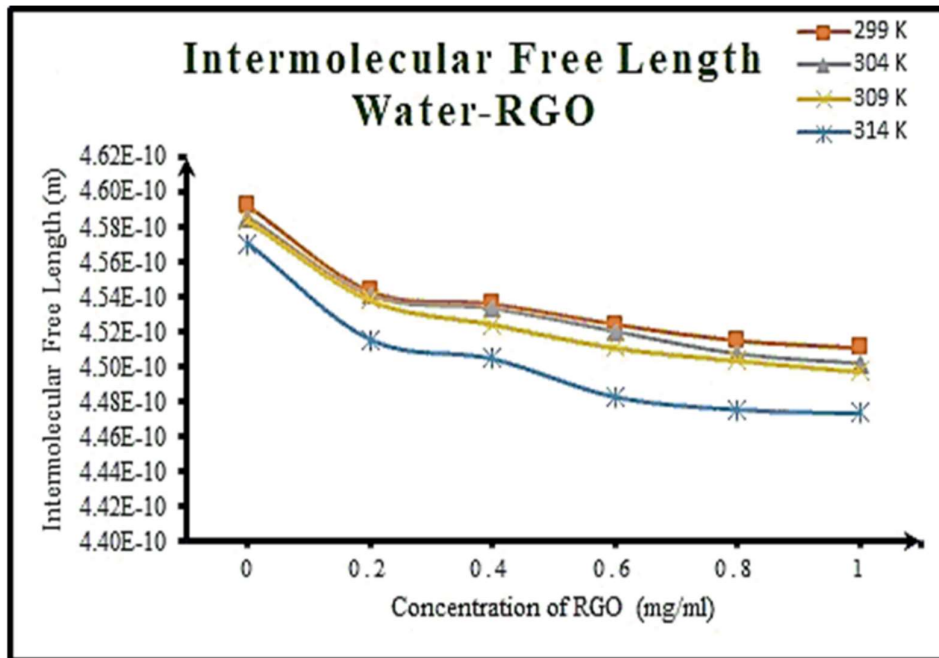


Figure 4.48 Intermolecular Free Length of Water-rGO Nanosuspension

4.17 References

- [1] J. Chen, B. Yao, C. Li, and G. Shi, *Carbon N. Y.* **64**, 225 (2013).
- [2] I. Roy, G. Sarkar, S. Mondal, D. Rana, A. Bhattacharyya, N.R. Saha, A. Adhikari, D. Khastgir, S. Chattopadhyay, and D. Chattopadhyay, *RSC Adv.* **6**, 10557 (2016).
- [3] L. Stobinski, B. Lesiak, A. Malolepszy, M. Mazurkiewicz, B. Mierzwa, J. Zemek, P. Jiricek, and I. Bieloshapka, *J. Electron Spectros. Relat. Phenomena* **195**, 145 (2014).
- [4] J. Pardeike, D.M. Strohmeier, N. Schrödl, C. Voura, M. Gruber, J.G. Khinast, and A. Zimmer, *Int. J. Pharm.* **420**, 93 (2011).
- [5] M. Rabbani, E. Mohseni, and M. Rao, *Int. Commun. Heat Mass Transf.* **76**, 308 (2016).
- [6] E. Sadeghinezhad, M. Mehrali, R. Saidur, M. Mehrali, S. Tahan Latibari, A.R. Akhiani, and H.S.C. Metselaar, *Energy Convers. Manag.* **111**, 466 (2016).
- [7] P.B. Kharat, S.D. More, S.B. Somvanshi, and K.M. Jadhav, *J. Mater. Sci. Mater. Electron.* **30**, 6564 (2019).
- [8] F. Torrisi, T. Hasan, W. Wu, Z. Sun, A. Lombardo, T. Kulmala, G.W. Hshieh, S.J. Jung, F. Bonaccorso, P.J. Paul, D.P. Chu, and A.C. Ferrari, *ACS Nano* **6**, 2992 (2012).
- [9] H. Zhang, S. Wang, Y. Lin, M. Feng, and Q. Wu, *Appl. Therm. Eng.* **119**, 132 (2017).
- [10] I.M. Mahbubul, R. Saidur, M.A. Amalina, E.B. Elcioglu, and T. Okutucu-Ozyurt, *Ultrason. Sonochem.* **26**, 361 (2015).
- [11] M.F. El-Kady, V. Strong, S. Dubin, and R.B. Kaner, *Science (80-.)*. **335**, 1326 (2012).

- [12] S. Ghosh, I. Calizo, D. Teweldebrhan, E.P. Pokatilov, D.L. Nika, A.A. Balandin, W. Bao, F. Miao, and C.N. Lau, *Appl. Phys. Lett.* **92**, 2008 (2008).
- [13] C. Lee, X. Wei, J.W. Kysar, and J. Hone, *Science* (80-.). **321**, 385 (2008).
- [14] S. Sheshmani and M.A. Fashapoyeh, 813 (2013).
- [15] W.S. Hummers and R.E. Offeman, *J. Am. Chem. Soc.* **80**, 1339 (1958).
- [16] S. Park, J. An, J.R. Potts, A. Velamakanni, S. Murali, and R.S. Ruoff, *Carbon N. Y.* **49**, 3019 (2011).
- [17] S. Naficy, R. Jalili, S.H. Aboutalebi, R.A. Gorkin, K. Konstantinov, P.C. Innis, G.M. Spinks, P. Poulin, and G.G. Wallace, *Mater. Horizons* **1**, 326 (2014).
- [18] L. Wang, Y. Huang, and H.J. Huang, *Mater. Lett.* **124**, 89 (2014).
- [19] Y. Wang, X. Wu, W. Zhang, J. Li, C. Luo, and Q. Wang, *Synth. Met.* **229**, 82 (2017).
- [20] G. Zhu, C. Xi, Y. Liu, J. Zhu, and X. Shen, *J. Mater. Chem. A* **3**, 7591 (2015).
- [21] Z. Luo, L. Zhu, Y. Huang, and H. Tang, *Synth. Met.* **175**, 88 (2013).
- [22] D. C.C. Marcano, D.. V. V Kosynkin, J.M. Berlin, A. Sinitskii, Z.Z. Sun, A. Slesarev, L.B. Alemany, W. Lu, and J.M. Tour, *ACS Nano* **4**, 4806 (2010).
- [23] J. Liu, H. Yang, S.G. Zhen, C.K. Poh, A. Chaurasia, J. Luo, X. Wu, E.K.L. Yeow, N.G. Sahoo, J. Lin, and Z. Shen, *RSC Adv.* **3**, 11745 (2013).
- [24] M. Zong, Y. Huang, and N. Zhang, *Appl. Surf. Sci.* **345**, 272 (2015).
- [25] P. Su, H.L. Guo, L. Tian, and S.K. Ning, *Carbon N. Y.* **50**, 5351 (2012).
- [26] W. Feng, Y. Wang, J. Chen, L. Wang, L. Guo, J. Ouyang, D. Jia, and Y. Zhou, *Carbon N. Y.* **108**, 52 (2016).
- [27] S. Stankovich, D.A. Dikin, R.D. Piner, K.A. Kohlhaas, A. Kleinhammes, Y. Jia,

- Y. Wu, S.B.T. Nguyen, and R.S. Ruoff, Carbon N. Y. **45**, 1558 (2007).
- [28] D. Li, M.B. Müller, S. Gilje, R.B. Kaner, and G.G. Wallace, Nat. Nanotechnol. **3**, 101 (2008).
- [29] J. Ma, J. Liu, W. Zhu, and W. Qin, Colloids Surfaces A Physicochem. Eng. Asp. **538**, 79 (2018).
- [30] H. Bao, Y. Pan, Y. Ping, N.G. Sahoo, T. Wu, L. Li, J. Li, and L.H. Gan, Small **7**, 1569 (2011).
- [31] M. Leena, S. Srinivasan, and M. Prabhakaran, Nanotechnol. Rev. **4**, 449 (2015).
- [32] S. Parveen, D. Shukla, S. Singh, K.P. Singh, M. Gupta, and J.P. Shukla, Appl. Acoust. **70**, 507 (2009).
- [33] R.S. Vajjha, D.K. Das, and B.M. Mahagaonkar, Pet. Sci. Technol. **27**, 612 (2009).
- [34] K. Ranjini, T. Mahalingam, and A.K.S. Jeevaraj, (2012).
- [35] H. Kumar, K. Kaur, S. Arti, and M. Singla, J. Mol. Liq. **221**, 526 (2016).
- [36] J. Hemalatha, T. Prabhakaran, and R. Pratibha Nalini, Microfluid. Nanofluidics **10**, 263 (2011).
- [37] Khushboo, A. Devi, P. Malik, and H. Kumar, J. Mol. Liq. **214**, 145 (2016).
- [38] V. Gupta, A.K. Sharma, and M. Sharma, J. Chem. Pharm. Res. **6**, 714 (2014).
- [39] K. Kaur and K.C.C. Juglan, Der Pharma Chem. **7**, 160 (2015).
- [40] B. Tajik, A. Abbassi, M. Saffar-Avval, and M.A. Najafabadi, Powder Technol. **217**, 171 (2012).
- [41] N.H. Ayachit, S.T. Vasan, F.M. Sannaningannavar, and D.K. Deshpande, J. Mol. Liq. **133**, 134 (2007).

[42] S. Elangovan and S. Mullainathan, *Indian J. Phys.* **87**, 659 (2013).

[43] A.B. Naik, *Indian J. Pure Appl. Phys.* **53**, 27 (2015).

[44] M. Joshi, A. Bhattacharyya, and S.W. Ali, *Indian J. Fibre Text. Res.* **33**, 304 (2008).

Section 2

Study of DMF-GO and DMF-rGO Nanosuspension

4.18 Introduction

Nanosuspensions are dilute liquid suspensions of nanoparticles with at least one of their principal dimensions between 100 nm to 500nm [1]. From prior investigations, nanosuspension has been found to possess superior thermophysical properties such as thermal conductivity [2], thermal diffusivity [3], viscosity, and convective heat transfer coefficients compared to those of base fluids like oil or water [4].

We know bats use ultrasound sound waves as a kind of navigational radar, and these waves are used to calculate sea level, positional signaling in ships, and mechanical cleaning, soldering, welding, anesthesia, washing, tube analysis, and non-destructive screening. In the non-destructive experiment, ultrasonic pulses allow us to "see-through" solid/opaque material and to identify surface or interior defects without impacting the object. Ultrasonic waves are commonly used in medical and clinical medicine. The unique feature of the sound wave is to provides direct and accurate information about the adiabatic properties of the solution [3]. Very few statistics on the speed of sound for fluids were available until 1930. The discovery of the interferometer and optical diffraction techniques strengthened the investigation both qualitatively as well as quantitatively [5]. The practical application of acoustic methods for physiochemical solution investigation is possible after the development of suitable conceptual strategies and techniques for accurate ultrasound velocity measurements in little volumes of fluids [6].

Not much study is available on the acoustical parameters of GO and rGO nanosuspension [7]. In this paper, nanosuspension of graphene oxide (GO) and reduced graphene oxide (rGO) with N, N-dimethylformamide (DMF) has been prepared, tested and Volumetric ultrasonic studies have been conducted at different temperatures over a wide range of concentrations. From the experimental values, a variety of thermodynamic parameters, including ultrasonic speed, adiabatic compressibility, acoustic impedance, relaxation time, free length, ultrasonic attenuation,

and attenuation, etc. has been determined. Variation of these parameters of concentration was found to be of use in understanding the nature of the interactions between the components [8][9].

4.19 Experimental

4.19.1 Materials and Methods

Graphite powder, sodium nitrate, Hydrazine monohydrate procured from Sigma Aldrich, KMnO_4 , HCL, H_2SO_4 , DMF, and Ammonia has been taken from CDH. H_2O_2 has been purchased from fisher scientific. All chemicals used in this research were of AR grade and used without additional purification. Throughout all the experiments, double distilled water was used when required.

Graphene Oxide was synthesized by the Hummers method. Graphite powder (6g) and Sodium Nitrate (6g) were mixed in 300 ml of sulphuric acid in 1000 ml vessel kept at 0 °C to 10 °C using an ice bath. The suspension was stirred for 3 hours at this temperature. Potassium Permanganate (18g) added to the mixture very slowly, and the temperature of the mix was maintained below 10 °C. After completing the addition of potassium permanganate, the mixture was kept at 35 °C until it becomes brown. After 24 hours mixture was added with 100 ml of water very gradually and keeping the temperature of the mix below 90 °C.

Further, 500 ml of the water was added to the mixture and stirred continuously. The reaction was treated with hydrogen peroxide (50 ml) to terminate the oxidation reaction. The mixture was washed with 10% HCL and distilled water several times after the filtration mixture was vacuum dried to obtain the GO powder [10].

In this study, we converted the GO into rGO; the prepared powder was divided into two equal parts. A suspension of GO powder in distilled water (2 mg/ml) was made by ultrasonication. Some drops of ammonia were added to the suspension to maintain the PH of the solution in a range of 8 to 10. Hydrazine Monohydrate (1 μl for 3 mg of GO) was added into the suspension. Constant stirring and keeping the temperature up to 90 °C for 5 hours produces the black precipitates of rGO. After cooling to room

temperature, the powder was filtered, washed, and dried in a vacuum [11]. Nanosuspension of concentrations (0 mg/ml, 0.2 mg/ml, 0.4 mg/ml, 0.6 mg/ml, 0.8 mg/ml, and 1.0 mg/ml) were prepared using ultrasonication for the continuous 24 hours with DMF.

4.19.2 Characterization of DMF-GO and DMF-rGO nanosuspension:

X-ray diffraction (XRD) graphs were recorded in the range of $2\theta = 20^\circ - 70^\circ$ using an X-ray diffractometer (Panalytical X'Pert Pro) with Cu K α radiation ($k = 1.5406 \text{ \AA}$) at 40 kV and 40 mA. FTIR spectra (KBr pellets) were recorded using a Shimadzu 8400S spectrometer. Nova Nano FESEM 450 with attached EDAX was used for the micro-level imaging of prepared samples. The Raman spectra were measured with the Confocal Raman Spectrometer Airix STR 500 with diode laser excitation in $800 - 2000 \text{ cm}^{-1}$ region at room temperature. UV-vis spectra were measured with Shimadzu UV-1800 spectrometer. The HRTEM was done with the help of Jeol JEM 2100 Plus, 2019. The average particle size in nanosuspension was verified with the help of Malvern Zetasizer Nano ZS90. The ultrasonic velocity of the prepared samples calculated with the support of Mittal Interferometer M – 81 with a static frequency of 2 MHz. Density was calculated with the help of a pycnometer. The labman model of LMDV-200 was used to calculate the viscosity of all prepared samples.

4.20 Data table

Table 4.6. DMF-GO Nanosuspension 1					
Concentration (mg/ml)	Temperature(T) (K)	Average Velocity(U) (m/s) $U = \lambda \times f$	Density(ρ) (Kg/m³)	Viscosity(η) (Pa-s)	Adiabatic Compressibility(β) (1/Pa) $\beta = 1/ (U^2 \times \rho)$
0	299	1455.39	955.8	0.00056	4.94E-10
0.2	299	1470.65	953.9	0.01588	4.85E-10
0.4	299	1464.62	953.2	0.01576	4.89E-10
0.6	299	1455.38	950.7	0.01512	4.97E-10
0.8	299	1452.31	950.4	0.01468	4.99E-10
1	299	1448.62	948.2	0.0153	5.03E-10
0	304	1440	952.2	0.00053	5.06E-10
0.2	304	1456.17	951.2	0.01531	4.96E-10
0.4	304	1446.15	951.6	0.01511	5.02E-10

0.6	304	1440.15	949	0.01488	5.08E-10
0.8	304	1436.92	948.2	0.01448	5.11E-10
1	304	1427.69	947.5	0.0145	5.18E-10
0	309	1424.62	949.9	0.0005	5.19E-10
0.2	309	1438.69	947.1	0.01495	5.10E-10
0.4	309	1424.46	947.6	0.01488	5.20E-10
0.6	309	1421.54	947	0.01464	5.23E-10
0.8	309	1418.31	946.6	0.01429	5.25E-10
1	309	1412.46	943.9	0.01423	5.31E-10
0	314	1403.08	942.3	0.00047	5.39E-10
0.2	314	1414.23	943.1	0.01475	5.30E-10
0.4	314	1403.92	941	0.01465	5.39E-10

0.6	314	1400.92	940.6	0.01437	5.42E-10
0.8	314	1396.15	940.3	0.0141	5.46E-10
1	314	1390.92	939.6	0.01386	5.50E-10

Standard uncertainties are $u(m) = 2 \times 10^{-5}$ kg, $u(T) = 0.3$ K, $u(\rho) = 4.6$ (kg/m³), $u(U) = 2.2$ (m/s-1), $u(\eta) = .005$ (Pa-s), $u(\beta) = 1.88 \times 10^{-11}$ (1/Pa)

Table 4.7 DMF-GO Nanosuspension 2

Concentration (mg/ml)	Temperature(T) (K)	Acoustical impedance(Z) (Pa. s/m³) Z = ρ × U	Attenuation (α/f²) (m⁻¹) α/f² = 8π²η /3ρU³	Bulk Modulus(K) (Pa) K = ρ U²	Relaxation Time(τ) (s) τ = 4βη/3	Intermolecular Free Length (L_f) (L_f = K_T × β^{1/2})
0	299	1391056.615	4.97923E-15	2024522397	3.67E-13	5.08E-10
0.2	299	1402853.035	1.37609E-13	2063105816	1.03E-11	4.98E-10
0.4	299	1396071.385	1.38388E-13	2044707628	1.03E-11	5.03E-10
0.6	299	1383634.154	1.35665E-13	2013719861	1.00E-11	5.10E-10
0.8	299	1380275.424	1.32532E-13	2004587801	9.76E-12	5.13E-10
1	299	1373577.108	1.3956E-13	1989784930	1.03E-11	5.17E-10

0	304	1371168	4.86405E-15	1974481920	3.55E-13	5.25E-10
0.2	304	1385108.904	1.37055E-13	2016954033	1.01E-11	5.14E-10
0.4	304	1376160	1.3806E-13	1990139077	1.01E-11	5.21E-10
0.6	304	1366702.35	1.37999E-13	1968256389	1.01E-11	5.27E-10
0.8	304	1362490.462	1.35284E-13	1957793986	9.86E-12	5.30E-10
1	304	1352738.462	1.38265E-13	1931294296	1.00E-11	5.37E-10
0	309	1353242.154	4.74831E-15	1927849591	3.43E-13	5.43E-10
0.2	309	1362583.299	1.39371E-13	1960334966	1.02E-11	5.34E-10
0.4	309	1349819.754	1.42793E-13	1922766323	1.03E-11	5.45E-10
0.6	309	1346196.923	1.41539E-13	1913670703	1.02E-11	5.47E-10
0.8	309	1342570.062	1.39093E-13	1904177446	1.00E-11	5.50E-10
1	309	1333222.446	1.40613E-13	1883125427	1.01E-11	5.56E-10

0	314	1322119.385	4.7579E-15	1855035198	3.39E-13	5.69E-10
0.2	314	1333760.313	1.45379E-13	1886243847	1.04E-11	5.59E-10
0.4	314	1321091.615	1.47927E-13	1854711006	1.05E-11	5.69E-10
0.6	314	1317708.246	1.46062E-13	1846007891	1.04E-11	5.72E-10
0.8	314	1312803.462	1.44871E-13	1832875602	1.03E-11	5.76E-10
1	314	1306911.323	1.44095E-13	1817813119	1.02E-11	5.80E-10

Standard uncertainties are $u(m) = 2 \times 10^{-5}$ kg, $u(T) = 0.3$ K, $u(Z) = 2.78 \times 10^2$ Pa. s/m³, $u(\alpha/f^2) = 5.16 \times 10^{-14}$ m⁻¹, $u(K) = 7.06 \times 10^6$ Pa, $u(\tau) = 3.74 \times 10^{-12}$ s, $u(Lf) = 2.47 \times 10^{-11}$ m

Table 4.8 DMF-rGO Nanosuspension 1

Concentration (mg/ml)	Temperature(T) (K)	Average Velocity(U)	Density(ρ) (Kg/m ³)	Viscosity(η) (Pa-s)	Adiabatic Compressibility(β)
		(m/s) $U = \lambda \times f$			(1/Pa) $\beta = 1/ (U^2 \times \rho)$
0	299	1455.385	955.8	0.000558	4.94E-10
0.2	299	1470.77	953.5	0.01368	4.85E-10
0.4	299	1461.54	952.8	0.014486	4.91E-10
0.6	299	1451.85	950.7	0.014586	4.99E-10
0.8	299	1444.61	950	0.01635	5.04E-10
1	299	1436.77	949.7	0.01735	5.10E-10
0	304	1440.00	952.2	0.000526	5.06E-10
0.2	304	1452.31	953.2	0.01317	4.97E-10

0.4	304	1443.85	952.8	0.014171	5.03E-10
0.6	304	1432.31	951.3	0.014386	5.12E-10
0.8	304	1422.15	950.7	0.015988	5.20E-10
1	304	1413.62	951.7	0.01685	5.26E-10
0	309	1424.62	949.9	0.000496	5.19E-10
0.2	309	1436.92	950.3	0.01286	5.10E-10
0.4	309	1427.54	948	0.013886	5.18E-10
0.6	309	1418	947.7	0.014214	5.25E-10
0.8	309	1409.92	947.9	0.015675	5.31E-10
1	309	1400.08	946.7	0.016388	5.39E-10
0	314	1403.077	942.3	0.000471	5.39E-10
0.2	314	1412.31	946.9	0.01257	5.29E-10

0.4	314	1403.08	944.3	0.013671	5.38E-10
0.6	314	1396.38	943.1	0.014014	5.44E-10
0.8	314	1388.46	942.1	0.01545	5.51E-10
1	314	1381.54	941.7	0.014888	5.56E-10

Standard uncertainties are $u(m) = 2 \times 10^{-5}$ kg, $u(T) = 0.3$ K, $u(\rho) = 3.9$ (kg/m³), $u(U) = 2.4$ (m/s-1), $u(\eta) = .005$ (Pa-s), $u(\beta) = 1.94 \times 10^{-11}$ (1/Pa)

Table 4.9 DMF-rGO Nanosuspension 2

Concentration (mg/ml)	Temperature(T) (K)	Acoustical impedance(Z)	Attenuation (α/f^2)	Bulk Modulus(K)	Relaxation Time(τ)	Intermolecular Free Length (L_f)
		(Pa. s/m ³) $Z = \rho \times U$	(m ⁻¹) $\alpha/f^2 = 8\pi^2\eta / 3\rho U^3$	(Pa) $K = \rho U^2$	(s) $\tau = 4\beta\eta/3$	($L_f = K_T \times \beta^{1/2}$)
0	299	1391056.615	4.97923E-15	2024522397	3.67E-13	5.08E-10
0.2	299	1402378.462	1.18566E-13	2062575091	8.84E-12	4.98E-10
0.4	299	1392553.846	1.28037E-13	2035271006	9.49E-12	5.05E-10
0.6	299	1380270.138	1.31811E-13	2003939892	9.70E-12	5.13E-10
0.8	299	1372379.5	1.50096E-13	1982553149	1.10E-11	5.19E-10
1	299	1364499.738	1.6195E-13	1960471240	1.18E-11	5.24E-10
0	304	1371168	4.86405E-15	1974481920	3.55E-13	5.25E-10
0.2	304	1384339.692	1.18592E-13	2010487184	8.73E-12	5.16E-10

0.4	304	1375696.615	1.2992E-13	1986294267	9.51E-12	5.22E-10
0.6	304	1362554.308	1.35311E-13	1951597016	9.83E-12	5.32E-10
0.8	304	1352041.662	1.53718E-13	1922811249	1.11E-11	5.40E-10
1	304	1345337.762	1.64791E-13	1901790157	1.18E-11	5.46E-10
0	309	1353242.154	4.74831E-15	1927849591	3.43E-13	5.43E-10
0.2	309	1365508	1.19924E-13	1962129957	8.74E-12	5.34E-10
0.4	309	1353306.462	1.32381E-13	1931897024	9.58E-12	5.42E-10
0.6	309	1343838.6	1.3831E-13	1905563135	9.95E-12	5.49E-10
0.8	309	1336466.085	1.55127E-13	1884314374	1.11E-11	5.56E-10
1	309	1325452.823	1.65834E-13	1855735910	1.18E-11	5.64E-10
0	314	1322119.385	4.7579E-15	1855035198	3.39E-13	5.69E-10
0.2	314	1337314.154	1.239E-13	1888699067	8.87E-12	5.59E-10

0.4	314	1324925.538	1.37812E-13	1858972448	9.81E-12	5.68E-10
0.6	314	1316930.331	1.43491E-13	1838941253	1.02E-11	5.74E-10
0.8	314	1308069.615	1.61086E-13	1816204351	1.13E-11	5.81E-10
1	314	1300994.769	1.57633E-13	1797374312	1.10E-11	5.87E-10

Standard uncertainties are $u(m) = 2 \times 10^{-5}$ kg, $u(T) = 0.3$ K, $u(Z) = 2.79 \times 10^2$ Pa. s/m³, $u(\alpha/l^2) = 5.4 \times 10^{-14}$ m⁻¹, $u(K) = 7.2 \times 10^6$ Pa, $u(\tau) = 3.8 \times 10^{-12}$ s, $u(L_t) = 2.5 \times 10^{-11}$ m

4.21 Result and Discussion

4.21.1 Morphological and elemental analysis

SEM was measured to characterize the morphology and microstructure of GO and rGO samples. The complete morphology of the individual layers could be observed from high- magnification SEM images 4.49 (a) and 4.49 (b) for GO and rGO, respectively [12]. SEM images in Fig. 1 (a) and (b) shows the wrinkled and folded graphene sheets [13].

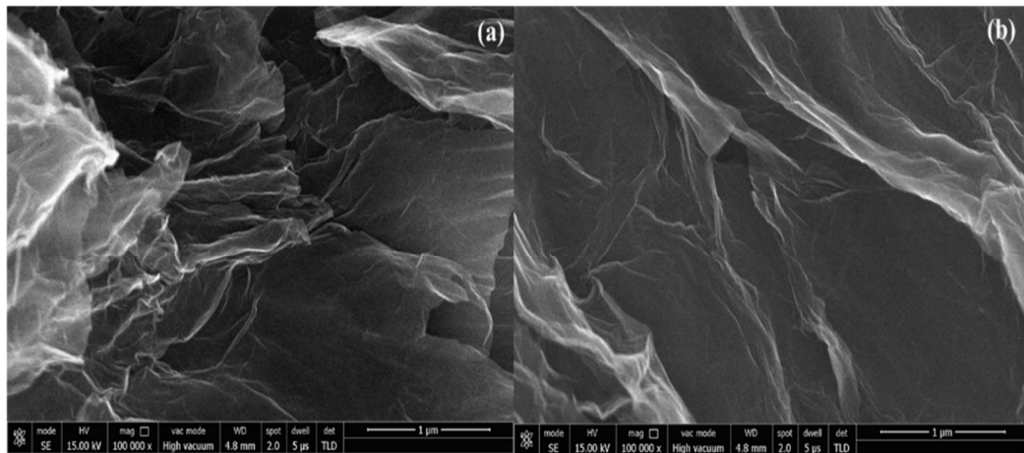


Figure 4.49 (a) FESEM micrograph of GO (b) FESEM micrograph of rGO

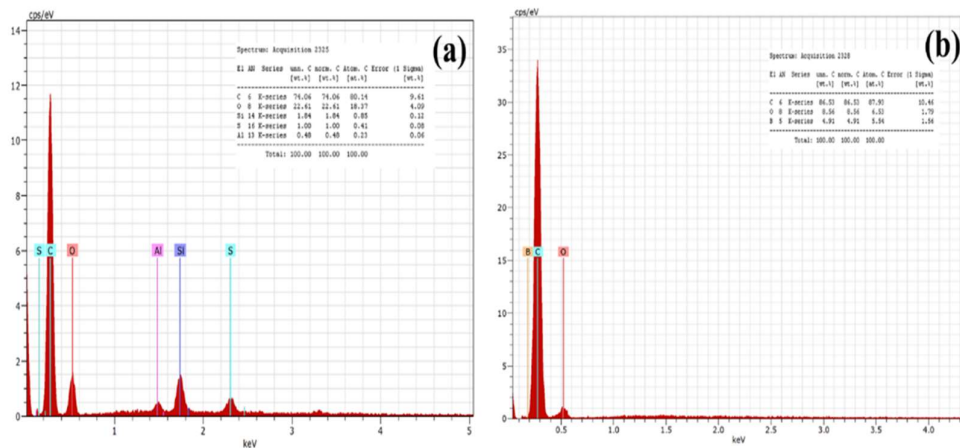


Figure 4.50 (a) EDS Spectra of GO (b) EDS Spectra of rGO

Besides, the EDS results are discussed in Fig. 4.50 (a) and 4.50 (b) for Go and rGO

respectively, it shows the distribution of significant elements, again confirming the existence of carbon and oxygen in the final sample. The ratio of carbon is 74.33% and 86.53% in GO and rGO, respectively, while oxygen content is 22.51% and 8.56% in GO and rGO. [14]

Figure 4.51 and 4.51 (b) shows the FTIR spectra of GO and rGO, respectively. Peaks at position 1095 cm^{-1} and 1116 cm^{-1} correspond to alkoxy and epoxy vibration of C and O bond [15]. Peaks at position 1614 cm^{-1} and 1618 cm^{-1} correspond to the skeletal vibration of C and C bond in unoxidized graphene.[16][17] The peak at positions 2345 cm^{-1} and 2347 cm^{-1} correspond to the hydroxyl group [18]. Besides, peaks at position 3435 cm^{-1} and 3443 cm^{-1} correspond to N and H stretching vibrations [19].

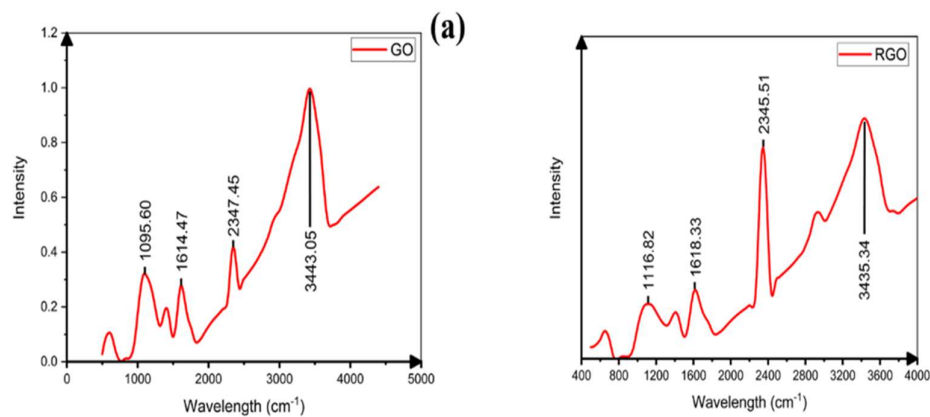


Figure 4.51 (a) FTIR Spectra of GO (b) FTIR Spectra of rGO

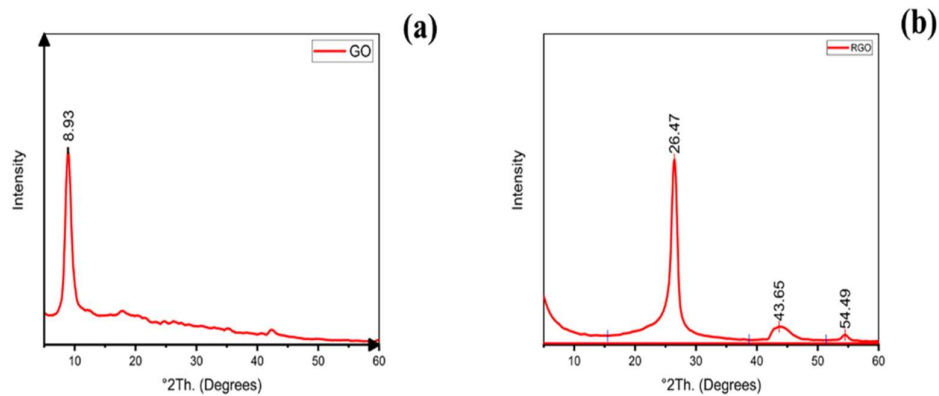


Figure 4.52 (a) XRD Spectra of GO (b) XRD Spectra of rGO

To further characterize the morphology of GO and rGO, XRD analysis was performed, which is shown in Fig. 4.52 (a) and 4.52 (b) respectively. After oxidation of GO peak at $8^{\circ}.93'$ (002 planes) vanished and a new peak at $26^{\circ}.47'$ (001 planes) generated [16][18]. A larger value of angle suggests the decrease in the space between the layers, which strengthens the removal of oxygen from the layers [20].

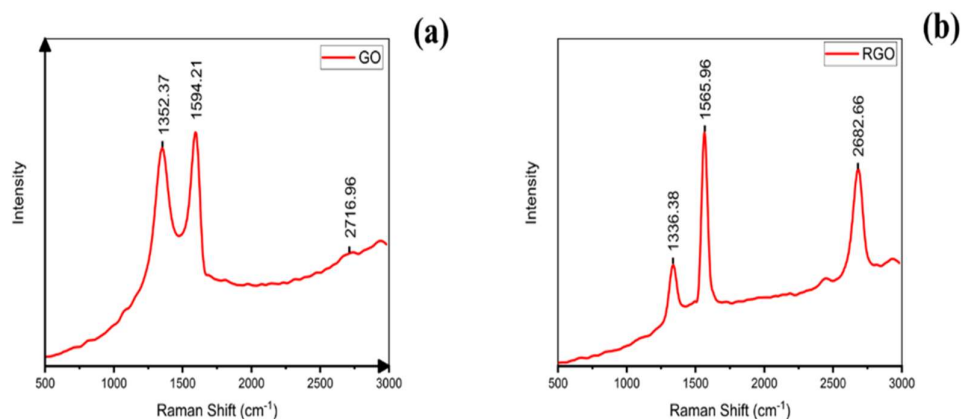


Figure 4.53 (a) RAMAN Spectra of GO (b) RAMAN Spectra of rGO

Raman Spectroscopy is an incredibly effective tool to illustrate the structural change of graphite to GO and rGO. The two main characteristics can illustrate the Raman Spectra, graphite structure retainment band, which is known as G band (1352.37 cm^{-1} and 1336.38 cm^{-1}), and Defect in the graphene structure, which is known as D Band (1594.21 cm^{-1} and 1565.96 cm^{-1}), as shown in Fig. 4.53 (a) and 4.53 (b) [21]. The intensity proportion of structural defect and Graphene network ratio is $I_D/I_G = 0.93$ and $I_D/I_G = 0.41$, which relates to good structure retainment of the graphene network [22].

4.21.2 Colloidal Stability analysis

Nano suspension of the GO and rGO with DMF was prepared with the support of extensive ultrasonication. Transmission electron microscopy is used to determine the morphology of the graphene sheets. A small sample of the GO and RGO suspension was taken, and HRTEM was performed on the same. The TEM image of GO and rGO is shown in figure 4.54 (a) and 4.54 (b), respectively. Figure 4.54 (a) shows the sheets

like graphene structure with wrinkles on the left side of the TEM image, while figure 6 (b) shows the stacking of the graphene layer one above another. Each figure shows the presence of the sheet-like structure in the nanosuspension, which gives confirmation of GO and rGO in the suspension [23]. Since the UV cutoff wavelength for the DMF is 268 nm and GO peak in UV is visible at 238nm [24], instead of that, no GO peak is visible in the UV spectra of DMF-GO nanosuspension as shown in Fig. 4.55 (a) [25]. In the case of the DMF-rGO nanosuspension shoulder of the peak starting from 270 nm is visible in Fig. 4.55 (b). This peak can be considered as the existence of rGO in the nanosuspension [23].

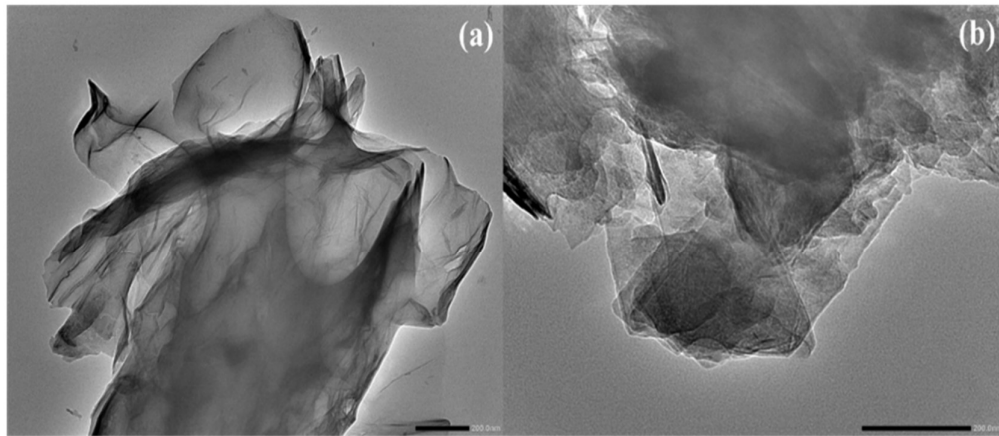


Figure 4.54 (a) TEM Spectra of GO (b) TEM Spectra of rGO

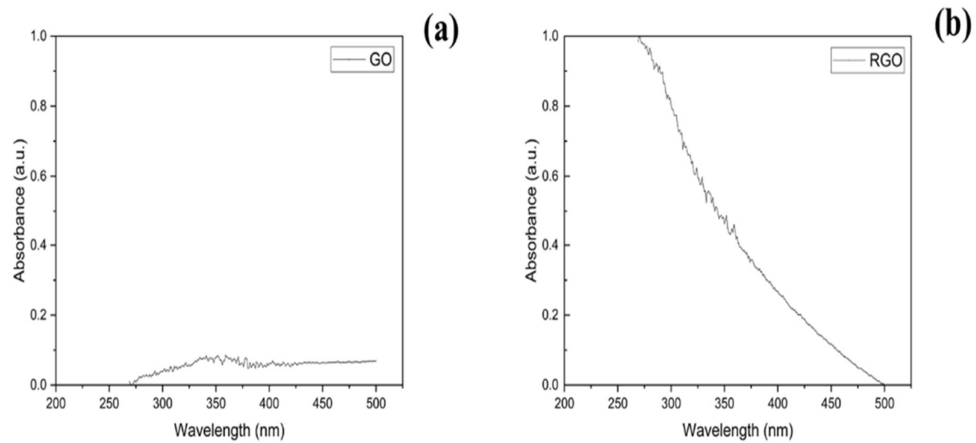


Figure 4.55 (a) UV-VIS Spectra of GO-DMF (b) UV-VIS Spectra of rGO-DMF

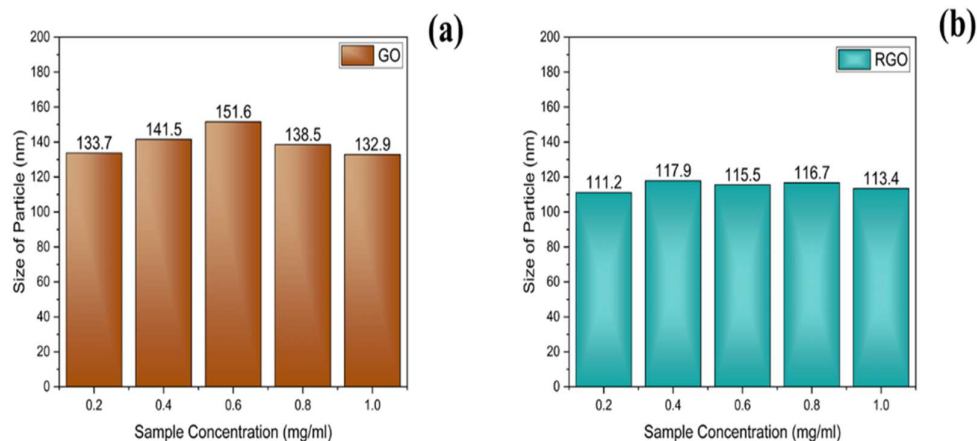


Figure 4.56 (a) DLS Study of GO-DMF (b) DLS Study of rGO-DMF

In this study, we used the DLS technique to analyze the size of GO and rGO particles in the DMF-GO and DMF-rGO nanosuspension [20]. This study helps to determine the size of the particle in the nanosuspension, which comes out to be in the range of 132 nm to 151 nm in the case of GO and 111 nm to 118 nm in the case of rGO. [26]

4.21.3 Thermoacoustic analysis: The following parameters have been measured in the study.

4.21.3.1 Ultrasonic Velocity

Ultrasonic velocity is one of the utmost significant parameters to qualitatively measure the interparticle and intermolecular interaction of the nanosuspension [9]. The ultrasonic velocity is measured for all the prepared samples of DMF-GO and DMF-rGO at four distinct temperatures (298, 303, 308, and 313K). Readings were measured repeatedly to avoid any experimental errors as well as readings of pure DMF is matched with the literature [27]. The increase and decrease of ultrasonic velocity with the concentration of the particles and temperature give an insight of intermolecular and intraparticle interactions, as shown in Fig. 4.57 (a) and 4.57 (b). It can be noticed in DMF-GO and DMF-rGO that ultrasonic velocity increases from the pure liquid and then decreases with the growth in the concentration of the particles. Further, it can similarly be noticed that as the temperature of the system increases from 298 K to 313 K, there is a decrease in the ultrasonic velocity. The decrease in the ultrasonic velocity

with the concentration is due to GO and DMF, rGO, and DMF interaction, it further explains the supremacy of intermolecular interaction over intraparticle interactions. The increase in concentration also reduces the Brownian motion of the system, which helps to reduce the ultrasonic velocity of the system. At the higher temperatures, the velocity decreases further as compared to the pure DMF, which helps to establish the fact that GO and DMF, rGO, and DMF having more interaction as compared to GO and GO, rGO, and rGO. The reduction of ultrasonic velocity with surging temperature proves that the nanosuspension follow the usual behavior of non- aqueous liquids, which can be described as the temperature of suspension increases, the average speed of the molecules surges, and the amount of time they employ in interaction with their nearest neighbors decreases. Thus, the increasing temperature leads to the fading of the intermolecular adhesive and cohesive forces, thereby enhancing the compressibility, which, in turn, reduces the ultrasonic velocity [28][29].

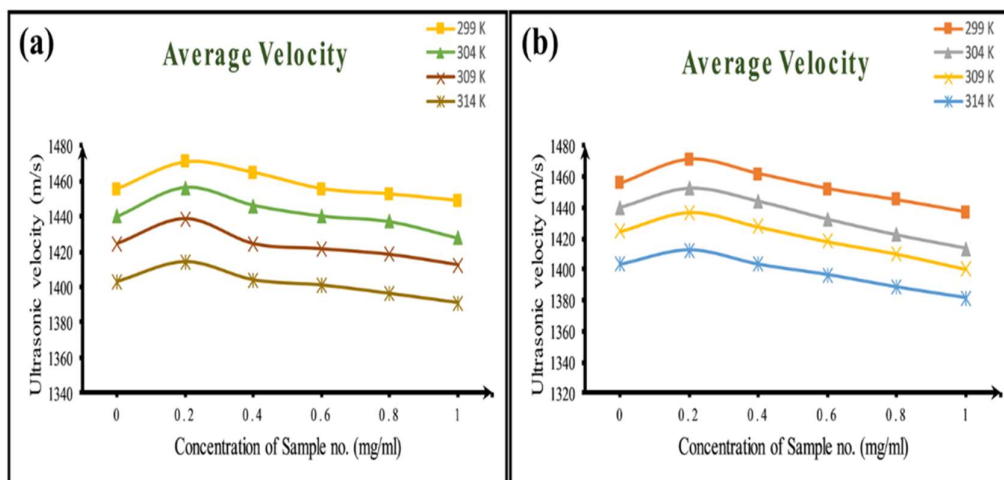


Figure 4.57 (a) Ultrasonic Velocity Study of GO-DMF (b) Ultrasonic Velocity Study of rGO-DMF

4.21.3.2 Density

It can be seen in Fig. 4.58 (a) and 4.58 (b) that the density of DMF-GO and DMF-rGO nanosuspension increase as the particles added to pure DMF. After this decrease in the density of formulated nanosuspension can be seen, the usual reflection is that density declines with temperature, which agrees well with the acceptable behavior of the fluids.

Density raises with concentration, as the nanoparticles being added are of higher density than the base fluid [30]. The decrease in density after increasing the concentration of the particles is due to the increase in intermolecular interaction instead that of interparticle communication [31].

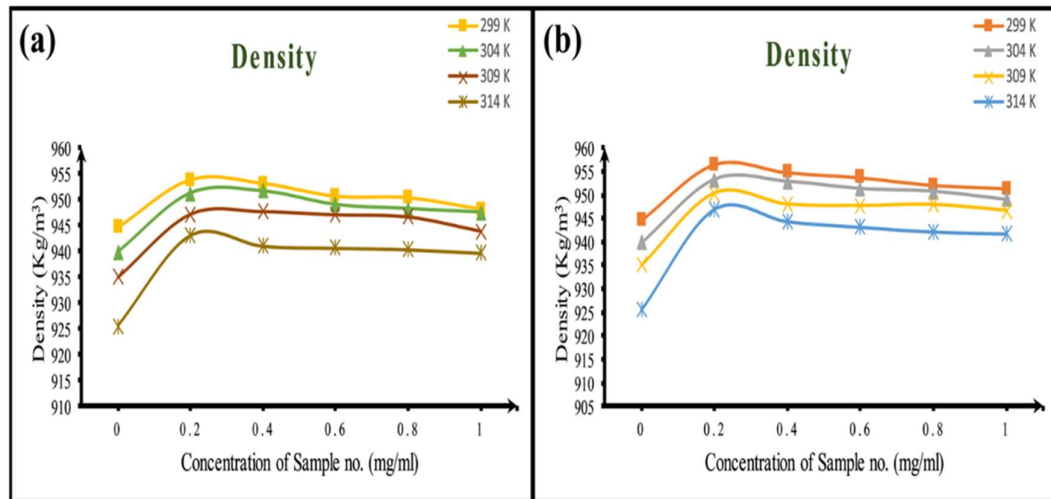


Figure 4.58 (a) Density of GO-DMF (b) Density of rGO-DMF

4.21.3.3 Viscosity

The viscosity of the DMF-GO and DMF-rGO nanosuspension rises very sharply with the addition of GO and rGO particles in the pure DMF solution, as displayed in figure 4.59 (a) and 4.59 (b), respectively.

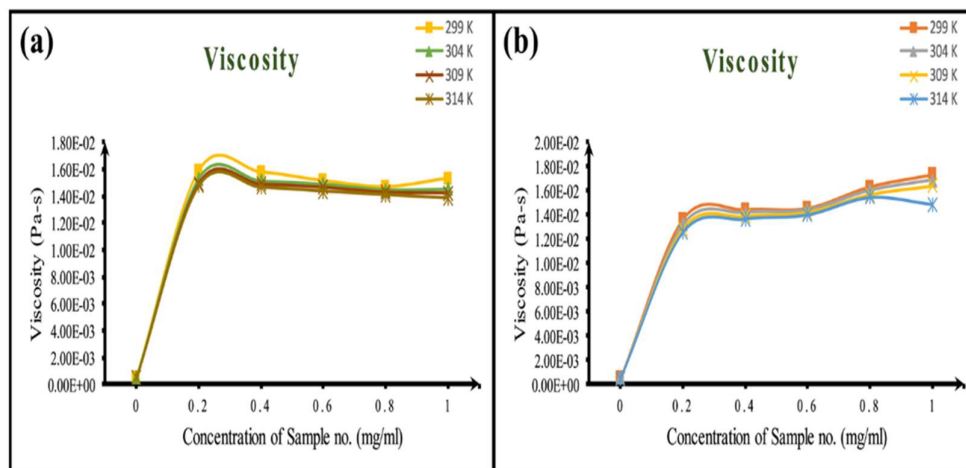


Figure 4.59 (a) Viscosity of GO-DMF (b) Viscosity of rGO-DMF

Viscosity similarly increases with increases the particle loading, which is due to the interlocking of GO and rGO particles while flow [8]. With the growth in the temperature, the viscosity of both nanosuspension decreases as normal fluid. The decrease in the viscosity can be understood by the rise in the Brownian motion of the particle present in the nanosuspension with the upsurge in the temperature. The decline in viscosity helps to flow the nanosuspension effortlessly at higher temperatures as compared to low temperature [32].

4.21.3.4 Adiabatic Compressibility

Fig. 4.60 (a) and 4.60 (b) shows the change in adiabatic compressibility with the increase in the particle loading in pure DMF. As the particles are added in the pure DMF, it shows a sudden decrease, which shows the weak particle fluid interaction [33]. The decline in the compressibility also leads to the conclusion that the particle added to the base fluid tries to form a complex structure in the nanosuspension. After this continuous rise in the adiabatic compressibility can be seen in both DMF-GO and DMF-rGO nanosuspension. The increase in the adiabatic compressibility shows the interaction in the particle and fluid decreases and omission of complex formation in the system. Adiabatic compressibility likewise increases with the increase in the temperature of the system, which is the cause of the rise in the Brownian motion of the particles. [3]

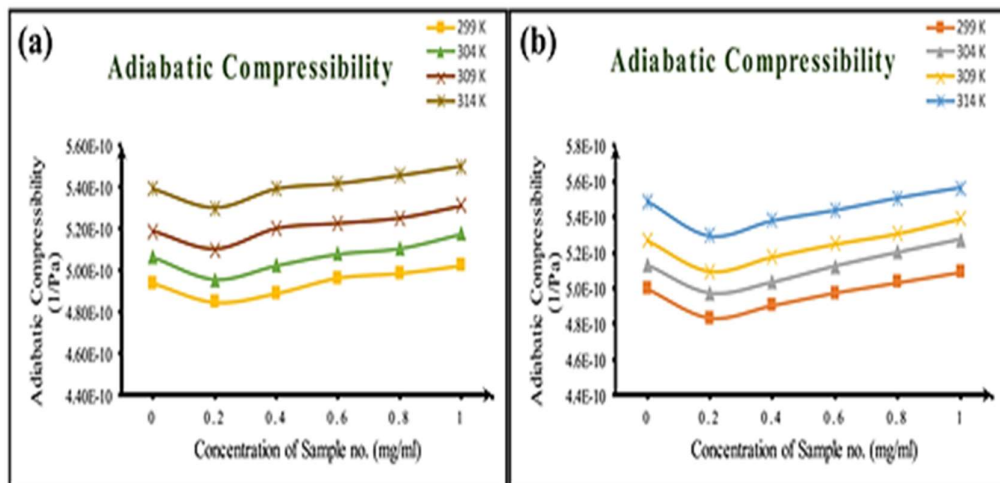


Figure 4.60 (a) Adiabatic Compressibility of GO-DMF (b) Adiabatic compressibility of rGO-DMF

4.21.3.5 Acoustic Impedance

Fig. 4.61 (a) and 4.61 (b) shows the values of acoustical impedance with particle loading in pure DMF. An upsurge in the amount of acoustical impedance shows the increase in interaction in solute and particle of the DMF-GO and DMF-rGO nanosuspension. This interaction decreases with the further addition of the particle concentration because particle-particle interaction increases as compare to particle-fluid interaction [34]. With the improvements in the temperature, the value of acoustic impedance decreases because of the Brownian motion of the particles in the fluid increases. Increasing particle-fluid interactions at lower concentrations widens the intermolecular gap, which provides resistance to the propagation of ultrasonic waves [35].

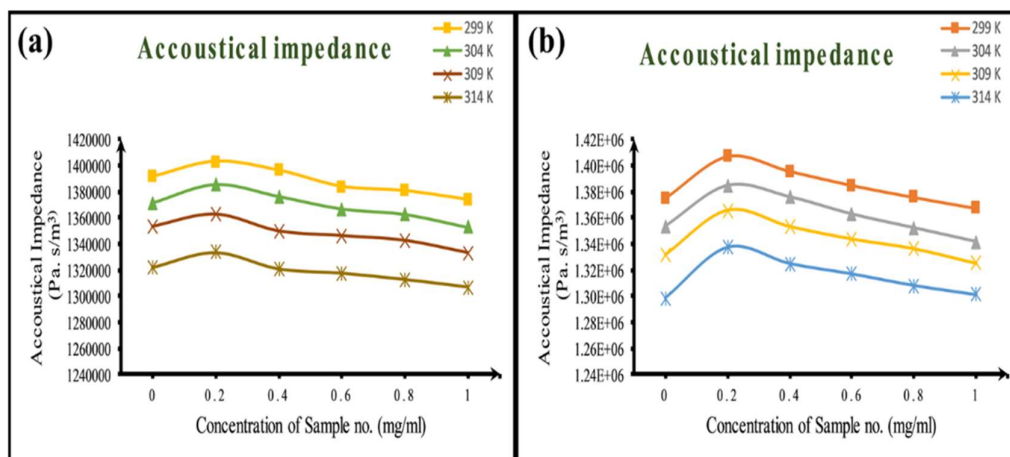


Figure 4.61 (a) Acoustical Impedance of of GO-DMF (b) Acoustical Impedance of rGO-DMF

4.21.3.6 Ultrasonic attenuation

Variation of the ultrasonic attenuation and concentration of the particles in DMF-GO and DMF-rGO nanosuspension is shown in Fig. 4.62 (a) and 4.62 (b) respectively. Ultrasonic attenuation increases as soon as the particle is added in the pure DMF fluid. Further increase in the ultrasonic attenuation can be seen in both DMF-GO and DMF-rGO nanosuspension, this increase in the attenuation is because both GO and rGO can form agglomeration by binding with each other. This blockage produced by the

agglomerated GO and rGO particles block the ultrasonic waves from reaching one end to the other. With the increase in the temperature value of the ultrasonic attenuation increases because of the increase in the Brownian motion of the fluid particles. [34]

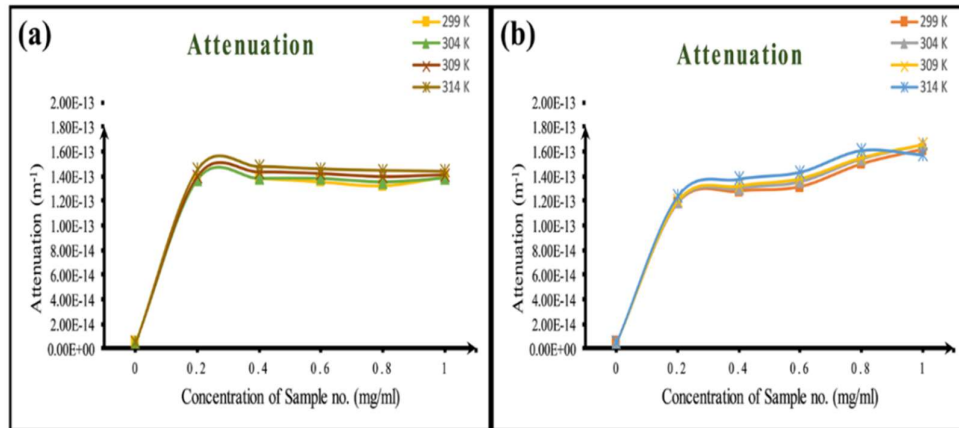


Figure 4.62 (a) Attenuation of sound wave in GO-DMF (b) Attenuation of sound wave in rGO-DMF

4.21.3.7 Bulk Modulus

It can be described as the resistance of the liquid or fluid to the stress applied. In Fig. 4.63 (a) and 4.63 (b), the bulk modulus tends to increase for the DMF-GO and DMF-rGO nanosuspension with the growth in the count of the particles in nanosuspension in the pure DMF.

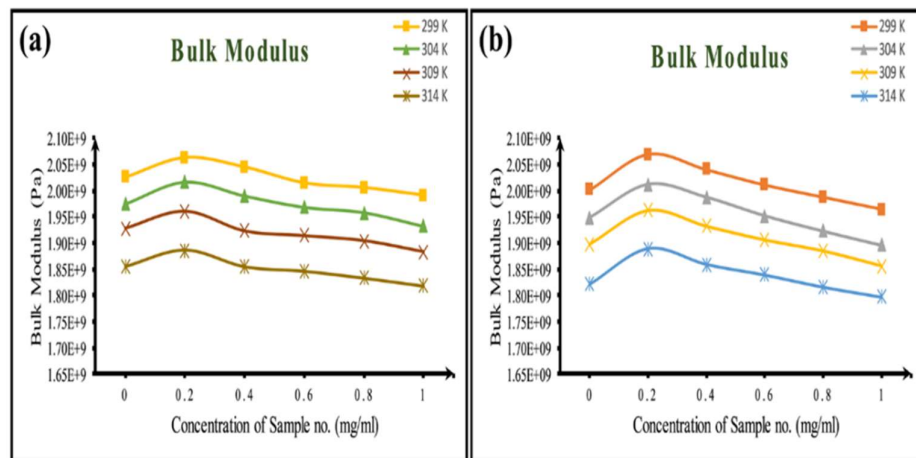


Figure 4.63 (a) Bulk Modulus of GO-DMF (b) Bulk Modulus of sound wave in rGO-DMF

4.21.3.8 Relaxation Time

Fig. 4.64 (a) and 4.64 (b) indicates the variation of relaxation time versus concentration of the particles for the DMF-GO and RO-DMF nanosuspension. Relaxation time is the duration of molecular re-arrangement during the propagation of ultrasonic waves from the fluid. It can be seen clearly in Fig. 4.64 (a) and 4.64 (b) that relaxation time rises abruptly as the particles added in pure DMF. Besides, a slight change in relaxation time is seen in nanosuspensions. Relaxation time increases with an increase in temperature as the Brownian motion of DMF molecules rises with an increase in temperature. [37]

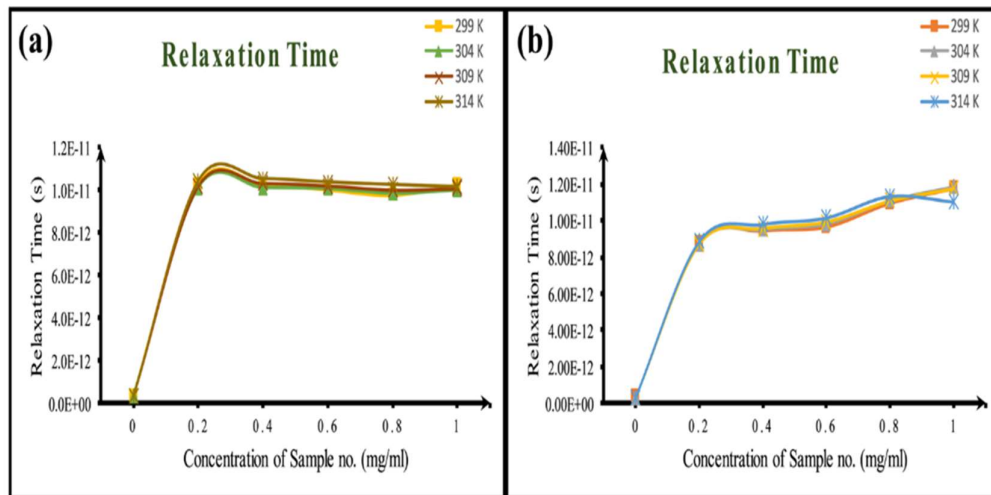


Figure 4.64 (a) Relaxation Time of GO-DMF (b) Relaxation Time of rGO-DMF

4.21.3.9 Intermolecular free length

It can be visible from Fig. 4.65 (a) and 4.65 (b) that the intermolecular free length is a function of temperature. As the temperature rises, the free intermolecular free length increases. This increase is due to a decrease in particle-particle interaction. The intermolecular free length increases with the loading of the particles. An increase in the intermolecular free is contributed to the fact that fluid-particle interaction decreases [38]

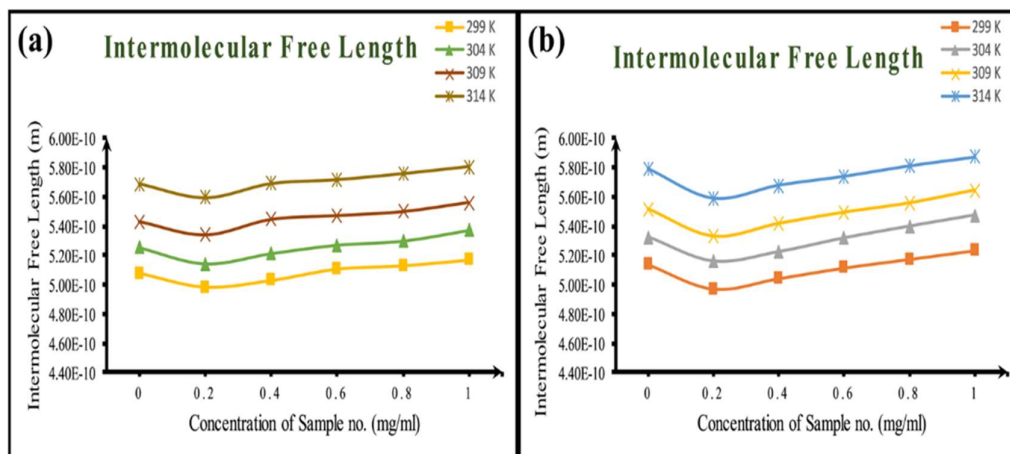


Figure 4.65 (a) Intermolecular Free Length of GO-DMF (b) Intermolecular Free Length of rGO-DMF

4.22 References

- [1] J. Pardeike et al., *Int. J. Pharm.*, **420**, 93, (2011)
- [2] C. Selvam, D. Mohan Lal, and S. Harish, *J. Therm. Anal. Calorim.*, **129**, 947, (2017).
- [3] A. Nanda, A. Tiadi, S. K. Mallik, R. Giri, and G. Nath, *IOP Conf. Ser. Mater. Sci. Eng.*, **360**, 1, (2018).
- [4] K. I. Bolotin et al., *Solid State Commun.*, **146**, 351, (2008).
- [5] I. Saxena, R. N. Pathak, V. Kumar, and R. Devi, *Int. J. Appl. Res.*, **1**, 562, (2015)
- [6] P. Gnana Kumari, P. Venkatesu, M. V. Prabhakara Rao, M. J. Lee, and H. mu Lin, *J. Chem. Thermodyn.*, **41**, 586, (2009)
- [7] Kenry, J. C. Yeo, J. Yu, M. Shang, K. P. Loh, and C. T. Lim, *Small*, **12**, 1593, (2016).
- [8] M. N. Rashin and J. Hemalatha, *Exp. Therm. Fluid Sci.*, **51**, 312, (2013).
- [9] M. N. Rashin and J. Hemalatha, *J. Mol. Liq.*, **197**, 257, (2014).

- [10] W. S. Hummers and R. E. Offeman, *J. Am. Chem. Soc.*, **80**, 1339, (1958).
- [11] S. Park, J. An, J. R. Potts, A. Velamakanni, S. Murali, and R. S. Ruoff, *Carbon N. Y.*, **49**, 3019, (2011).
- [12] H. J. Ryu, S. S. Mahapatra, S. K. Yadav, and J. W. Cho, *Eur. Polym. J.*, **49**, 2627, (2013).
- [13] S. Zhou, H. Zhang, Q. Zhao, X. Wang, J. Li, and F. Wang, *Carbon N. Y.*, **52**, 440, (2013).
- [14] L. Wang, Y. Huang, and H. J. Huang, *Mater. Lett.*, **124**, 89, (2014)
- [15] X. Jiang et al., *Carbon N. Y.*, **67**, 662, (2014).
- [16] R. Muzyka, M. Kwoka, Ł. Smędowski, N. Díez, and G. Gryglewicz, *Xinxing Tan Cailiao/New Carbon Mater.*, **32**, 15, (2017).
- [17] J. Luo, Y. Xu, W. Yao, C. Jiang, and J. Xu, *Compos. Sci. Technol.*, **117**, 315, (2015).
- [18] N. I. Zaaba, K. L. Foo, U. Hashim, S. J. Tan, W. W. Liu, and C. H. Voon, *Procedia Eng.*, **184**, 469, (2017)
- [19] J. Zhang et al., *Electrochim. Acta*, **199**, 70, (2016).
- [20] J. Ma, J. Liu, W. Zhu, and W. Qin, *Colloids Surfaces A Physicochem. Eng. Asp.*, **538**, 79, (2018).
- [21] Y. Guo, X. Sun, Y. Liu, W. Wang, H. Qiu, and J. Gao, *Carbon N. Y.*, **50**, 2513, (2012).
- [22] J. L. Lv, S. R. Zhai, C. Gao, N. Zhou, Q. Da An, and B. Zhai, *Chem. Eng. J.*, **289**, 261, (2016).
- [23] I. Roy et al., *RSC Adv.*, **6**, 10557, (2016)
- [24] Q. Lai, S. Zhu, X. Luo, M. Zou, and S. Huang, *AIP Adv*, **2**, 3, (2012).

- [25] J. I. Paredes, A. Marti, J. M. D. Tasco, and A. Marti, *Langmuir*, **24**, 10560, (2008).
- [26] S. Sen Gupta et al., *J. Chem*, **084302**, 1352, (2011).
- [27] D. Papamatthaiakis, F. Aroni, and V. Havredaki, *J. Chem. Thermodyn.*, **40**, 107, (2008).
- [28] M. Nabeel Rashin and J. Hemalatha, *J. Mol. Liq.*, **197**, 257, (2014),
- [29] M. N. Rashin and J. Hemalatha, *Ultrasonics*, **52**, 1024, (2012).
- [30] R. S. Vajjha, D. K. Das, and B. M. Mahagaonkar, *Pet. Sci. Technol.*, **1**, 612, (2009),
- [31] S. N. Shoghl, J. Jamali, and M. K. Moraveji, *Exp. Therm. FLUID Sci.* **12**, 205, (2016).
- [32] M. R. Esfahani, E. M. Languri, M. R. Nunna, M. Rabbani, E. Mohseni, and M. Rao, *Int. Commun. Heat Mass Transf.*, **76**, 308, (2016).
- [33] Khushboo, A. Devi, P. Malik, and H. Kumar, *J. Mol. Liq.*, **214**, 145, (2016)
- [34] S. Tiwari, B. S. Kusmariya, A. Tiwari, V. Pathak, and A. P. P. Mishra, *J. Taibah Univ. Sci.*, **11**, 101, (2017)
- [35] N. H. Ayachit, S. T. Vasan, F. M. Sannaningannavar, and D. K. Deshpande, *J. Mol. Liq.*, **133**, 134, (2007).
- [36] F. Chen, Z. Yang, Z. Chen, J. Hu, C. Chen, and J. Cai, *Journal of Molecular Liquids*, **209**, 683, (2015)
- [37] K. Kaur and K. C. Juglan, *Der Pharma Chem.*, **7**, 160, (2015).
- [38] A. Singh, *Journal of Molecular Liquids*, **47**, 1020, (2008).

Section 3 (Part A)

Study of NMP-GO

4.23 Introduction

When we disperse nanoparticles in the solvent under the controlled condition, the suspension mixture prepared is called the nanosuspension. Many definitions of nanosuspensions; nanofluids are available in the literature; in this study, we are considering the size of the solute particles are in the range of 100 to 500nm than the suspension is called nanosuspension [1]. A lot of examples of nanosuspension are available in the literature most of the example available is based on nanoparticles of carbon like carbon nanotubes, nanoparticles of metals and metal oxides, ceramics, etc. all these nanoparticles shows some remarkable properties when compared to their micrometer counterpart. It is discussed in the literature that most of the impressive features of the nanoparticles are because of the larger surface area. The addition of nanoparticles with the larger surface enhances the overall properties of the fluid in which we are mixing it [2-5]. Since the size of the nanoparticles is very small, they can interact with the molecules of the solvent. When we apply heat, the molecules of the liquid will start random zigzag motion. Due to this motion, molecules collide with the nanoparticle of the suspension. During this process, heat is transferred to the nanoparticles, and they start moving at a rapid pace in the suspension. This rapid movement in the suspension helps to give higher thermal conductivities in the case of nanofluids. Therefore, it is a perfect opportunity to study the nanosuspension of these available solute and solvent.

Ultrasonication is a recognized method for studying these crisscross motions of particles and diffusing accumulated nanoparticles for aqueous nanosuspension preparation [6-7]. Since as per literature, it has been observed that when we add ordinary particles with micron-size, it causes changes in ultrasonic velocity and ultrasonic attenuation. So, the size of particles also plays an essential role in the study of nanosuspension. The demand of the ultrasonication in the research also increases the curiosity of the research groups to study the effect of passing the ultrasonic waves

through the nanosuspensions. Many researchers are studying the ultrasonic velocity, density, and viscosity of nanosuspensions. Since we know the surface to volume percentage of the nanoparticles is very high, they can significantly improve the thermoacoustic properties of the nanosuspension. Hence it is essential to discuss the impact of the density of the solid particles on the properties of pure liquids to predict the final properties of the nanosuspensions.

In the last decade, graphene was one of the essential materials which we able to discover and study. After its discovery in 2004, a series of properties have been considered and reported by many research groups. Firstly, the manufacturing process of the graphene is itself a topic of research; many research groups are working to find a clean and green way to produce graphene. As far as the properties of graphene are concerned, it has been reported that this material is having high mobility of electron, impermeable to gasses, most potent content available, very high thermal conductivity, etc. Graphene offers a lot of opportunities in the field of research and development, but still, there are some gaps available like production of the graphene at the industry scale is not possible, the creation of the graphene involves toxic gasses, there are very less available solvents in which graphene can be suspended [8-11].

In this paper, we are studying the thermoacoustic properties of the prepared NMP-GO nanosuspension at different temperatures as well as different concentrations of GO. Different thermodynamically, physical, and fluid-particle interaction studies have been done and related. Various acoustical parameters like ultrasonic velocity, density, viscosity were calculated at a temperature range of 298 to 313 K and explained.

4.24 Material and Method

4.24.1 Reagent and Chemicals

Graphite powder, sodium nitrate procured from Sigma Aldrich, KMnO_4 , HCL, H_2SO_4 , and Ammonia has taken from CDH. H_2O_2 has been obtained from fisher scientific. NMP has been acquired from Sigma Aldrich. All chemicals employed during this research were of AR quality and utilized without additional purification. Throughout the whole experiment, double distilled water was used.

4.24.2 Methods

As mentioned earlier, GO was prepared by the novel Hummers method. In this method, 4g of carbon powder was mixed with 8 g of sodium nitrate. On the other side, a flask of 1 liter was taken and placed on the magnetic agitator. An ice bath has been formed all around the flask, and a thermometer is set inside the flask to measure the temperature. Now 160 ml of sulphuric acid was added to the flask with a mixture of carbon powder and sodium nitrate. Keeping the check on the temperature and makes sure that it should be close to zero. As soon as the temperature of the mixture reaches zero and carbon is fully dissolved in the sulphuric acid, we can move to the next step. Now we add potassium permanganate in the mixture very slowly because the reaction of the potassium permanganate with the mixture is exothermic. The rate of adding the potassium permanganate in the mixture should be so slow that the temperature of the reaction should not go above 90 °C. We have done continuous stirring for 3 hours. After 3 hours, the ice bath was removed, and the flask was moved to a water bath where 40 °C temperature was maintained. This increase in temperature boosts the oxidation process in the reaction mixture. After half an hour, the flask is again transferred to a magnetic stirrer without an ice bath, now again keeps the mixture on a magnetic stirrer until the shade of the combination adjusts from black to yellowish-brown, keep a rotation of the magnetic stirrer to the lowest. After 24 hours, the 30 % hydrogen peroxide was added to the mixture, which stops the further oxidation of the mixture. Further water was added to the mixture very slowly. More water was added to the mixture, and the mixture was divided into two parts for easy handling. Leaving the mixture overnight helps to remove the excess water from the final product. Furthermore, water was used for washing, and the mixture was washed with hydrochloric acid two times. The hydrochloric wash will remove the excess metal ions from the final product and will increase the purity of the sample after that sample was again washed and kept for 3 hours of continuous ultrasonication. Then the filtered result was dried up in a vacuum at the temperature of 40 °C. After drying, brown color powder of the GO was obtained. This GO powder was used to make nanosuspension of the different concentrations with the help of ultrasonication. [7], [12-14].

4.25 Characterization of GO and NMP-GO nanosuspension

In this study for the SEM analysis, we have used Nova Nano FESEM 450 with the attached EDS for the micrograph studies. For the preliminary investigation of the sample, the FTIR spectrum has been calculated with the help of Shimadzu 8400S spectrometer, appearing in the scope of 4000 to 400 cm^{-1} . XRD has been calculated with the help of Panalytical Xpert Pro. The final testing of the sample has been done with the Raman spectrometer model Airix STR 500 at wavelength 1.54 Å. The average size of the particle size in the formulated nanosuspension in conjunction with Malvern Zetaster Nano Z290. The velocity of the ultrasonic wave inside the liquid sample, together with the use of Mittal Interferometer M-81 with a static frequency of 2 MHz. We have calculated the density of the prepared nanosuspension with a pycnometer. In this study, the viscosity of the sample has been calculated with rotatory viscometer model Labman LMDV-200.

4.26 DATA TABLE

Table 4.10 NMP-GO Nanosuspension 1					
Concentration (mg/ml)	Temperature(T) (K)	Average Velocity(U) (m/s) $U = \lambda \times f$	Density(ρ) (Kg/m³)	Viscosity(η) (Pa-s)	Adiabatic Compressibility(β) (1/Pa) $\beta = 1/ (U^2 \times \rho)$
0	299	1547.69	1028.316	0.001661	4.06E-10
0.2	299	1556.69	1046.763	0.001794	3.94E-10
0.4	299	1567.69	1053.713	0.001839	3.86E-10
0.6	299	1576.46	1061.288	0.001989	3.79E-10
0.8	299	1583.46	1064.063	0.002134	3.75E-10
1	299	1592.38	1066.813	0.002277	3.70E-10
0	304	1526.15	1023.823	0.001523	4.19E-10

0.2	304	1535.69	1042.713	0.001643	4.07E-10
0.4	304	1545.92	1049.688	0.00175	3.99E-10
0.6	304	1552.15	1057.213	0.001865	3.93E-10
0.8	304	1559.15	1060.438	0.002	3.88E-10
1	304	1570	1061.904	0.002128	3.82E-10
0	309	1504.69	1019.33	0.001413	4.33E-10
0.2	309	1514.69	1038.538	0.00155	4.20E-10
0.4	309	1521.69	1046.663	0.001635	4.13E-10
0.6	309	1529.62	1053.163	0.001717	4.06E-10
0.8	309	1539.69	1055.513	0.001844	4.00E-10
1	309	1549.77	1057.263	0.001966	3.94E-10
0	314	1483.00	1014.72	0.001259	4.48E-10

0.2	314	1489.23	1035.338	0.001375	4.36E-10
0.4	314	1497.23	1042.263	0.00153	4.28E-10
0.6	314	1507.08	1049.063	0.001649	4.20E-10
0.8	314	1515.23	1052.263	0.001743	4.14E-10
1	314	1526.15	1054.438	0.001887	4.07E-10

Table 4.11 NMP-GO Nanosuspension 2

Concentration (mg/ml)	Temperature(T) (K)	Acoustical impedance(Z)	Attenuation (α/f^2)	Bulk Modulus(K)	Relaxation Time(τ)	Intermolecular Free Length (L_f)
		(Pa. s/m ³) $Z = \rho \times U$	(m ⁻¹) $\alpha/f^2 = 8\pi^2\eta / 3\rho U^3$	(Pa) $K = \rho U^2$	(s) $\tau = 4\beta\eta/3$	($L_f = K_T \times \beta^{1/2}$)
0	299	1591516.763	1.14556E-14	2463178252	8.99E-13	4.17E-10
0.2	299	1629487.132	1.19433E-14	2536610083	9.43E-13	4.05E-10
0.4	299	1651896.981	1.1909E-14	2589666190	9.47E-13	3.97E-10
0.6	299	1673078.925	1.25794E-14	2637544576	1.01E-12	3.90E-10
0.8	299	1684902.043	1.32835E-14	2667977582	1.07E-12	3.85E-10
1	299	1698775.813	1.38963E-14	2705104471	1.12E-12	3.80E-10
0	304	1562511.409	1.10016E-14	2384632797	8.51E-13	4.35E-10

0.2	304	1601285.565	1.14405E-14	2459081925	8.91E-13	4.22E-10
0.4	304	1622736.13	1.18639E-14	2508625231	9.30E-13	4.14E-10
0.6	304	1640956.448	1.24025E-14	2547016862	9.76E-13	4.07E-10
0.8	304	1653385.207	1.3085E-14	2577881904	1.03E-12	4.02E-10
1	304	1667189.542	1.36121E-14	2617487580	1.08E-12	3.96E-10
0	309	1533778.16	1.07009E-14	2307864200	8.17E-13	4.54E-10
0.2	309	1573064.763	1.12931E-14	2382709095	8.67E-13	4.39E-10
0.4	309	1592698.275	1.16563E-14	2423596714	8.99E-13	4.32E-10
0.6	309	1610933.563	1.19779E-14	2464108761	9.29E-13	4.25E-10
0.8	309	1625164.477	1.25865E-14	2502253244	9.83E-13	4.18E-10
1	309	1638512.891	1.31357E-14	2539316863	1.03E-12	4.12E-10
0	314	1504829.76	9.99993E-15	2231662534	7.52E-13	4.73E-10

0.2	314	1541856.462	1.05725E-14	2296180084	7.98E-13	4.59E-10
0.4	314	1560507.485	1.14968E-14	2336439822	8.73E-13	4.52E-10
0.6	314	1581017.885	1.20714E-14	2382715569	9.23E-13	4.43E-10
0.8	314	1594420.517	1.25195E-14	2415915027	9.62E-13	4.37E-10
1	314	1609233.846	1.32351E-14	2455938424	1.02E-12	4.30E-10

4.27 Result and Discussion

Figure 4.66 shows the FESEM image of the prepared GO sample at 20000X magnification. The stacking of the carbon layers can be seen in the picture very clearly. The side layers of the carbon sheets are visible, which confirms the conversion of the carbon powder into graphene oxide.

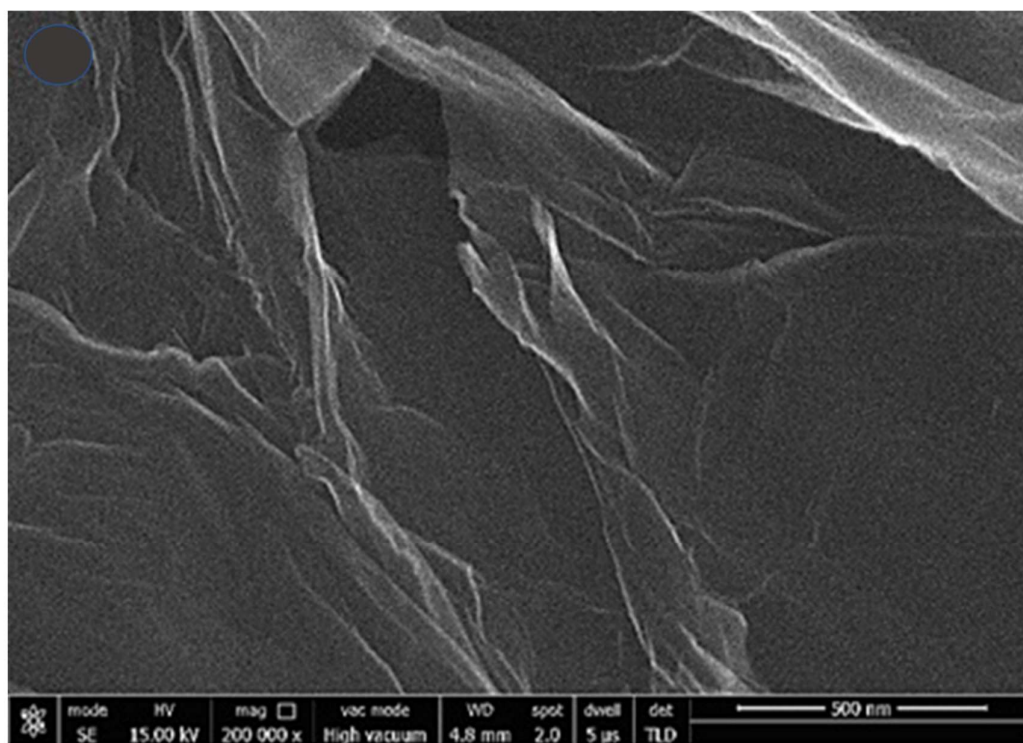


Figure 4.66 FESEM of GO

In figure 4.67, elemental analysis of the prepared sample is given; this EDS is taken with FESEM with EDS attachment, which uses backscattered electrons. The carbon content present in the sample is 74.33 %, and oxygen is 24.46%. The amount of oxygen present in the sample shows good oxidation of the prepared sample. The amount of oxygen confirms the conversion of carbon powder into graphene oxide. [15], [16]

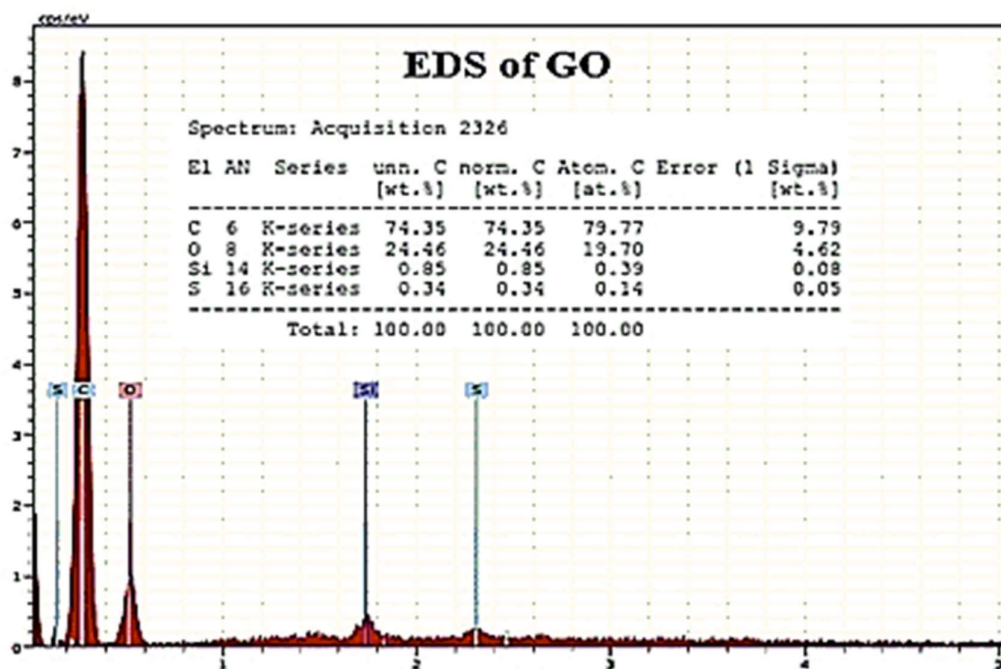


Figure 4.67 EDS of GO

FTIR of the prepared sample is given in figure 3. Peaks at 1116.8 cm^{-1} confirm the presence of a carbon-oxygen stretching bond, which again strengthens the existence of oxygen inside the sample.

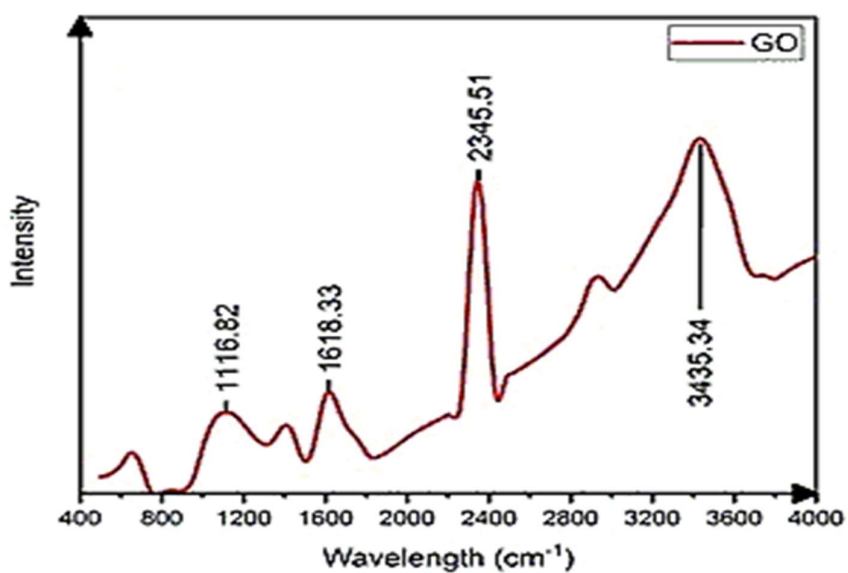


Figure 4.68 FTIR of GO

The peaks at 1618.3 cm^{-1} confirm the bonding between carbon and carbon, the mountain in the range of 1400 cm^{-1} to 1700 cm^{-1} confirms the presence of graphene in the sample under study as per literature. 2445.5 cm^{-1} corresponds to the presence of carbon dioxide in the sample [17-19].

The study of the XRD spectrum shows a peak at $8^{\circ}.93'$, as per figure 4.69. We know XRD works on the principle of Bragg's law. As per this law, if the separation between two planes is large, then the angle corresponding to the material will be less. In our sample, the peak comes at a shallow angle, which shows the separation of the layer with a larger distance. This large distance may be due to the presence of a big oxygen atom in between the layers of carbon. [22-22].

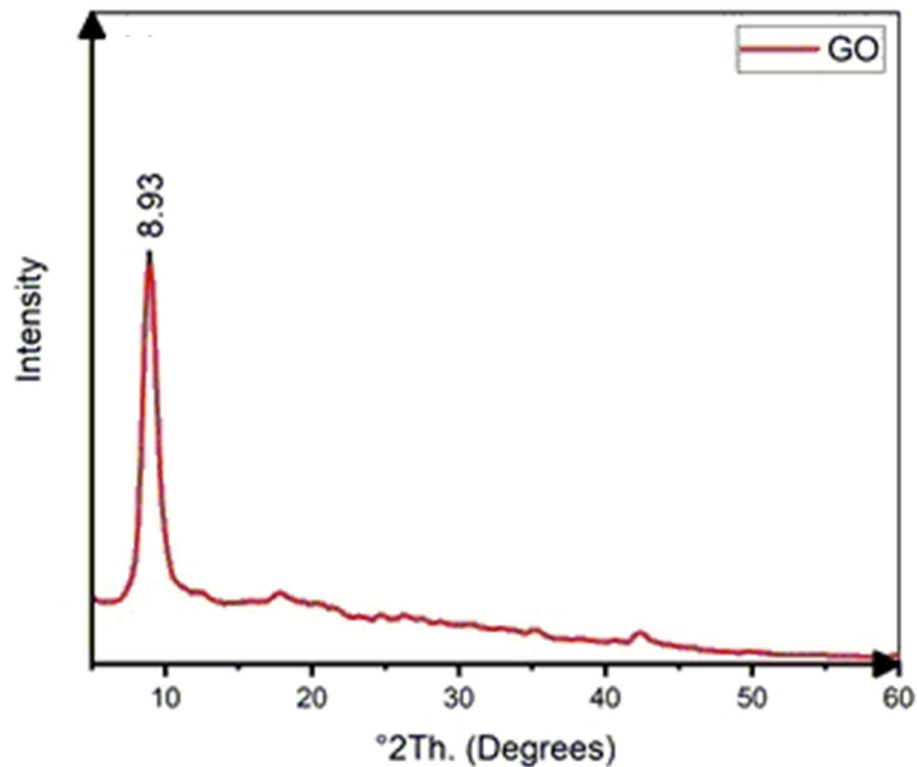


Figure 4.69 XRD of GO

Raman spectrum is shown in figure 4.70. two peaks are visible in the Raman spectra;

the first peak is at 1352.3 cm^{-1} , and the second peak is at 1595.2 cm^{-1} . as per the literature, the first zenith resembles the imperfection appear in the graphene network, and the second peak corresponds to the excellent structure of the graphene network. the ratio of the intensity of defect peak and good structure peak is $I_D/I_G = 0.84$, which shows the presence of a good graphene network in the sample preparation. [23-25]

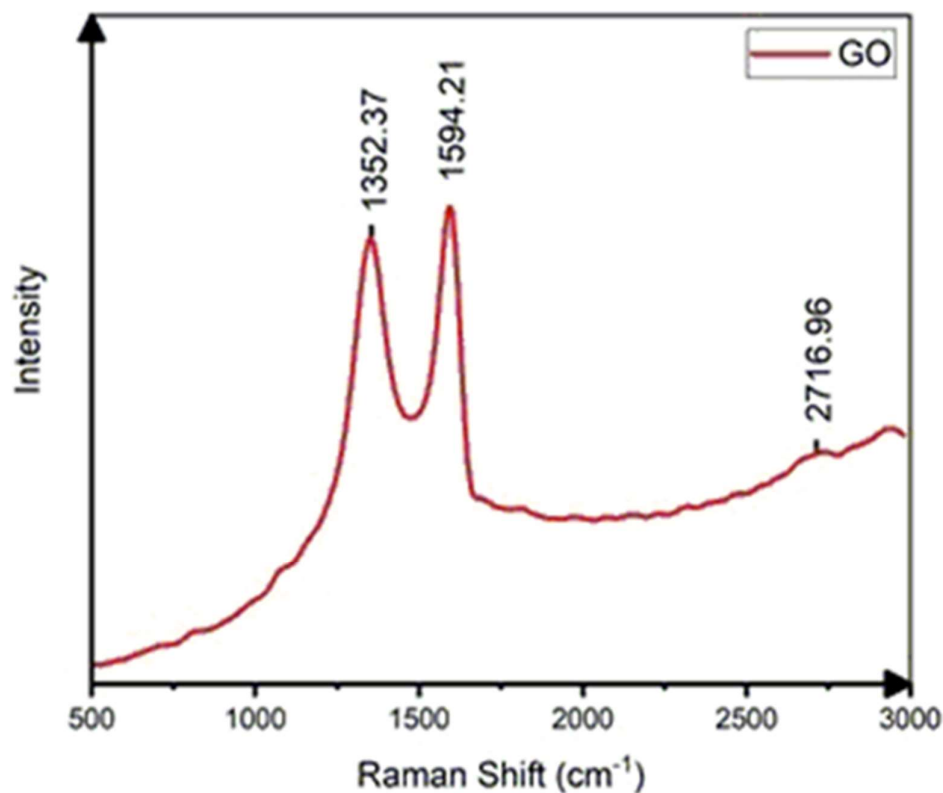


Figure 4.70 Raman of GO

As discussed earlier, nanosuspension has been prepared with intensive ultrasonication. So the presence of the GO can be shown with the help of UV-Vis, but in this study, we are using NMP as the solvent, which has a UV cut off wavelength 285 nm , but we know the peak of the GO comes near 230 nm but here which cannot be measured. So, we are not discussing UV-Vis spectra in this study [26-27]. The size of the particles and their distribution has been calculated with the help of the Dynamic light scattering method. The results of DLS have been plotted in figure 4.71. It is visible from the figure

that the size of the particle in the solvent is between 130 to 155 nm. [16], [28-29]. Since the particle size is above 100 nm, we call our sample as nanosuspension, not nanofluid.

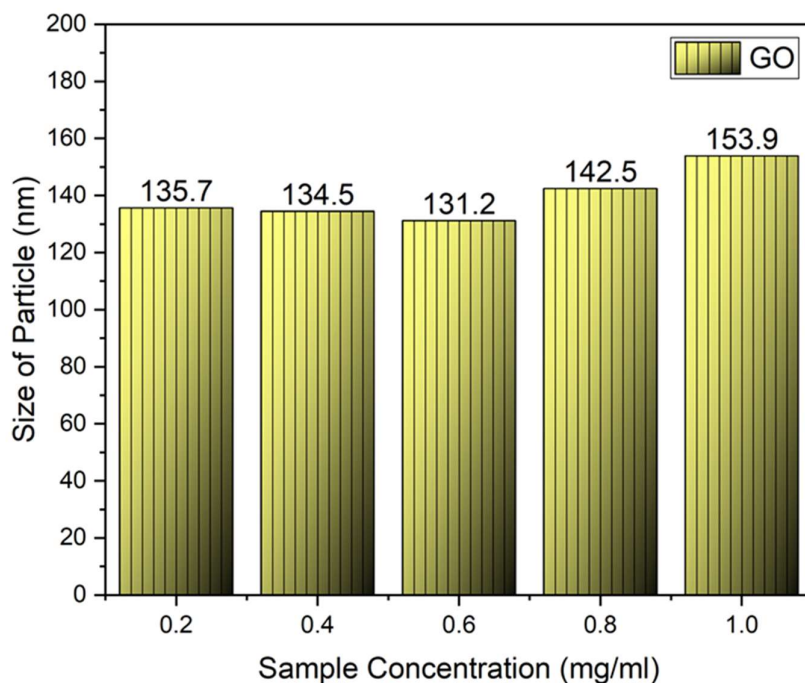


Figure 4.71 DLS of GO

To understand the intermolecular and intraparticle interaction among the solute molecule and solvent, it is essential to study the ultrasonic parameters of the nanosuspension. The ultrasonic velocity of all prepared samples has been calculated at the temperature 298, 303, 308, and 313K. Approximately 20 reading has been taken for each concentration to avoid any experimental error. In figure 4.72, it is visible that the ultrasonic velocity increases with the increase of concentration of the particles inside the solvent. This behaviour is in line with the rise of intramolecular interaction over intermolecular interaction, which means particles are attracted to the solvent. The growth of the number of particles present with increasing concentration also contributes to the outer layer, which additionally increases the speed inside the sample. An increase in the temperature decreases the ultrasonic velocity in the sample; that is might be because the zigzag motion of the solvent molecules increases with the rise in the heat,

which hinders the passage of ultrasonic waves through the sample[30-31]. From figure 4.72, the density of the liquid increases with the addition of GO particles in the NMP.

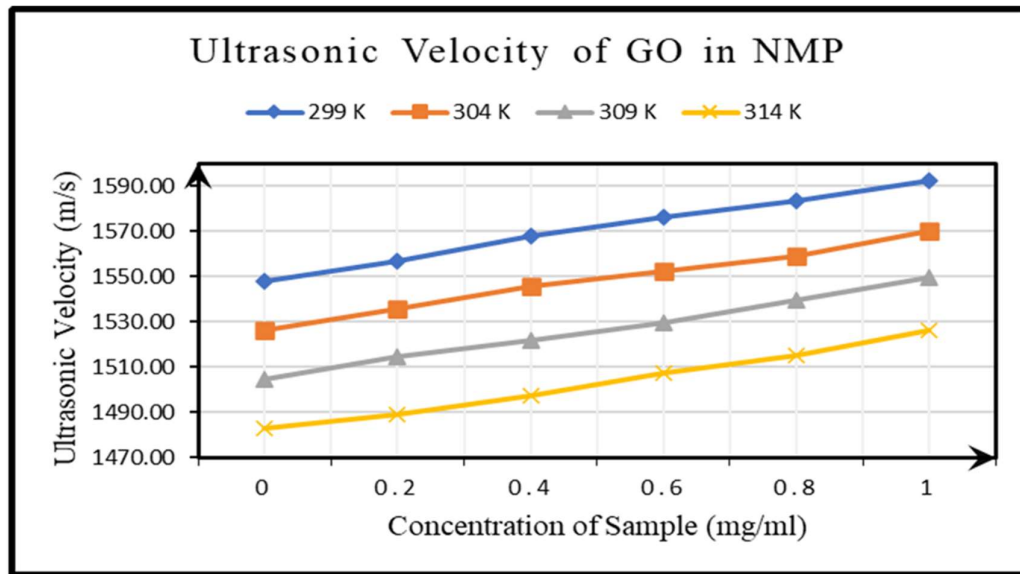


Figure 4.72 Ultrasonic Velocity of GO-NMP Nanosuspension

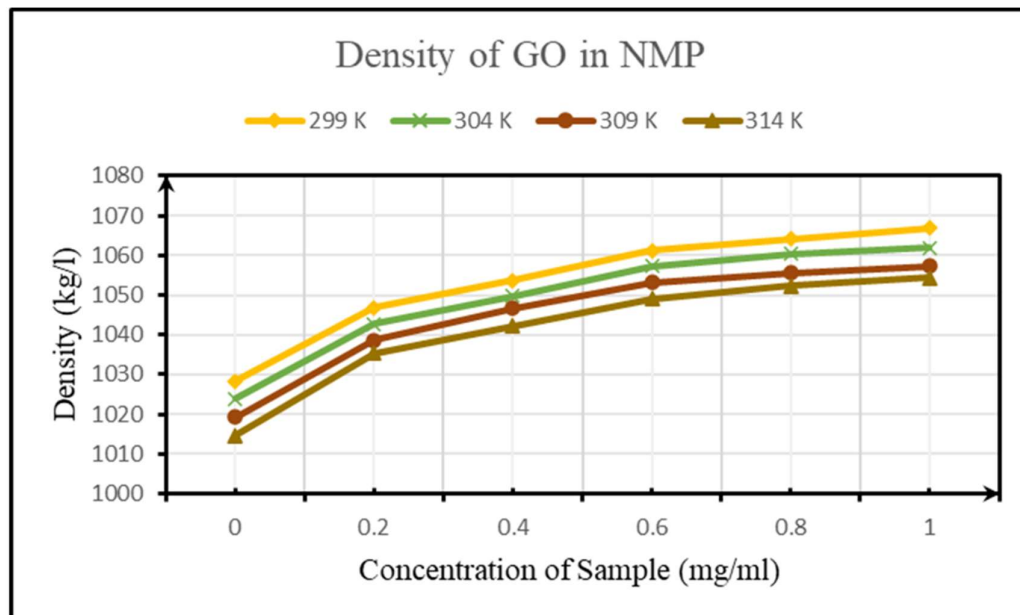


Figure 4.73 Density of GO-NMP Nanosuspension

The values increase from range 1010 kg/m³ to 1050 Kg/m³. As seen in the image, as soon as GO powder is added to the liquid, there is a sudden jump in the density. After

this, there is a slight increase in the density of nanosuspension. The rise in the density is because of increased intramolecular collaboration than intermolecular collaboration. The density of the nanosuspension decrease with the increase in the heat of the nanosuspension, as shown in figure 4.73. The reason can be intermolecular interaction improve with an increase in the temperature [32-33].

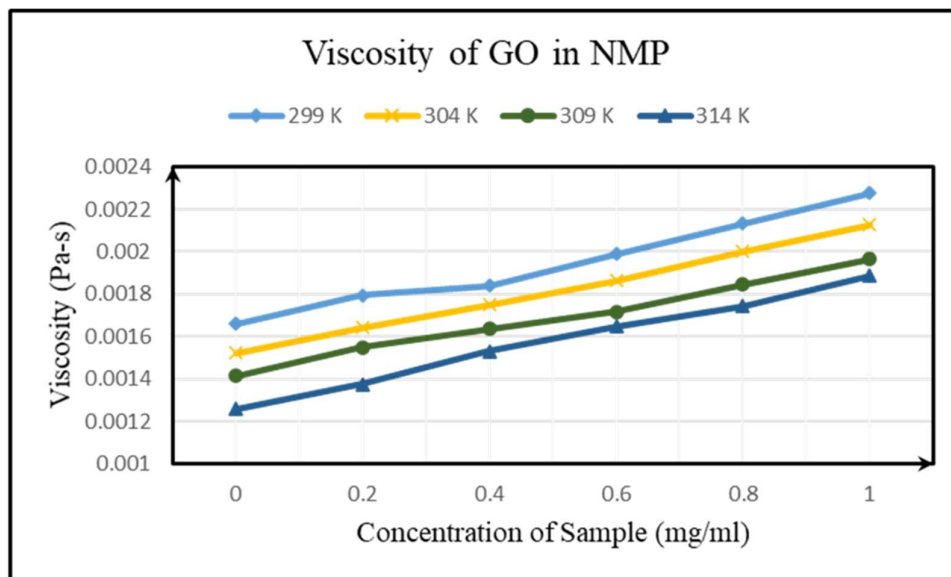


Figure 4.74 Viscosity of GO-NMP Nanosuspension

In figure 4.74, it can be seen clearly that the viscosity of the NMP-GO nanosuspension rises with a rise in the particle concentrations. The increase in the viscosity with particle loading can be due to the rise in the particle-solvent interaction, which increases the viscosity. On the other hand, the viscosity of the NMP-GO nanosuspension declines with an upsurge in the temperature. The fundamental reason behind this decrease is the rise in the zigzag movement of the NMP solvent molecules increases with increasing temperature [2], [31].

Figure 4.75 shows the continuous decline in the adiabatic compressibility with the increase in the particle loading of the GO particle in the NMP. This decrease is because of increased particle and solute molecule interaction. Adiabatic compressibility increases with an increase in the temperature that might be because of increasing intermolecular interaction between solvent molecules. [34-35]. Figure 4.76 shows the

continuous increase in the acoustical impedance with the increase in the GO particles in the NMP solvent. The increase in the impedance value suggests the increased interaction between molecules of the solvent and solute, which also affects the structural change.

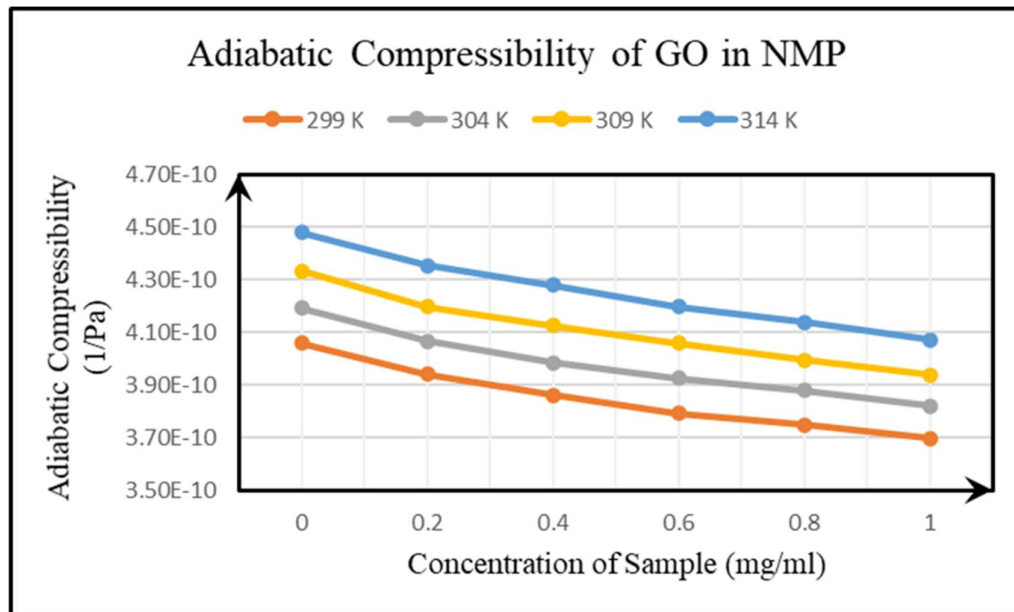


Figure 4.75 Adiabatic Compressibility of GO-NMP Nanosuspension

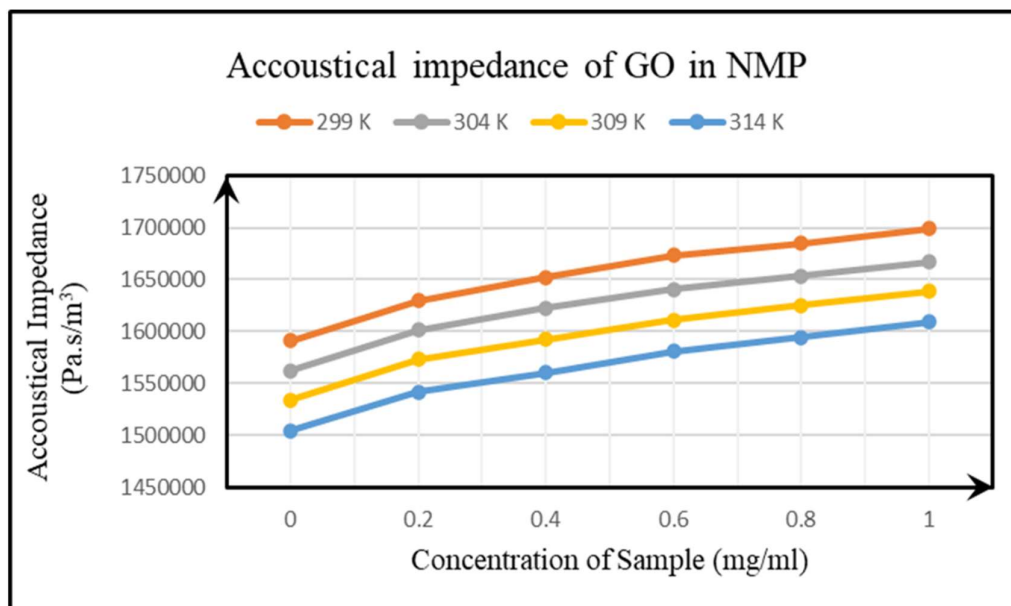


Figure 4.76 Acoustical Impedance of GO-NMP Nanosuspension

The acoustic impedance decreases because the Zigzag movement of the solvent increases with the rise in the heat, and the solvent molecule interacts with nanoparticles, which creates a gap between the molecules, which helps the ultrasonic waves to pass through the liquid easily. [36-37]. Figure 4.77 shows the attenuation of the ultrasonic wave inside the NMP-GO nanosuspension. With the rise in the particle loading in the fluid, attenuation of the ultrasonic wave decreases. The decline in attenuation may be due to network formation by GO particles, which reduces the intensity of the ultrasonic wave to reach from one end to the other. Attenuation declines with the rise in the heat of the sample. The decline in attenuation might be due to the increase in the particle and solute interaction as this interaction increases the gap between molecules increases, which helps to pass the ultrasonic wave easily [38-39]. Bulk modulus is the fluid's opposition to the stress being applied.

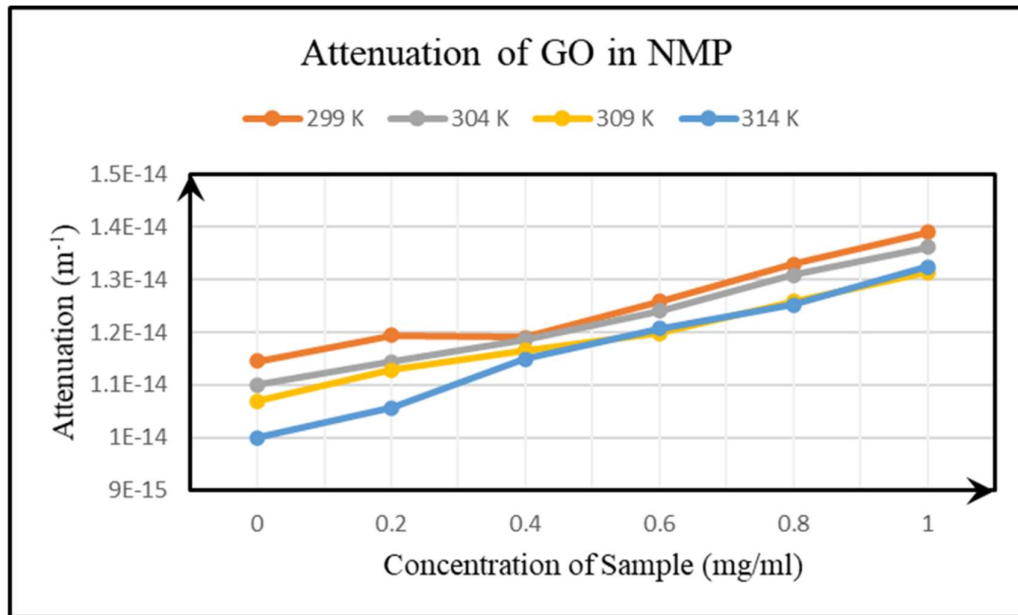


Figure 4.77 Attenuation of Ultrasound in GO-NMP Nanosuspension

In figure 4.78, it can be seen clearly that the value of bulk modulus rises with the increase in the particle loading in the solvent. Interaction between the particle and fluid increases as the concentration of the NMP-GO nanosuspension increases. The value of the bulk modulus decreases with the rise in the heat of the nanosuspension. The resistance of the nanosuspension decreases to the externally applied stress at a higher

temperature because the interaction between particle and solute increases creates the gap between molecules, which helps in reducing bulk modulus [40-41]. The relaxation time of the NMP-GO sample increase with the increase in the particle concentration in the NMP-GO nanosuspension, as shown in figure 7.79. Since the interaction between the solvent molecules and solute increases. The reordering time for the solute molecules increases. When the heat of the NMP-GO nanosuspension rises, the zigzag movement of the solvent molecule increases, which helps to reorder the molecules quickly because of fast motion [41-42].

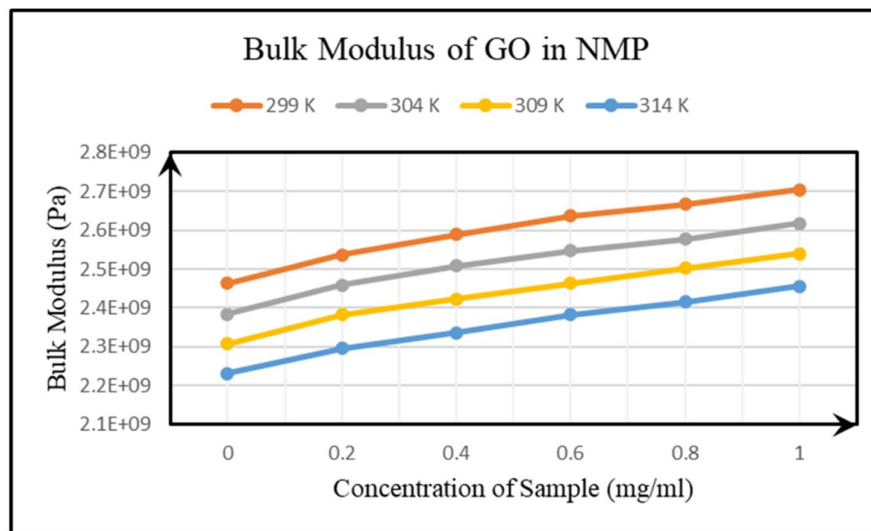


Figure 4.78 Bulk modulus of GO-NMP Nanosuspension

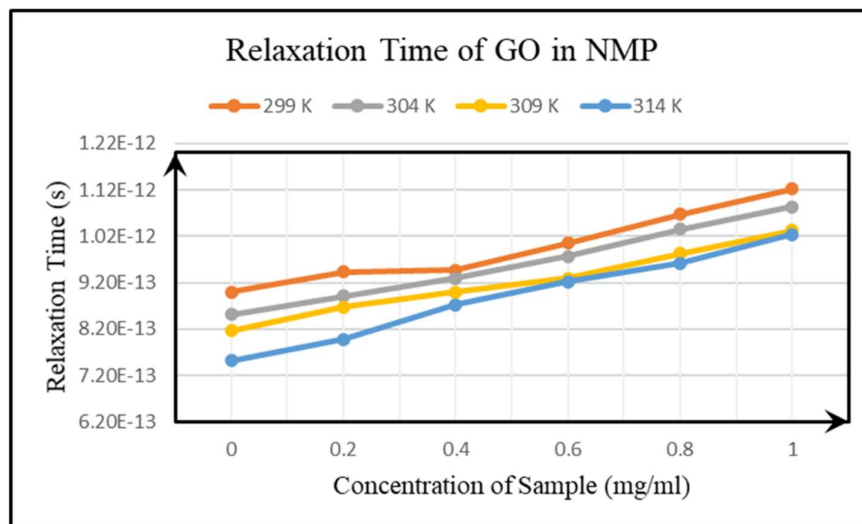


Figure 4.79 Relaxation Time of GO-NMP Nanosuspension

The intermolecular length of the sample rises with a rise in the particle loading in the NMP-GO nanosuspension, as in figure 4.80.

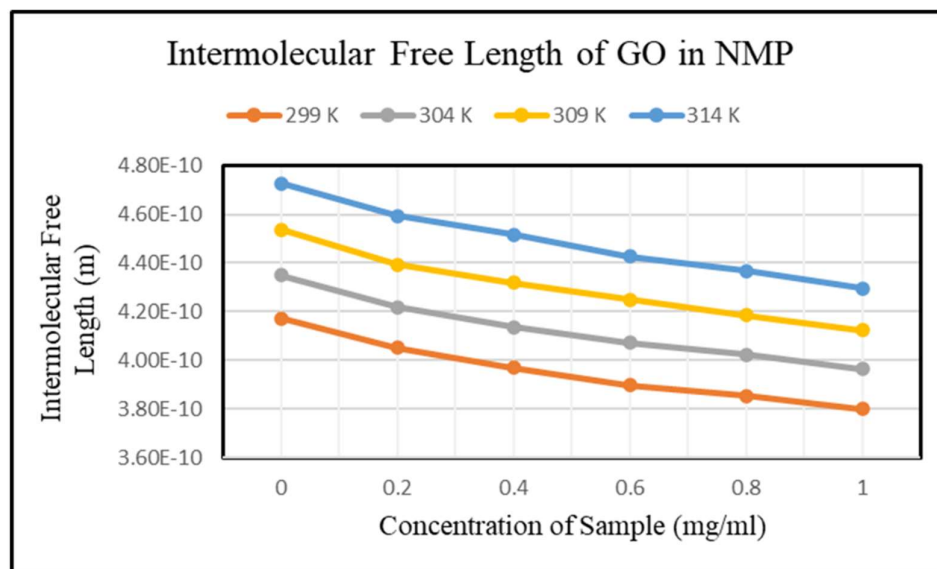


Figure 4.80 Intermolecular Free Length of GO-NMP Nanosuspension

It shows the interaction between particle and solvent molecules increases. The increase in the intermolecular length with the rise in the heat is because the zigzag movement of the solvent molecules rises, and this movement increases the solute and solvent molecule interaction [36-37].

4.28 References.

- [1] J. Chen, B. Yao, C. Li, and G. Shi, *Carbon N. Y.* **64**, 225 (2013).
- [2] I. Roy, G. Sarkar, S. Mondal, D. Rana, A. Bhattacharyya, N.R. Saha, A. Adhikari, D. Khastgir, S. Chattopadhyay, and D. Chattopadhyay, *RSC Adv.* **6**, 10557 (2016).
- [3] L. Stobinski, B. Lesiak, A. Malolepszy, M. Mazurkiewicz, B. Mierzwa, J. Zemek, P. Jiricek, and I. Bieloshapka, *J. Electron Spectros. Relat. Phenomena* **195**, 145 (2014).
- [4] J. Pardeike, D.M. Strohmeier, N. Schrödl, C. Voura, M. Gruber, J.G. Khinast, and A. Zimmer, *Int. J. Pharm.* **420**, 93 (2011).

- [5] M. Rabbani, E. Mohseni, and M. Rao, *Int. Commun. Heat Mass Transf.* **76**, 308 (2016).
- [6] E. Sadeghinezhad, M. Mehrali, R. Saidur, M. Mehrali, S. Tahan Latibari, A.R. Akhiani, and H.S.C. Metselaar, *Energy Convers. Manag.* **111**, 466 (2016).
- [7] P.B. Kharat, S.D. More, S.B. Somvanshi, and K.M. Jadhav, *J. Mater. Sci. Mater. Electron.* **30**, 6564 (2019).
- [8] F. Torrisi, T. Hasan, W. Wu, Z. Sun, A. Lombardo, T. Kulmala, G.W. Hshieh, S.J. Jung, F. Bonaccorso, P.J. Paul, D.P. Chu, and A.C. Ferrari, *ACS Nano* **6**, 2992 (2012).
- [9] H. Zhang, S. Wang, Y. Lin, M. Feng, and Q. Wu, *Appl. Therm. Eng.* **119**, 132 (2017).
- [10] I.M. Mahbulul, R. Saidur, M.A. Amalina, E.B. Elcioglu, and T. Okutucu-Ozyurt, *Ultrason. Sonochem.* **26**, 361 (2015).
- [11] M.F. El-Kady, V. Strong, S. Dubin, and R.B. Kaner, *Science (80-.)*. **335**, 1326 (2012).
- [12] S. Ghosh, I. Calizo, D. Teweldebrhan, E.P. Pokatilov, D.L. Nika, A.A. Balandin, W. Bao, F. Miao, and C.N. Lau, *Appl. Phys. Lett.* **92**, 2008 (2008).
- [13] C. Lee, X. Wei, J.W. Kysar, and J. Hone, *Science (80-.)*. **321**, 385 (2008).
- [14] S. Sheshmani and M.A. Fashapoyeh, 813 (2013).
- [15] W.S. Hummers and R.E. Offeman, *J. Am. Chem. Soc.* **80**, 1339 (1958).
- [16] S. Park, J. An, J.R. Potts, A. Velamakanni, S. Murali, and R.S. Ruoff, *Carbon N. Y.* **49**, 3019 (2011).
- [17] S. Naficy, R. Jalili, S.H. Aboutalebi, R.A. Gorkin, K. Konstantinov, P.C. Innis, G.M. Spinks, P. Poulin, and G.G. Wallace, *Mater. Horizons* **1**, 326 (2014).

- [18] L. Wang, Y. Huang, and H.J. Huang, *Mater. Lett.* **124**, 89 (2014).
- [19] Y. Wang, X. Wu, W. Zhang, J. Li, C. Luo, and Q. Wang, *Synth. Met.* **229**, 82 (2017).
- [20] G. Zhu, C. Xi, Y. Liu, J. Zhu, and X. Shen, *J. Mater. Chem. A* **3**, 7591 (2015).
- [21] Z. Luo, L. Zhu, Y. Huang, and H. Tang, *Synth. Met.* **175**, 88 (2013).
- [22] D. C.C. Marcano, D. V. V Kosynkin, J.M. Berlin, A. Sinitskii, Z.Z. Sun, A. Slesarev, L.B. Alemany, W. Lu, and J.M. Tour, *ACS Nano* **4**, 4806 (2010).
- [23] J. Liu, H. Yang, S.G. Zhen, C.K. Poh, A. Chaurasia, J. Luo, X. Wu, E.K.L. Yeow, N.G. Sahoo, J. Lin, and Z. Shen, *RSC Adv.* **3**, 11745 (2013).
- [24] M. Zong, Y. Huang, and N. Zhang, *Appl. Surf. Sci.* **345**, 272 (2015).
- [25] P. Su, H.L. Guo, L. Tian, and S.K. Ning, *Carbon N. Y.* **50**, 5351 (2012).
- [26] W. Feng, Y. Wang, J. Chen, L. Wang, L. Guo, J. Ouyang, D. Jia, and Y. Zhou, *Carbon N. Y.* **108**, 52 (2016).
- [27] S. Stankovich, D.A. Dikin, R.D. Piner, K.A. Kohlhaas, A. Kleinhammes, Y. Jia, Y. Wu, S.B.T. Nguyen, and R.S. Ruoff, *Carbon N. Y.* **45**, 1558 (2007).
- [28] D. Li, M.B. Müller, S. Gilje, R.B. Kaner, and G.G. Wallace, *Nat. Nanotechnol.* **3**, 101 (2008).
- [29] J. Ma, J. Liu, W. Zhu, and W. Qin, *Colloids Surfaces A Physicochem. Eng. Asp.* **538**, 79 (2018).
- [30] H. Bao, Y. Pan, Y. Ping, N.G. Sahoo, T. Wu, L. Li, J. Li, and L.H. Gan, *Small* **7**, 1569 (2011).
- [31] M. Leena, S. Srinivasan, and M. Prabhakaran, *Nanotechnol. Rev.* **4**, 449 (2015).
- [32] S. Parveen, D. Shukla, S. Singh, K.P. Singh, M. Gupta, and J.P. Shukla, *Appl. Acoust.* **70**, 507 (2009).

- [33] R.S. Vajjha, D.K. Das, and B.M. Mahagaonkar, *Pet. Sci. Technol.* **27**, 612 (2009).
- [34] K. Ranjini, T. Mahalingam, and A.K.S. Jeevaraj, (2012).
- [35] H. Kumar, K. Kaur, S. Arti, and M. Singla, *J. Mol. Liq.* **221**, 526 (2016).
- [36] J. Hemalatha, T. Prabhakaran, and R. Pratibha Nalini, *Microfluid. Nanofluidics* **10**, 263 (2011).
- [37] Khushboo, A. Devi, P. Malik, and H. Kumar, *J. Mol. Liq.* **214**, 145 (2016).
- [38] V. Gupta, A.K. Sharma, and M. Sharma, *J. Chem. Pharm. Res.* **6**, 714 (2014).
- [39] K. Kaur and K.C.C. Juglan, *Der Pharma Chem.* **7**, 160 (2015).
- [40] B. Tajik, A. Abbassi, M. Saffar-Avval, and M.A. Najafabadi, *Powder Technol.* **217**, 171 (2012).
- [41] N.H. Ayachit, S.T. Vasan, F.M. Sannaningannavar, and D.K. Deshpande, *J. Mol. Liq.* **133**, 134 (2007).
- [42] S. Elangovan and S. Mullainathan, *Indian J. Phys.* **87**, 659 (2013).
- [43] A.B. Naik, *Indian J. Pure Appl. Phys.* **53**, 27 (2015).
- [44] M. Joshi, A. Bhattacharyya, and S.W. Ali, *Indian J. Fibre Text. Res.* **33**, 304 (2008).

Section 3 (Part B)

Study of NMP-rGO

In Section 3 (Part A), we discussed the study of NMP with GO. In the current section, we will discuss the NMP with rGO. In the present study, the characterization of the rGO powder was already considered in 4.2.

4.29 Introduction

When we disperse nanoparticles in the solvent under the controlled condition, the suspension mixture prepared is called the nanosuspension. Many definitions of nanosuspensions; nanofluids are available in the literature; in this study, we are considering the size of the solute particles are in the range of 100 to 500nm than the suspension is called nanosuspension. A lot of examples of nanosuspension are available in the literature most of the example available is based on nanoparticles of carbon like carbon nanotubes, nanoparticles of metals and metal oxides, ceramics, etc. all these nanoparticles shows some remarkable properties when compared to their micrometer counterpart. It is discussed in the literature that most of the impressive features of the nanoparticles are because of the larger surface area. The addition of nanoparticles with the larger surface enhances the overall properties of the fluid in which we are mixing it. Since the size of the nanoparticles is very small, they can interact with the molecules of the solvent. When we apply heat, the molecules of the liquid will start random zigzag motion. Due to this motion, molecules collide with the nanoparticle of the suspension. During this process, heat is transferred to the nanoparticles, and they start moving at a rapid pace in the suspension. This rapid movement in the suspension helps to give higher thermal conductivities in the case of nanofluids. Therefore, it is a perfect opportunity to study the nanosuspension of these available solute and solvent.

Ultrasonication is a recognized method for studying these crisscross motions of particles and diffusing accumulated nanoparticles for aqueous nanosuspension preparation. Since as per literature, it has been observed that when we add ordinary particles with micron-size, it causes changes in ultrasonic velocity and ultrasonic attenuation. So, the size of particles also plays an essential role in the study of

nanosuspension. The demand of the ultrasonication in the research also increases the curiosity of the research groups to study the effect of passing the ultrasonic waves through the nanosuspensions. Many researchers are studying the ultrasonic velocity, density, and viscosity of nanosuspensions. Since we know the surface to volume percentage of the nanoparticles is very high, they can significantly improve the thermoacoustic properties of the nanosuspension. Hence it is essential to discuss the impact of the density of the solid particles on the properties of pure liquids to predict the final properties of the nanosuspensions.

In the last decade, graphene was one of the essential materials which we able to discover and study. After its discovery in 2004, a series of properties have been considered and reported by many research groups. Firstly, the manufacturing process of the graphene is itself a topic of research; many research groups are working to find a clean and green way to produce graphene. As far as the properties of graphene are concerned, it has been reported that this material is having high mobility of electron, impermeable to gasses, most potent content available, very high thermal conductivity, etc. Graphene offers a lot of opportunities in the field of research and development, but still, there are some gaps available like production of the graphene at the industry scale is not possible, the creation of the graphene involves toxic gasses, there are very less available solvents in which graphene can be suspended.

In this paper, we are studying the thermoacoustic properties of the prepared NMP-rGO nanosuspension at different temperatures as well as different concentrations of rGO. Different thermodynamically, physical, and fluid-particle interaction studies have been done and related. Various acoustical parameters like ultrasonic velocity, density, viscosity were calculated at a temperature range of 298 to 313 K and explained.

4.30 Material and Method:

4.30.1 Materials

Graphite powder, sodium nitrate obtained from Loba Chemical, KMnO_4 , HCl, NMP, and Ammonia was taken from CDH, and H_2SO_4 was obtained from Avantar. H_2O_2 was gathered from a fisher scientific, Hydrazine monohydrate was purchased from Sigma

Aldrich with an AR grade. All the chemicals used in work are AR grade. Double distilled water was used throughout the experiment.

4.30.2 Methods

The original Hummers Method is used to prepare to GO. In 1000 ml beaker, 345 ml of H₂SO₄ has been taken and put to the continuous magnetic stirrer. An ice bath has been made around the beaker to maintain the temperature of the bath below ten °C. 15 gm of Graphite Powder, and 7.5 gm of NaNO₃ has been added to continuously stirring H₂SO₄ with the heat of the bath is close to zero Celsius. After 30 minutes of continuous stirring, 45 gm of KMnO₄ has been added to the mixture very slowly, such as to maintain the reaction temperature below 90 °C. The mixture is left for continuous stirring for 2 hours after that beaker has been placed in a water bath at the temperature of 40 °C for 1 hour to increase the rate of oxidation. The color of the mixture changes from black to greenish-brown. After 1 hour, the mixture is placed on the magnetic stirrer and ice bath. With continuous stirring, the mixture is diluted with 500 ml of distilled water very slowly, maintaining the reaction temperature below 90 °C. After leaving the mixture overnight, distilled water 100 ml with 30% H₂O₂ added to the mix to remove any excess KMnO₄ and to stop the oxidation reaction. The further mixture was diluted with distilled water and left for the decantation process overnight. Then we remove the top layer of water, and the remaining solution is filtered. Continuous addition of distilled water has been added during the filtration process helps to remove excess KMnO₄ and metal ions. Approximately 5 liters of distilled water was used during the filtration process. Following the completion of the filtration, the processed mixture was again mixed with 500 ml of distilled water and added to 8-hour ultrasonication, which helps to reduce GO.

The mixture was left to dry in the vacuum and to grinded for GO powder. A colloidal suspension of GO powder in double-distilled water (2 mg/ml) is prepared by ultrasonication of GO in 500 mL of liquid for 1 hour. A few drops of Ammonia have been added to the solution to adjust the PH of the solution in a range of 9 to 10. Hydrazine monohydrate (1 µl for 3 mg of GO) was then added to the suspension. Continuous magnetic string and temperature maintenance up to 95 °C for 3 hours

yielded black precipitate of RGO powder. After cooling to room temperature, the powder was filtered through the filter, and the vacuum was dried. Synthesized RGO nanoparticles are dispersed in NMP by ultrasound for 24 h to obtain a homogenous suspension of different concentrations without any phase separation and sedimentation. As with many peer groups, it is indisputable that ultrasound improves reliability and dispersion of the suspension. Nanosuspensions with different concentrations (0.2mg / ml, 0.4mg / ml, 0.6mg / ml, 0.8mg / ml and 1.0mg / ml) are prepared without the introduction of any surfactants.

4.31 Characterization of NMP-RGO Nanosuspension

4.30.1 UV-VIS: The UV-Vis characterization of prepared NMP-rGO nanosuspension is discussed in section 4.3.

4.31.2 HRTEM: The HRTEM image of the prepared NMP-rGO is shown in figure 4.81. We have used a drop of Nanosuspension for the study of the sample of NMP-rGO under HRTEM.

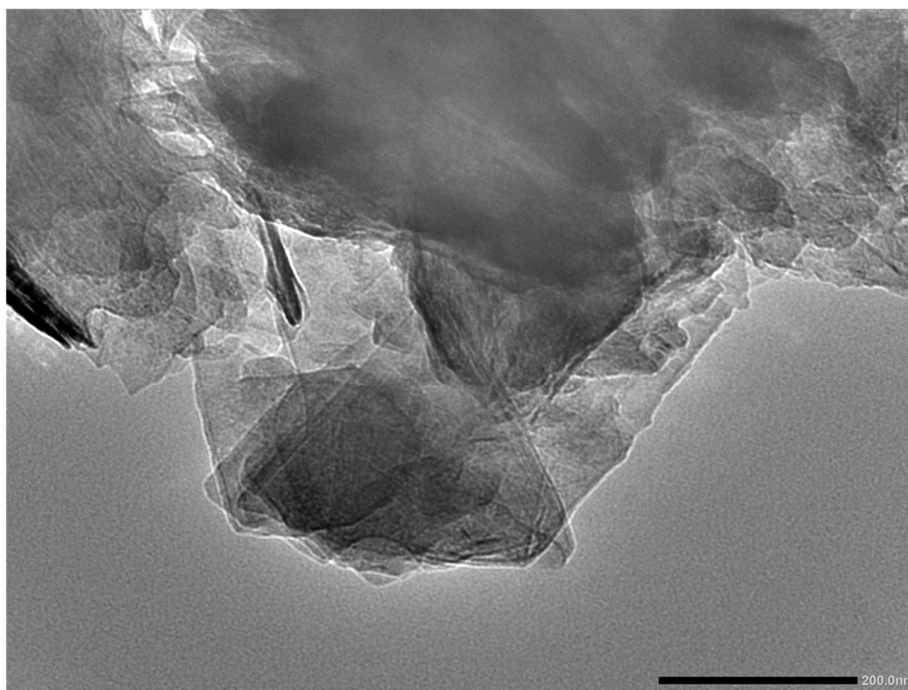


Figure 4.81 HRTEM image of rGO

Figure 4.81 shows the layer of the graphene sheets stacked over each other. The light portion of the image shows the stack of a smaller number of the sheets, and the darker part shows many layers stacked or maybe the presence of the oxygen atom in between the sheets. Image 4.81 indicated the presence of the rGO sheets in the drop of NMP under the HRTEM study.

4.31.3 DLS: We can depict the size of the rGO sheets with the help of the DLS technique. Figure 4.82 shows the particle size of rGO in the NMP with different concentrations of rGO particles.

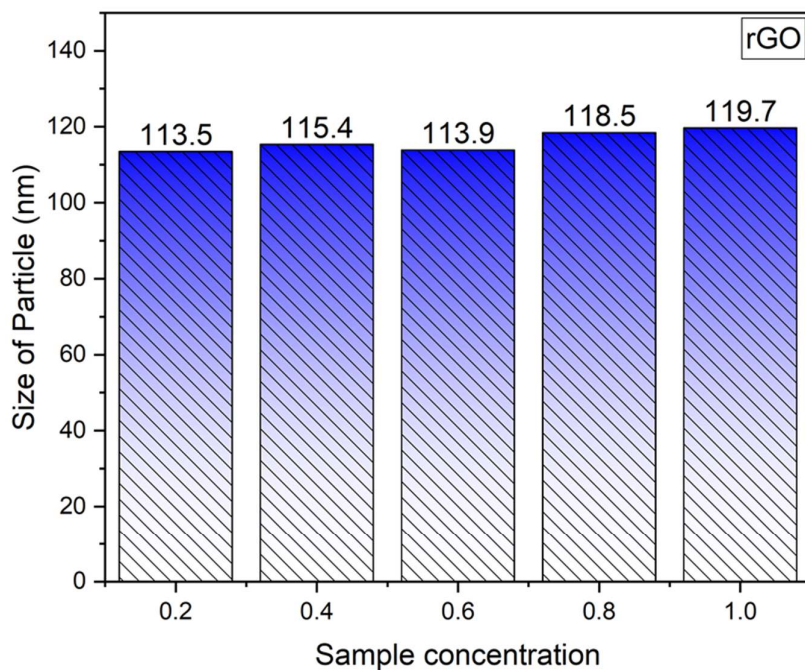


Figure 4.82 DLS particle size of the NMP-rGO Nanosuspension

We deployed ultrasonication for the formulation of nanosuspension. The size of the particles significantly reduced if compared with GO. The size of the rGO particles comes out in the range of 113 nm to 120 nm, which helps to name our suspension as nanosuspension.

4.32 Data Table:

Table 4.12 NMP-rGO Nanosuspension 1					
Concentration (mg/ml)	Temperature (in K)	Average Velocity (m/s) $U = \lambda \times f$	Density (Kg/m ³)	Viscosity (Pa-s)	Adiabatic Compressibility (1/Pa) $\beta = 1/(U^2 \times \rho)$
0	299	1547.692	1028.316	0.001661	4.06E-10
0.2	299	1556.077	1050.488	0.001907	3.93E-10
0.4	299	1567.308	1052.363	0.00211	3.87E-10
0.6	299	1576.923	1052.863	0.002139	3.82E-10
0.8	299	1587.538	1056.338	0.002208	3.76E-10
1	299	1597.333	1057.389	0.00232	3.71E-10
0	304	1520.154	1023.823	0.001523	4.23E-10
0.2	304	1529.615	1047.513	0.001812	4.08E-10
0.4	304	1540	1049.013	0.001957	4.02E-10
0.6	304	1550.615	1049.288	0.001985	3.96E-10
0.8	304	1560.923	1052.063	0.002054	3.9E-10
1	304	1570	1053.763	0.002236	3.85E-10

0	309	1495.692	1019.33	0.001413	4.39E-10
0.2	309	1505.077	1043.463	0.001695	4.23E-10
0.4	309	1515.692	1045.388	0.001816	4.16E-10
0.6	309	1525.231	1046.113	0.001898	4.11E-10
0.8	309	1536.692	1048.113	0.00197	4.04E-10
1	309	1543.846	1049.438	0.002076	4E-10
0	314	1473	1014.72	0.001259	4.54E-10
0.2	314	1480.538	1038.488	0.001526	4.39E-10
0.4	314	1491.154	1041.413	0.001706	4.32E-10
0.6	314	1501.538	1043.313	0.001736	4.25E-10
0.8	314	1512.077	1044.063	0.001805	4.19E-10
1	314	1522.308	1046.013	0.00192	4.13E-10

Table 4.13 NMP-rGO Nanosuspension 2

Concentration (mg/ml)	Temperature (T) (K)	Acoustical impedance (Z) (Pa. s/m³) Z = ρ × U	Attenuation (α/f²) (m⁻¹) α/f² = 8π²η /3ρU³	Bulk Modulus(K) (Pa) K = ρ U²	Relaxation Time(τ) (s) τ = 4βη/3	Intermolecular Free Length (L_f) (L_f = K_T × β^{1/2})
0.6	299	1660283.2	1.36187E-14	2618138850	1.08907E-12	3.92645E-10
0.8	299	1676976.4	1.37375E-14	2662264549	1.10597E-12	3.86137E-10
1	299	1689002.3	1.41574E-14	2697899669	1.14681E-12	3.81037E-10
0	304	1556368.5	1.11323E-14	2365919518	8.58193E-13	4.38519E-10
0.2	304	1602291.2	1.27046E-14	2450889325	9.85494E-13	4.23316E-10
0.4	304	1615479.3	1.34268E-14	2487838045	1.04858E-12	4.17029E-10
0.6	304	1627041.3	1.33426E-14	2522915334	1.04919E-12	4.11231E-10
0.8	304	1642188.6	1.3495E-14	2563330136	1.06823E-12	4.04747E-10
1	304	1654407.1	1.44142E-14	2597419186	1.14762E-12	3.99435E-10
0	309	1524604.2	1.08953E-14	2280338759	8.26401E-13	4.59142E-10
0.2	309	1570491.3	1.25285E-14	2363710257	9.5624E-13	4.42948E-10
0.4	309	1584485.8	1.31141E-14	2401592927	1.008E-12	4.35961E-10

0.6	309	1595563	1.34422E-14	2433601741	1.03972E-12	4.30227E-10
0.8	309	1610626.4	1.36199E-14	2475037225	1.06138E-12	4.23024E-10
1	309	1620170	1.41317E-14	2501293297	1.1064E-12	4.18583E-10
0	314	1494682.6	1.0205E-14	2201667411	7.623E-13	4.79182E-10
0.2	314	1537520.7	1.19013E-14	2276358510	8.9356E-13	4.6346E-10
0.4	314	1552906.3	1.29914E-14	2315622135	9.824E-13	4.55601E-10
0.6	314	1566573.8	1.29246E-14	2352270883	9.84156E-13	4.48503E-10
0.8	314	1578702.8	1.31455E-14	2387120091	1.008E-12	4.41955E-10
1	314	1592352.9	1.36771E-14	2424051030	1.05586E-12	4.35222E-10

4.33 Result and Discussion: We measured the following parameter to study the thermoacoustic analysis.

4.33.1 Ultrasonic Velocity: Ultrasonic velocity is one of the utmost significant parameters to qualitatively measures the interparticle and intermolecular interaction of the nanosuspension [1]. The ultrasonic speed is measured for all the prepared samples of NMP-rGO at four distinct temperatures (298, 303, 308, and 313K). Readings were measured repeatedly to avoid any experimental errors as well as readings of pure NMP is matched with the literature [2]. The increase and decrease of ultrasonic velocity with the concentration of the particles and temperature give an insight of intermolecular and intraparticle interactions, as shown in Fig. 4.83. We can notice in NMP-rGO and NMP-rGO that ultrasonic velocity consistently increases from the pure liquid with the growth in the concentration of the particles.

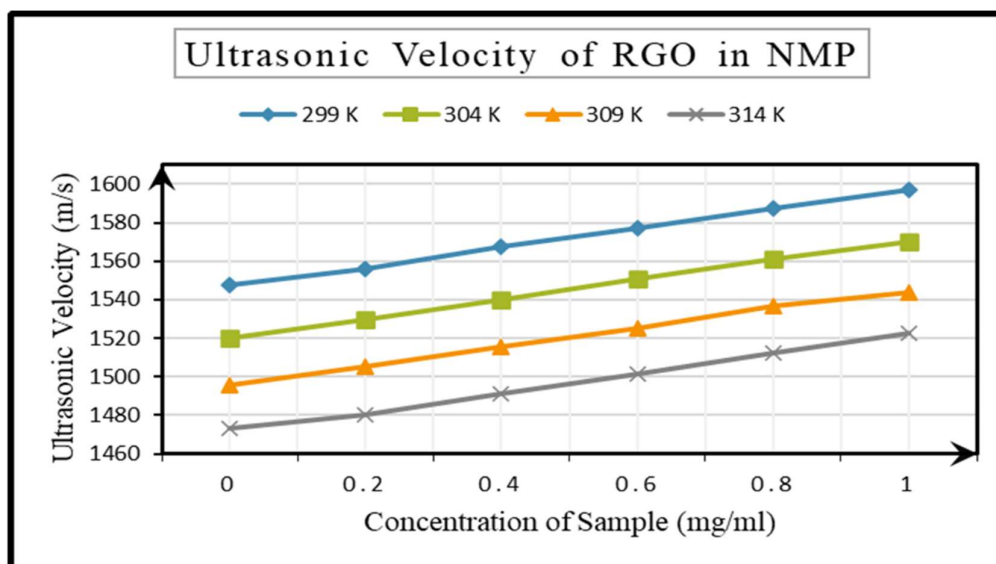


Figure 4.83 Ultrasonic study of NMP-rGO Nanosuspension

Further, we can notice that as the temperature of the system increase from 298 K to 313 K, there is a decrease in the ultrasonic velocity. The reduction in the ultrasonic speed with the concentration is due to rGO and NMP interaction; it further explains the supremacy of intermolecular interaction over intraparticle interactions. The increase in concentration also reduces the Brownian motion of the system, which helps to increase

the ultrasonic velocity of the system because the interaction of rGO particles with solvent molecule increases. At the higher temperatures, the speed decreases further as compared to the pure NMP, which helps to establish the fact that rGO and NMP had more interaction as compared to rGO and rGO. The reduction of ultrasonic velocity with surging temperature proves that the nanosuspension follow the usual behavior of non- aqueous liquids, which can be described as the temperature of suspension increases, the average speed of the molecules surges, and the amount of time they employ in interaction with their nearest neighbors decreases. Thus, the increasing temperature leads to the fading of the intermolecular adhesive and cohesive forces, thereby enhancing the compressibility, which, in turn, reduces the ultrasonic velocity [3][4].

4.33.2 Density: It can be seen in Figure 4.84 that the density of NMP-rGO nanosuspension increases as the particles added to pure NMP. After this slight increase in the density of formulated nanosuspension can be seen, the usual reflection is that density declines with temperature, which agrees well with the acceptable behavior of the fluids. Density raises with concentration, as the nanoparticles being added are of higher density than the base fluid [5]. The small rise in the density after increasing the concentration of the particles is due to the increase in intermolecular interaction instead that of interparticle communication [6].

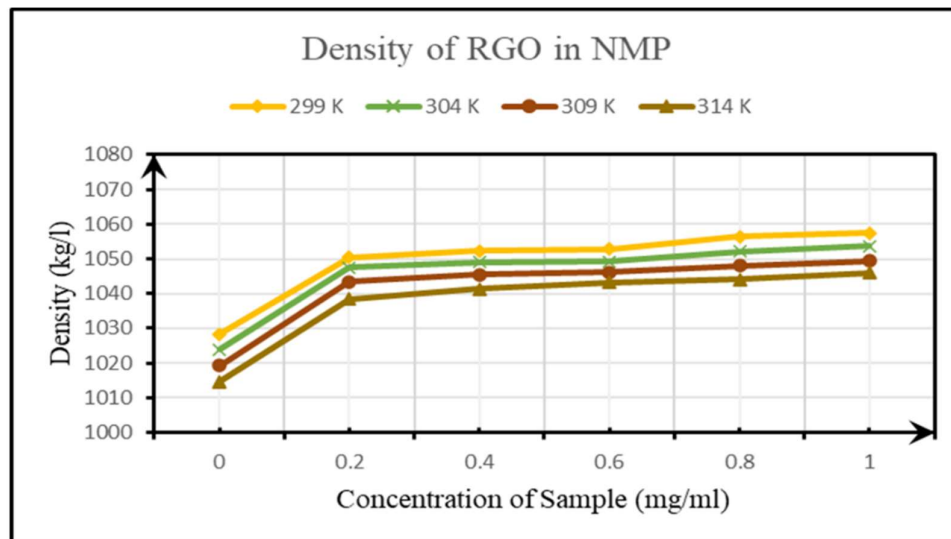


Figure 4.84 Density of NMP-rGO Nanosuspension

The density of the NMP-rGO nanosuspension decreases with the increase in the temperature of the system. With the rise in the heat, the Brownian motion of the solvent molecules also starts to rise. The increase in random motion tends to decrease the density of the system.

4.33.3 Viscosity: Viscosity of the NMP-rGO nanosuspension rises very sharply with the addition of rGO particles in the pure NMP solution, as displayed in figure 4.85. Viscosity similarly increases with increases the particle loading, which is due to the interlocking of rGO particles while flow [7]. With the growth in the temperature, the viscosity of NMP-rGO nanosuspension decreases as normal fluid. The decrease in the viscosity with a rise in temperature can be understood by the increase in the Brownian motion of the particle present in the nanosuspension with the upsurge in the heat. The decrease in viscosity with temperature helps to flow the nanosuspension effortlessly at higher temperatures as compared to low temperatures [8].

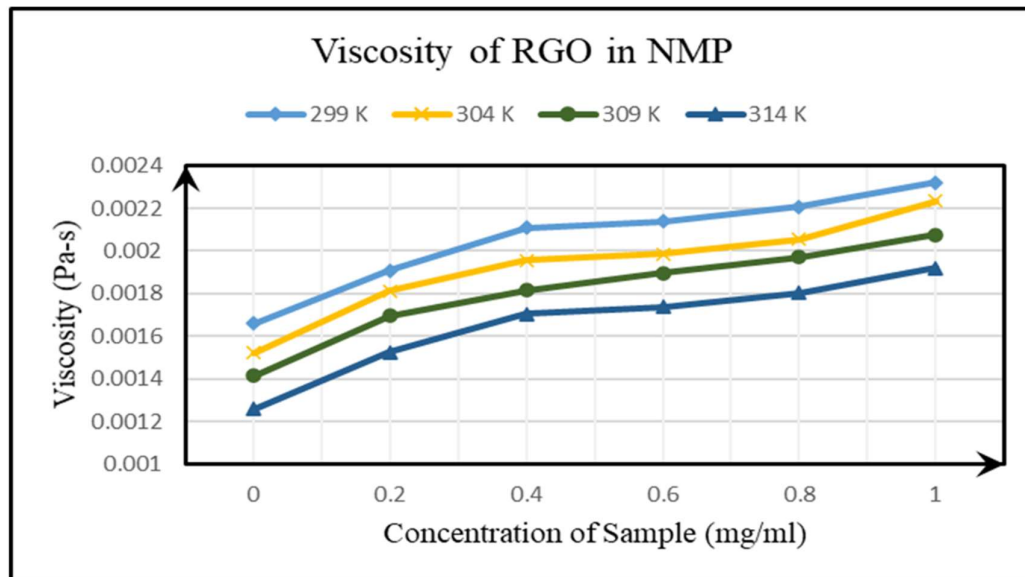


Figure 4.85 Viscosity of NMP-rGO Nanosuspension

4.33.4 Adiabatic Compressibility: Fig. 4.86 shows the change in adiabatic compressibility with the increase in the particle loading in pure NMP. As the particles are added in the pure NMP, it shows a sudden decrease, which shows the weak particle and fluid interaction [9]. The decline in the compressibility also leads to the conclusion that the particle added to the base fluid tries to form a complex structure in the nanosuspension. The reduction in the adiabatic compressibility shows the interaction in the particle and fluid increases and complex formation in the system. Adiabatic compressibility likewise increases with the increase in the temperature of the system, which is the cause of the rise in the Brownian motion of the particles. [10]

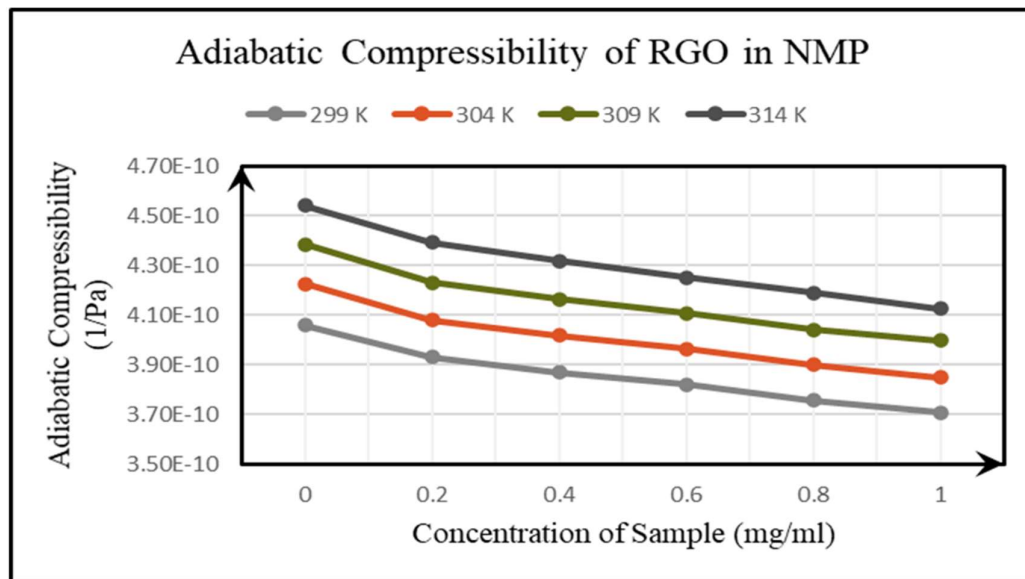


Figure 4.86 Adiabatic Compressibility of NMP-rGO Nanosuspension

4.33.5 Acoustical Impedance: Fig. 4.87 shows the values of acoustical impedance with particle loading in pure NMP. An upsurge in the amount of acoustical impedance shows the increase in interaction in solute and particle of the NMP-rGO nanosuspension [11]. With the improvements in the temperature, the value of acoustic impedance decreases because of the Brownian motion of the particles in the fluid increases. Increasing particle-fluid interactions at lower concentrations widen the intermolecular gap, which provides resistance to the propagation of ultrasonic waves [12].

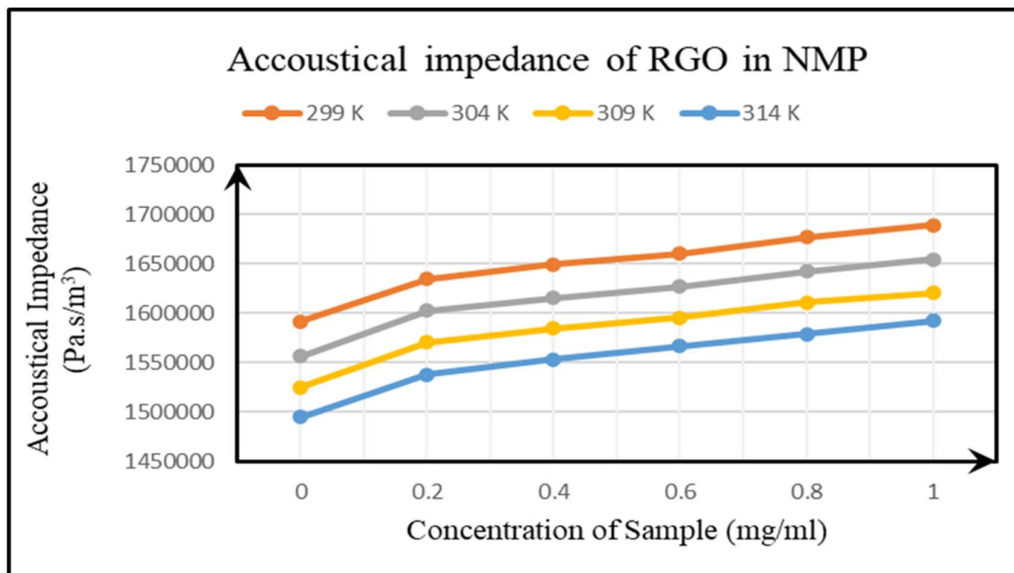


Figure 4.87 Acoustical Impedance of NMP-rGO Nanosuspension

4.33.6 Attenuation: Variation of the ultrasonic attenuation and concentration of the particles in NMP-rGO nanosuspension is shown in Fig. 4.88. Ultrasonic attenuation increases as soon as the particle is added in the pure DMF fluid.

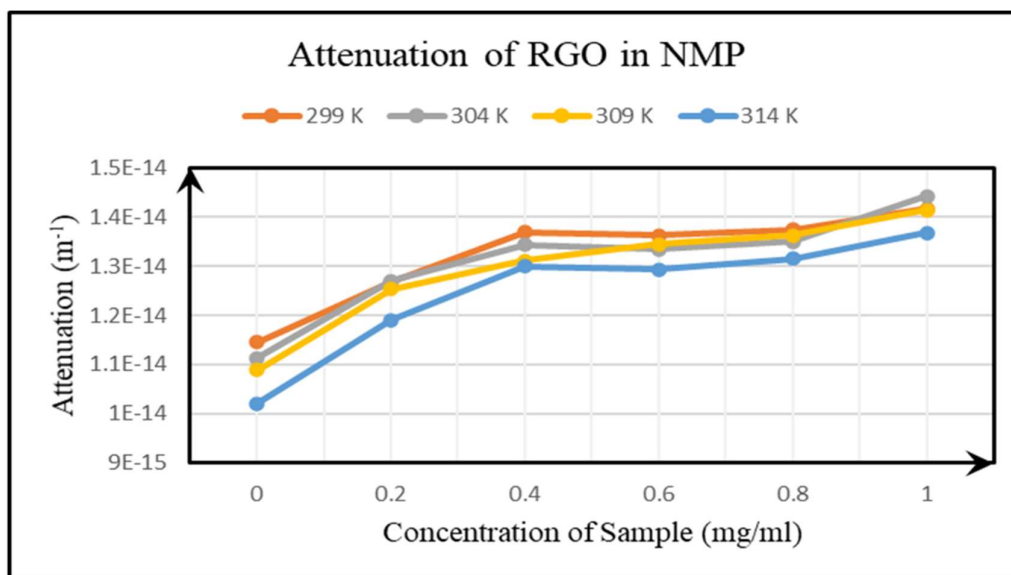


Figure 4.88 Attenuation of ultrasound waves in NMP-rGO Nanosuspension

Further increase in the ultrasonic attenuation can be seen in NMP-rGO nanosuspension; this increase in the mitigation is because rGO can form agglomeration by binding with each other. This blockage produced by the agglomerated rGO particles blocks the ultrasonic waves from reaching one end to the other. The increase in the temperature value of the ultrasonic attenuation decrease because of a reduction in the interaction of NMP and rGO particles. Here we cannot deny the complex formation in the suspension. [11]

4.33.7 Bulk Modulus: In figure 4.89, it can be seen clearly that the value of bulk modulus rises with the increase in the particle loading in the solvent. Interaction between the particle and fluid increases as the concentration of the NMP-rGO nanosuspension increases. The value of the bulk modulus decreases with the rise in the heat of the nanosuspension. The resistance of the nanosuspension decreases to the externally applied stress at a higher temperature because the interaction between particle and solute increases creates the gap between molecules, which helps in reducing bulk modulus [13],[14]

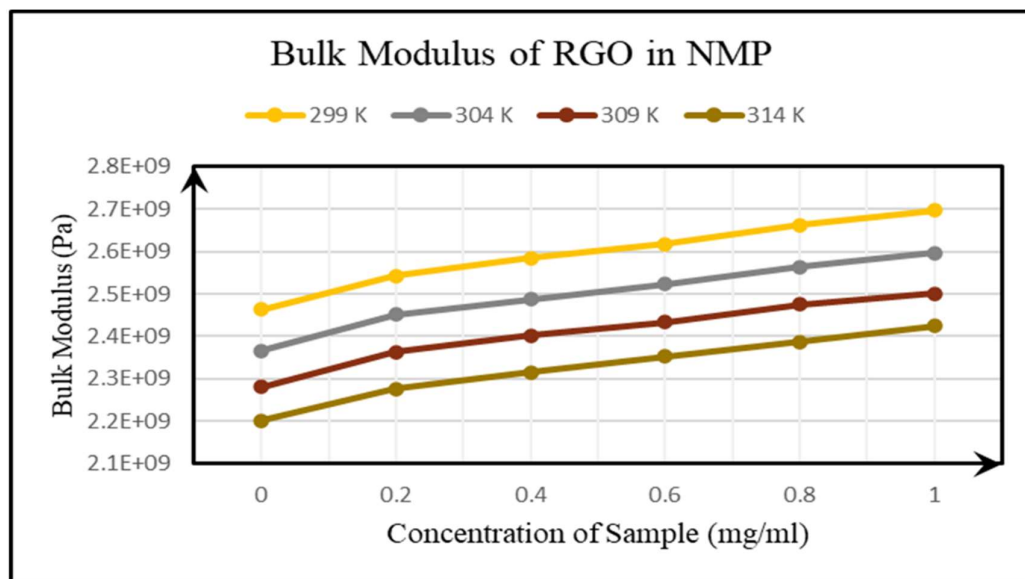


Figure 4.89 Bulk Modulus of NMP-rGO Nanosuspension

4.33.8 Relaxation Time: The relaxation time of the NMP-rGO sample increase with the increase in the particle concentration in the NMP-rGO nanosuspension, as shown

In figure 4.90. Since the interaction between the solvent molecules and solute increases. The reordering time for the solute molecules increases. When the heat of the NMP-rGO nanosuspension rises, the zigzag movement of the solvent molecule increases, which helps to reorder the molecules quickly because of fast motion [14],[15].

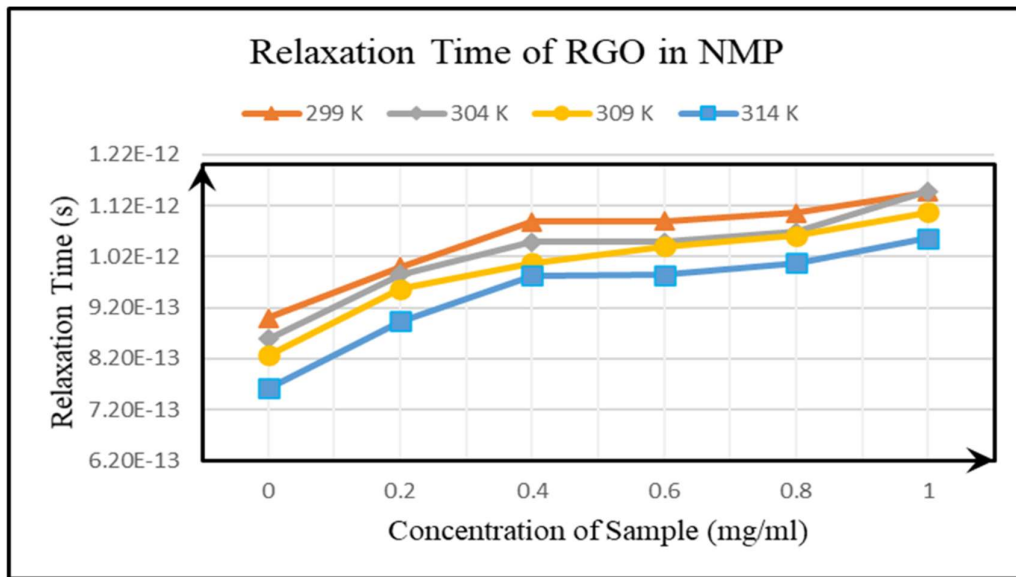


Figure 4.90 Relaxation Time of NMP-rGO Nanosuspension

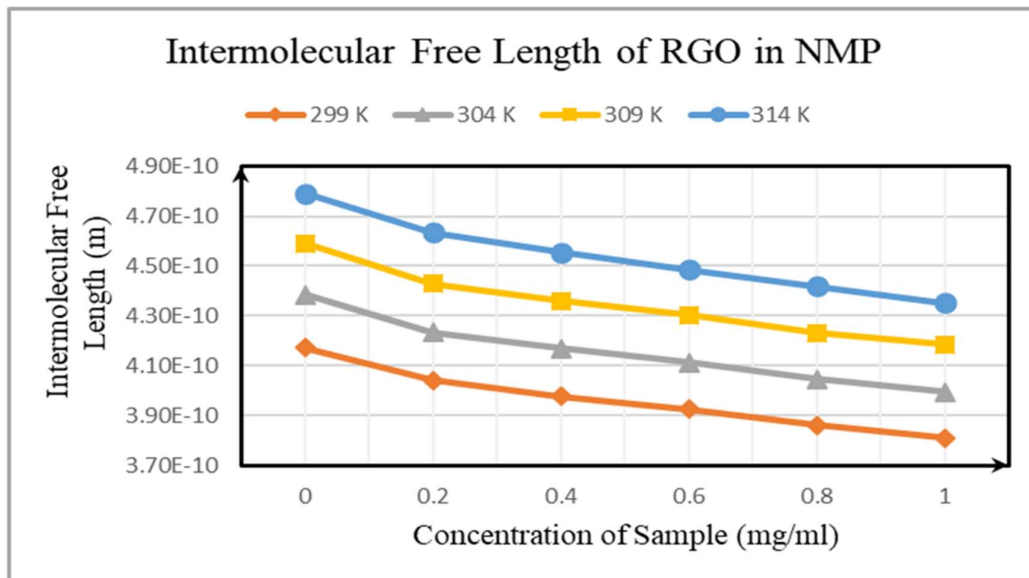


Figure 4.91 Intermolecular free length of NMP-rGO Nanosuspension

4.33.9 Intermolecular free length: The intermolecular length of the sample decreases

with a rise in the particle loading in the NMP-rGO nanosuspension, as shown in figure 4.91. It shows the interaction between particle and solvent molecules decreases. The increase in the intermolecular length with the increase in the heat is because the zigzag movement of the solvent molecules rises, and this movement increases the solute and solvent molecule interaction [16-17]

4.34 References:

- [1] M. N. Rashin and J. Hemalatha, *J. Mol. Liq.*, **197**, 257, (2014).
- [2] D. Papamatthaiakis, F. Aroni, and V. Havredaki, *J. Chem. Thermodyn.*, **40**, 107, (2008).
- [3] M. Nabeel Rashin and J. Hemalatha, *J. Mol. Liq.*, **197**, 257, (2014).
- [4] M. N. Rashin and J. Hemalatha, *Ultrasonics*, **52**, 1024, (2012).
- [5] R. S. Vajjha, D. K. Das, and B. M. Mahagaonkar, *Pet. Sci. Technol.*, **27**, 612, (2009).
- [6] S. N. Shoghl, J. Jamali, and M. K. Moraveji, *Exp. Therm. FLUID Sci.*, **27**, 12, (2016).
- [7] M. N. Rashin and J. Hemalatha, *Exp. Therm. Fluid Sci.*, **51**, 312, (2013).
- [8] M. R. Esfahani, E. M. Languri, M. R. Nunna, M. Rabbani, E. Mohseni, and M. Rao, *Int. Commun. Heat Mass Transf.*, **76**, 308, (2016).
- [9] Khushboo, A. Devi, P. Malik, and H. Kumar, *J. Mol. Liq.*, **214**, 145, (2016).
- [10] A. Nanda, A. Tiadi, S. K. Mallik, R. Giri, and G. Nath, *IOP Conf. Ser. Mater. Sci. Eng.*, **360**, 1, (2018).
- [11] S. Tiwari, B. S. Kusmariya, A. Tiwari, V. Pathak, and A. P. P. Mishra, *J. Taibah Univ. Sci.*, **11**, 101, (2017).
- [12] N. H. Ayachit, S. T. Vasan, F. M. Sannaningannavar, and D. K. Deshpande, *J. Mol. Liq.*, **133**, 134, (2007).

- [13] B. Tajik, A. Abbassi, M. Saffar-Avval, and M.A. Najafabadi, *Powder Technol.* **217**, 171, (2012).
- [14] N.H. Ayachit, S.T. Vasan, F.M. Sannaningannavar, and D.K. Deshpande, *J. Mol. Liq.* **133**, 134 (2007).
- [15] S. Elangovan and S. Mullainathan, *Indian J. Phys.* **87**, 659 (2013).
- [16] F. Chen, Z. Yang, Z. Chen, J. Hu, C. Chen, and J. Cai, *Journal of Molecular Liquids*, **209**, 683, (2015).
- [17] K. Kaur and K. C. Juglan, *Der Pharma Chem.*, **7**, 160, (2015)

Section 4

Study of THF-GO and THF-rGO Nanosuspension

In Section 3, we discussed the study of NMP with GO and rGO. In the present study, we will examine the THF with GO and rGO. In the present study, the characterization of the GO and rGO powder is already discussed in sections 4.1 and 4.2, respectively.

4.35 Introduction

Nanosuspension is a colloidal dispersion of nanoparticles that can be controlled by various techniques. The particle size range for solid particles in nanosuspensions is typically smaller than one micron with a median particle size ranging between 100 and 500 nm. Dispersion of nanoparticle in a base fluid can offer a tremendous change in its properties, and because of the extraordinary properties shown by various nanoparticles of metals, metals oxides, ceramic, and Carbon, it becomes the attraction for many researchers. One fascinating feature of nanofluids is that they have an anomalously high thermal conductivity, which makes nanosuspension durable material for the next generation of coolants for improving the design and performance of thermal management systems. The Brownian motion of nanoparticles in a base liquid is proposed to be one of the significant physical mechanisms of the thermal conduction of nanofluids. Therefore, it is vital to investigate the movements of nanoparticles in nanosuspension. Ultrasonication is an accepted technique for the study of such Brownian motion and dispersing aggregated nanoparticles for the preparation of aqueous nanosuspensions. Most of the studies have focused on the effect of sonication time on the stability of nanosuspensions, and all of them used continuous ultrasonic waves to sonication. The ultrasonic properties of solid-liquid suspensions in the micrometer size of the particles can cause changes in ultrasonic velocity and ultrasonic attenuation that can affect the thermal conductivity of nanofluids. More specifically, there is an increasing interest mostly in the acoustic properties for acoustic telemetry suspensions via drilling fluids, as well as the rising market for ultrasonic components. Several scientists have researched ultrasonic propagation behaviour by suspending solid particles, especially in the nanometre scale of a fluid, intending to find a process

that allows vital information to be derived from the behaviour of ultrasonic materials, such as particle size, density, and mechanical properties of the constituents. Due to their relatively large surface-to-volume ratio, nanoparticles arrested in base liquid substantially expose some new features that are not always present in either of the pure components. Hence it is essential to investigate the influence of nanoparticles on the properties of the base liquid to anticipate the final properties of the complex fluids effectively.

Graphene is one of the most significant finds of the last decade in terms of many physical and chemical properties. Since its evolution in 2004 range of features has been reported like: high electron mobility, high thermal conductivity, impermeable to gasses, most durable material ever published, etc. Despite all of these excellent properties still, there are several challenges associated with this material, like industrial-scale productivity, the stability of GO in different available solvents.

In the present work, we have conducted a study of ultrasonic waves in colloidal dispersion of GO and rGO nanoparticles with different concentrations in THF to take advantage of the GO and rGO properties in the form of nanosuspension. Structural, morphological, and fluid-particle interaction studies have been completed and compared. Various acoustical parameters like ultrasonic velocity, density, viscosity were calculated at a temperature range of 298 to 313 K and explained.

4.36 Material and Method

4.36.1 Materials

Graphite powder, sodium nitrate obtained from Loba Chemical, KMnO_4 , HCl , THF, and Ammonia was taken from CDH, and H_2SO_4 was obtained from Avantar. H_2O_2 was gathered from a fisher scientific, Hydrazine monohydrate was purchased from Sigma Aldrich with an AR grade. All the chemicals used in work are AR grade. Double distilled water was used throughout the experiment.

4.36.2 Methods

The original Hummers Method is used to prepare to GO. In 1000 ml beaker, 345 ml of

H₂SO₄ has been taken and put to the continuous magnetic stirrer. An ice bath has been made around the beaker to maintain the temperature of the bath below ten °C. 15 gm of Graphite Powder, and 7.5 gm of NaNO₃ has been added to continuously stirring H₂SO₄ with the heat of the bath is close to zero Celsius. After 30 minutes of continuous stirring, 45 gm of KMnO₄ has been added to the mixture very slowly, such as to maintain the reaction temperature below 90 °C. The mixture is left for continuous stirring for 2 hours after that beaker has been placed in a water bath at the temperature of 40 °C for 1 hour to increase the rate of oxidation. The color of the mixture changes from black to greenish-brown. After 1 hour, the mixture is placed on the magnetic stirrer and ice bath. With continuous stirring, the mixture is diluted with 500 ml of distilled water very slowly, maintaining the reaction temperature below 90 °C. After leaving the mixture overnight, distilled water 100 ml with 30% H₂O₂ added to the mix to remove any excess KMnO₄ and to stop the oxidation reaction. The further mixture was diluted with distilled water and left for the decantation process overnight. Then we remove the top layer of water, and the remaining solution is filtered. Continuous addition of distilled water has been added during the filtration process helps to remove excess KMnO₄ and metal ions. Approximately 5 liters of distilled water was used during the filtration process. Following the completion of the filtration, the processed mixture was again mixed with 500 ml of distilled water and added to 8-hour ultrasonication, which helps to reduce GO.

The mixture was left to dry in the vacuum and to grinded for GO powder. A colloidal suspension of GO powder in double-distilled water (2 mg/ml) is prepared by ultrasonication of GO in 500 mL of liquid for 1 hour. A few drops of Ammonia have been added to the solution to adjust the PH of the solution in a range of 9 to 10. Hydrazine monohydrate (1 µl for 3 mg of GO) was then added to the suspension. Continuous magnetic string and temperature maintenance up to 95 °C for 3 hours yielded black precipitate of RGO powder. After cooling to room temperature, the powder was filtered through the filter, and the vacuum was dried. Synthesized RGO nanoparticles are dispersed in THF by ultrasound for 24 h to obtain a homogenous suspension of different concentrations without any phase separation and sedimentation. As with many peer groups, it is indisputable that ultrasound improves reliability and

dispersion of the suspension. Nanosuspensions with different concentrations (0.2mg / ml, 0.4mg / ml, 0.6mg / ml, 0.8mg / ml and 1.0mg / ml) are prepared without the introduction of any surfactants.

4.37 Characterization of THF-GO and THF-rGO Nanosuspension

4.37.1 UV-VIS: The UV-Vis characterization of prepared THF-GO and THF-rGO nanosuspension is discussed in sections 4.3 and 4.4, respectively.

4.37.2 HRTEM: The HRTEM image of the prepared suspension is shown in figure 4.92. We have used a drop of Nanosuspension for the study of the sample of THF-GO and THF-rGO nanosuspension under HRTEM.

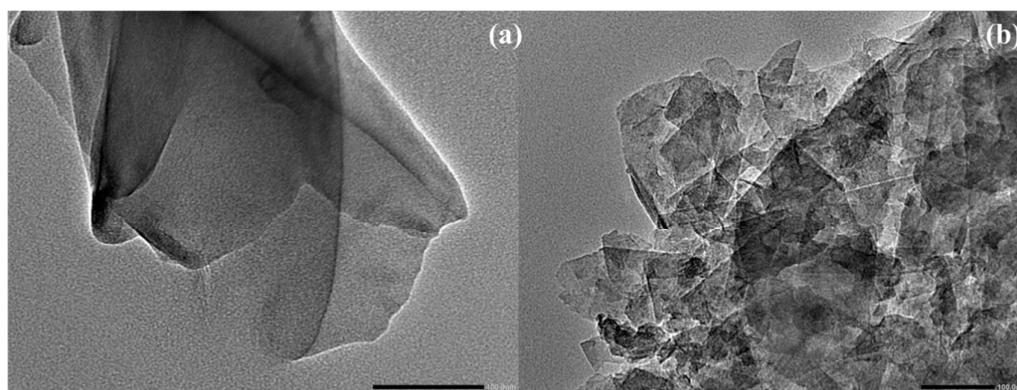


Figure 4.92 (a) HRTEM image of GO (b) HRTEM image of rGO

Figure 4.92 (a) shows the layer of the graphene sheets stacked over each other. The light portion of the image shows the stack of a smaller number of the sheets, and the darker part shows many layers stacked or maybe the presence of the oxygen atom in between the sheets. Image 4.92 (a) indicated the presence of the GO sheets in the drop of NMP under the HRTEM study. Figure 4.92 (b) shows the number of smaller sheets in the sample under investigation. The small size of graphene sheets indicates that while reducing the GO chemically with hydrazine hydrate, big sheets split into small sheets because of oxygen atom escape from the layers by breaking the structure. The dark portion shows either the pile of rGO sheets or the presence of an oxygen atom in the layers of graphene. It is confirmed from HRTEM that sheets like structures are present in the drop of THF-rGO Nanosuspension.

4.37.3 DLS: We can depict the size of the GO and rGO sheets with the help of the DLS technique. Figure 4.93 shows the particle size of GO and rGO in the THF with different concentrations of GO and rGO particles, respectively.

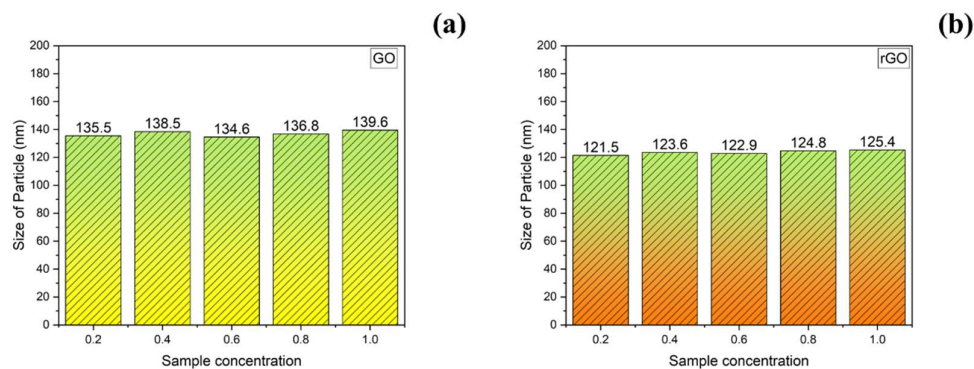


Figure 4.93 (a) DLS image of GO-THF Nanosuspension (b) DLS image of rGO-THF Nanosuspension

We deployed ultrasonication for the formulation of nanosuspension. The size of the rGO particles significantly reduced if compared with GO. The size of the rGO particles comes out in the range of 113 nm to 120 nm, and GO particles have the size range from 134 to 140 nm. This size confirmation helps to name our suspension as nanosuspension.

4.38 Data Table

Table 4.14 THF-GO Nanosuspension 1

Concentration (mg/ml)	Temperature (in K)	Average Velocity (m/s) $U = \lambda \times f$	Density (Kg/m ³)	Viscosity (Pa-s)	Adiabatic Compressibility (1/Pa) $\beta = 1 / (U^2 \times \rho)$
0	299	1280	898.2625	0.00046	6.7948E-10
0.2	299	1282.857143	898.7625	0.000465103	6.76081E-10
0.4	299	1285.923077	899.8375	0.000468404	6.72057E-10
0.6	299	1289.846154	900.9875	0.000472457	6.67122E-10
0.8	299	1291.076923	901.7375	0.000480111	6.65297E-10
1	299	1293.923077	902.0375	0.000490617	6.62153E-10
0	304	1253.076923	894.3875	0.000451295	7.12064E-10
0.2	304	1256.153846	895.7705	0.000454747	7.07486E-10
0.4	304	1260.076923	896.2375	0.000459249	7.02721E-10
0.6	304	1262.230769	897.2125	0.000464352	6.99564E-10
0.8	304	1264.307692	897.243	0.000470881	6.97243E-10
1	304	1265.230769	897.3625	0.000480561	6.96134E-10

0	309	1224.615385	890.8625	0.000439439	7.48497E-10
0.2	309	1226.384615	892.3125	0.000443791	7.45126E-10
0.4	309	1228.846154	892.8875	0.000448143	7.41666E-10
0.6	309	1232.692308	892.9975	0.000454447	7.36954E-10
0.8	309	1235.769231	893.1125	0.00046105	7.33194E-10
1	309	1240.846154	893.7875	0.000472156	7.26658E-10
0	314	1198.846154	887.3125	0.000428783	7.84145E-10
0.2	314	1201.3	888.3625	0.000435537	7.80022E-10
0.4	314	1204.230769	888.8375	0.000440039	7.75815E-10
0.6	314	1206.142857	889.0625	0.000445967	7.73161E-10
0.8	314	1208.153846	889.2875	0.000452308	7.70395E-10
1	314	1211.153846	889.7375	0.0004609	7.66195E-10

Table 4.15 THF-GO Nanosuspension 2

Concentration (mg/ml)	Temperature (T) (K)	Acoustical Impedance (Z) (Pa. s/m³) $Z = \rho \times U$	Attenuation (α/f^2) (m⁻¹) $\alpha/f^2 = 8\pi^2\eta / 3\rho U^3$	Bulk Modulus(K) (Pa) $K = \rho U^2$	Relaxation Time(τ) (s) $\tau = 4\beta\eta/3$	Intermolecular Free Length (L_f) ($L_f = K_T \times \beta^{1/2}$)
0	299	1149776	6.42026E-15	1471713280	4.17E-13	6.99E-10
0.2	299	1152983.893	6.44462E-15	1479113623	4.19E-13	6.95E-10
0.4	299	1157121.807	6.43636E-15	1487969634	4.20E-13	6.91E-10
0.6	299	1162135.262	6.42477E-15	1498975697	4.20E-13	6.86E-10
0.8	299	1164212.477	6.50479E-15	1503087863	4.26E-13	6.84E-10
1	299	1167167.138	6.60116E-15	1510224494	4.33E-13	6.81E-10
0	304	1120736.337	6.74264E-15	1404368840	4.28E-13	7.39E-10
0.2	304	1125225.559	6.73399E-15	1413456414	4.29E-13	7.34E-10
0.4	304	1129328.191	6.73383E-15	1423040392	4.30E-13	7.29E-10
0.6	304	1132489.224	6.7665E-15	1429462744	4.33E-13	7.26E-10
0.8	304	1134391.227	6.82764E-15	1434219554	4.38E-13	7.23E-10
1	304	1135370.646	6.95184E-15	1436505876	4.46E-13	7.22E-10

0	309	1090963.923	7.06182E-15	1336011204	4.39E-13	7.84E-10
0.2	309	1094318.322	7.0894E-15	1342055155	4.41E-13	7.80E-10
0.4	309	1097221.37	7.11141E-15	1348316261	4.43E-13	7.77E-10
0.6	309	1100791.149	7.14327E-15	1356936782	4.47E-13	7.72E-10
0.8	309	1103680.947	7.19214E-15	1363894955	4.51E-13	7.68E-10
1	309	1109052.782	7.26986E-15	1376163879	4.57E-13	7.61E-10
0	314	1063751.178	7.37392E-15	1275274008	4.48E-13	8.27E-10
0.2	314	1067189.871	7.43546E-15	1282015192	4.53E-13	8.23E-10
0.4	314	1070365.466	7.45363E-15	1288967029	4.55E-13	8.18E-10
0.6	314	1072336.384	7.51627E-15	1293390870	4.60E-13	8.16E-10
0.8	314	1074396.113	7.58322E-15	1298035797	4.65E-13	8.13E-10
1	314	1077608.995	7.66611E-15	1305150279	4.71E-13	8.08E-10

Table 4.16 THF-rGO Nanosuspension 1

Concentration (mg/ml)	Temperature (T) (K)	Average Velocity (m/s) $U = \lambda \times f$	Density (Kg/m³)	Viscosity (Pa-s)	Adiabatic Compressibility (1/Pa) $\beta = 1/ (U^2 \times \rho)$
0	299	1280	898.2625	0.00046	6.79E-10
0.2	299	1281.615	899.5875	0.00047	6.77E-10
0.4	299	1284.231	900.8625	0.00048	6.73E-10
0.6	299	1287.077	901.8175	0.000485	6.69E-10
0.8	299	1288.154	901.9375	0.000495	6.68E-10
1	299	1289.077	902.5375	0.000502	6.67E-10
0	304	1263.077	894.3875	0.000451	7.01E-10
0.2	304	1264.692	895.2875	0.000462	6.98E-10
0.4	304	1266.615	896.3875	0.000466	6.95E-10
0.6	304	1267.308	897.3575	0.000476	6.94E-10
0.8	304	1269.385	897.2625	0.000485	6.92E-10
1	304	1271.923	898.0575	0.000493	6.88E-10
0	309	1241.615	890.8625	0.000439	7.28E-10

0.2	309	1243.923	891.7125	0.000452	7.25E-10
0.4	309	1245.154	892.5375	0.000456	7.23E-10
0.6	309	1247.846	892.8975	0.000464	7.19E-10
0.8	309	1249.846	893.2125	0.000473	7.17E-10
1	309	1250.923	893.7575	0.000479	7.15E-10
0	314	1221.846	887.3125	0.000429	7.55E-10
0.2	314	1222.808	888.1125	0.000441	7.53E-10
0.4	314	1224.538	888.9375	0.000445	7.5E-10
0.6	314	1226.462	889.8125	0.000454	7.47E-10
0.8	314	1229.308	890.7663	0.000463	7.43E-10
1	314	1231.308	891.0375	0.000469	7.4E-10

Table 4.17 THF-rGO Nanosuspension 2

Concentration (mg/ml)	Temperature (T) (K)	Acoustical impedance (Z) (Pa. s/m³) $Z = \rho \times U$	Attenuation (α/f^2) (m⁻¹) $\alpha/f^2 = 8\pi^2\eta / 3\rho U^3$	Bulk Modulus(K) (Pa) $K = \rho U^2$	Relaxation Time(τ) (s) $\tau = 4\beta\eta/3$	Intermolecular Free Length (L_f) ($L_f = K_T \times \beta^{1/2}$)
0	299	1149776	6.42E-15	1.47E+09	4.17E-13	6.99E-10
0.2	299	1152925	6.53E-15	1.48E+09	4.24E-13	6.96E-10
0.4	299	1156915	6.61E-15	1.49E+09	4.3E-13	6.92E-10
0.6	299	1160708	6.63E-15	1.49E+09	4.33E-13	6.88E-10
0.8	299	1161834	6.75E-15	1.5E+09	4.41E-13	6.87E-10
1	299	1163440	6.83E-15	1.5E+09	4.46E-13	6.85E-10
0	304	1129680	6.58E-15	1.43E+09	4.22E-13	7.27E-10
0.2	304	1132263	6.71E-15	1.43E+09	4.3E-13	7.25E-10
0.4	304	1135378	6.72E-15	1.44E+09	4.32E-13	7.21E-10
0.6	304	1137228	6.85E-15	1.44E+09	4.4E-13	7.2E-10
0.8	304	1138971	6.95E-15	1.45E+09	4.47E-13	7.18E-10
1	304	1142260	7.01E-15	1.45E+09	4.52E-13	7.14E-10
0	309	1106109	6.78E-15	1.37E+09	4.27E-13	7.62E-10

0.2	309	1109222	6.92E-15	1.38E+09	4.37E-13	7.59E-10
0.4	309	1111347	6.95E-15	1.38E+09	4.39E-13	7.57E-10
0.6	309	1114199	7.03E-15	1.39E+09	4.45E-13	7.53E-10
0.8	309	1116378	7.13E-15	1.4E+09	4.52E-13	7.5E-10
1	309	1118022	7.2E-15	1.4E+09	4.57E-13	7.49E-10
0	314	1084159	6.97E-15	1.32E+09	4.32E-13	7.96E-10
0.2	314	1085991	7.14E-15	1.33E+09	4.43E-13	7.94E-10
0.4	314	1088538	7.17E-15	1.33E+09	4.45E-13	7.91E-10
0.6	314	1091321	7.27E-15	1.34E+09	4.52E-13	7.88E-10
0.8	314	1095026	7.35E-15	1.35E+09	4.58E-13	7.84E-10
1	314	1097141	7.41E-15	1.35E+09	4.62E-13	7.81E-10

4.39 Result and Discussion: We measured the following parameter to study the thermoacoustic analysis.

4.39.1 Ultrasonic Velocity: Ultrasonic velocity is one of the utmost significant parameters to qualitatively measures the interparticle and intermolecular interaction of the nanosuspension [1]. The ultrasonic speed is measured for all the prepared samples of THF-GO and THF-rGO at four distinct temperatures (298, 303, 308, and 313K). Readings were measured repeatedly to avoid any experimental errors as well as interpretations of pure THF is matched with the literature [2]. The increase and decrease of ultrasonic velocity with the concentration of the particles and temperature give an insight of intermolecular and intraparticle interactions, as shown in Fig. 4.94. We can notice in THF-GO and THF-rGO that ultrasonic velocity consistently increases from the pure liquid with the growth in the concentration of the particles.

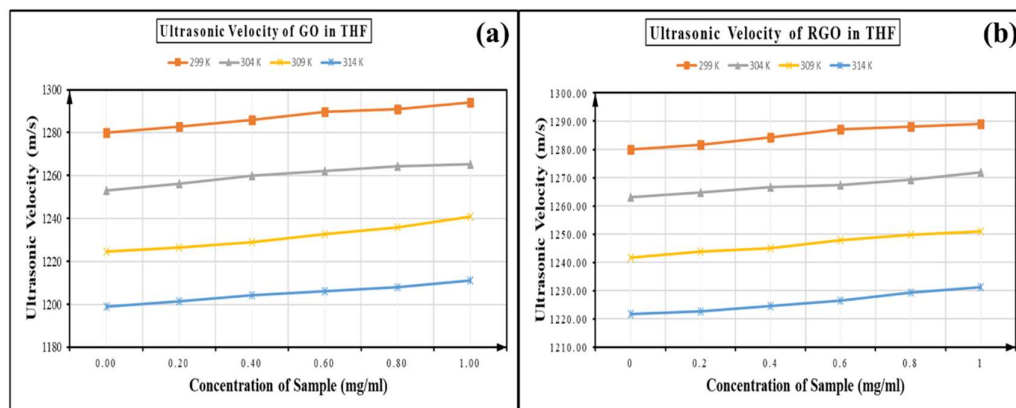


Figure 4.94 (a) Ultrasonic Velocity of GO-THF Nanosuspension (b) Ultrasonic Velocity of rGO-THF Nanosuspension

Further, we can notice that as the temperature of the system increase from 298 K to 313 K, there is a decrease in the ultrasonic velocity. The reduction in the ultrasonic speed with the concentration is due to the interaction of the GO and rGO particles with THF interaction; it further explains the supremacy of intermolecular interaction over intraparticle interactions. The increase in concentration also reduces the Brownian motion of the system, which helps to increase the ultrasonic velocity of the system because the interaction of GO and rGO particles with solvent molecule increases. At the higher temperatures, the speed decreases further as compared to the pure THF,

which helps to establish the fact that GO, rGO, and THF had more interaction as compared to GO-GO and rGO-rGO. The reduction of ultrasonic velocity with surging temperature proves that the nanosuspension follow the usual behavior of non- aqueous liquids, which can be described as the temperature of suspension increases, the average speed of the molecules surges, and the amount of time they employ in interaction with their nearest neighbors decreases. Thus, the increasing temperature leads to the fading of the intermolecular adhesive and cohesive forces, thereby enhancing the compressibility, which, in turn, reduces the ultrasonic velocity [3],[4].

4.39.2 Density: It can be seen in Figure 4.95 that the density of THF-rGO nanosuspension increases as the amount of GO and rGO particles added to pure THF. After this slight increase in the density of formulated nanosuspension can be seen, the usual reflection is that density declines with temperature, which agrees well with the acceptable behavior of the fluids. Density raises with concentration, as the nanoparticles being added are of higher density than the base fluid [5]. The small rise in the density after increasing the concentration of the particles is due to the increase in intermolecular interaction instead that of interparticle communication [6].

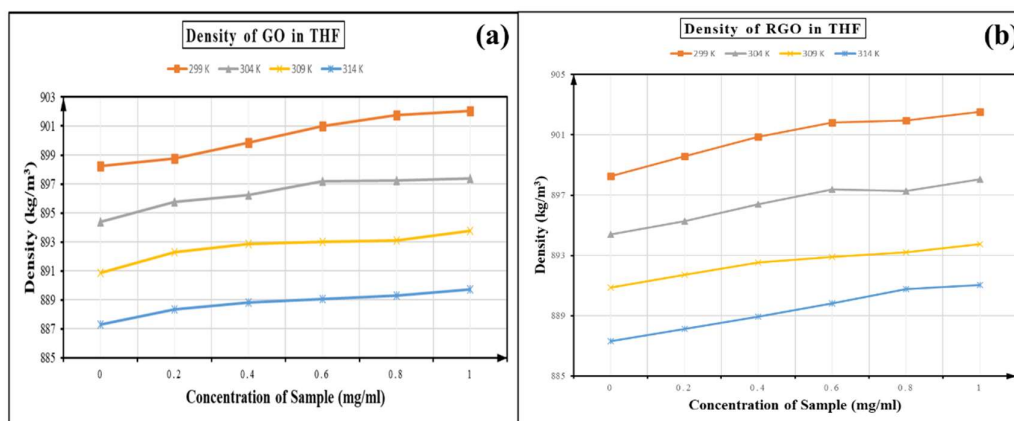


Figure 4.95 (a) Density of GO-THF Nanosuspension (b) Density of rGO-THF Nanosuspension

The density of the THF-GO and THF-rGO nanosuspension decreases with the increase in the temperature of the system. With the rise in the heat, the Brownian motion of the solvent molecules also starts to rise. The increase in random motion tends to decrease the density of the system.

4.39.3 Viscosity: Viscosity of the THF-GO and THF-rGO nanosuspension rises very sharply with the addition of rGO particles in the pure THF solution, as displayed in figure 4.96. Viscosity similarly increases with increases the particle loading, which is due to the interlocking of GO and rGO particles while flow [7]. With the growth in the temperature, the viscosity of THF-GO and THF-rGO nanosuspension decreases as normal fluid. This decrease in the viscosity of the sample can be understood by the rise in the Brownian motion of the particle present in the nanosuspension with the upsurge in the temperature. This decrease in viscosity with temperature helps to flow the nanosuspension effortlessly at higher temperatures as compared to low temperatures [8].

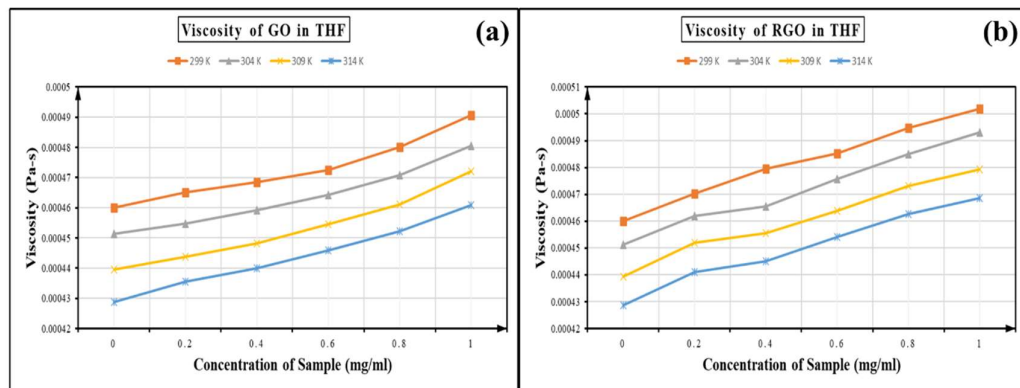


Figure 4.96 (a) Viscosity of GO-THF Nanosuspension (b) Viscosity of rGO-THF Nanosuspension

4.39.4 Adiabatic Compressibility: Fig. 4.97 shows the change in adiabatic compressibility with the increase in the particle loading in pure THF. As the particles are added in the pure THF, it shows a constant decrease, which shows the weak particle and fluid interaction [9]. The decline in the compressibility also leads to the conclusion that the particle added to the base fluid tries to form a complex structure in the nanosuspension. The reduction in the adiabatic compressibility shows the interaction in the particle and fluid increases and complex formation in the system. Adiabatic compressibility likewise increases with the increase in the temperature of the system, which is the cause of the rise in the Brownian motion of the particles. [10]

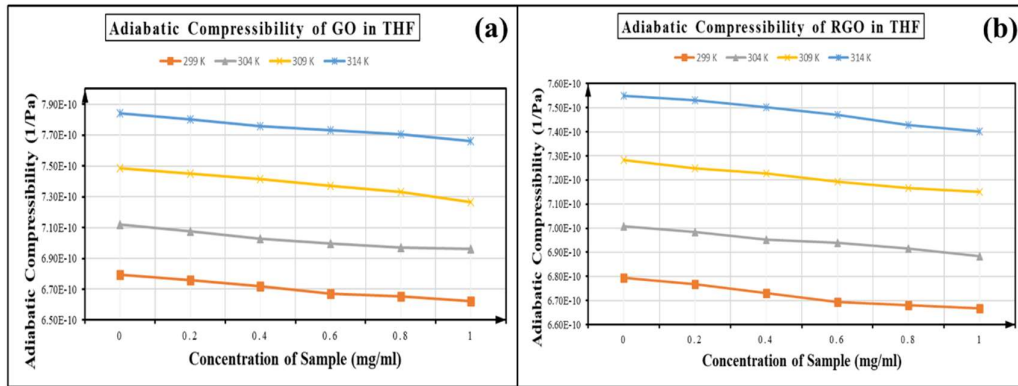


Figure 4.97 (a) Adiabatic Compressibility of GO-THF Nanosuspension (b) Adiabatic Compressibility of rGO-THF Nanosuspension

4.39.5 Acoustical Impedance: Fig. 4.98 shows the increase in the values of acoustical impedance with particle loading in pure THF. An upsurge in the amount of acoustical impedance shows the increase in interaction in solute and particle of the THF-GO and THF-rGO nanosuspension [11]. With the improvements in the temperature, the value of acoustic impedance decreases because of the Brownian motion of the particles in the fluid increases. Increasing particle-fluid interactions at lower concentrations widen the intermolecular gap, which provides resistance to the propagation of ultrasonic waves [12].

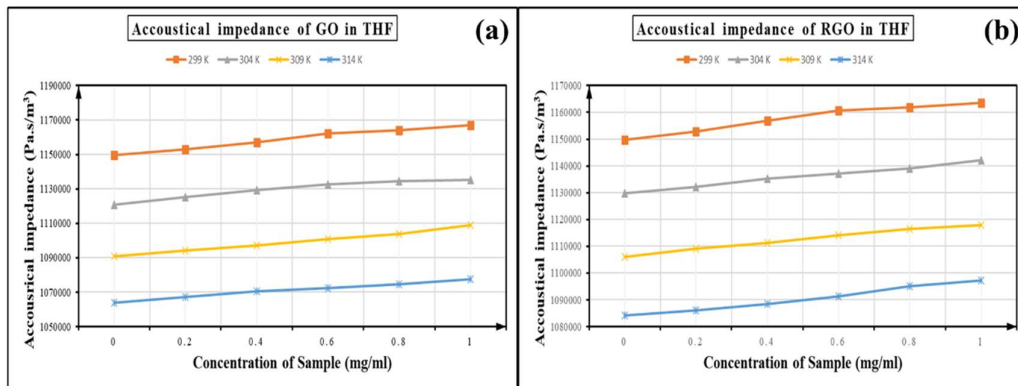


Figure 4.98 (a) Acoustical Impedance of GO-THF Nanosuspension (b) Acoustical Impedance of rGO-THF Nanosuspension

4.39.6 Attenuation: Variation of the ultrasonic attenuation and concentration of the particles in THF-GO and THF-rGO nanosuspension is shown in Fig. 4.99. Ultrasonic attenuation starts increasing as soon as the particle is added in the pure THF fluid.

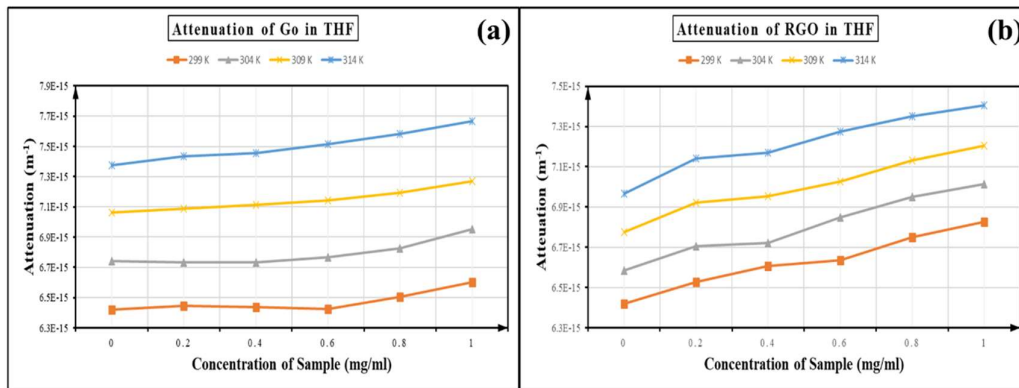


Figure 4.99 (a) Attenuation of Ultrasonic Wave in GO-THF Nanosuspension (b) Attenuation of Ultrasonic Wave in rGO-THF Nanosuspension

Further increase in the ultrasonic attenuation can be seen in both GO and rGO nanosuspension; this increase in the mitigation is because GO and rGO can form agglomeration by binding with each other. This blockage produced by the agglomerated GO and rGO particles block the ultrasonic waves from reaching one end to the other. The increase in the temperature value of the ultrasonic attenuation increases because of an increase in the interaction of THF molecules with GO and rGO particles. Here we can deny the complex formation in the suspension. [11]

4.39.7 Bulk Modulus: In figure 4.100, it can be seen clearly that the value of bulk modulus rises with the increase in the particle loading in the solvent. Interaction between the particle and fluid increases as the concentration of the GO and rGO in nanosuspension increases.

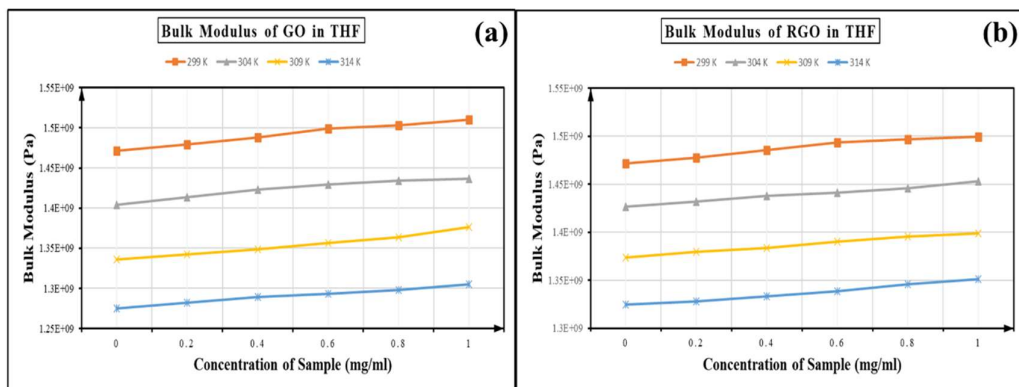


Figure 4.100 (a) Bulk Modulus of GO-THF Nanosuspension (b) Bulk Modulus of rGO-THF Nanosuspension

The value of the bulk modulus decreases with the rise in the heat of the nanosuspension. The resistance of the nanosuspension decreases to the externally applied stress at a higher temperature because the interaction between particle and solute increases creates the gap between molecules, which helps in reducing bulk modulus [13-14]

4.39.8 Relaxation Time: The relaxation time of the THF-GO and THF-rGO sample increase with the increase in the concentration of GO and rGO in the THF-GO and THF-rGO nanosuspension, respectively, as shown in figure 4.101. Since the interaction between the solvent molecules and solute increases. The reordering time for the solute molecules increases. When the heat of the THF-GO and THF-rGO nanosuspension rises, the zigzag movement of the solvent molecule increases, which helps to reorder the molecules quickly because of fast motion [14-15].

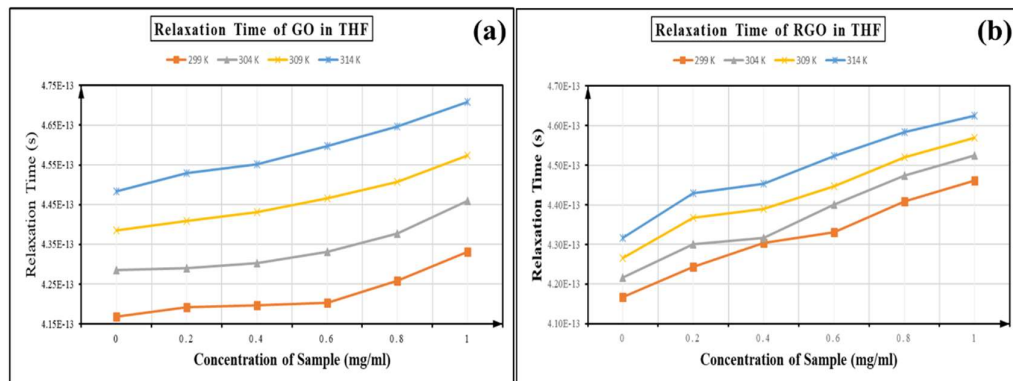


Figure 4.101 (a) Relaxation Time of GO-THF Nanosuspension (b) Relaxation Time of rGO-THF Nanosuspension

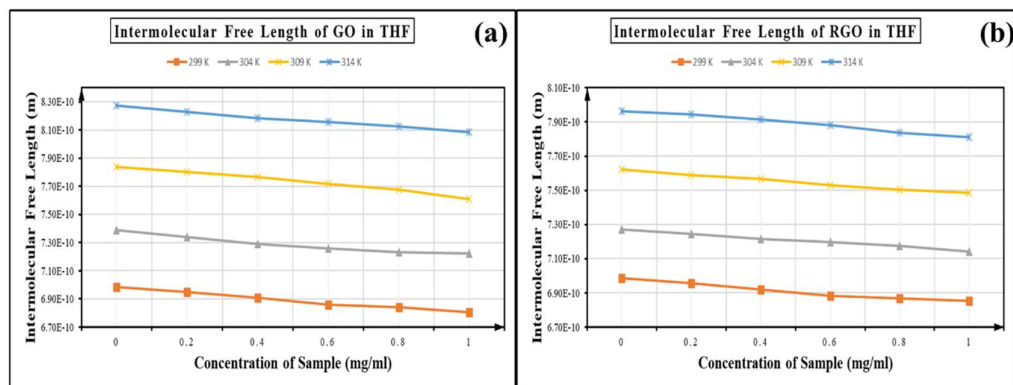


Figure 4.102 (a) Intermolecular free Length of GO-THF Nanosuspension (b) Intermolecular free Length of rGO-THF Nanosuspension

4.39.9 Intermolecular free length: The intermolecular length of the sample decreases with a rise in the particle loading in the THF-GO and THF-rGO nanosuspension, as shown in Figure 4.102. It shows the interaction between particle and solvent molecules decreases. The increase in the intermolecular length with the rise in the heat is because the zigzag movement of the solvent molecules rises, and this movement increases the solute and solvent molecule interaction [16-17]

4.40 References

- [1] M. N. Rashin and J. Hemalatha, *J. Mol. Liq.*, **197**, 257, (2014).
- [2] D. Papamatthaiakis, F. Aroni, and V. Havredaki, *J. Chem. Thermodyn.*, **40**, 107, (2008).
- [3] M. Nabeel Rashin and J. Hemalatha, *J. Mol. Liq.*, **197**, 257, (2014).
- [4] M. N. Rashin and J. Hemalatha, *Ultrasonics*, **52**, 1024, (2012).
- [5] R. S. Vajjha, D. K. Das, and B. M. Mahagaonkar, *Pet. Sci. Technol.*, **27**, 612, (2009).
- [6] S. N. Shoghl, J. Jamali, and M. K. Moraveji, *Exp. Therm. FLUID Sci.*, **27**, 12, (2016).
- [7] M. N. Rashin and J. Hemalatha, *Exp. Therm. Fluid Sci.*, **51**, 312, (2013).
- [8] M. R. Esfahani, E. M. Languri, M. R. Nunna, M. Rabbani, E. Mohseni, and M. Rao, *Int. Commun. Heat Mass Transf.*, **76**, 308, (2016).
- [9] Khushboo, A. Devi, P. Malik, and H. Kumar, *J. Mol. Liq.*, **214**, 145, (2016).
- [10] A. Nanda, A. Tiadi, S. K. Mallik, R. Giri, and G. Nath, *IOP Conf. Ser. Mater. Sci. Eng.*, **360**, 1, (2018).
- [11] S. Tiwari, B. S. Kusmariya, A. Tiwari, V. Pathak, and A. P. P. Mishra, *J. Taibah Univ. Sci.*, **11**, 101, (2017).
- [12] N. H. Ayachit, S. T. Vasan, F. M. Sannaningannavar, and D. K. Deshpande, *J.*

Mol. Liq., **133**, 134, (2007).

[13] B. Tajik, A. Abbassi, M. Saffar-Avval, and M.A. Najafabadi, Powder Technol. **217**, 171, (2012).

[14] N.H. Ayachit, S.T. Vasan, F.M. Sannaningannavar, and D.K. Deshpande, J. Mol. Liq. **133**, 134 (2007).

[15] S. Elangovan and S. Mullainathan, Indian J. Phys. **87**, 659 (2013).

[16] F. Chen, Z. Yang, Z. Chen, J. Hu, C. Chen, and J. Cai, Journal of Molecular Liquids, **209**, 683, (2015).

[17] K. Kaur and K. C. Juglan, Der Pharma Chem., **7**, 160, (2015)

Section 5

Study of EG-GO and EG-rGO Nanosuspension

In Section 4, we discussed the study of THF with GO and rGO. In the existing section, we will discuss the EG with GO and rGO. We have already discussed the characterization of the GO and rGO powder in sections 4.1 and 4.2, respectively.

4.41 Introduction

Nanosuspensions are the colloidal dispersion of nanosized particles ranging from 100 – 500 nm in the base fluid. The nanoparticles used in the nanosuspension are typically made from metals, oxides, carbides, or nanotubes of Carbon. As we know, heat transfer takes place on the surface of the particle, so for the better heat transfer application, nanosized particles can play a very vital role because of the extremely high surface area available in these particles. Nanosized particles have a high thermal conductivity that can be used in various fields like electronics, where the dissipation of heat from the electronic components is always a challenge. Another potential area can be the use of these particles in ink for electronic device printing to produce flexible and more conductive electronic devices. The choice of the base fluid in these nanosuspensions can further increase the properties, e.g., the use of water as a base fluid can help to improve the process of heat exchange as water is one of the best coolant available. But, the main objective and goal in nanosuspension research are to develop nanosuspension with stability for industrial applications. Ultrasonication is an accepted technique for dispersing aggregated nanoparticles for the preparation of aqueous nano-suspensions. It has been found in the literature that the increase in the stability of nanosuspension with the rise in the sonication time. Stabilization of the nanosuspension also depends on the choice of the nanoparticle and the choice of sonication time. So, the first challenge is to prepare stable nanosuspension, which can be used for industrial applications.

Graphene is one of the most significant finds in the last decade in terms of many physical and chemical properties. Since its evolution, the number of features like high electron mobility, high electron density, high thermal conductivity, the most durable

material, etc. Despite all these excellent properties, there are some difficulties associated with this material like industrial-scale productivity and preparation of the good stable suspension. A different peer group has reported many methods to produce graphene (G), graphene oxide (GO) and reduced graphene oxide (RGO), and the stable suspension.

In this paper, we prepared GO and rGO nanosuspension with different concentrations in EG. Structural, morphological, and fluid interaction studies have been completed and compared. Intermolecular interaction between EG-GO and EG-rGO nanosuspension was observed at different concentrations and temperatures in the range of 298 K to 313 K. The adiabatic compressibility, acoustic impedance, mean free pathway were evaluated and examined by ultrasonic approach. Nonetheless, the attenuation coefficient of the ultrasonic wave propagating through all specimens is calculated.

4.42 Material and Method

4.42.1 Materials

Graphite powder, sodium nitrate obtained from Loba Chemical, KMnO_4 , HCl , and Ammonia was taken from CDH, and H_2SO_4 was obtained from Avantar. H_2O_2 was gathered from a fisher scientific, Hydrazine monohydrate, and EG was purchased from Sigma Aldrich with an AR grade. All the chemicals used in work are AR grade. Double distilled water was used throughout the experiment.

4.42.2 Methods

The original Hummers Method is used to prepare to GO. In 1000 ml beaker, 345 ml of H_2SO_4 has been taken and put to the continuous magnetic stirrer. An ice bath has been made around the beaker to maintain the temperature of the bath below ten $^\circ\text{C}$. 15 gm of Graphite Powder, and 7.5 gm of NaNO_3 has been added to continuously stirring H_2SO_4 with the heat of the bath is close to zero Celsius. After 30 minutes of continuous stirring, 45 gm of KMnO_4 has been added to the mixture very slowly, such as to maintain the reaction temperature below 90 $^\circ\text{C}$. The mixture is left for continuous stirring for 2 hours after that beaker has been placed in a water bath at the temperature

of 40 °C for 1 hour to increase the rate of oxidation. The color of the mixture changes from black to greenish-brown. After 1 hour, the mixture is placed on the magnetic stirrer and ice bath. With continuous stirring, the mixture is diluted with 500 ml of distilled water very slowly, maintaining the reaction temperature below 90 °C. After leaving the mixture overnight, distilled water 100 ml with 30% H₂O₂ added to the mix to remove any excess KMnO₄ and to stop the oxidation reaction. The further mixture was diluted with distilled water and left for the decantation process overnight. Then we remove the top layer of water, and the remaining solution is filtered. Continuous addition of distilled water has been added during the filtration process helps to remove excess KMnO₄ and metal ions. Approximately 5 liters of distilled water was used during the filtration process. Following the completion of the filtration, the processed mixture was again mixed with 500 ml of distilled water and added to 8-hour ultrasonication, which helps to reduce GO.

The mixture was left to dry in the vacuum and to grinded for GO powder. A colloidal suspension of GO powder in double-distilled water (2 mg/ml) is prepared by ultrasonication of GO in 500 mL of liquid for 1 hour. A few drops of Ammonia have been added to the solution to adjust the PH of the solution in a range of 9 to 10. Hydrazine monohydrate (1 µl for 3 mg of GO) was then added to the suspension. Continuous magnetic string and temperature maintenance up to 95 °C for 3 hours yielded black precipitate of RGO powder. After cooling to room temperature, the powder was filtered through the filter, and the vacuum was dried. Synthesized RGO nanoparticles are dispersed in EG by ultrasound for 24 h to obtain a homogenous suspension of different concentrations without any phase separation and sedimentation. As with many peer groups, it is indisputable that ultrasound improves reliability and dispersion of the suspension. Nanosuspensions with different concentrations (0.2mg / ml, 0.4mg / ml, 0.6mg / ml, 0.8mg / ml and 1.0mg / ml) are prepared without the introduction of any surfactants.

4.43 Characterization of EG-GO and EG-rGO Nanosuspension

4.43.1 UV-VIS: The UV-Vis characterization of prepared EG-GO and EG-rGO nanosuspension a discussed in sections 4.3 and 4.4, respectively.

4.43.2 HRTEM: The HRTEM image of the prepared suspension is shown in figure 4.103. We have used a drop of Nanosuspension for the study of the sample of EG-GO and EG-rGO nanosuspension under HRTEM.

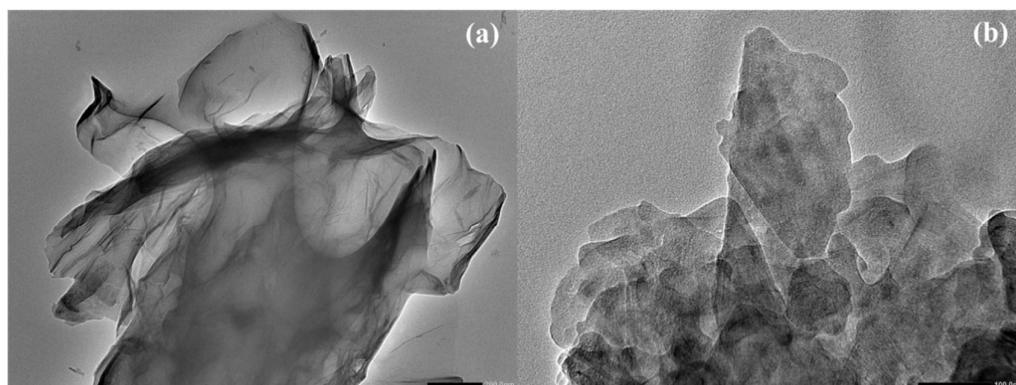


Figure 4.103 (a) HRTEM image of GO (b) HRTEM image of rGO

Figure 4.103 (a) shows the layer of the graphene sheets stacked over each other. The light portion of the image shows the stack of a smaller number of the sheets, and the darker part shows many layers stacked or maybe the presence of the oxygen atom in between the sheets. Image 4.103 (a) indicated the presence of the GO sheets in the drop of NMP under the HRTEM study. Figure 4.103 (b) shows the number of smaller sheets in the sample under investigation. The small size of graphene sheets indicates that while reducing the GO chemically with hydrazine hydrate, big sheets split into small sheets because of oxygen atom escape from the layers by breaking the structure. The dark portion shows either the pile of rGO sheets or the presence of an oxygen atom in the layers of graphene. It is confirmed from HRTEM that sheets like structures are present in the drop of EG-rGO Nanosuspension.

4.43.3 DLS: We can depict the size of the GO and rGO sheets with the help of the DLS technique. Figure 4.104 shows the particle size of GO and rGO in the EG with different concentrations of GO and rGO particles, respectively.

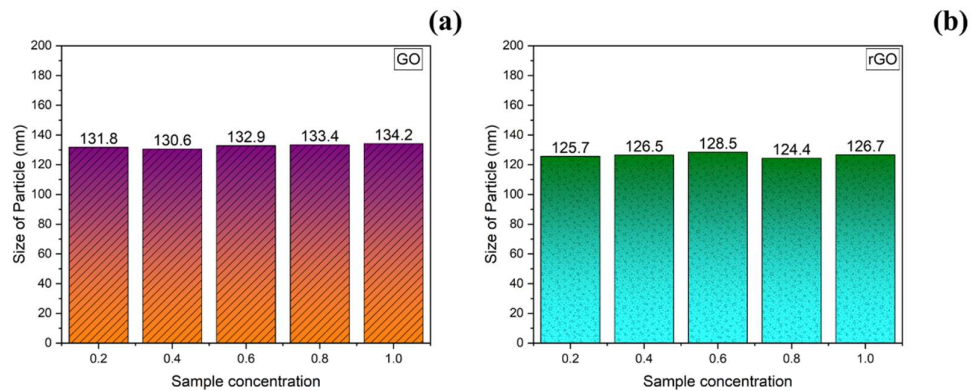


Figure 4.104 (a) DLS image of GO-EG Nanosuspension (b) DLS image of rGO-EG Nanosuspension

We deployed ultrasonication for the formulation of nanosuspension. The size of the rGO particles significantly reduced if compared with GO. The size of the rGO particles comes out in the range of 113 nm to 120 nm, and GO particles have the size range from 134 to 140 nm. This size confirmation helps to name our suspension as nanosuspension.

4.44 Data Table

Table 4.18 EG-GO Nanosuspension 1

Concentration (mg/ml)	Temperature (in K)	Average Velocity (m/s) $U = \lambda \times f$	Density (Kg/m ³)	Viscosity (Pa-s)	Adiabatic Compressibility (1/Pa) $\beta = 1 / (U^2 \times \rho)$
0	299	1670.769	1121.1	0.012193	3.2E-10
0.2	299	1670.069	1120.9	0.016103	3.2E-10
0.4	299	1669.091	1120.7	0.01363	3.2E-10
0.6	299	1665.333	1120.2	0.012383	3.22E-10
0.8	299	1663.538	1119.8	0.012126	3.23E-10
1	299	1661.077	1119.4	0.010806	3.24E-10
0	304	1653.077	1118.4	0.01103	3.27E-10
0.2	304	1652.231	1117.8	0.014249	3.28E-10
0.4	304	1651.154	1117.3	0.012378	3.28E-10
0.6	304	1649.154	1116.8	0.011573	3.29E-10
0.8	304	1645.231	1116.3	0.010988	3.31E-10
1	304	1636.923	1116	0.0102	3.34E-10

0	309	1633.846	1115.4	0.01036	3.36E-10
0.2	309	1631.23	1114.7	0.012795	3.37E-10
0.4	309	1628.692	1114.1	0.011148	3.38E-10
0.6	309	1625.538	1114.1	0.010336	3.4E-10
0.8	309	1622.923	1113.8	0.010171	3.41E-10
1	309	1621.538	1113.4	0.009789	3.42E-10
0	314	1618.462	1113.6	0.00944	3.43E-10
0.2	314	1615.077	1113.1	0.010765	3.44E-10
0.4	314	1613.462	1112.3	0.010288	3.45E-10
0.6	314	1612.154	1112	0.009604	3.46E-10
0.8	314	1608.615	1111	0.009346	3.48E-10
1	314	1605.385	1110.5	0.009213	3.49E-10

Table 4.19 EG-GO Nanosuspension 2

Concentration (mg/ml)	Temperature (T) (K)	Acoustical Impedance (Z) (Pa. s/m³) $Z = \rho \times U$	Attenuation (α/f^2) (m⁻¹) $\alpha/f^2 = 8\pi^2\eta / 3\rho U^3$	Bulk Modulus(K) (Pa) $K = \rho U^2$	Relaxation Time(τ) (s) $\tau = 4\beta\eta/3$	Intermolecular Free Length (L_f) ($L_f = K_T \times \beta^{1/2}$)
0	299	1873099.4	6.1312E-14	3129516818	5.19484E-12	3.28485E-10
0.2	299	1871980.6	8.1087E-14	3126337202	6.86746E-12	3.28819E-10
0.4	299	1870550.2	6.8769E-14	3122118303	5.82083E-12	3.29264E-10
0.6	299	1865506.4	6.2927E-14	3106689991	5.31434E-12	3.30899E-10
0.8	299	1862830.4	6.1847E-14	3098889967	5.21746E-12	3.31732E-10
1	299	1859409.5	5.5376E-14	3088622224	4.66467E-12	3.32834E-10
0	304	1848801.2	5.7402E-14	3056210650	4.81206E-12	3.39473E-10
0.2	304	1846863.6	7.4307E-14	3051444790	6.22601E-12	3.40003E-10
0.4	304	1844834.2	6.4704E-14	3046105072	5.41785E-12	3.40599E-10
0.6	304	1841775	6.0743E-14	3037370350	5.08005E-12	3.41578E-10
0.8	304	1836571.1	5.8112E-14	3021583296	4.84845E-12	3.43363E-10
1	304	1826806.2	5.4787E-14	2990341150	4.54798E-12	3.4695E-10

0	309	1822392	5.5992E-14	2977508160	4.63923E-12	3.51636E-10
0.2	309	1818332.1	6.9529E-14	2966117840	5.75163E-12	3.52987E-10
0.4	309	1814526.1	6.0893E-14	2955304701	5.02937E-12	3.54278E-10
0.6	309	1811012.4	5.679E-14	2943870311	4.68148E-12	3.55654E-10
0.8	309	1807611.7	5.617E-14	2933614779	4.62285E-12	3.56898E-10
1	309	1805420.9	5.4216E-14	2927559466	4.45827E-12	3.57636E-10
0	314	1802318.8	5.2573E-14	2916983608	4.31496E-12	3.61675E-10
0.2	314	1797742.1	6.0357E-14	2903491817	4.94347E-12	3.63356E-10
0.4	314	1794653.3	5.7895E-14	2895604025	4.73707E-12	3.64345E-10
0.6	314	1792715.1	5.4193E-14	2890132506	4.43059E-12	3.65035E-10
0.8	314	1787171.7	5.3137E-14	2874871879	4.33469E-12	3.66973E-10
1	314	1782779.6	5.272E-14	2862046967	4.29203E-12	3.68617E-10

Table 4.20 EG-rGO Nanosuspension 1

Concentration (mg/ml)	Temperature (T) (K)	Average Velocity (m/s) $U = \lambda \times f$	Density (Kg/m ³)	Viscosity (Pa-s)	Adiabatic Compressibility (1/Pa) $\beta = 1/ (U^2 \times \rho)$
0	299	1665.769	1121.1	0.012193	3.21E-10
0.2	299	1663.385	1120.2	0.01397	3.23E-10
0.4	299	1659.462	1119.7	0.013781	3.24E-10
0.6	299	1655.385	1119.5	0.013685	3.26E-10
0.8	299	1653.385	1119.2	0.01298	3.27E-10
1	299	1650.385	1118.7	0.012516	3.28E-10
0	304	1653.077	1118.4	0.01103	3.27E-10
0.2	304	1651.846	1117.7	0.012539	3.28E-10
0.4	304	1648.846	1117.1	0.012243	3.29E-10
0.6	304	1645.923	1116.3	0.011473	3.31E-10
0.8	304	1642.923	1115.8	0.011168	3.32E-10
1	304	1640	1115.2	0.010779	3.33E-10
0	309	1638.846	1115.4	0.01036	3.34E-10

0.2	309	1635.769	1114.7	0.011225	3.35E-10
0.4	309	1632.692	1113.9	0.011041	3.37E-10
0.6	309	1629.769	1113.4	0.01025	3.38E-10
0.8	309	1626.846	1112.8	0.009879	3.4E-10
1	309	1623.846	1111.8	0.0095	3.41E-10
0	314	1618.462	1113.6	0.00944	3.43E-10
0.2	314	1615.385	1112.3	0.009728	3.45E-10
0.4	314	1612.308	1111.7	0.009518	3.46E-10
0.6	314	1609.462	1111.1	0.008904	3.47E-10
0.8	314	1605.462	1110.4	0.008421	3.49E-10
1	314	1602.462	1109.4	0.008134	3.51E-10

Table 4.21 EG-rGO Nanosuspension 2

Concentration (mg/ml)	Temperature (T) (K)	Acoustical impedance (Z) (Pa. s/m³) $Z = \rho \times U$	Attenuation (α/f^2) (m⁻¹) $\alpha/f^2 = 8\pi^2\eta / 3\rho U^3$	Bulk Modulus(K) (Pa) $K = \rho U^2$	Relaxation Time(τ) (s) $\tau = 4\beta\eta/3$	Intermolecular Free Length (L_f) ($L_f = K_T \times \beta^{1/2}$)
0	299	1867494	6.19E-14	3.11E+09	5.23E-12	3.3E-10
0.2	299	1863323	7.12E-14	3.1E+09	6.01E-12	3.32E-10
0.4	299	1858099	7.08E-14	3.08E+09	5.96E-12	3.33E-10
0.6	299	1853203	7.09E-14	3.07E+09	5.95E-12	3.35E-10
0.8	299	1850468	6.75E-14	3.06E+09	5.66E-12	3.36E-10
1	299	1846285	6.54E-14	3.05E+09	5.48E-12	3.37E-10
0	304	1848801	5.74E-14	3.06E+09	4.81E-12	3.39E-10
0.2	304	1846268	6.54E-14	3.05E+09	5.48E-12	3.4E-10
0.4	304	1841926	6.43E-14	3.04E+09	5.37E-12	3.42E-10
0.6	304	1837344	6.06E-14	3.02E+09	5.06E-12	3.43E-10
0.8	304	1833174	5.93E-14	3.01E+09	4.94E-12	3.44E-10
1	304	1828928	5.76E-14	3E+09	4.79E-12	3.46E-10
0	309	1827969	5.55E-14	3E+09	4.61E-12	3.49E-10

0.2	309	1823392	6.05E-14	2.98E+09	5.02E-12	3.51E-10
0.4	309	1818656	5.99E-14	2.97E+09	4.96E-12	3.53E-10
0.6	309	1814585	5.59E-14	2.96E+09	4.62E-12	3.54E-10
0.8	309	1810354	5.42E-14	2.95E+09	4.47E-12	3.55E-10
1	309	1805392	5.25E-14	2.93E+09	4.32E-12	3.57E-10
0	314	1802319	5.26E-14	2.92E+09	4.31E-12	3.62E-10
0.2	314	1796792	5.45E-14	2.9E+09	4.47E-12	3.63E-10
0.4	314	1792402	5.37E-14	2.89E+09	4.39E-12	3.65E-10
0.6	314	1788273	5.05E-14	2.88E+09	4.13E-12	3.67E-10
0.8	314	1782704	4.82E-14	2.86E+09	3.92E-12	3.69E-10
1	314	1777771	4.68E-14	2.85E+09	3.81E-12	3.7E-10

4.45 Result and Discussion: We measured the following parameter to study the thermoacoustic analysis.

4.45.1 Ultrasonic Velocity: Ultrasonic velocity is one of the utmost significant parameters to qualitatively measure the interparticle and intermolecular interaction of the nanosuspension [1]. The ultrasonic speed is measured for all the prepared samples of EG-GO and EG-rGO at four distinct temperatures (298, 303, 308, and 313K). Readings were measured repeatedly to avoid any experimental errors as well as interpretations of pure EG is matched with the literature [2]. The increase and decrease of ultrasonic velocity with the concentration of the particles and temperature give an insight of intermolecular and intraparticle interactions, as shown in Fig. 4.105. We can notice in EG-GO and EG-rGO that ultrasonic velocity consistently decreases from the pure liquid with the progression in the concentration of the particles.

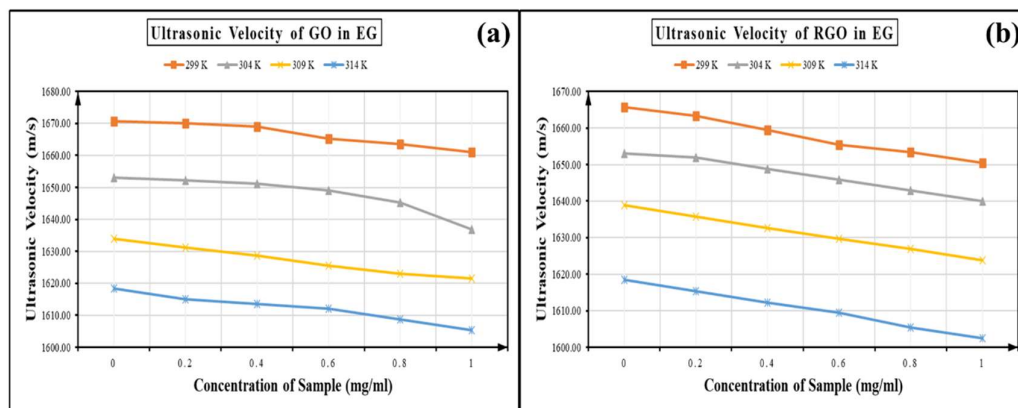


Figure 4.105 (a) Ultrasonic Velocity of GO-EG Nanosuspension (b) Ultrasonic Velocity of rGO-EG Nanosuspension

Further, we can notice that as the temperature of the system increase from 298 K to 313 K, there is a decrease in the ultrasonic velocity. The reduction in the ultrasonic speed with the concentration is due to the interaction of the GO and rGO particles with EG interaction; it further explains the supremacy of intermolecular interaction over intraparticle interactions. The increase in concentration also reduces the Brownian motion of the system, which helps to decrease the ultrasonic velocity of the system because the interaction of GO and rGO particles with solvent molecule decreases. At the higher temperatures, the speed decreases further as compared to the pure EG, which

helps to establish the fact that GO, rGO, and EG had more interaction as compared to GO-GO and rGO-rGO. The reduction of ultrasonic velocity with surging temperature proves that the nanosuspension follow the usual behavior of non- aqueous liquids, which can be described as the temperature of suspension increases, the average speed of the molecules surges, and the amount of time they employ in interaction with their nearest neighbors decreases. Thus, the increasing temperature leads to the fading of the intermolecular adhesive and cohesive forces, thereby enhancing the compressibility, which, in turn, reduces the ultrasonic velocity [3][4].

4.45.2 Density: It can be seen in Figure 4.106 that the density of EG-rGO nanosuspension decreases as the amount of GO and rGO particles added to pure EG. After this slight decrease in the density of formulated nanosuspension can be seen, the usual reflection is that density declines with temperature, which agrees well with the acceptable behavior of the fluids. Density declines with concentration, as the nanoparticles being added are of higher density than the base fluid [5]. The continuous reduction in the density after increasing the concentration of the particles is due to the decrease in intermolecular interaction instead that of interparticle communication [6].

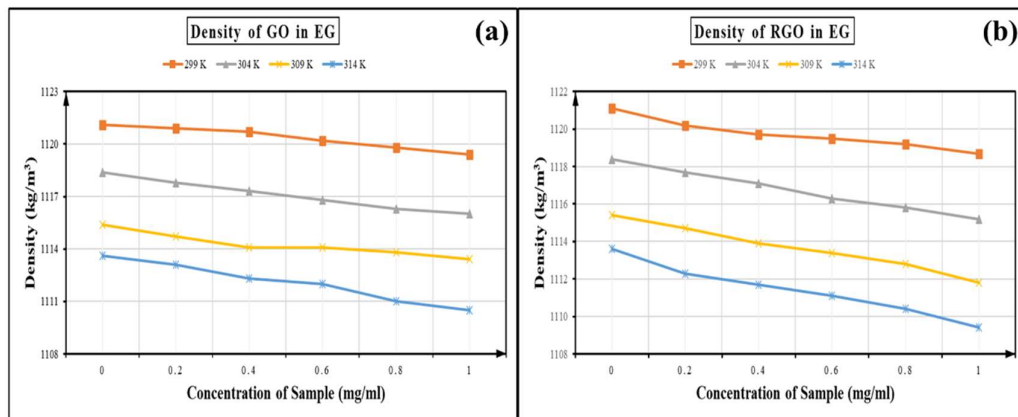


Figure 4.106 (a) Density of GO-EG Nanosuspension (b) Density of rGO-EG Nanosuspension

The density of the EG-GO and EG-rGO nanosuspension decreases with the increase in the temperature of the system. With the rise in the heat, the Brownian motion of the solvent molecules also starts to rise. The increase in random motion tends to decrease the density of the system.

4.45.3 Viscosity: Viscosity of the EG-GO and EG-rGO nanosuspension rises very sharply with the addition of GO and rGO particles in the pure EG solution, as displayed in figure 4.107. Viscosity decreases with increases the particle loading, which is due to the ease of GO and rGO particles while flow [7]. With the growth in the temperature, the viscosity of EG-GO and EG-rGO nanosuspension decreases as normal fluid. The decrease in the viscosity can be understood by the rise in the Brownian motion of the particle present in the nanosuspension with the upsurge in the temperature. The reduction in velocity helps to flow the nanosuspension effortlessly at higher temperatures as compared to low temperatures [8].

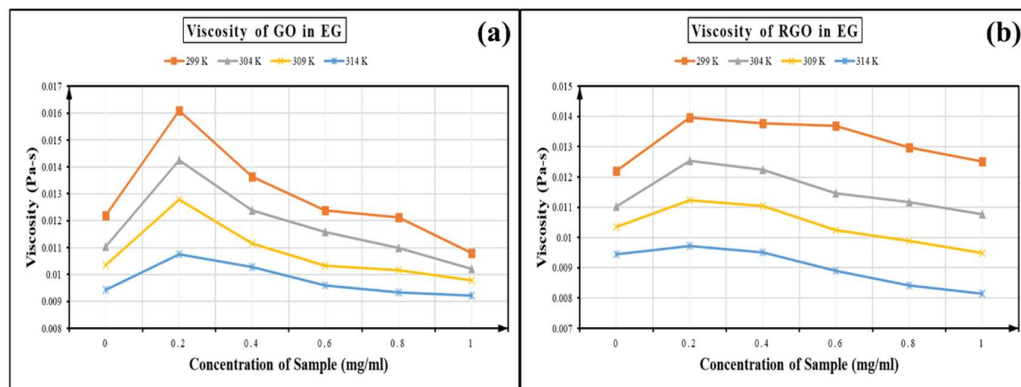


Figure 4.107 (a) Viscosity of GO-EG Nanosuspension (b) Viscosity of rGO-EG Nanosuspension

4.45.4 Adiabatic Compressibility: Fig. 4.108 shows the change in adiabatic compressibility with the increase in the particle loading in pure EG.

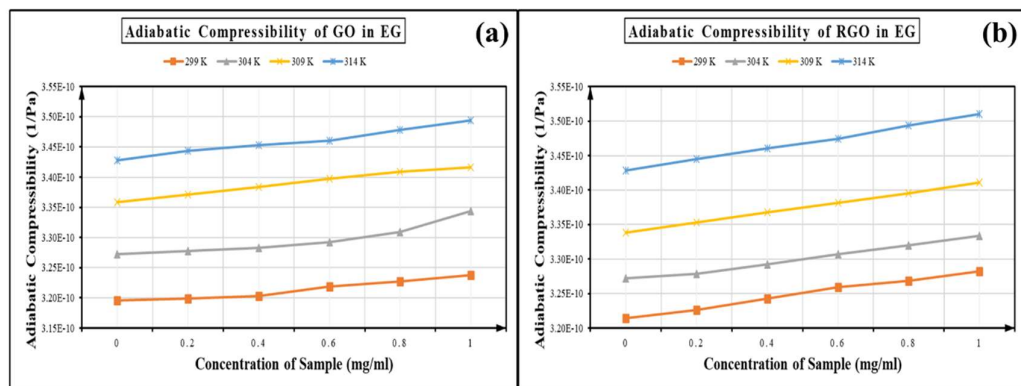


Figure 4.108 (a) Adiabatic Compressibility of GO-EG Nanosuspension (b) Adiabatic Compressibility of rGO-EG Nanosuspension

As the particles are added in pure EG, it shows a constant rise, which shows the stable particle and fluid interaction [9]. The increase in the compressibility also leads to the conclusion that the particle added to the base fluid is not forming any complicated structure in the nanosuspension. The increase in the adiabatic compressibility shows the interaction in the particle and fluid decreases. Adiabatic compressibility likewise increases with the increase in the temperature of the system, which is the cause of the rise in the Brownian motion of the particles. [10]

4.45.5 Acoustical Impedance: Fig. 4.109 shows the decrease in the values of acoustical impedance with particle loading in pure EG. A reduction in the amount of acoustical impedance shows the decline in interaction in solute and particle of the EG-GO and EG-rGO nanosuspension [11]. With the increases in the temperature, the value of acoustic impedance decreases because of the Brownian motion of the particles in the fluid increases. Increasing particle-fluid interactions at lower concentrations widen the intermolecular gap, which provides resistance to the propagation of ultrasonic waves [12].

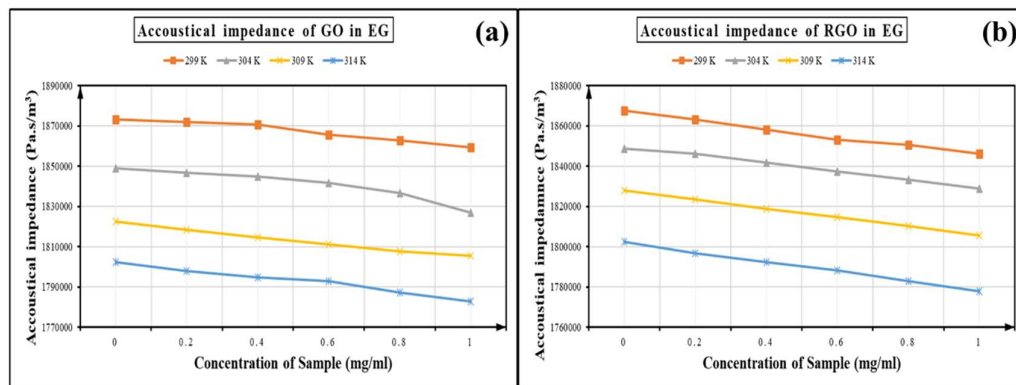


Figure 4.109 (a) Acoustical Impedance of GO-EG Nanosuspension (b) Acoustical Impedance of rGO-EG Nanosuspension

4.45.6 Attenuation: Variation of the ultrasonic attenuation and concentration of the particles in EG-GO and EG-rGO nanosuspension is shown in Fig. 4.110. Ultrasonic attenuation starts increasing as soon as the particle is added in the pure EG fluid.

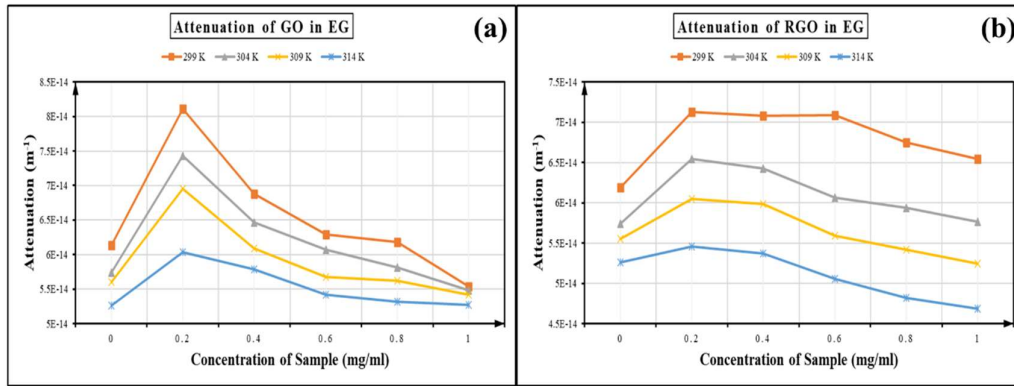


Figure 4.110 (a) Attenuation of Ultrasonic Wave in GO-EG Nanosuspension (b) Attenuation of Ultrasonic Wave in rGO-EG Nanosuspension

Further decrease in the ultrasonic attenuation can be seen in both GO and rGO nanosuspension; this decrease in the mitigation is because GO and rGO cannot form agglomeration by binding with each other. This help produced by the GO and rGO particles in the nanosuspension passes the ultrasonic waves from reaching one end to the other. The increase in the temperature value of the ultrasonic attenuation decrease because of a reduction in the interaction of EG molecules with GO and rGO particles. Here we cannot deny the complex formation in the suspension. [11]

4.45.7 Bulk Modulus: In figure 4.111, it can be seen clearly that the value of bulk modulus declines with the increase in the particle loading in the solvent. Interaction between the particle and fluid decreases as the concentration of the GO and rGO in nanosuspension increases.

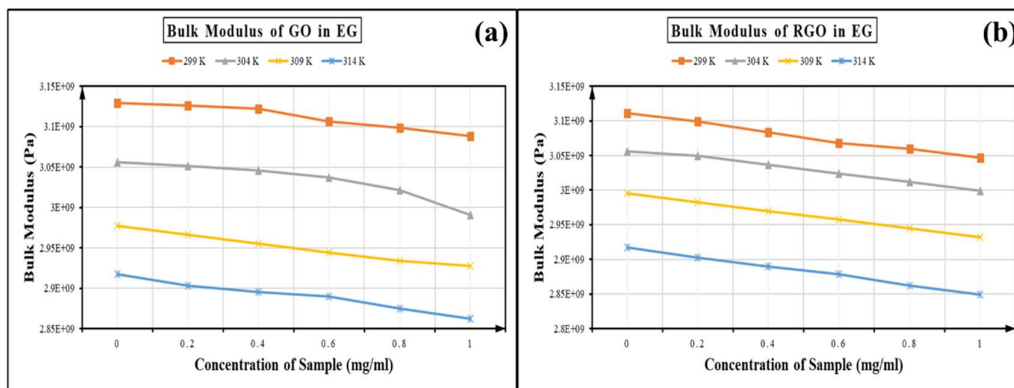


Figure 4.111 (a) Bulk Modulus of GO-EG Nanosuspension (b) Bulk Modulus of rGO-EG Nanosuspension

The value of the bulk modulus decreases with the rise in the heat of the nanosuspension. The resistance of the nanosuspension decreases to the externally applied stress at a higher temperature because the interaction between particle and solute increases creates the gap between molecules, which helps in reducing bulk modulus [13],[14]

4.45.8 Relaxation Time: The relaxation time of the EG-GO and EG-rGO sample decrease with the increase in the concentration of GO and rGO in the G)-EG and EG-rGO nanosuspension, respectively, as shown in figure 4.112. Since the interaction between the solvent molecules and solute decreases. The reordering time for the solute molecules increases. When the heat of the EG-GO and EG-rGO nanosuspension rises, the zigzag movement of the solvent molecule increases, which helps to reorder the molecules quickly because of fast motion [14],[15].

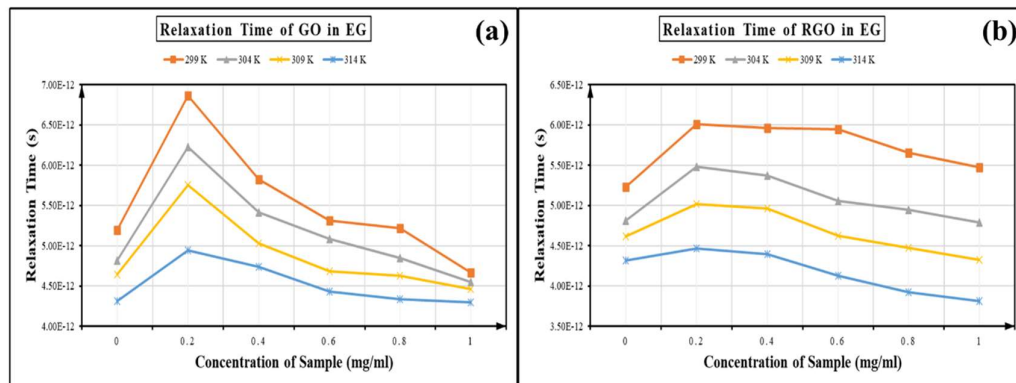


Figure 4.112 (a) Relaxation Time of GO-EG Nanosuspension (b) Relaxation Time of rGO-EG Nanosuspension

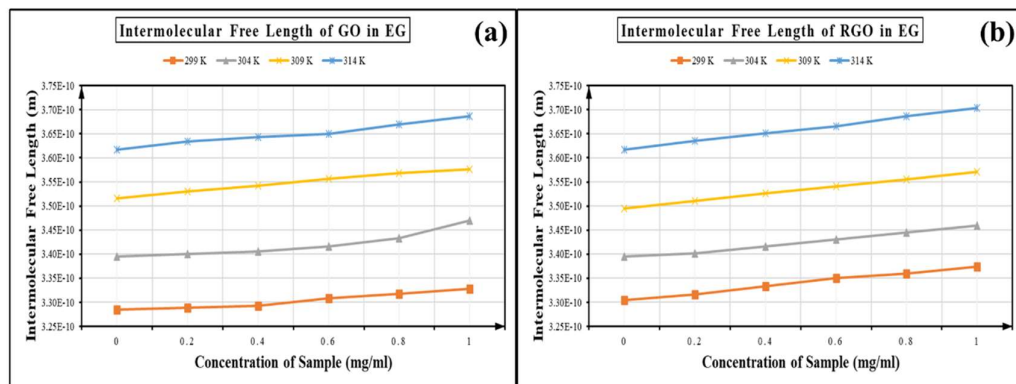


Figure 4.113 (a) Intermolecular free Length of GO-EG Nanosuspension (b) Intermolecular free Length of rGO-EG Nanosuspension

4.45.9 Intermolecular free length: The intermolecular free length of the sample increases with a rise in the particle loading in the EG-GO and EG-rGO nanosuspension, as shown in Figure 4.113. It shows the interaction between particle and solvent molecules increases. The increase in the intermolecular length with the rise in the heat is because the zigzag movement of the solvent molecules rises, and this movement increases the solute and solvent molecule interaction [16],[17]

4.46 References

- [1] M. N. Rashin and J. Hemalatha, *J. Mol. Liq.*, **197**, 257, (2014).
- [2] D. Papamatthaiakis, F. Aroni, and V. Havredaki, *J. Chem. Thermodyn.*, **40**, 107, (2008).
- [3] M. Nabeel Rashin and J. Hemalatha, *J. Mol. Liq.*, **197**, 257, (2014).
- [4] M. N. Rashin and J. Hemalatha, *Ultrasonics*, **52**, 1024, (2012).
- [5] R. S. Vajjha, D. K. Das, and B. M. Mahagaonkar, *Pet. Sci. Technol.*, **27**, 612, (2009).
- [6] S. N. Shoghl, J. Jamali, and M. K. Moraveji, *Exp. Therm. FLUID Sci.*, **27**, 12, (2016).
- [7] M. N. Rashin and J. Hemalatha, *Exp. Therm. Fluid Sci.*, **51**, 312, (2013).
- [8] M. R. Esfahani, E. M. Languri, M. R. Nunna, M. Rabbani, E. Mohseni, and M. Rao, *Int. Commun. Heat Mass Transf.*, **76**, 308, (2016).
- [9] Khushboo, A. Devi, P. Malik, and H. Kumar, *J. Mol. Liq.*, **214**, 145, (2016).
- [10] A. Nanda, A. Tiadi, S. K. Mallik, R. Giri, and G. Nath, *IOP Conf. Ser. Mater. Sci. Eng.*, **360**, 1, (2018).
- [11] S. Tiwari, B. S. Kusmariya, A. Tiwari, V. Pathak, and A. P. P. Mishra, *J. Taibah Univ. Sci.*, **11**, 101, (2017).
- [12] N. H. Ayachit, S. T. Vasan, F. M. Sannaningannavar, and D. K. Deshpande, *J.*

Mol. Liq., **133**, 134, (2007).

[13] B. Tajik, A. Abbassi, M. Saffar-Avval, and M.A. Najafabadi, Powder Technol. **217**, 171, (2012).

[14] N.H. Ayachit, S.T. Vasan, F.M. Sannaningannavar, and D.K. Deshpande, J. Mol. Liq. **133**, 134 (2007).

[15] S. Elangovan and S. Mullainathan, Indian J. Phys. **87**, 659 (2013).

[16] F. Chen, Z. Yang, Z. Chen, J. Hu, C. Chen, and J. Cai, Journal of Molecular Liquids, **209**, 683, (2015).

[17] K. Kaur and K. C. Juglan, Der Pharma Chem., **7**, 160, (2015)

CHAPTER 5: SUMMARY AND CONCLUSION

5.1 SUMMARY

The thesis entitled “*Study of acoustical and thermodynamic properties of graphene oxide (GO) and reduced graphene oxide (rGO) in water and some organic solvents*” tells us about the acoustical and thermodynamic behaviour of the nanosuspension of GO and rGO with water, NMP, DMF, THF, and EG. We have measured the thermodynamic properties of the nanosuspension. Out of measured properties, ultrasonic velocity, density, and viscosity are measured with the help of an interferometer, densimeter, and viscometer. All these measured values are calculated at temperatures 298, 303, 308, and 313 K. we have derived specific parameters like adiabatic compressibility, Bulk modulus, etc. with the help of the calculated properties

In this study, we converted carbon to GO chemically with the help of the Hummers method. In this method, oxidation of the graphite powder is done with the help of oxidation reagents like KMnO_4 and NaNO_3 . These reagents add oxygen in between the layers of the carbon if done correctly. With the addition of the big oxygen atoms, the gap between the layers of the graphite increases. Now, these layers are loosened enough and can be detached from the graphite structure. This detachment of the layers can be done by removing the oxygen from the layers of the carbon. This removal of the oxygen produces the layers of the graphene, which is known as rGO. Prepared GO was reduced with the help of hydrazine hydrate to receive rGO as a final product. Both GO and rGO were characterized with the help of FESEM, EDS, XRD, FTIR, and RAMAN. The presence of layers like structure in FESEM, peak at a higher angle in GO, and lower angle in rGO shows the presence and absence of oxygen in between the sheets, respectively. EDS provides the amount of carbon and oxygen present in the prepared GO and rGO. The presence of I_d/I_g ratio confirms the conversion of carbon to GO and GO to rGO. The characterization of the samples confirms the transformation of both GO and rGO.

There are very fewer fluids available in which GO and rGO make a stable suspension. Out of many liquids, water, EG, THF, DMF, and NMP are few fluids which

make stable suspension with the GO and rGO. In this study, we have made the suspension for all five liquids with concentration 0.2mg/ml, 0.4 mg/ml, 0.6 mg/ml, 0.8 mg/ml and 1.0 mg/ml. after the addition of the GO and rGO in the liquid, we have done the intense ultrasonication of the liquid sample. This ultrasonication helps to provide a stable suspension for the liquids under study. Ultrasonication also helps to loosen up the more layers from the graphite structure by providing energy from outside. This process helps to break the layers into smaller parts. HRTEM, UV-Vis, and DLS are used to characterize the prepared suspension. IN HRTEM, layers of the GO and rGO were visible for both GO and rGO. The size of the graphene sheets was larger in the case of GO as compare to rGO. The smaller size of the sheets in the rGO is because of the chemical removal of the oxygen atoms from the layers, which breaks the structure of the graphene sheets. UV-Vis confirms the presence of the GO and rGO by showing their respective peaks in the graphs. DLS was used to determine the average size of the GO and rGO sheets. All these techniques help to prove the presence of the GO and rGO in the solution and the size of the GO and rGO particles in the solution.

In the ultrasonic velocity study of GO and rGO with solvents, it can be seen that the ultrasonic velocity rises with particle loading for Water-GO, Water-rGO, NMP-GO, NMP-rGO, THF-GO, and THF-rGO. This shows the dominating interaction between the Solute and solvent molecules. DMF-GO, DMF-rGO, EG-GO, and EG-rGO show the decrease in the ultrasonic velocity with an increase in the particle loading in the solvent. This decrease in the ultrasonic speed indicates the dominating solute-solute and solvent-solvent interaction as the temperature of the system increases the ultrasonic velocity of the Water-GO and Water-rGO increases and the decrease in the ultrasonic velocity observed in the DMF-GO, DMF-rGO, NMP-GO, NMP-rGO, THF-GO, THF-rGO, EG-GO, and EG-rGO. This increase in the ultrasonic speed with a hike with the temperature is due to the rise in the particle fluid interaction, and a decrease in the velocity shows the weakening of the particle fluid interaction. In the density study of the GO and rGO with different solvent, it can be seen that the density of the prepared nanosuspension decreases for Water-GO, Water-rGO, DMF-GO, DMF-rGO, EG-GO, and EG-rGO with the increase in the particle loading and increases for NMP-GO, NMP-rGO, THF-GO and THF-rGO nanosuspension with the increase in the particle loading.

The rise in density shows the fair amount of the interaction between the solute and the solvent molecules. This interaction weakens when the density decreases with the particle loading as the temperature of the system increases, the value of the density decreases for all the prepared nanosuspensions. The reduction in the density suggests that with increases in the heat, the solute-solvent interaction decreases. In the study of the viscosity, the value of the viscosity increases with an increase in the particle loading for Water-GO, Water-rGO, NMP-GO, NMP-rGO, THF-GO, and THF-rGO and decreases for DMF-GO, DMF-rGO, EG-GO, and EG-rGO. The viscosity of the fluid increases because the GO and rGO particles tangle with each other to restrict the flow of the suspension. The decrease in the viscosity shows the addition of the GO, and rGO helps to flow the suspension easily; when the temperature of the fluid increases, the viscosity of all the prepared nanosuspension decreases because of the Brownian motion of the solvent molecules increases, which helps to flow the nanosuspension. In the study of the Adiabatic compressibility, the value of adiabatic compressibility increases in DMF-GO, DMF-rGO, EG-GO, and EG-rGO with an increase in the particle loading. The decrease in the adiabatic compressibility observed in the Water-GO, Water-rGO, NMP-GO, NMP-rGO, THF-GO, and THF-rGO. This decrease in the adiabatic compressibility is the due formation of the complex structure in the nanosuspension, and an increase in the adiabatic compressibility is due to the absence of any complex structures in the nanosuspension. With the rise in the temperature, the adiabatic compressibility of Water-GO and Water-rGO decreases, and all other nanosuspension shows the increase in the adiabatic compressibility. An increase in the adiabatic compressibility shows the decrease in the fluid and solute interaction with the rise in the temperature. In the study of acoustic impedance, the value of acoustic impedance increases in Water-GO, Water-rGO, NMP-GO, NMP-rGO, THF-GO, and THF-rGO and value decreases for DMF-GO, DMF-rGO, EG-GO, and EG-rGO. The increase in the acoustic impedance suggests the excellent interaction between solute and solvent molecule, and the decrease in the impedance suggests the superb cooperation between the solvent-solvent molecule and particle-particle of solute. With the increase in the temperature, the value of acoustic impedance increase in Water-GO and Water-rGO only, and the value of the acoustic impedance decreases in DMF-GO, DMF-rGO, NMP-GO, NMP-rGO, THF-GO, THF-rGO, EG-GO, and EG-rGO. The decrease in the value

of acoustic impedance is due to the rise in the Brownian motion of base fluid molecules with the increase in the heat, and the solvent molecule interacts with nanoparticles, which creates a gap between the molecules, which helps the ultrasonic waves to pass through the liquid quickly. On the other hand, an increase in the acoustic impedance increase because the particle-particle interaction stops the ultrasonic waves from passing through the sample. In this study, the attenuation of the ultrasonic wave has been measured in the sample. The value of the attenuation increase in Water-GO, Water-rGO, DMF-rGO, NMP-GO, NMP-rGO, THF-GO, and THF-rGO and the value of the attenuation decreases for DMF-GO, EG-GO, and EG-rGO with the increase in the particle concentration. The value of the attenuation increases with the increase in the concentration because GO and rGO particles form the network of the particles, which blocks the ultrasonic waves. On the other hand, the decrease in the attenuation is because particle-particle interaction is not their presence in the suspension. With an increase in the temperature, the value of the attenuation increases in DMF-rGO, THF-GO, and THF-rGO. On the other hand, attenuation decreases in Water-GO, Water-rGO, DMF-GO, NMP-GO, NMP-rGO, EG-GO, and EG-rGO. The ultrasonic attenuation decreases because of a reduction in the interaction of EG molecules with GO and rGO particles. In this study, the value of the bulk modulus increases in Water-GO, Water-rGO, NMP-GO, NMP-rGO, THF-GO, and THF-rGO, and the value decreases for DMF-GO, DMF-rGO, EG-GO, and EG-rGO with the increase in the particle concentration in the suspension. The bulk modulus increases with particle and solvent interaction and decreases with increases in solvent-solvent and solution-solution interaction. The value of bulk modulus increases in Water-GO and Water-rGO, on the other hand, DMF-GO, DMF-rGO, NMP-GO, NMP-rGO, THF-GO, THF-rGO, EG-GO, and EG-rGO. The decrease in the value of the bulk modulus is because of the interaction between particle and solute increases creates the gap between molecules, which helps in reducing bulk modulus. The increase in the value of the bulk modulus is because of a decrease in the interaction of particle and particle and solvent molecule and solvent molecule. In this study, we have calculated the relaxation time increases in Water-GO, Water-rGO, DMF-rGO, NMP-GO, NMP-rGO, THF-GO, and THF-rGO and decrease in DMF-GO, EG-GO, and EG-rGO with the increase in the particle loading in the nanosuspension. The relaxation time increases because of the interaction

between the solvent molecules and solute decreases, and the reordering time for the solute molecules increases. On the other hand, reordering time increases as the solvent molecules and solute increases. When the temperature of the suspension increases, the value of the relaxation time increases in DMF-GO, DMF-rGO, THF-GO, and THF-rGO and decreases for Water-GO, Water-rGO, NMP-GO, NMP-rGO, EG-GO, and EG-rGO. The value of the relaxation time decreases because the zigzag movement of the solvent molecule increases, which helps to reorder the molecules quickly because of fast motion and vice versa. In this study, we have calculated the intermolecular free length increases in DMF-GO, DMF-rGO, EG-GO, and EG-rGO and decreases in Water-GO, Water-rGO, NMP-GO, NMP-rGO, THF-GO, and THF-rGO. The intermolecular free length decreases with the increase in the particle solute interaction and vice-versa. The value of the intermolecular free length decreases with an increase in the temperature in Water-GO and Water-rGO and increases in DMF-GO, DMF-rGO, NMP-GO, NMP-rGO, THF-GO, THF-rGO, EG-GO, and EG-rGO. The increase in the intermolecular length with the rise in the heat is because the zigzag movement of the solvent molecules rises, and this movement increases the solute and solvent molecule interaction and vice-versa.

5.2 CONCLUSION

This study helps to conclude the acoustical and thermodynamical parameter study as an easy and cheap method to find stable nanosuspension. It has been observed that both GO and rGO nanosuspension behaves similarly for all the prepared samples. The intramolecular interaction is dominated in Water-GO, Water-rGO, NMP-GO, NMP-rGO, THF-GO, and THF-rGO. This shows the strong interaction between solvent molecules and solute particles. On the other hand, DMF-GO, DMF-rGO, EG-GO, and EG-rGO shows the domination of intermolecular interaction over intramolecular communication. The intermolecular interaction suggests the strong interaction between either solvent and solvent molecules or solute and solute particles. The interaction of the solute and solute particles also hints towards the agglomeration of the particles in the samples. With the study of data, we found that there is no complex formation in Water-GO, Water-rGO, NMP-GO, NMP-rGO, THF-GO, and THF-rGO. On the other

hand, the increase in the adiabatic compressibility shows the creation of some complicated structures in DMF-GO, DMF-rGO, EG-GO, and EG-rGO the nanosuspension. As per data, it can be said that out of prepared nanosuspension, Water, NMP, and THF show better stable nanosuspension properties as compare to DMF and EG.

5.3 FUTURE PROSPECTIVE

1. As we know, the heat conductive properties of the GO and rGO are excellent so, further studies on the thermal conductivity of the sample can be conducted. This study will help to find the use of GO and rGO stable nanosuspension as a coolant application.
2. The study on the flow behaviour of GO and rGO has an excellent future scope in the field of rheology. This study can solve the problem of conductive ink.

CHAPTER 6: LIST OF PUBLICATIONS

6.1 List of publications

- ❖ Alok Jain, Parminder Kaur and K. C. Juglan. al, “Synthesis and Ultrasonic Investigation of Reduced Graphene Oxide Nanosuspension with Water”, J. Phy : conf. Ser. 1531, 012022, 2020.
- ❖ Alok Jain, Parminder Kaur and K. C. Juglan, “Rheological study of Reduced Graphene Oxide – Ethylene Glycol nanosuspension for ink” Russian Journal of Physical Chemistry A”, 2020. (Accepted)
- ❖ Alok Jain Parminder Kaur and K. C. Juglan, “Synthesis and ultrasonic investigation of graphene oxide nanosuspension with water”, Plant Archieve, 2020,
- ❖ Alok Jain and K. C. Jug“Acoustical and Thermodynamical study of Graphite Oxide-N-Methyl-2-Pyrrolidon nanosuspension.”, Indian journal of Mechanical and Production Engineering, 2020.

6.2 Paper Communicated

- ❖ Alok Jain and K. C. Jug, “Synthesis and ultrasonic investigation of graphene oxide and reduced graphene oxide nanosuspension with n, n-dimethylformamide” Rasayan Journal of Chemistry, 2020

6.3 Research paper presented in conferences

- ❖ Alok Jain, Parminder Kaur and K. C. Juglan, “Synthesis and Ultrasonic Investigation of Reduced Graphene Oxide Nanosuspension with Water”, J. Phy : conf. Ser. 1531, 012022, 2020.
- ❖ Alok Jain, Parminder Kaur and K. C. Juglan, “Synthesis and ultrasonic investigation of graphene oxide and reduced graphene oxide nanosuspension with n, n- dimethylformamide”. Russian Journal of Chemistry B, 2020